PETROPHYSICAL AND MINERALOGICAL EVALUATION OF SHALE GAS RESERVOIRS (A COOPER BASIN CASE STUDY)

Maqsood Ahmad

Master of Science in Applied Geology
University of The Punjab, Lahore Pakistan
Master of Information Technology
Queensland University of Technology, Brisbane Australia
Master of Engineering Science in Petroleum Engineering
The University of New South Wales, Sydney Australia

Thesis submitted
in fulfilment of the requirements for the degree of

Doctor of Philosophy

Australian School of Petroleum

Faculty of Engineering, Computer and Mathematical Sciences

The University of Adelaide
Australia

January 2014

Table of Contents

CHAPTER 3: Mineralogy and Petrophysical Evaluation Using QEMSCAN, Micro and Nano CT-Scanning, FIB/SEM and X-Ray Diffraction Techniques

Page No.

CHAPTER 4: Evaluation of Porosity Using Core Analysis

CHAPTER 5: Water Saturation Evaluation Using Wireline Logs, Focused Ion Beam Milling and Scanning Electron Microscopy

CHAPTER 6: Conclusions

Page No.

Abstract

Unconventional shale gas reservoirs are over-mature potential source rocks and possess commercial quantities of hydrocarbons in a mechanism which is different from conventional gas reservoirs. These organically rich shale rocks also known as continuous hydrocarbon reservoirs represent a voluminous, long-term, global source of thermo-genic methane and other hydrocarbon gases and could be referred to as shale gas. Roseneath and Murteree shale formations in Cooper Basin have been identified as potential shale gas reservoirs in South Australia. Core samples from these carbonaceous shales were selected for this study.

Petrophysical and mineralogical characterization of shale gas reservoirs is still a challenge due to ultra-fine grained micro-fabric, micro level heterogeneity and anisotropic characteristics of these sedimentary rocks. Unlike conventional gas reservoirs, shale gas reservoirs have very low effective porosity and micro to nano-scale permeability. Conventional standards applications to characterize unconventional gas reservoirs give contradictory results about the mineralogy and rock characteristics, effective and total porosity as well as estimated brine saturation. These uncertainties in the results raised the question, which tools/standards are suitable for petrophysical and mineralogical evaluation of shale gas reservoir.

This research outcome tried to answer the above questions and tells how mineralogy and rock characterization, total porosity, reasons of very low effective porosity and saturation which play a key role in selection and development of a shale gas play, can be evaluated and estimated using both conventional and unconventional techniques

The Roseneath and Murteree shale formations in Cooper Basin have been identified as potential shale gas reservoirs in South Australia. Two core samples from these carbonaceous shales intercepted in Della4 and Moomba46 wells were selected for this project. Core samples were used for number of reservoir characterization phases namely, a) minerals quantification and rock classification, b) visual identification and density of pores location in grains and matrix, c) their types, size classification and interconnectivity, d) evaluation of effective and total interstitial/intergranular and intragranular porosity. While log data from Della# 4 was applied in various resistivity models for water saturation estimation in Murteree shale.

QEMSCAN (Quantitative Evaluation of Minerals using Scanning Electron Microscopy) aided by X-Ray Diffraction techniques was used for mineral and rock characterization. Based on QEMSCAN analysis, we found that Murteree shale has, 42.78% quartz, 6.75% siderite, 28.96% illite, 14.09% koalinite, 1.91% Total Organic Content and 0.04% pyrite, while rutile, sphalerite and some other silicates minerals were identified as accessory minerals. Computerized Tomography (CT), Focused Ion Beam Milling and Scanning Electron Microscopy (FIB/SEM) were employed for identification of pores, network of fractures and their interconnectivity in scanned samples. FIB/SEM combined with CT scanning significantly enhanced shale rock characterization and reservoir petrophysical quality assessment. Helium porosimetry and mercury injection capillary pressure (MICP) techniques were applied for effective porosity and liquid pyknometry was used to estimate the total pore volume. While water saturation was estimated using wireline logs data from Della#4 well completion report and later correlation of results with data found in well completion reports of recent wells drilled through Roseneath and Murteree shale interval.

QEMSCAN results when correlated with XR-diffraction quantitative analyses are found in good agreement with each other for Murteree shale samples. Total free porosity found to be 2 percent is close to total porosity calculated using Wyllie's formula with Hilchie's correction factor. Stieber formula was applied to estimate clay volume (52.3%) from Gamma Ray logs data and this figure

is close to estimated clays volume in XR-diffraction and QEMSCAN techniques 50.59% and 47.30% respectively. QEMSCAN coloured maps revealed the location of lamination, quartz and clay rich zones, high and low porosity zones as well as high and low sorption areas. FIB/SEM scanned images showed that free porosity is largely associated with clay and siderite rich zones. Pores are intergranular and linear, isolated by clays microfabric lamination, and elongated wedge shaped. All pores types and morphology are described.

Since individual pores and porosity evaluation found in QEMSCAN and FIB/SEM technique are not possible to be imaged using CT-scanning, only a network of micro-fracture system in Murteree shale sample was identified in CT-scanned samples. Therefore, no porosity evaluation is possible using CT-scanning. To check the interconnectivity of the pores and fractures network, helium porosimetry was used to measure effective porosity revealing very low effective porosity less than 2.0 % on all samples. Also MICP techniques revealed that samples were mainly comprised of meso-pore throat sized pores, with pore throat diameters range between 2–50 nanometres and an effective porosity of less than 2%. Pores aperture size was documented by 2D imaged pores size and their interconnectivity in FIB/SEM results. The MICP based pores throat classification confirms ultra-low permeability in these reservoirs. The contradiction between imaged pore sizes and the effective porosity led to estimate the total porosity using liquid pyknometry.

Liquid pyknometry method was applied on crushed/powder samples to measure total porosity. It estimated an average absolute porosity of 30.5% for Murteree shale and 39% for Roseneath shale, much higher than MCIP technique and helium porosimetry results, revealing very high isolated porosity and very low permeability. The findings were investigated and analysed using of extensive FIB/SEM images. These 2D images displayed high amounts of isolated porosity supporting high porosity existence estimated from pyknometry technique. Therefore, it was envisaged that total porosity assessment was not possible by helium porosimetry and mercury injection capillary pressure techniques. The pyknometry technique supported by the SEM images is an alternative method which measures total rather than effective porosity.

From our FIB/SEM experimental work and observations we believe Roseneath and Murteree formations have high level of heterogeneity, anisotropy and possess macro and micro-level natural fracture systems. The observed pores and fractures system strongly support that total porosity is much higher than 2.00% estimated from QEMSCAN, sonic and density porosity from logs data as well as effective porosity from helium porosimetry and MICP techniques.

Later selected water saturation models were applied for water saturation estimation in Murteree shale. Based on cumulative effect and interaction of minerals, fluids and organic content application of Archie's equation and other resistivity models such as Indonesian, Siamandoux and Total shale model were investigated. Wire-line logs data was calibrated with QEMSCAN, XRD and FIB/SEM images for clay volumes and total porosity. Evaluation of Archie's parameters (cementation exponent, m, tortuosity factor, a, and saturation exponent, n) were re-examined through sensitivity analysis before applying these models. Using Simandoux and Indonesian models we found 86.00% (S_w) and 84.00% (S_w) respectively when original porosity 2.00% was considered for Murteree shale. However, when total porosity based on 2D FIB/SEM images was considered to be more than or equal to 10.00%, Archie model gave an estimation of 89.00% and with humble formula 84.00% water saturations respectively. Total shale model estimated 58.00% and 70.00% water saturations when cementation exponent (m) was taken as 2.00 and 2.15 respectively in same Murteree shale interval with a total porosity 10.00%.

Declaration

I certify that this work contains no material which has been accepted for the award of any other degree or diploma in any university or other tertiary institutions and, to the best of my knowledge and belief, contains no material previously published or written by another person except where due reference has been made in the text. I certify that no part of this work will, in future, be used in submission for any other degree or diploma in any university or other tertiary institution without the prior approval of the University of Adelaide and where applicable, any partner institution responsible for the joint-award of this degree.

I gave consent for this copy of my thesis, when deposited in the University Library, being made available, for loan and photocopying, subjected to the provisions of the Copyright Act 1968.

The author acknowledges that copy right of published works contained within this thesis resides with the copy right holders of those works. I also give permission for the digital version of my thesis to be made available on the web, via the University's digital research repository, the Library catalogue and also through web search engines, unless permission has been granted by the University to restrict access for a period of time.

Maqsood Ahmad

Signed: Date: April 14, 2014

Australian School of Petroleum
The University of Adelaide
South Australia; Australia

Acknowledgment

The author is especially indebted to Faculty of Engineering, Computer and Mathematical Sciences, The University of Adelaide, for providing me a generous double divisional Ph.D. scholarship and research funding, later on as well. I would like to express my profound gratitude, appreciation and recognition to my principal supervisor, Associate Professor Manouchehr Haghighi and co-supervisor Professor Pavel Bedrikovetsky for their engagement and support throughout this highest research degree project. Each contributed in their unique professional way to guide me to achieve my goal.

It is worth mentioning with gratitude, Head of School, Professor Steve Begg and Professor Ainsworth Bruce for their annual retreat arrangements to closely monitor the post graduate students research activity and feedback received later at the end of retreats, in the last four years. I appreciate their attention and time for this sincere effort to train future research students for presentations and communication skills in their future role. I would like to acknowledge the many people who assisted me during this research. I also extend my thanks to research and teaching staff at Australian School of Petroleum, Kathryn Amos, Mary Gonzalez, Carageorgos Themis, Richard Daniel, You Zhenjiang and Badalyan Alexander. I am pleased to thank Senior Lecture, Andy Mitchell for sending email about the approval of my scholarship and to join ASP, in Adelaide University. Thanks, Andy!

The support and feedback from my fellow research postgraduate colleagues were invaluable in the conduct of this work as well. Special thanks go to all the people at the Australian School of Petroleum. However, I would like to mention Maureen Sutton, Hollands Delise, Ian West, Jodie Norman, Conny Meyer and Eileen Flannery for their support and cooperation in all administrative matters, laboratory work and computer matters especially.

The author strongly acknowledges the help and support of laboratory staff in Ian Wark Research Institute, University of South Australia for QEMSCAN and CT scanning analysis. The support in preparing results of QEMSCAN, Microtomography and Nanotomography Dr Jeremy Deverrel, Zofia Swierczek and Simon Dove support is worth appreciation for conducting experimental work on priority levels. I am also pleased to express my appreciation to Mr Gelb Jeff for his expert advice about Nano-CT Scanning data interpretation after repeating the Nanotomographic and Microtomographic run on Murteree core sample in Xradia Lab Inc. Pleasanton, CA, USA.

The help from laboratory and technical staff at the department of Geology and Geophysics, as well as the Adelaide Microscopy staff to conduct the FIB/SEM µ -CT scanning experimental work has been much appreciated in publications as well. Staff at Adelaide Microscopy facility, in University of Adelaide especially microscopist Mr Leonard Green, Mr Ken Neubauer, Miss Aoife McFadden and Mr John Terlet help is very much appreciated in the use of FEI-FIB/SEM, FEI

Quanta 450, and X-ray Micro-CT radiation techniques in preparing very high quality images for this project. I am also humbled by the support of principal geologist, Dr Nick Lemon, in SANTOS Ltd. Adelaide for sending emails mentioning the availability of Murteree and Roseneath shales core samples in PIRSA Core Library, in Adelaide. David Groom, Michael Willison and their fellow colleagues help in PIRSA Core Library is highly appreciable as well. I also want to thank to Associate Professor Dr Cristopher Sumby, School of Chemistry and Physics, University of Adelaide for timely help and running XRD experiments on some shale samples and later in interpretation as well.

Finally, I would like to extend my gratitude and sincere thanks to my brother Aziz, for his overwhelming support until the submission of my thesis. And my mother, Hajran, her prayers for my success was the biggest source of this humble achievement in my life.

List of Figures

Figure No.	List of Figures (continued) Title	Page No.

Figure No.	List of Figures (continued) Title	Page No.

List of Tables

Dedication

This thesis is dedicated to my parents, brothers, and sister

Research Activity Flow Chart 2010-2011

2010

Literature Review

Research Title/Topic Selection & Registration:
Petrophysical and Mineralogical Evaluation of Shale Gas Reservoirs
A Cooper Basin - Case Study

Experimental Techniques & Methodology Selection & Applied:

1. Helium Porosimetry
2. Mercury Injection Techniques
3. Liquid Pyknometry
4. QEMSCAN, XRD & FIB/SEM
5. Micro and Nano CT-Scanning
6. Wireline Logging Techniques

Objectives/Tasks:

1. Mineral and Rock Characterization
2. Effective and Total Porosity
3. Pore Throat and Pore Size, Morphology and Micro Fracture System Study and Interconnectivity
4. Water Saturation Evaluation

Wells & Cores Selection (Della#4 and Moomba#46)
Samples Collection & Experimental Setup

2011

Sample Preparation for:

1. QEMSCAN Radiation
2. Micro and Nano CT-Scanning
3. XRD – Technique
4. SEM Imaging of QEMSCAN samples

Experimental Results:

1. Organics and Various Minerals Phase Identification & Quantification
2. Weight % & Volumetric % of each Mineral Phase
3. False Colour Map Preparation of Scanned Samples
4. Fractures & Pores Identification in QEMSCAN Used Sample
5. XRD – Minerals Identification and Quantification
6. Micro and Nano CT-Scanning for Pores and Micro Fracture system

Results Correlation:

1. QEMSCAN and XRD Results Correlation
2. Pores Correlation between FIB/SEM Images and QEMSCAN Results
3. Micro – CT Scanning and FIB/SEM Images Correlation for Micro Fracture System

Research Activity Flow Chart 2012-2013

Literature Review

2012

Sample Preparation for :

1. Helium Porosimetry
2. MICP(Mercury Injection Capillary Pressure)
3. Liquid Pyknometry
4. FIB/SEM

Experimental Results:

1. Effective Porosity by Helium and MICP
2. Pores Throat size and Pores Size Description by MICP & FIB/SEM
3. Total Porosity by Liquid Pyknometry

Results Correlation:

1. Helium Porosimetry and MICP Results Correlation
2. Pores Correlation between MICP and FIB/SEM
3. Total Porosity from Liquid Pyknometry & FIB/SEM Images & MICP Graphs

2013

Well Completion Reports Selection:

1. Della#4 & Wireline Log Data Digitization
2. Moomba#46 & Wireline Log Data Digitization
3. Recently drilled Well Completion Reports in Cooper Basins for Murteree and Roseneath Shale
4. Use of FIB/SEM Images from Murteree & Roseneath Shales

Experimental Results:

1. FIB/SEM images Description for Organics and Clays
2. Fluids, Organics and Mineral Interaction
3. Resistivity and Conductivity Analysis
4. a, m, n, R_w and R_{cl} from Published Data
5. Water Saturation Calculation Using Archie, Indonesian, Simandoux and Total Shale Models

Results Correlation:

1. Diagenesis Related Changes in Mineralogy and Fluid Production
2. Interaction between Clays, Methane and Brine
3. Interaction Impact on Resistivity
4. Use of Archie's Formula for Water Saturation and Correlation with Indonesian , Simandoux and Total Shale Model

Three research papers were produced and published based on this research as given below with the titles and name of Journal and Conference venues, presented.

EVALUATION OF FREE POROSITY IN SHALE GAS RESERVOIRS (ROSENEATH AND MURTEREE FORMATIONS CASE STUDY)

M. Ahmad, A. Alamar, R.Koo, H. Nguyen and M. Haghighi
Australian School of Petroleum , North Terrace Campus
The University of Adelaide SA 5005
mahmad@asp.adelaide.edu.au

APPEA Journal 2012, pp 603-610

SPE-158461-PP¶

Mineralogy·and·Petrophysical·Evaluation·of·Roseneath·and·Murteree·Shale· Formations,·Cooper·Basin,·Australia·Using·QEMSCAN·and·CT-Scanning·¶

Maqsood·Ahmad,·and·Manouchehr· Haghighi,·SPE,·Australian·School·of·Petroleum,·The· University·of· Adelaide,·SA·5005,· Australia¶

Maqsood Ahmad and Manouchehr Haghighi SPE
Australian School of Petroleum , North Terrace Campus
The University of Adelaide SA 5005
mahmad@asp.adelaide.edu.au

SPE 167080

Water Saturation Evaluation of Murteree and Roseneath Shale Gas Reservoirs, Cooper Basin, Australia Using Wire-line Logs, Focused Ion Beam Milling and Scanning Electron Microscopy

Maqsood Ahmad, ASP, the University of Adelaide
Manouchehr Haghighi, ASP, the University of Adelaide

Maqsood Ahmad and Manouchehr Haghighi SPE
Australian School of Petroleum , North Terrace Campus
The University of Adelaide SA 5005
mahmad@asp.adelaide.edu.au

CHAPTER 1

Introduction

1.1 Shale Gas Reservoirs-History

Previously known as essential component of a petroleum system as a source rock, a seal and cap rock, mature and organically rich source rocks are now being developed as most promising alternative source of natural gas globally. Albeit complex multiphase gas storage and flow mechanisms, carbonaceous shale characterization techniques have reasonably improved and taken appreciable strides forward, especially in the last decade. Development of shale gas reservoir had been a challenge until 2000, but due to rigorous efforts and highly sought after fast improvement in multilateral horizontal drilling, hydraulic fracturing and multistage state of the art completion techniques have made all these reservoirs economically fit to develop and produce commercial quantities of natural gas from them. Before going into details about geological, geochemical and petrophysical nature of shale gas reservoirs summarized historical background about unconventional shale gas industry in the World is given in table 1.1.

Table 1.1 Shale gas history (Green C. 2012; Bustin et al., 2013)

Year	Events & Development in Geoscientific Research and Engineering Innovation
1821	First commercial gas well drilled in USA/Appalachian Basin/Devonian Shale, Fredonia, New York
1859	Commercial oil well drilled in USA
1860's-1920's	Consumption of natural gas starts from Appalachian and Illinois Basin in local markets
1930's	Natural gas supply/transmission through pipelines
1940's	Hydraulic fracturing experimented on gas well Kelpper Well No. 1 in Grant County, Kansas
1970's	Directional drilling is introduced in industry
1970's-1980's	Department of Energy announced the extensive unconventional gas potential country wide in USA
1980's-1990's	Department of Energy and Gas Research Institute announced multi-disciplinary projects: To improve large hydraulic fracturing design, reservoir characterization and completion techniques; To improve technology and make Barnett shale an economical success by multi-lateral horizontal drilling hydraulic fracturing in shale gas formations for commercial production
2001 to 2004	Barnett shale proved big success – A milestone in shale gas Industry
2005 - 2010	Major shale gas plays development intensifies in USA
2010	USA/Canadian Oil and Gas upstream operators took interest in overseas shale gas plays/systems

1.2 Organic Shales Importance as a Natural Gas Resource

Conventional oil and gas reservoirs received the most attention and were focus of much exploitation in 19th and 20th century. In 20th century petroleum industry made a highly appreciable improvement in applied technology and techniques to evaluate accurately conventional reservoirs

and exploit the petroleum reserves all over the world. This exponential exploitation of conventional hydrocarbon resources lead to a serious thought about total world reserves available at the end of the 20th century, future energy demand in 21st century and beyond. Therefore, taking consequences of likely depletion of conventional petroleum reserves seriously, not in very distance future, the upstream petroleum sector set its focus on the unconventional natural gas to fulfil the future energy demands of the world in present century and later. Global coalbed methane (CBM), tight gas, gas hydrates and shale gas resources were considered as an alternative economical source of energy to face world energy demands. North American upstream sector in petroleum natural resource industry did most of pioneering work in last two decades of 20th century and built the faith to develop these natural gas plays successfully all over the world. They contributed through progressive improvement in scientific tools and procedures to help better characterize, estimate and enhancing manyfold production. Improvements in fraccing, drilling and completion techniques, ultimately encouraged operators to focus in their own petroleum plays and zones of interest worldwide. Barnett shale gas play successful development is one of such examples in North America. Now due to enormous volumes and core component of most of the developed conventional oil and gas plays in world, overmature potential source rocks have attained full attention and are being revaluated and characterized as best alternative cheap source of energy. Consequently organically rich mature source rocks are in focus of upstream petroleum industry operators.

Shales are ubiquitous sedimentary rocks in the world. It is believed that more than half of sedimentary rocks in earth crust are shales of various mineralogical and textural natures. They play a vital role as source rock if impregnated with enough mature organic content as well as a cap/seal in a petroleum system (North F. K., 1985). After original organic matter conversion into kerogen, and later into petroleum (oil, gas and solid hydrocarbons) as a consequence of progressive increase in temperature, pressure and overburden on source rocks, oil and gas will only leave and migrate from shales source rocks to reservoirs rocks if they have saturated their parent rocks and have surplus to move through carrier bed into and ultimately stored in under or overlying porous media, where it is trapped. In case of conventional sandstones and carbonates reservoirs with commercial hydrocarbon potential, source rocks (organically rich mature and overmature shales) in the same sedimentary basins, are the most probable shale gas reservoirs and worth investigation as potential shale gas formations for future, albeit their very low permeability and complex storage mechanism. Shale formations holding natural gas are laterally extensive and thicker compared to conventional sandstones and carbonates reservoirs. Consequently they promise to become best alternative source of natural gas supply due to their enormous volumes.

Shale-gas resources have been estimated 16,000 to 25000 Tcf, (Kawata and Fujita 2001, Rogner 1997, USA-IEA/ARE 2011) worldwide as shown in figure 1.1 and table 1.2. Consequently search for potential shale gas reservoirs has gained momentum on global level. In Europe, China and

Australia the shale gas exploration activity is getting serious, taking example of successful emergence of unconventional natural gas industry from source rocks in lower eastern states of North American. Similarly shale gas potential in Australia is enormous as given in table 1.2.

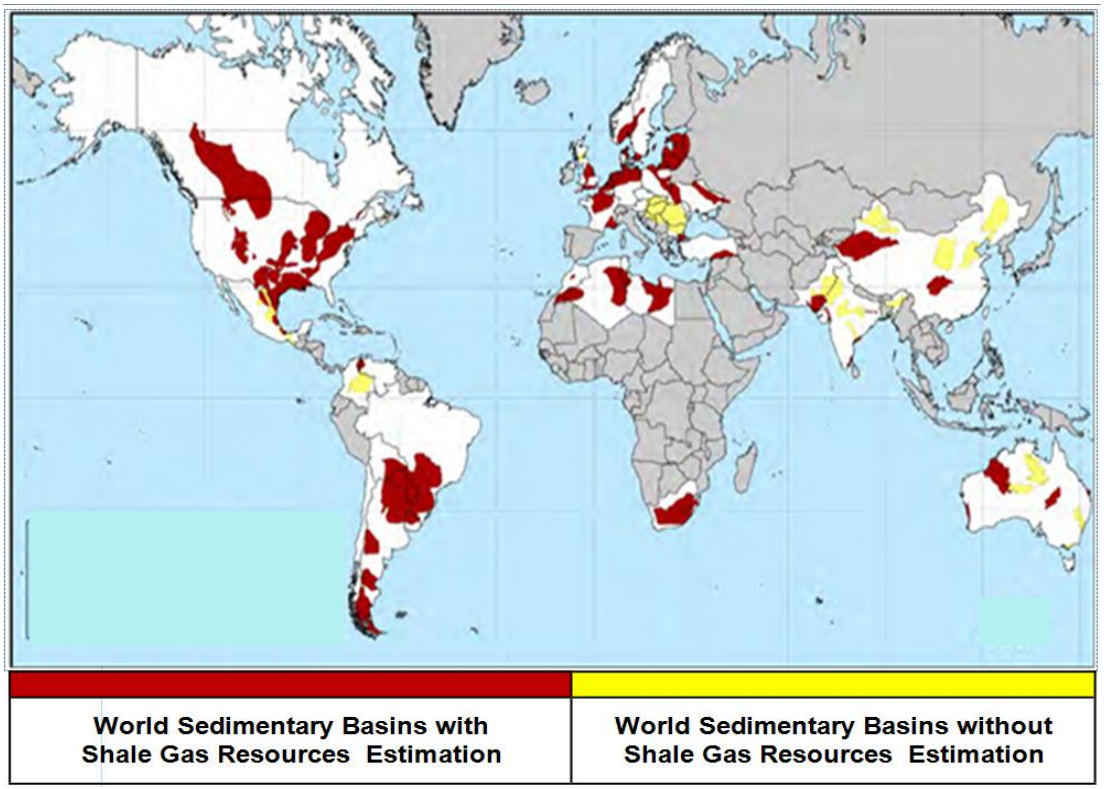

Figure 1.1: World major shale gas resources in 32 countries (US EIA 2011)

Table 1.2 World estimates of shale gas resources in-place

Continent	H.H. Rogner World Estimates (Tcf)	EIA/ARI World Estimates (Tcf)	EIA/ARI Risked Gas in Place (Tcf)	EIA/ARI Risked Technically Recoverable (Tcf)
1. North America	3,842	7,140	3,856	1,069
2. South America	2,117	4,569	4,569	1,225
3. Europe	549	2,587	2,587	624
4. Africa	1,548	3,962	3,962	1,042
5. Asia	3,528	5,661	5,661	1,404
6. Australia	**2,313**	**1,381**	**1,381**	**396**
7. Others	2,215	n/a		
Total (Trillion cubic feet)	**16,112**	**25,300**	**22,016**	**5,760**

Rogner, H. H., "An Assessment of World Hydrocarbon Resources", Rev. Energy Environ. 1997, 22:217-62.
EIA/ARI : USA Energy Information Administration: World Shale Gas Resources: An Initial Assessment of 14 Regions Outside the United States April 2011(http://www.adv-res.com/pdf/A_EIA_ARI_2013)

In the light of natural shale gas resources worldwide as shown in figure 1.1 and table 1.2 and current world energy needs, these shales must be evaluated with reference to generation and production potential to satisfy the energy requirements and demands in near future. Therefore unconventional reservoirs have become the target of latest and sophisticated evaluation and

production technological investigation due to attractive volumes of natural gas they hold. The gradual increase in natural gas prices, all over the world and global environmental impact of this natural gas usage have also escalated the interest of the world petroleum industry operators and organizations related to environmental greenhouse issues. There are number of proven advantages once the shale gas reserves become economical to develop:

1. Alternative future energy source
2. Saving exploration and appraisal costs by converting conventional plays into unconventional plays
3. Saving transportation costs on oil and gas supply to local markets through already built in infrastructure in conventional plays
4. Reduce CO_2 emission by using cheap environmentally friendly methane gas as energy source
5. Turning past exhausted conventional oil/gas plays into unconventional shale gas plays

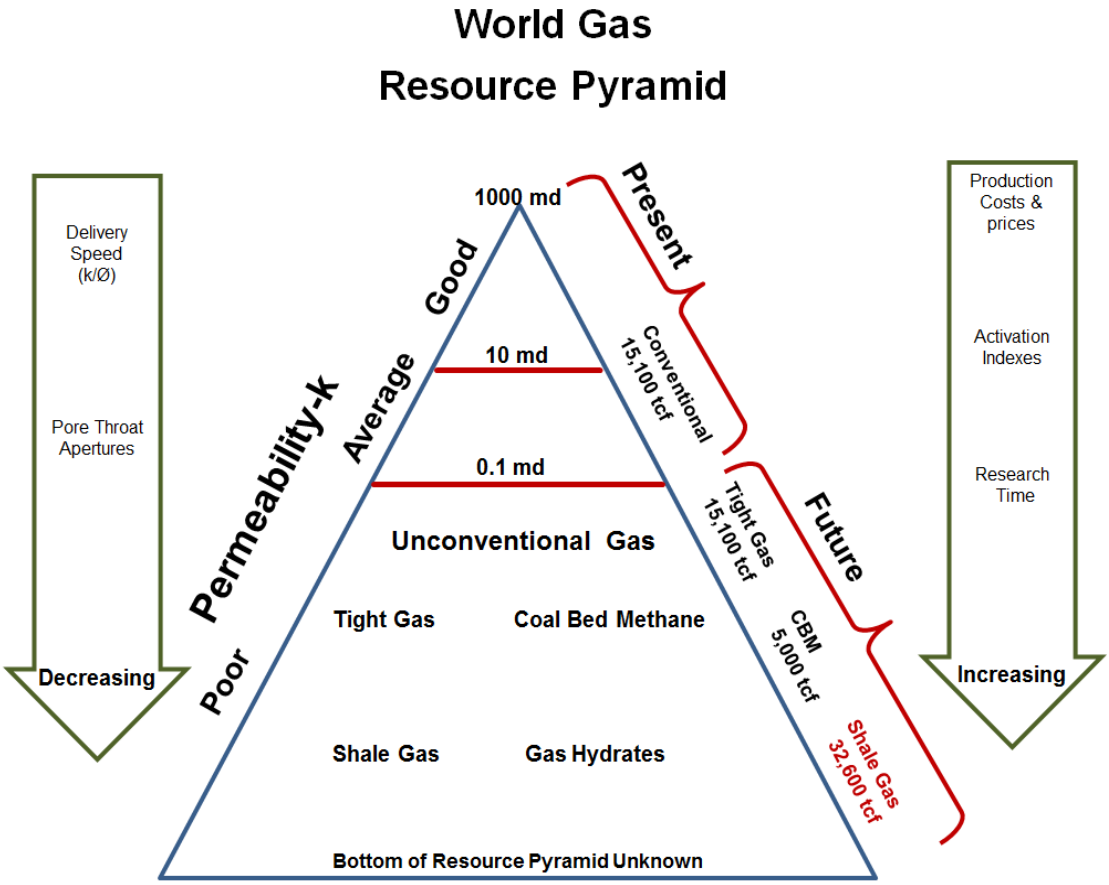

Figure 1.2: World conventional and unconventional gas resources (Aguilera 2013)

1.3 Shale Gas Resources in Australia

Due to progressive improvement in techniques and methodology to characterize and produce liquid and solid petroleum resources, petroleum industry has entered into new phase of exploration, development and production, especially when dealing with shale gas resources

globally. The examples of use and application of such improved scientific approach can be seen in the successful development of Barnett, Haynesville, Marcellus, Woodford and Fayetteville shale plays in North America. In the last decade, North American has made a worthy progress to produce natural gas from these unconventional resources to fulfil part of its domestic energy demands. This successful adventure to exploit the shale gas resources has built the confidence in other countries round the world to explore their prospective shale gas reservoirs as an alternative energy source locally, as well.

North American, shale plays can provide some analogy how to develop and produce natural gas from these resources. But the ground truth is that, all shale gas reservoirs in the world are unique, in source rock and reservoir characteristics even two potential gas shales in same sedimentary basin. Therefore in same sedimentary basin, as well as between different sedimentary basins, different geological, geochemical and geomechanical considerations will be applied in the selection of any shale gas formation for any further investment. These considerations are related to reservoir characterization techniques, production planning and strategies implemented in the future shale gas play in Australia as well.

Australia has fifty to sixty sedimentary and sub named sedimentary basins (Lewis et al. 2010, Mackie 1987). They have sedimentary successions, favouring the likely existence of commercial unconventional petroleum resources as shown in figure 1.3. The thick source rocks interval have not been explored and characterized as likely future shale gas formations yet like Murteree and Roseneath shales in Cooper Basin apart from a limited number of these sedimentary basins as given in table 1.3.

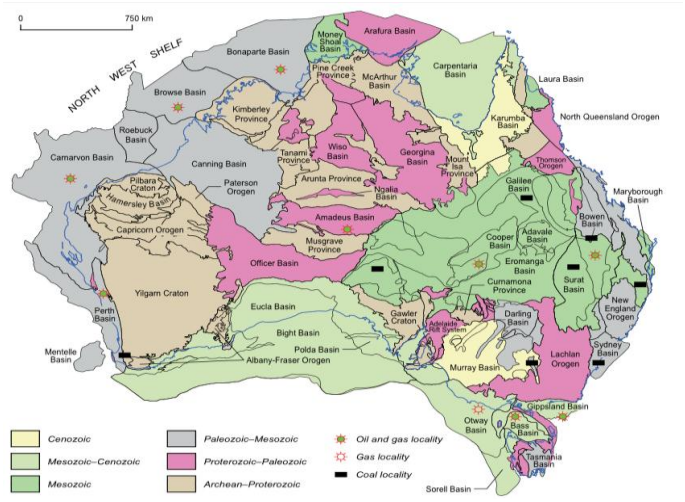

Figure 1.3: Australian sedimentary basins map, showing basin age and major oil, gas and coal occurrences. (Bradshaw et. al., 2007)

The estimated shale 'gas-in-place' resources in Australia as independently assessed by Baker and Bare (2011) and USA EIA/ARI (2013) are in range of 1380–2300 trillion cubic feet (Tcf) of which over 400 Tcf could be technically recovered. The major contributors in this estimation of gas in place are Cooper Basin, South Australia, Canning and Perth Basins Western Australia,

Maryborough in Queensland (Kuuskraa et al. 2011). Although Australia is third largest country according to some experts assessment in shale resources, commercial production for local consumption markets has not commenced yet. Shale industry in Australia is still in its preliminary development stages, waiting for a concerted effort by the upstream industry operators to evaluate total national gas shale resources applying all available means of evaluation and estimation at hand.

Table 1.3: Shale gas potential in major Australian Sedimentary Basins (Richard et al., 2010)

Sedimentary Basin	Reservoir Physical Extent		Reservoir Properties	Total Resources
Cooper Basin **Basin Gross Area:** 46,900 mi^2 **Prospective Area**: 5,810 mi^2 **Age** : Permian **Shale Formations :** Roseneath, Epsilon and Murteree	Thickness (ft.)	**Interval** : 0-1800 ft. **Organically Rich**: 500 ft. **Net**: 300 ft.	**Reservoir Pressure**: Moderately Overpressured **Average TOC wt.%:** 2.5 % **Thermal Maturity:** 2.00% **Clay Content :** Low	**GIP Concentration (Tcf):** 105 **Risked GIP (Tcf):** 342 **Risked Recoverable (Tcf)** : 85
	Depth (ft.)	**Interval** : 6000-13000 ft. **Average**: 8,500 ft.		
Maryborough Basin **Basin Gross Area** : 4,290 mi^2 **Prospective Area** : 1,555 mi^2 **Age** : Cretaceous **Shale Formations :** Goodwood And Cherwell Mudstone	Thickness (ft.)	**Interval** : 300-3000 ft. **Organically Rich**: 1,250 ft. **Net**: 250 ft.	**Reservoir Pressure**: Slightly Over pressured **Average TOC wt.%:** 2.00 % **Thermal Maturity:** 1.50% **Clay Content :** Low	**GIP Concentration (Tcf):** 110 **Risked GIP (Tcf):** 77 **Risked Recoverable (Tcf)** : 23
	Depth (ft.)	**Interval** : 5000-16, 5000 ft. **Average**: 9,500 ft.		
Perth Basin **Basin Gross Area** : 12,560 mi^2 **Prospective Area** : 2,180 mi^2 **Age** : Upper Permian **Shale Formation :** Carynginia Shale	Thickness (ft.)	**Interval** : 300-1,500 ft. **Organically Rich:** 950 ft. **Net**:250 ft.	**Reservoir Pressure**: Normal **Average TOC wt.%:** 4.00 % **Thermal Maturity:** 1.40% **Clay Content :** Low	**GIP Concentration (Tcf):** 107 **Risked GIP (Tcf):** 98 **Risked Recoverable (Tcf)** : 29
	Depth (ft.)	**Interval** : 4000-16, 5000 ft. **Average**: 10,700 ft.		
Perth Basin **Basin Gross Area** : 12,560 mi^2 **Prospective Area** : 2,180 mi^2 **Age** : Lower Triassic **Shale Formation :** Kockatea	Thickness (ft.)	**Interval** : 300-3,000 ft. **Organically Rich:** 2,300 ft. **Net**:230 ft.	**Reservoir Pressure**: Normal **Average TOC wt.%:** 5.6 % **Thermal Maturity:** 1.30% **Clay Content :** Low	**GIP Concentration (Tcf):** 110 **Risked GIP (Tcf):** 100 **Risked Recoverable (Tcf)** : 30
	Depth (ft.)	**Interval** : 3,300-16, 5000 ft. **Average**: 10,000 ft.		
Canning Basin **Basin Gross Area** : 181,000 mi^2 **Prospective Area** : 48,100 mi^2 **Age** : M. Ordovician **Shale Formation :** Goldwyer Formation	Thickness (ft.)	**Interval** : 300-2,414 ft. **Organically Rich**: 1,300 ft. **Net**: 250 ft.	**Reservoir Pressure**: Normal **Average TOC wt.%:** 3.00 % **Thermal Maturity:** 1.40% **Clay Content :**Low	**GIP Concentration (Tcf):** 106 **Risked GIP (Tcf):** 764 **Risked Recoverable (Tcf)** : 229
	Depth (ft.)	**Interval** : 3,300-16, 5000 ft. **Average**: 12,000 ft.		

Current applied and experimented technology in USA, and existing knowledge of specific Australian shale gas sequences, support a positive view that production is feasible from these

source rocks. Cooper and Perth basins are best understood and there is existing production infrastructure and pipelines. Other prospective basins are Canning, Georgina and Beetaloo basins. Geologically and geochemically they are not well understood and source rock quality in question is substandard creating some apprehensions about generation capacity, production potential and transport infrastructure is absent as well. Bowen Basin in Queensland and Sydney basin in New South Wales also have thick sedimentological and stratigraphic sequence, but little is known about hydrocarbon generation potential and rock fraccability due to lack of data required for their reservoir characteristics (Bergenheier 2010). Commercial production from shale has not been seriously attempted in Australia. Australian petroleum industry may plan a robust strategy for its future energy challenges by developing its own evaluation and production techniques according to the local reservoirs geological and geochemical constraints and requirements.

Development and production from few appraisals wells drilled in Roseneath shale, Epsilon formation (tight sandstone) and Murteree shale (RESM interval) in Cooper Basin is being considered as an example to pave the way for further investment in establishment of shale gas industry in Australia.

1.4 Geology of Cooper Basin and Nappmerrie Trough

Being part of the super continent Gondwana, geology of the shale gas reservoirs in all prospective source rocks in Australian Sedimentary Basins, are different from shale gas plays which are actively being produced in the world. These variations in the source rock character are ascribed to the unique fauna and flora, water circulation in Panthalassan Ocean, climatic and pale-latitude of Gondwana. These characteristics have strong impact on Australian source rocks, their lateral extension, geochemical and geomechanical character and later becoming shale gas formations. Due to periodic glaciation and upwelling of the cold high latitude, Panthalassan water was rich in organic matter, in late Palaeozoic (Bergenheier 2010). As a consequence of these prevailing climatic conditions, Permian organically rich marine shales in the Sydney and Bowen Basins were deposited. However, the deep troughs in Sydney, Bowen and Nappamerrie Trough in Cooper Basins are thought to be shallow marine or deltaic organically rich shales, only capable of producing natural gas (Bergenheier 2010).

Cooper Basin in Australia, initially known as Cooper's Creek Basin comprises 130,000 km^2, and is situated at the boundary of Queensland and South Australia states. Cooper Basin is one of most prolific and productive onshore petroleum sedimentary basin and has record of thousands of exploration, development and production wells (Hill and Gravestock 1995). It is a Late Carboniferous to Middle Triassic, non-marine sedimentary basin. It does not outcrop and is completely covered by the Eromanga Basin and approximately covering 35,000 km^2 in South Australia as shown in figure 1.4. Jackson-Wackett-Arrabury trend divides Cooper Basin into south and north region. Cooper Basin has been further divided into three sub basins or troughs, called Patchawarra, Nappamerri, and Tenappera troughs, by two other trends in south region (Lindsay

2000). Due to subsidence, the major depocentre, Nappamerri trough has the thickest stratigraphic succession, reaching a maximum thickness of 1200m as shown in figure 1.5., on next page.

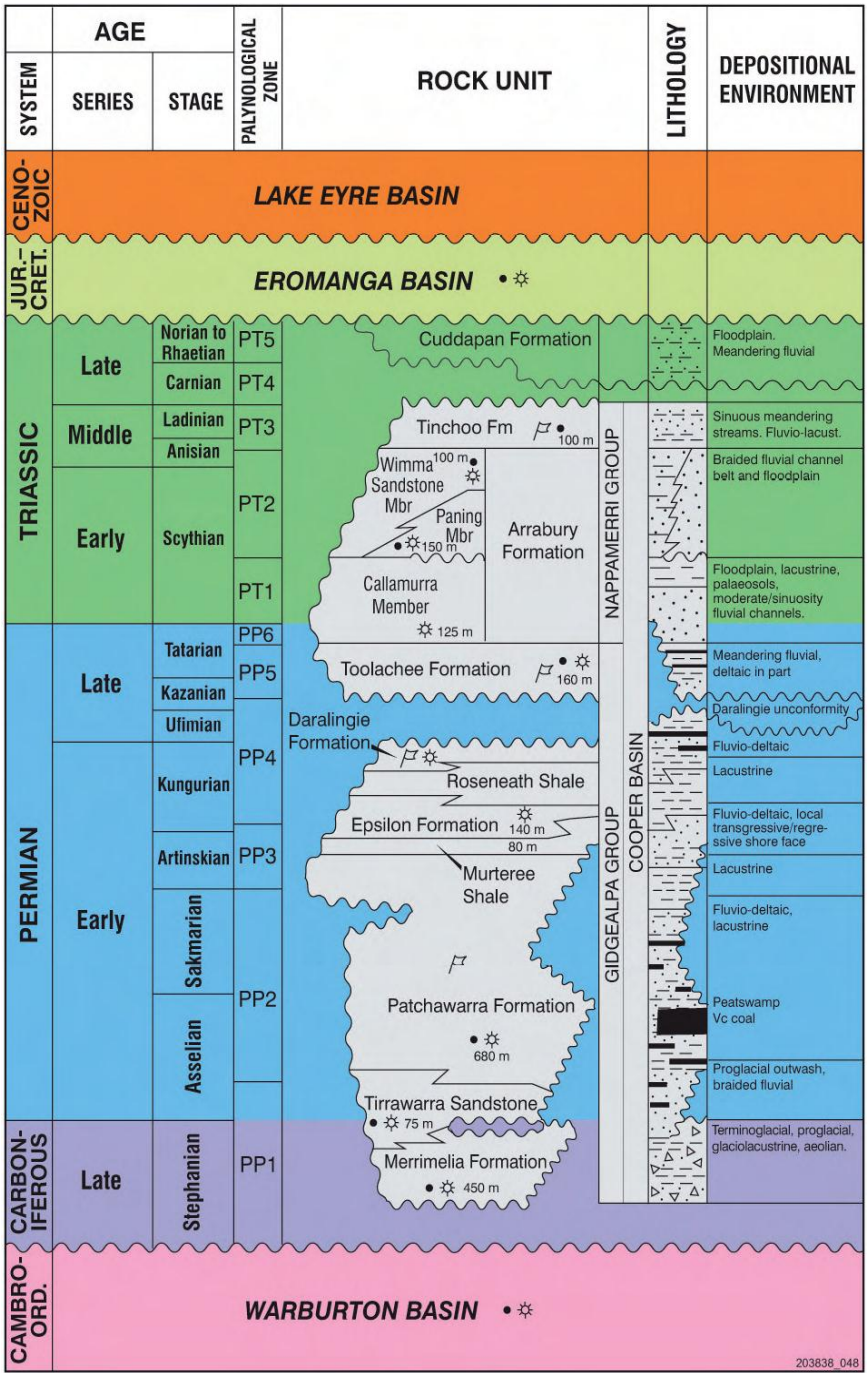

Figure 1.4: Stratigraphy of Cooper Basin and location of Roseneath, Epsilon and Murteree Formations (REM) interval. (PIRSA 200171_002 and 200171_004)

Cooper Basin shares its boundaries by two unconformities of various thicknesses, between Eromanga and Warburton Basins on the top and bottom respectively. Due to glacial retreat from the basal depressions and three times repetition of a cycle of braided streams, meandering streams and lacustrine depositional environments, a number of very productive petroleum systems in Eromanga and Cooper Basins were developed. The whole stratigraphic sequence in

Cooper Basin has been divided into two groups, namely Gidgealpa and Nappamerri Groups of early Permian and late Permian age respectively. The stratigraphic succession comprised nonmarine sandstones, siltstone, shale and coals. Murteree and Roseneath shales are part of depositional sequence called Gidgealpa Group. Later on when subjected to number of orogenic events and gradual burial and higher geothermal gradient due to Carboniferous granite intrusion these fine grained clastic rocks, Roseneath and Murteree became potential source rocks (Mackie 1987). The two formations have acted as seal to the intercalated sandstones reservoirs as well. Due to close vicinity of the provenance to the site of deposition, the clast which turned into Murteree and Roseneath shales lack in sorting and roundness leaving considerable inter-granular porosity in these carbonaceous shales (Ahmad M. and M Haghighi 2012). A formation is a geological term, representing a distinct unit of rock with particular set of rock characteristics, which make the formation recognizable from one location of outcrop or well to another location or in another well. While a Group is always consist of two or more contiguous or associated formations based on some common lithological and diagnostic properties as expressed in figure 1.5.

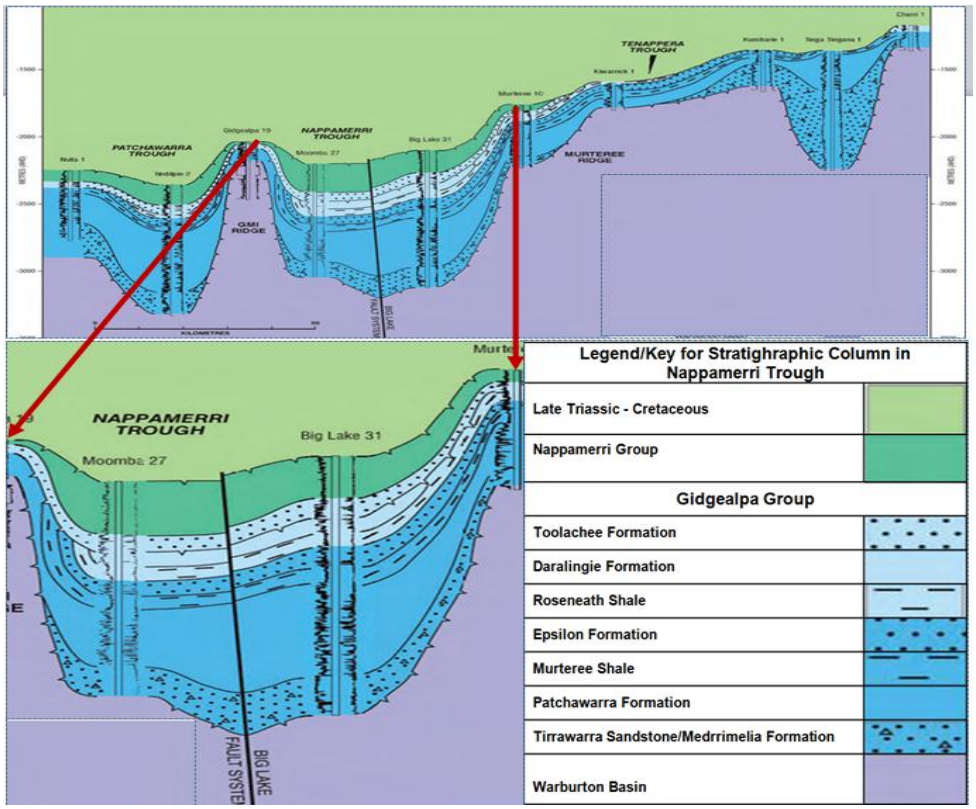

Figure 1.5: Stratigraphy column thickness in Nappamerri Trough of Cooper Basin and location of Roseneath, Epsilon and Murteree Formations (REM) interval**.** (PIRSA 200171_002 and 200171_004)

Early Permian Murteree shale is widely spread in Cooper Basin. Lying between Patchawarra and Epsilon Formations, it has average thickness of 50m, while reaches maximum thickness to 80m in Nappamerrie Trough. Stuart (1976), Thornton (1979) and Gravestock et al. (1998) believed that Murteree shale has an open deep lacustrine and/or marine environment but there are some

concerns about its marine origin due to lack of microplankton organic content as source of hydrocarbons, Gravestock et al., (1998) believed. Whilst Roseneath Shale is not extensive laterally as Murteree formation and its absence in some of the petroleum wells, has been ascribed to tectonic events causing uplift and erosion. Like Murteree, Roseneath shale is nonmarine, thickness 100m, with variable thickness in major troughs like Nappamerrie, Patchawarra and Arrabury Troughs (Stuart, 1976; Thornton, 1979). These two potential, predominantly fine grained shale formations with kerogen type - II, and vitrinite reflectance value greater 3% (PIRSA 2010; Stuart, 1976; Thornton, 1979) make very good representative of unconventional shale gas reservoirs in Cooper Basin.

In intracratonic Cooper Basin onshore sedimentary basin, first natural gas discovery well (Gidgealpa-2) was drilled in 1963, and Permian discovery oil well, in Tirrawara field in 1970, Gravestock D. (1988) and Mackie (1987) have reported. Since then, serving the energy needs of South Australia and neighbouring states in Australia, once again in 2010, Cooper Basin became target of upstream operator's attention for its retained huge potential of unconventional natural gas. Permian shale formations, Roseneath, and Murteree, separated by tight sand formation, Epsilon, commonly known as REM interval are being re-evaluated for economic values from the appraisal wells (Moseby 2010). It is believed that hydrocarbons in Cooper Basin were sourced from Permian coals and shales, mainly from plant remains preserved in sediments. Oil and wet gas reservoiring in Patchawarra Trough were sourced from local source rocks. Nappamerrie Trough due to granitic intrusion in the base and geothermal gradient reaching up to 40-50 °C/Km is over mature and largely contains dry gas, methane. Previously considered as lean source rocks, Murteree and Roseneath shale are considered now, organically rich over mature source rocks based on latest geochemical analysis (PIRSA 2010). The TOC 5 Wt. % has attained a vitrinite reflectance maturity level of 3.0%. Epsilon formation in between the two Permian shales, Roseneath and Murteree shales is typical example of tight gas sand reservoir in Cooper basin. Roseneath shale provides seal to Epsilon while Patchawarra formation was sealed by overlying Murteree formation.

There are state of the art production, processing and transmission systems developed in last half century since the first gas and oil wells were drilled in Cooper Basin. The data and information about the petroleum conventional reservoirs seals, cap rocks and source rocks range from megascopic to microscopic level. Also the produced hydrocarbons (oil and gas) are close to local and interstate consumption markets, and are transported expeditiously through the infrastructure in place at Moomba and Port Bonython facility in South Australia, to Adelaide, Sydney and in Queensland for domestic use.

Cooper Basin is an ultra-mature petroleum province, with reference to unconventional natural gas from Roseneath and Murteree shales, but major potential is the consequence of ideal succession acting both reservoirs and sources in its deepest part, Nappamerrie Trough which have received

considerable exploration and development interest in the past five years. This succession is shown in figure 1.6 below.

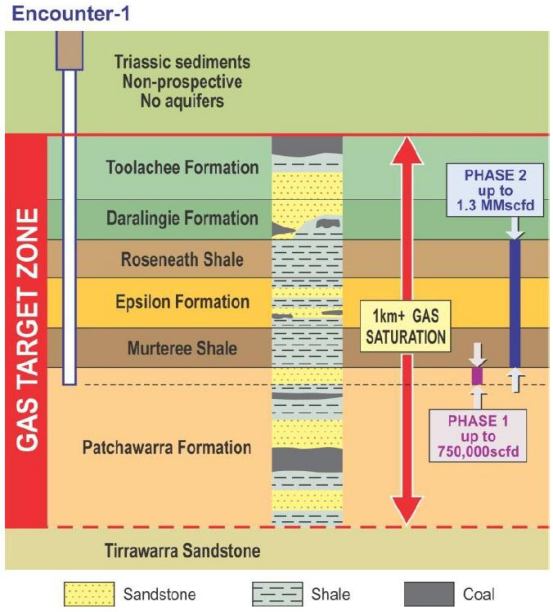

Figure 1.6: Natural gas potential from conventional and unconventional gas reservoirs (Roseneath Epsilon and Murteree) interval in Cooper Basin. (beachenrgy.com.au)

Without knowing the fundamental geological and georganic characteristics of shales it is not possible to understand these sedimentary rocks as potential shale gas reservoirs in Cooper Basin. Therefore in the next topic mudrocks/shales and their geological, geochemical and petrophysical characteristics have been elaborated.

1.5 Mudrocks and Shales (Geological, Geochemical and Petrophysical characteristics)

Shale is a fissile, fine grained ubiquitous clastic sedimentary rock composed of various amount of minerals like quartz, carbonates and clays (David et al. 1995, Schieber 1998, Peters E.J. 2004, katahara, 2006, Sondergeld et. al. 2010), making up over 50% of sedimentary rock. The fissile character is thin parallel layering and bedding caused by alignment of clay minerals and tendency to break into flakes and plates like structures (Strahler 1981; Jacobi et al., 2009; Javadpour 2009).The property of fissility in mudstones, claystones, and siltstones make them shale, clayey shale and silty shales as shown in table 1.4.

Table 1.4: Classification of argillaceous sedimentary rocks (Chapman 1975)

Silt and Clay Particles Size Range	Fissile	Massive/ Non-fissile
Silt:62.50 – 3.906µm	Silty-Shale	Siltstone
Mud Silt <Mud Particle size> Clay	Shale	Mudstone
Clay <3.906 – 0.9765µm	Clayey Shale	Claystone

Shales gas reservoirs have clays (Koalinite, Illite, and Chlorite etc.) one of the core minerals components of having flakes like structure, carbonates (limestone, dolomite, and siderite) and silica (Quartz, Opal) grains and particles in various amounts and ratios. It has medium to fine silt

grains (31.25 – 7.812 µm), and clays flakes less than 3.906 µm (Passey et al 2010). Clays and silica belongs to silicate mineral family and are subdivided into phyllosilicates and tectosilicates (Strahler 1981). The weathering product of feldspars, clays or phyllosilicates, are hydrous layered silicate materials, made of two or three layers of silica or alumina joined into sheets. Clay's platelets are charged positively at the edges and negatively on faces. Kaolinite is a two layer ($(Al_4[Si_4O_{10}](OH)_8$ 1:1 silica:alumina) the weathering product of feldspar in an acidic environment while three layer (2:1 silica:alumina) clay minerals are smectite (Ca, Na)(Al, Mg, Fe)$[(Si, Al)_8 O_{20}](OH)_4.nH_2O$, and Illite $(KAl_4[Si_7AlO_{20}](OH)_4$. The latter have the crystal structure of the micas, muscovite and biotite. Chlorite (Mg, Al, Fe) $_{12}[(Si, Al)_8O_{20}](OH)_{16}$ is a four layer clay and when rich in iron becomes camosite $(Fe_5$ Al)(Al $Si_3)O_{10}$ $(OH)_8$). Shale can have two types of tectosilicates, microcrystalline and crystalline opal and quartz respectively, where the former is abundant in sandstones and the later can have organic origin from the diatoms, in carbonaceous shale. They are both silica with common chemical formula SiO_2.

In oxygen deficient depositional environments iron oxide hematite (Fe_2O_3 Ferric Oxide), is commonly transformed into siderite ($FeCO_3$, ferrous carbonate) or pyrite (FeS_2). Heavy minerals like rutile, sphalerite and zircon make a minor constituent in carbonaceous shales. Shale can also have ankerite Ca (Fe Mg Mn) $(CO_3)_2$, dolomite Ca Mg $(CO_3)_2$ and calcite Ca CO_3. Their various amounts depend on the chemistry of transported detrital clast and nature of the sediments already present in the depositional environment as a consequence of post depositional digenesis. Sandstones conventional reservoirs have negligible amount of preserved organic matter, therefore only organically rich shales and sometime carbonates with certain amount of preserved organic content have a role to become potential source rocks in a conventional petroleum system or become a shale gas reservoir in the former case.

Shales possess about 95% of the total organic matter found in all sedimentary rocks making them the potential source rocks for both conventional and unconventional reservoirs. Shales can be classified on the basis of environment of clast deposition (terrestrial lacustrine or marine), type of retained organic matter which makes them oil or gas prone as well as the amount of silt and clay they possess. Terrestrial depositional environments usually produce coals mainly while lacustrine and marine environments save sapropelic organic matter from oxidation due to very oxygen deficient, very low energy levels at the interface of brackish water and sediments (Sam Boggs 2006). Shales especially marine are laterally extensive and show great deal of heterogeneity in organic richness as a consequence of changes in water level, geological conditions and organic matter supply (Passey et al. 2010).

Hutton Adrian C. (1987, 1994) developed oil shales classification based on petrographic terms from coal terminology. Hutton classification designates oil shales as terrestrial, lacustrine (lake-bottom-deposited), or marine (ocean bottom-deposited), based on the environment of the initial biomass deposition. Hutton's classification scheme has proven useful in estimating the yield and

composition of the extracted oil and gas. The organic matter found in these shales is transformed into kerogen as a consequence of progressive burial under overburden, gradual increase in temperature and pressure over geological time span. Sam Boggs (2006) divides the sedimentary organic matter (SOM) found in sedimentary rocks shales, into, humus, peat and sapropel. They are sourced by the remains of plants and organic matter which accumulate and deposit in soils, lakes, lagoons, and marine basins. The sapropelic organic matter belongs to remains of phytoplankton (algae), zooplankton (foraminifers) spores and pollens from higher plants and is the major contributor in the oil and gas generation (Boggs 2006). Ultimately the residual organic matter prior to oxidation and preserved in the sediments is converted into kerogen. The source rock found with reasonable amount of kerogen in preliminary exploration phase undergoes through strict selection criteria before identification as a potential shale gas reservoir and selection procedure is described in the next topic.

1.6 Selection Criteria for Potential Shale Gas Reservoirs

The selection criteria for shale gas reservoir base on the values of geochemical and petrophysical variables generated using geological, geochemical, geomechanical and petrophysical analytical techniques. The fundamental prerequisite to become a potential petroleum source rock or unconventional shale gas reservoir, shales must possess a certain amount of mature organic matter, commonly known as Total Organic Carbon (TOC % wt.). Without certain amount of TOC wt.% and its transformation level into oil and gas even organically rich shale cannot become the favourite candidate to be investigated further for gas in place assessment. Once the organically rich and mature intervals of shales have been identified, they will be scrutinized for the mineralogical character to evaluate free porosity, adsorption and desorption characteristics and geomechanical character for fraccing operations to generate artificial permeability. Potential shale gas reservoirs are extremely heterogeneous in rock character, have multiple hydrocarbons storage mechanism which requires a number of scientific methods and skills for their characterization as potential reservoirs and later to produce commercially. All world active petroleum plays have source rocks, the essential part of a petroleum system, so discovery of a shale gas reservoir is not impossible. The special challenge lies in production of commercial quantities from source rock using traditional methods to justify cost. Mitchell Energy took seventeen years to develop a successful technique to produce natural gas commercially from the Barnett shales (Sondergeld 2010). After the calibration of the seismic data with well logs data from appraisal well, a number of techniques and methods are used to extensively investigate prospective shale mineralogy, reactive organic carbon and organic matter maturity level, porosity, permeability and fraccability as given in the table 1.5.

Table 1.5: Source rock identification and petrophysical variables evaluation techniques for shale gas reservoir characterization

Variable/Reservoir Property	Evaluation Source (Technique/Method Applied)
Shale Interval Identification	SP (Self-Potential), GR (Gamma Ray), Shallow and Deep Resistivity, Density, Neutron and Sonic Logs
Thickness & Lateral Extension	SP (Self-Potential), GR (Gamma Ray) and Correlation of Logs data between wells and seismic data
Vitrinite Reflectance (Maturity)	Fast and inexpensive technique to determine maturity of source rock and coals macerals, based on amount of reflected light from oil immersed, Vitrinite maceral surface, VR_0 measured as %.
Rock / Mineral Composition	QEMSCAN (Quantitative Evaluation of Minerals, using Scanning Electron Microscopy), XRD (X-Ray Diffraction Method), EDS/SEM (Energy Dispersive Spectroscopy and Scanning Electron Microscope), FTIR (Fourier Transform Infrared spectroscopy),
TOC wt.% (Total Organic Carbon)	Rock Evaluation Pyrolysis Method, and Leco CR 412 for TOC Wt.%. Fast and inexpensive source rock maturity and kerogen type classification techniques
Free and Adsorbed Gas Content	Canister Desorption and Langmuir Isotherm
Porosity	Helium Porosimetry, MICP (Mercury Injection Capillary Pressure), NMR (Nuclear Magnetic Resonance) and Density, Neutron and Sonic Logs, SAN and USAN (Small Angle Neutron Scattering and Ultra Small Angle Neutron Scattering)
Water Saturation	SP (Self-Potential), GR (Gamma Ray), Shallow and Deep Resistivity, Density, Neutron and Sonic Logs, Dean Stark and Retort Method
Pore Size Classification	MICP and FIB/SEM(Focused Ion Beam Milling and Scanning Electron Microscopy) STEM (Scanning Transmission Electron Microscopy),
3D-Volumetric Modelling	FIB/SEM – Sectioning and Imaging Techniques

Three phases, A B and C are followed and investigated strictly in the same order as given in table 1.5 before making a decision about fate of a shale play. Phase A, deals with source rock identification. It also deals with its lateral extension and vertical thickness giving some assessment about the total volume of the source rock in the prospective play. The later judgment will lead ultimately to closer observation about type, amount and its maturity level to make a prediction about the total hydrocarbon generation potential. whether it is retained or migrated into porous reservoirs in the play. Based on satisfactory estimation about the volume of source rock, organic matter type and maturity, the next phase B deals with the petrophysical evaluation of the potential source rock based on type and amount of minerals, porosity and pores size classification, permeability and flow mechanism during production phase. While in the last phase C we largely deals with the field development planning, fraccing planning and number of wells per acre based on data from some appraisal wells as given in table 1.6.

Table 1.6: Reservoir characterization of potential source rocks phases (Deshpande 2010, Shaw et al. 2006, and Sondergeld et al. 2010)

Properties for source rock identification Phase A
1. Source rock bulk volume 2. Type of source rock – marine, lacustrine and terrestrial 3. Organic matter – type of kerogen I, II, III or IV 4. Amount of organic matter – TOC wt.% 5. Maturation level – level of organic matter conversion into petroleum/hydrocarbons 6. Hydrocarbon generation potential – hydrocarbons generated / ton of source rock 7. Hydrocarbons retained or migrated to conventional reservoirs
Properties for potential shale gas reservoir identification Phase B
1. Type of minerals 2. Amount of minerals 3. Lamination/parallel layering and bedding – shaly or non-shaly siltstones/mudstones/claystone 4. Pores classification, density and interconnectivity 5. Natural fracture system and interconnectivity 6. Total compressed gas content 7. Total adsorbed gas content 8. Gas type - biogenic and thermogenic 9. Permeability – vertical and horizontal 10. Initial reservoir pressure 11. Initial reservoir temperature
Production Strategy and Planning Phase C
1. Well locations & no. of well /acre. 2. Initial permeability – mD, µD, and nD (milli Darcy, micro Darcy and nano-Darcy) 3. Horizontal drilling techniques planning 4. Multilateral horizontal drilling strategy & program 5. Fraccability, & stimulation completion requirements

Before describing the role of the diagenesis in conversion of the organic matter into kerogen in next few paragraphs a flow chart has been given in figure 1.7 below. This figure shows all the sequential steps taken to reach a potential shale reservoir and finally decide and plan a strategy for its development and production.

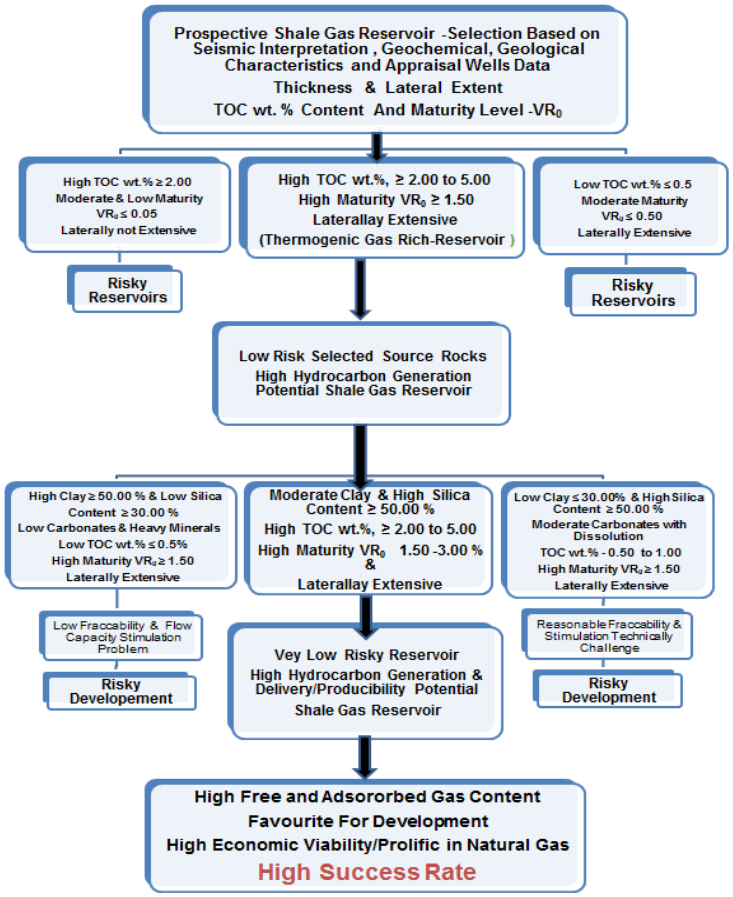

Figure 1.7: Shale gas reservoir selection criteria based on geological, geochemical and mineralogical characteristics

Kerogen is an organic geochemistry term which defines the organic matter found in organic sedimentary rocks and could be separated from these sediments using hydrochloric acid or hydrofluoric acid (Durand 1980; Hutton et al 1994, Hunt 1996). Kerogen is a mixture of many organic compounds with massive molecular weight (insoluble in organic solvents) and bitumen (soluble in organic solvents) and has complex formulas. This complex organic compound, product of diagenesis of the deposited organic matter has low density, high sonic velocity, neutron porosity and resistivity. Due to these physical properties it is important to estimate kerogen content in weight and volume both and their impact on the petrophyiscal evaluation of the formation (Colin and Paul 2007; Glorioso and Rattia 2012).

Kerogen classification is very important for number of reasons and special laboratory technique have been designed called Rock-Evaluation Pyrolysis, to have some idea about likely amount and type of hydrocarbons (oil and gas) generated after transformation of organic matter in source rock into kerogen. A known amount of crushed source rock is burned in oxygen free chamber/oven in Rock Evaluation Pyrolysis experimental apparatus/system to generate hydrocarbons to be used for geochemical data. During heating process the free hydrocarbons and kerogen is converted into hydrocarbon vapours. These vapours are split into two separate streams and are passed to flame ionization detector in the system The ionization of hydrocarbons in this step of experiment

generates voltage which is used to calibrate the amount/mass of hydrocarbons present in the source sample (Espitalie et al, 1977) and the output of this technique is illustrated figure 1.8.

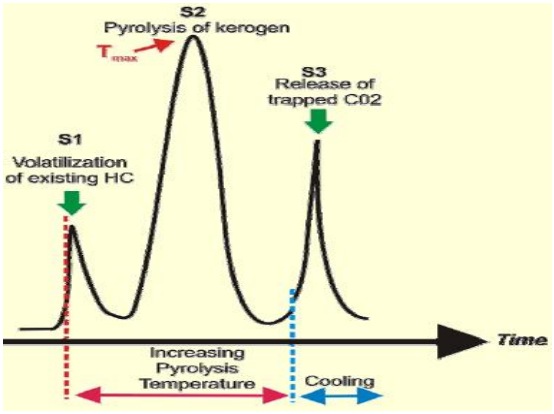

Figure 1.8: Graphical expression of Rock Evaluation Pyrolysis output, denoted by S_1, S_2 and S_3 peaks and temperature used in the kerogen classification, TOC (Wt.%) and source rock hydrocarbon generation potential (Espitalei 1977).

The data is used to identify kerogen type, TOC %wt. for grading of source rock into poor (0.50 - 1.00 % wt.%), fair (1.00-2.00 wt.%), good (2.00 -5.00 wt.%), very good and excellent (> 5.00 Wt.%), as well as type of hydrocarbons generated (Kevin McCarthy 2011). The results can also predict the kerogen metamorphism/maturity level, achieved known as diagenesis (Immature), metagenesis (mature) and catagenesis (postmature) (Peters and Cassa 1994). Van Krevelen (Van Krevelen 1961) diagram assigns kerogen types, using ratios between hydrogen and oxygen organic matter predicted from Rock Evaluation Pyrolysis technique, contained in potential shales, to predict the type of hydrocarbons generation potential. The immature stage represents kerogen not ready for conversion into oil and gas, mature prone to generate while over mature stage, indicates the most of oil cracking into dry gas. Based on Rock-Evaluation Pyrolysis results, data can be plotted to classify organic matter into four kerogens as shown in table 1.7 (Hunt 1996, Colin and Paul 2007, Killops and Vanessa 2009; Passey et al., 2010, Glorioso and Rattia 2012) as a source of gas and oil contained in source rock formations.

Table 1.7: Type of kerogens representing source of various hydrocarbons

Kerogen type	Organic matter source	Organic matter depositional environment	Likely hydrocarbons (Oil and Gas) generated
Type I	Algal and Amorphous Botryococcus type - ball like algal remains and resin bodies equivalent to alginite A and liptinite group of macerals	Highly anoxic/oxygen deficient lacustrine shallow marine lagoonal environment	Liquid Hydrocarbons (mainly Oil)
Type IIa	Marine Plankton and Fibrous /filamental algae called alginite B or Lamalginite group of macerals	Marine and lacustrine subtidal and supratidal anoxic/Oxygen deficient environments	Oil and gas prone organic matter
Type IIb	Plant spores and pollens – all other liptinite group of macerals, most abundant source of oil in shale source rocks		
Type III	Woody and Humic Vitrinite group of macerals	Brackish water swamps mainly	Gas and Coal, may yield oil as well
Type IV	Cannot Generate liquid and gas hydrocarbons Inertinite group of macerals	Oxic swampy and oxic marine environments	Only Coal with little amount of gas

The four kerogens as a consequence of evolution toward production of gas and hydrocarbons are shown in figure 1.9 below, with calibration to vitrinite reflectance and thermal alteration index. By knowing hydrogen and oxygen indices from Rock Evaluation pyrolysis, optical properties vitrinite reflectance and thermal alteration index, some predictions can be made about the maturity of organic matter and likely hydrocarbon products from this diagram called Van Krevelen Diagram in figure 1.9.

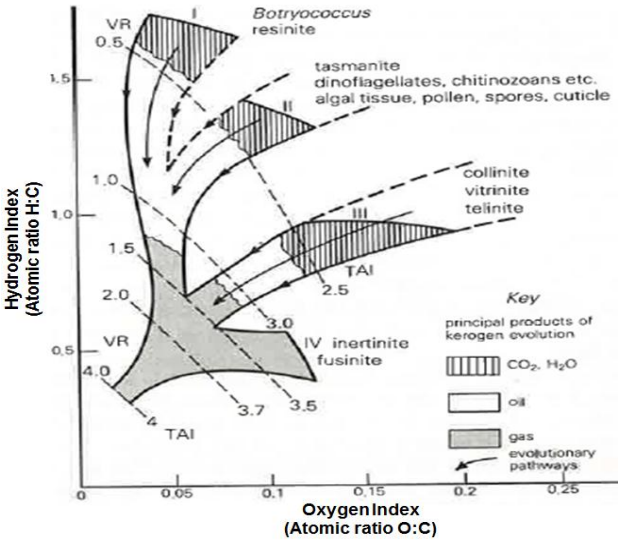

Figure 1.9: Four kerogen types (I, II III and IV) evolution paths with correlating values of Vitrinite reflectance (VR) and Thermal alteration index (TAI) (F. K. North 1985).

The geochemical data generated using Rock Evaluation Pyrolysis is correlated with other direct optical methods like thermal alteration index (colour of the organic matter gradually changing with increase in temperature and pressure – originally yellow, then orange, brown black and black sequentially), with some additional information from vitrinite reflectance (amount (%) of reflected light from organic matter surface) to further validate accuracy and authenticity of outcome from Rock Evaluation Pyrolysis techniques as given in figure 1.10.

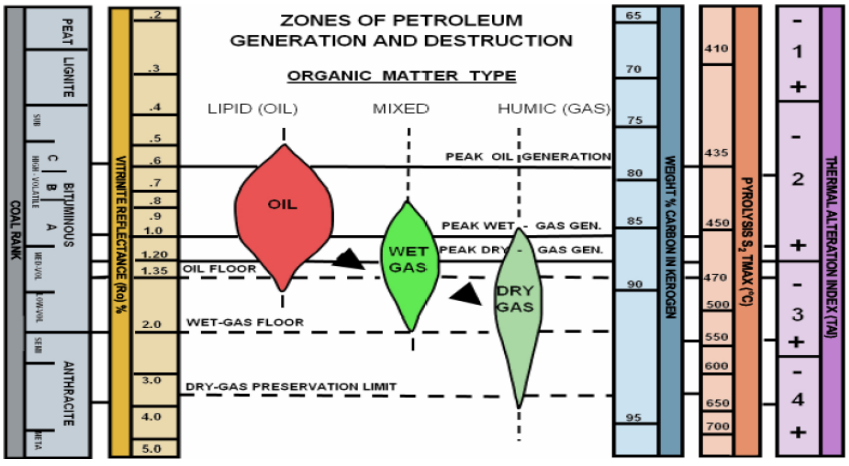

Figure 1.10: Schematic illustrating use of coal rank, vitrinite reflectance, Rock Evaluation Pyrolysis (Temperature (T_{max}) TOC wt.%) and accompanied changes in colour of organic matter used to predict source rock richness, maturity and hydrocarbons generation potential (Talukdar 2010).

TOC wt.%, its type, amount and maturity level, total reservoir volume, depth, temperature, pressure, porosity and mineralogical composition are key parameters required in a shale gas reservoir characterization (Passey et al. 2010). TOC (wt.%). Type and total organic carbon content, its maturity and shale reservoir volume dictate the hydrocarbon generation potential of any prospective shale gas reservoirs. The inorganic minerals volume and type of minerals like quartz, carbonates, clays and any other heavy mineral will have impact on free porosity, pores interconnectivity and on deliverability during field production phase of any shale gas play. It has been found that reservoir temperature, pressure and depth can influence relative adsorbed and compressed gas fraction in the shale formations. Therefore petrophysical characteristics of source shale rocks and reservoirs rocks vary a large from each other when they are evaluated as natural gas reservoir.

The constituent micron and submicron size inorganic clast and sedimentary organic matter found in shales and deposited in a lake or marine depositional environment undergo parallel changes like compaction, cementation, diagenesis, loss of water and porosity under sediments overburden and gradual increase in pressure and temperature. These chemical and physical changes in minerals and organic matter found in shales are different from the changes which sediments in sandstones and carbonates reservoirs suffer from after deposition. As a consequence shale gas reservoirs develop multiphase natural gas storage mechanism, complex porous system and flow networks which are far different in their nature and whose evaluation requires different standards and methodology, making shale gas reservoir characterization a very expensive and time consuming venture. Due to negligible content of organics, heavy minerals and comparatively low volumes of clays, porosity evaluation in conventional reservoirs is easier, compared to over mature shale gas formations. Texture, grain size and grain size distribution, pore size, type and distribution can readily be evaluated using conventional methods and prevalent standards in commercial service laboratories for sandstones and carbonates reservoirs. The grain size and pore size and interconnectivity are much higher than shale formations. While in shale gas reservoirs total pore volume, pores size and shape, their distribution, and interconnectivity all depend on type and amount of inorganic matrix and organic matter, level of post depositional diagenesis and conversion of organic matter into oil and gas leaving behind bitumen and pyrobitumen. Primary and secondary free porosity in a shale gas reservoir is a result of complex physical and chemical interaction among the constituent clasts before and after the deposition in marine, lacustrine and fluviodeltic environments. Passey et al.(2010) have mentioned the major factors controlling retained primary porosity and secondary porosity as the consequence of the post depositional changes in the organic and inorganic content of a shale interval as follow:

1. Kerogen (TOC wt.%)
2. Kerogen maturity level
3. Silica/Quartz
4. Carbonates: calcite, dolomite and siderite
5. Clays : Illite, Koalinite and Chlorite

These organic and inorganic constituents play a key role in the amount of free versus adsorbed gas. Clays, carbonates, silica/quartz, heavy minerals and mature/overmature organic matter affect total free porosity regardless of their origin in the reservoir. The range of these pore sizes vary considerably, from nanoscale to macroscale, depending on the type of minerals and their origin. Pores in kerogen mass have secondary origin, and can adsorb large quantities of gas. Pores related to quartz are of two types, detrital quartz transported with other clast, contribute to free porosity, post-depositional biogenic quartz tends to decrease the primary free porosity in the formation. Carbonates in shale are of authigenic origin. Siderite, ankerite dolomite and calcite are common form of carbonates in shale formations. Siderite, iron carbonate helps in the hydraulic fraccing operations while dolomite on diagenesis will lead to increase the secondary porosity as well as secondary permeability as a consequence of carbonate dissolution (Schieber 2010). Porosity related to detrital clays content contributes to the free porosity. Role of clays in a shale gas reservoir is different from the role in conventional reservoirs. They are essential part of the source rocks acting as reservoir rocks and primary porosity is preserved in their morphological structure during deposition among the hard inorganic matter in the shales. Also clays provide sites for adsorption (Barker C. 1972; Hartman et al. 2008) after the saturation of organic matter with adsorbed gas. The distribution style of the clays in shales reservoir does not matter much as it has a role in affecting the total porosity and permeability of conventional reservoirs (Peters E.J. 2007). The estimation of porosity is difficult using any available technique due to intrinsic heterogeneous character, laterally and vertically in a shale gas formation.

Techniques used to determine effective and total porosity helium porosimetry, mercury injection capillary pressure techniques, wireline logging, liquid and gas pyknometry are indirect methods. Radiation techniques like nuclear magnetic resonance, focused ion beam milling and scanning electron microscopy, micro and nano computerized tomography SANS and USAN are also in use especially in shale gas reservoirs. All these standard techniques have their merits and demerits, advantages and disadvantages when applied in conventional and unconventional reservoirs. The shale gas reservoirs give rise to more doubts and uncertainties, when these evaluation tools are applied for porosity measurement without required modification suitable for shale gas formations. These concerns are consequence of very complex micro fabric nature and lateral and vertical anisotropy and heterogeneity in prospective shale gas reservoirs.

Porosity in a reservoir is shared by brine, oil and gas. Overmature organic shale formations do not have oil, so the total void space comprise intergranular pores and natural fractures is occupied by two fluids, brine and gas. The free compressed gas is held in interstitial pores or fractures/fissures or vugs, and adsorbed gas onto clay minerals and kerogen, acting as adsorbents. The total gas in place is the fraction of the total void space, occupied by free compressed gas and adsorbed gas on the kerogen, organic matter and adsorbent clay content minus the brine saturation. To determine the total gas in place, a number of techniques have been employed by researchers. To evaluate the fraction of adsorbed gas and free gas content two separate techniques are

recommended in shale gas reservoir. All the voids/pores in a porous medium are seldom connected altogether, and the state of connectivity leads to definitions of effective and total porosity in a reservoir rock. The total volume occupied by pores whether they are connected or not, is known as total porosity, while the fraction of this total pore volume interconnected and which can communicate fluids is called effective porosity of a formation. These total and effective porosity definitions and concepts work well in conventional petroleum reservoirs. When porosity term is applied in shale gas reservoirs, in the context of storage capacity of a rock, it is required to add the fraction of the adsorbed gas on clays and organic matter into the total porosity/storage capacity, whether these adsorbent are interconnected or not. Based on the amount of liquid fluids, brine, oil and gas fractions, a number of empirical definitions of effective and total porosities have been derived for conventional reservoirs as shown in the figure 1.11. These concepts of porosity, total and effective, and rock characteristics are much complicated in shale gas reservoirs than conventional sandstones and carbonates reservoirs as given in figure 1.12 on next page.

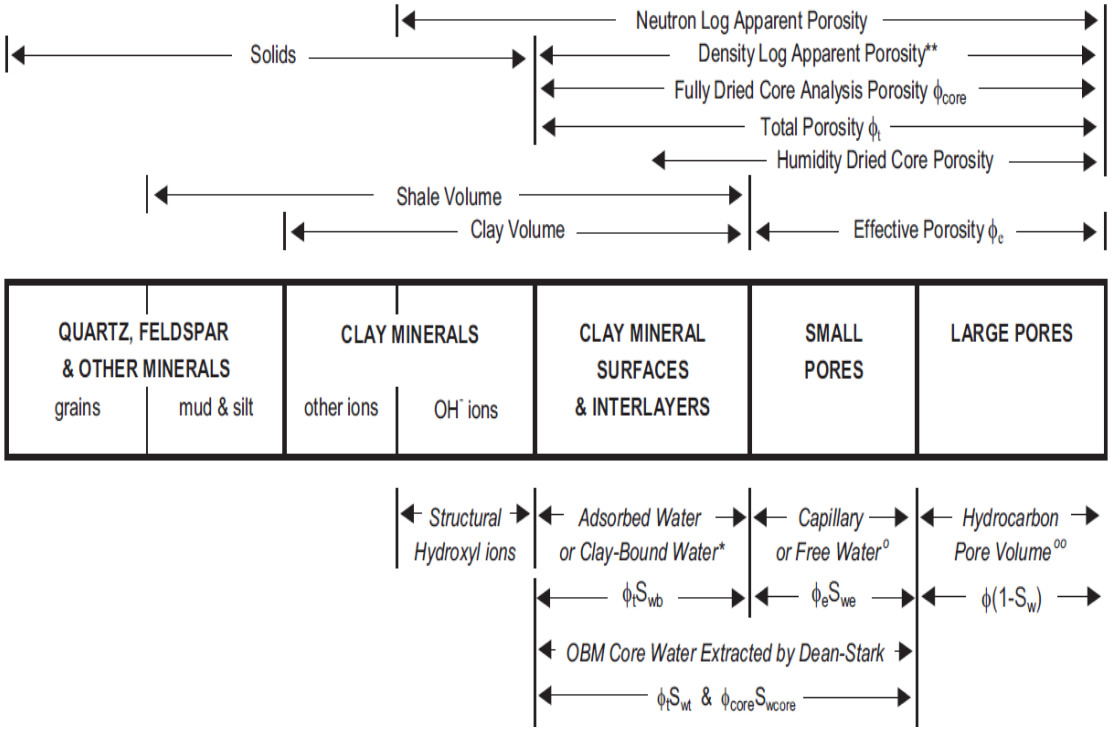

Figure 1.11: Schematic showing total effective and core porosity and their associated water saturations in shaly sands (adopted from Core Laboratories 2011)

Key:

**Density log apparent porosity using the grain density of the dried core and correct invaded-zone fluid density.

*Smectite clays have a large capacity to adsorb water, whereas most other clay minerals have little or no adsorbed (or bound) water.

°°This model has no mobile water, and the model will produce water-free hydrocarbons during its initial production phase.

°As height above the hydrocarbon –water contact increases, capillary water volume decreases and hydrocarbons displace capillary water. Humidity dried core analysis porosity is shown as including some of the clay bound water (Box sizes are schematic and arbitrary)

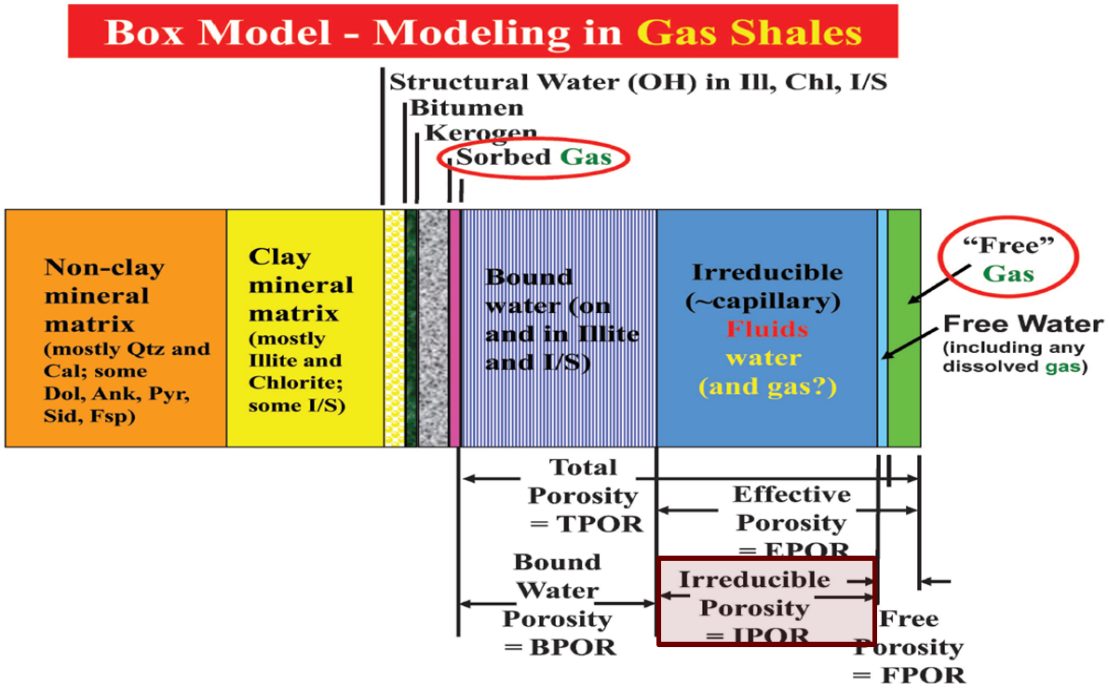

FIGURE 1.12: Box model used for modelling components of gas shales (with modification from Hill et al., 1979; Kanckstedt et al., 2010; Passet et al., 2010; Eslinger and Evertt 2012; Quihein et al., 2013); where; **Ill** = illite; **Chl** = chlorite; **I/S** = illite/smectite; **Qtz** = quartz; **Dol** = dolomite; **Cal** = calcite; **Ank** = ankerite; **Pyr** = pyrite; **Sid** = siderite; **Fsp** = feldspar; **OH** = hydroxyl groups, **IPOR** (Irreducible Porosity, shaded rectangle)= capillary bound water, and kerogen microporosity.

It is found that qualitative and quantitative results after evaluation of shale rocks do not corroborate each other received from different service providers for same shale gas reservoir. Measurement of total porosity and water saturation are not free of uncertainty and lack in consistency with serious suspicions, if applied to determine the initial gas in place in a reservoir. Traditional procedures like helium porosimetry and mercury injection capillary pressure techniques can be tried to ascertain the effective porosity and pores throat size distribution but due to very low effective porosity and permeability, these techniques do not work well. Therefore, to select the proper technique for effective, total porosity evaluation in these ultra-fine grained source rocks, pore network systems must be probed using FIB/SEM, Micro and Nano Computerised Tomographic techniques. When Argon ion milled samples are scanned at very high resolution and magnification, a much better image and insight about interconnectivity of the pore throats connecting micro, meso and macro pores emerges. The observation and understanding of pore network can help in both storage mechanism and flow paths during production, and later to plan a better production strategy using desired techniques.

All the salient geological and geochemical features of Roseneath and Murteree shales making them most promising unconventional gas reservoirs are given below and a description of selection of appropriate methodology for visual and loge derived porosity as well.

1.7 Roseneath and Murteree shale Geological and Geochemical Characteristics

Nappmerrie Trough hosting overmature, overpressure carbonaceous Roseneath and Murteree shale is the most extensive trough comprising 15,000 km^2 and having more than 10, 000 ft. depth in the centre, is focus of attention as a richest shale gas play in Cooper Basin. Widely spreading across Cooper Basin, Murteree formation has an average 50 m thick, while achieving maximum thickness of 80 m in Nappamerri Trough. Roseneath shale is not widely spread as Murteree shale, and has an average thickness of 37 m and maximum thickness of 100m in Nappamerrie Trough. The organic matter or kerogen is type II, and not type III, and amount of TOC Wt. % also varies all over Cooper Basin, ranging from 1.00 to 5 00 % as reported in the latest geochemical analysis prepared for these two formations (PIRSA1972, PIRSA 1982, PIRSA2011). Similarly maturity level expressed by vitrinite reflectance shows a range of maturity in both shale formations across Cooper Basin, VR_0 1.00 – to – 3.00%, indicating thermogenic gas presence. The geothermal gradient in Nappamerrie trough is highest compared to other neighbouring troughs like Tenappera, Araburry and Patchawarra due to radioactive granite basement, making the Roseneath and Murteree shale overmature. Nappamerrie Trough at depth of 9000 ft. has temperature 300 °F and thermal gradient of 3.42 °F/100 ft. (PIRSA1972, PIRSA 1982, PIRSA2011). The geological and geochemical properties of this shale in brief are given in figure 1.13.

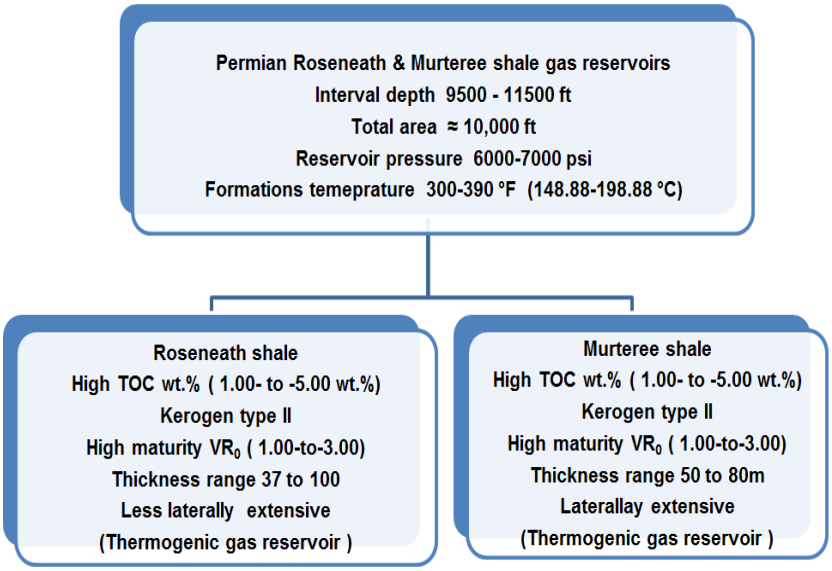

Figure 1.13: Geological and geochemical properties of Murteree and Roseneath shales

1.8 Methodology

As a consequence of ultra-complex microfabric conversion into number of authigenic minerals and transformation of organic matter into hydrocarbon fluids, creating vertical and lateral heterogeneity, more often unconventional shale gas reservoirs require an integrated conventional and unconventional reservoir characterization approach. Fluids injection techniques are readily

available in conventional petroleum laboratories with some doubts about accuracy of evaluated variables. Radiation techniques are able to scan shales at nanoscale level. These techniques are very time consuming, expensive and the results have some valid concerns and issues when applied on reservoir scale and make a decision to continue with the ongoing evaluation process before development of any shale gas play. Therefore, we have made a selection of suitable methods and techniques based on understanding about the mineralogy and petrophysical properties of Roseneath and Murteree shales which play a key role in the assessment of initial gas of a play. A brief description is given below.

Core samples of Murteree and Roseneath shales were used for QEMSCAN, XR-Diffraction, Micro and Nano CT-Scanning, FIB/SEM, Helium Porosimetry, Mercury Injection Capillary Pressure (MICP) techniques, liquid pyknometry and wireline log data. The objective was to investigate total and effective porosity, mineralogy and rock characterization, pore size identification and classification, water saturation. Murteree core sample was divided into 7 parts before all these aforementioned analyses and techniques were applied before analyses as shown in figure 1.14 and a short description of each experimental phase is given in the following pages.

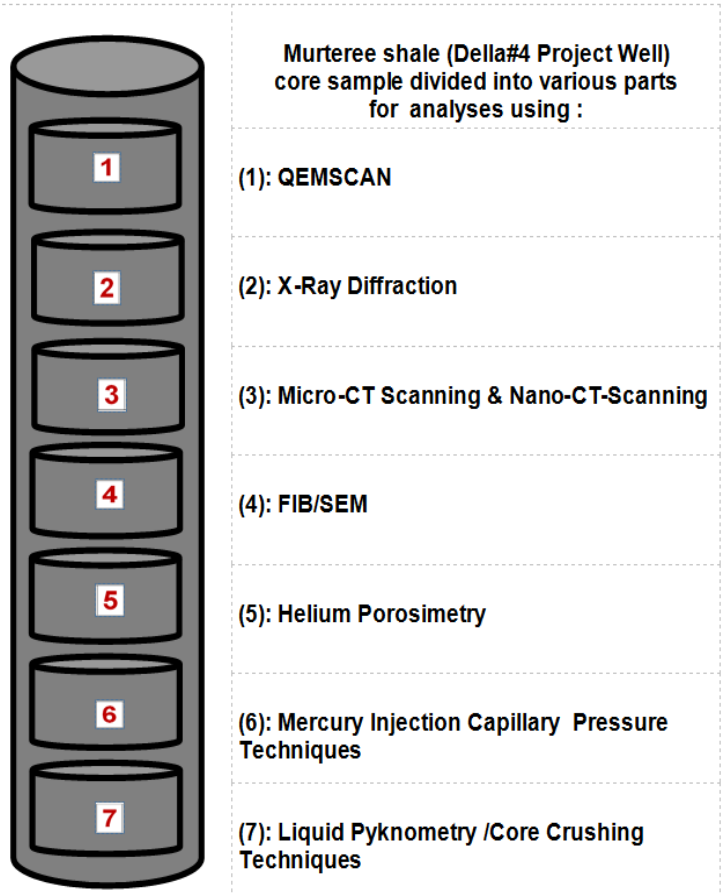

Figure 1.14: Murteree shale- core sample divided into various parts for (1) QEMSCAN, (2) Micro-CT Scanning and (3) Nano CT-Scanning, (4) FIB/SEM, (5) Helium Porosimetry, (6) MICP and (7) Liquid Pyknometry experimental work.

1.8.1 QEMSCAN, XRD, Micro and Nano CT-Scanning, FIB/SEM

High energy electron beam from electron gun in a QEMSCAN system is focused on sample surface. The high speed and energy electron eliminates an electron from inner energy shells like K and L in a targeted atom of an element creating empty space or a hole in the targeted shell. After the ejection of electron from K or L, an electron from higher energy shell drops in the hole and the difference of energy in the two shells is emitted as a characteristic x-rays. These x-rays have characteristics energy and wavelength for atom of that element from which they are emitted and are detected by a number of Energy Dispersive X-ray Spectrometers (EXDS). Calcium(Ca), magnesium(Mg) and iron(Fe) for example, all have characteristic x-rays, emitted when their atoms are irradiated for their identification and quantification. The interaction of high energy focused beam of electron to eject electron and filling the hole by dropping an electron with a release of particular x-ray having certain amount of energy and wavelength makes the basis of QEMSCAN automated mineralogy system. The EDS in system are governed by the Plank's and Duane – Hunt equations as given below, to identify the elements found in the sample and later grading into rock types. Plank's (1901) Equation:

$E = hv$

where, h (Joules)= Planks Constant, 6.6260×10^{-34}

v = Frequency in cyles/second, Hertz

Electromagnetic Radiation, $v = c/\lambda$

where c = speed of light (2.99782×10^{8} metre/second) and λ = wavelength (meter)

and substition yields, $E = hc/\lambda$;

Conversion of λ to nanometer ($1 \text{ meter} = 10^{-9}$)

Energy, into electronvolts ($1 \text{ eV} = 1.6021 \times 10^{-19}$ Joules)

Duane- Hunt Equation (1913):

$$E = \frac{\left(6.6260 \times 10^{-34}\right) \times \left(2.99782 \times 10^{8}\right)}{\lambda}$$

$$E = \frac{1239.84}{\lambda} \qquad \text{where } \lambda, \text{ is in nanometers and E, energy is in electron volts} \ldots\ldots (1.1)$$

Once we know the energy of the x-ray or its wavelength as expressed in the above equation (1.1), we can identify, quantify elements in the scanned sample. This information can be applied later for mineral identification, quantification as well as into certain rock type. The resin coated on sample surface is separated by backscattered electron signal detector from the rock sample, after that grains and particles mapping begins pixel by pixel with an arbitrary resolution set by QEMSCAN operator for analysis. This process is very fast and each pixel takes less than 1µs reaching a speed of 1 million pixels per hour (Sliwinski 2010).

In XRD techniques, x-ray diffraction pattern produced by diffracted x-rays from amorphous or crystalline rock sample is unique and serves as fingerprint for analysed samples. In samples under investigation the constituent atoms can be arranged randomly or in a regular pattern. The diffracted rays are measured based on intensity of the photons and angle at which they are

diffracted. The angle measures the distance between discrete crystallographic planes in sample which is function of the geometry of the sample grain size orientation and can have strong effect on the measurement. Therefore powder samples are recommended. The intensity of the peak estimated in photons under the peaks indicates the quantity of minerals. QEMSCAN and XRD can perform quantitative analyses for rock analyses. We need powder or pulverized sample form for XRD while QEMSCAN is able to scan solid rock samples qualitatively and quantitatively for mineralogical analyses at much higher speed. In the latter we retain the natural texture and lithology of the rock samples and results can be correlated with 2D images taken using SEM for further verification of grains morphology, contact and pore size classification at much higher resolution and magnification (Sliwinski 2010).

Microfocus and Nanofocus X-ray CT (Computed Tomography) is a non-destructive radiation technique. It is used for imaging and visualizing desired features of objects and obtaining digital information on their 3-D geometries, properties and interior details. A CT image of a certain thickness of the object scanned is called a slice. A typical digital image captured using X-rays is composed of pixels (picture elements, having width and length only), while a CT slice, image is composed of voxels (volume element, having width, length and height). The attenuation of x-rays after transmission through the sample are represented by gray levels in CT slice reflecting the proportion of X-rays scattered or absorbed as they pass through each voxel. Attenuation is a function of X-ray energy applied, density and atomic number of sample being imaged. A CT image is created by directing X-rays through the sample plane from multiple orientations and directions –sample rotating at 360° (degrees) in front of a beam of x-rays as shown in figure 1.15 and resultant decrease in x-ray intensity is estimated on an X-ray detector screen. To reconstruct the distribution of X-ray attenuation (decrease) in the slice plane a special algorithm embedded in the X-ray system is applied. (Coenen et al. 2004; Diaz 2009). The attenuation coefficient passing through each point of 2D-XY slice is expressed by CT-Number, whose numerical value represents the density and the chemical composition of sample at that point. The focal spot diameter of x-ray source, detector resolution, distance between the focal spot and centre of object scanned are crucial parameters which are considered important to achieve desired resolution and information about scanned sample (Coenen et al. 2004; Long et al. 2009).

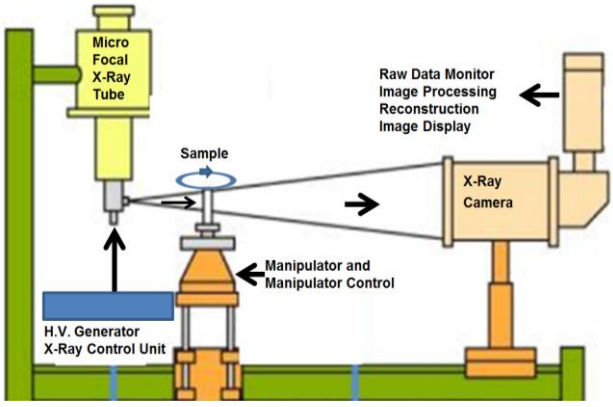

Figure 1.15: Schematic showing the principles of Micro X-ray Tomography (with modification from Coenen et al., 2004)

In the FIB/SEM dual microprobe, the sample is prepared using Argon ions or gallium ions from a focused ion beam (FIB) milling part of the system, and later electron beam from electron gun is applied to image the topography and other characteristics of the sample. These scattered electrons after colliding with atoms in sample, are of three types produced from various depth of irradiated sample. Each collected electron beam has its role in visual characterization of sample as they return back to the scanning electron microscope (Volkert and Minor, 2007). Two types of detectors, secondary electron beam detector and backscattered electron detector are of special interest in FIB/SEM probes. In order to image the topography at ultra-high level of magnification and resolution secondary electrons are useful. Magnification of SEM is simple enlargement of image and or part of image while resolution is the smallest separation achievable at which two points or objects in irradiated sample using SEM can be seen as distinct entities. Resolution depends on the wavelength, lens refractive index as well as numerical aperture (Wu and Aguilera 2012). Very small De Broglie wavelength of electrons beam helps FIB/SEM dual system in the identification of shale microfabric distinctly as given in the mathematical expression below;

$$d = \frac{\lambda}{2NA} \text{..... ....} (1.2)$$

Where:

d = Microscope resolution
λ= Wavelength of the electron beam
NA = Numerical aperture

The back scattered electrons are used to identify the different types of mineral phases based on density. While characteristic x-rays are used for the identification of elements in minerals in the samples as used in QEMSCAN technology. The sample is coated with carbon or gold to make it conductive for current before imaging the surface to have better quality images.

1.8.2 Helium Porosimetry

Helium porosimetry is valid technique and has been used for effective porosity evaluation in petroleum industry since very long time. Due to helium gas inert nature and very small molecular diameter—0.260 nanometres (Sondergeld et al, 2010b), it has capability to penetrate pores with very small pore openings/pores throat size, in the rock samples. This technique is reliable and insensitive to any chemical reactivity with mineralogy and possesses lowest adsorption trend on grain and pore surfaces, especially when dealing with organic matter and adsorbent clays in the carbonaceous shales sample. Issler and Katsube (1994) claimed that helium porosimetry values are more reflective of the total interconnected pore space (effective porosity) than values obtained by mercury porosimetry because of the molecular diameter difference between helium and mercury. But due to extremely low permeability and micro-porosity when applied to shale samples helium needs extra time to equilibrate in the porous media by diffusion. Neglecting to allocate sufficient time for total diffusion of helium gas molecules during such experimental work there is likelihood of generate higher grain volumes and lower effective porosities in shale samples. The equilibrium pressure recorded during these experiments allows the computer software to calculate

the porosity by applying Boyle's Law to calculate the grain volume, and subtracting it from the bulk volume to obtain the effective pore volume.

1.8.3 Mercury Injection Capillary Pressure (MICP) Techniques

Samples in MICP experimental work do not require very special and time consuming treatments. They are usually prepared using a diamond saw readily available in core laboratories. After a routine cleaning and drying session, these samples having a suitable size are loaded into a penetrometer, which is installed into the Micromeritics AutoPore-III Model, for effective porosity and pore throat size classification analysis. At low applied pressure, rock sample surface artefacts, imperfections and open surface pores are not saturated with the mercury surrounding in the sample holder because of the nonwetting nature of mercury. Later, on gradual increase in pressure leads the mercury to fill the open pores and artificial cracks on the sample's surface and mercury volume, which enters into these surface pores and cracks, is not counted into total mercury intrusion. This deduction from the total final mercury intrusion is called the conformance value (Vavra et al, 1992). The volume of intruded mercury , pressure applied at each successive increment and diameter recorded in Washburn equation are used for classification of the pore openings (pore throat size) leading to the pores and effective porosity in the sample.

1.8.4 Core Crushing Method/Liquid Pyknometry

Core crushing procedure to evaluate the grains volume reliably was applied by Luffel et al (1992) to investigate porosity core samples for various Eastern Devonian gas shales. They argued that all pores are connected in these carbonaceous shales but interconnecting connections were so small that even helium molecules will require substantial amount of time to equilibrate and reach all the interconnecting pore space, documenting the idea of possessing very low permeability. They tried to evaluate total pore volume and porosity using this technique, not the absolute total free porosity, which is porosity when water molecules are still adsorbed by the clays. Due to smectite-illite conversion, the amount of the adsorbed water by the illite is usually assumed very low and negligible in this case. Consequently, there is no loss of porosity when measuring total porosity in samples using the crushed sample in pyknometry method. In core crushing and liquid pyknometry experimental work core samples are cut, pulverised and ground first by using a mortar and pestle, and then by a vibrating grinder, to prepare a suitable amount of powder for tests. The powder is usually sieved using a 40 μm sieve. The microfabric of carbonaceous shale is less than 40 μm. Distilled water in the pyknometry method is used to find the most reliable volume of shale grains/matrix in the samples for the calculation of total interstitial free porosity.

1.8.5 Log Interpretation

Wireline log and core samples in project well Della004 were selected to estimate water saturation. Composite log of Della4 (PIRSA1972) was digitized to find caliper, gamma ray, sonic velocity, true resistivity and bulk density. These digitized values were used to estimate clay/shale volumes

and various types of total porosity. Focused ion beam milling and scanning electron microscopy (FIB/SEM) results/2D images were also used for mineralogical and petrophysical understanding, evaluation and correlation with results from QEMSCAN and XRD results of Murteree shale. Considering the ultra-complex nature of Mureteree and Roseneath shale formations and sensitivity of estimated water saturation on initial resources, we opted to use four resistivity models rather conductivity models and results were correlated to improve the understanding of water content in Murteree shale. Although we have not used any sample from Roseneath formation for water saturation estimation except FIB/SEM images, early Permian Roseneath and Murteree organic shales have similar lithological, mineralogical and geochemical characteristics as they were sourced from same provenance and were laid down in same type of depositional environment in Cooper Basin (Gravestock 1988).

In nutshell we largely relied on QEMSCAN, XRD for minerals, rock characterization and applied EDXS techniques for elemental maps during FIB/SEM applications for verification. Clay's content outcome in QEMSCAN and XRD was verified by Steiber formula as well using gamma ray log in Della4 project well. Pores types, their morphology, density and location in matrix, connectivity and microfracture systems were mainly investigated using FIB/SEM extensive work and Micro computerized tomography. Helium porosimetry and MICP conventional laboratory techniques to check the effective porosity and pores throat size in Murteree and Roseneath shale, while liquid pyknometry for total porosity. For water saturation wireline logs aided by FIB/SEM 2D images were used.

1.9 Study Area

Cores samples to evaluate Murteree and Roseneath shales mineralogical and petrophysical properties were obtained from Della4 and Moomba46. Murteree and Roseneath cores samples depths, range between 6,619.00–6,620.00ft., in Della4 and 8096.0–8097.6ft., in Moomba46 respectively and were received from PIRSA's (Primary Industries and Resources South Australia) core library in Adelaide South Australia. Della4 in PPL15 (Petroleum Production License 15) was drilled to evaluate the hydrocarbon potential and reserves of the Della Structure in the Della oil and gas field. Moomba46 in PPL8 (Petroleum Production License 8) was spudded in Moomba oil and gas field located at a distance of 9 km from the Moomba gas treatment plant, to evaluate and develop Daralingie and Toolachee formations for gas content. The location of the wells in research project area is given in table 1.8 with approximate location of wells are shown in figure 1.16 below.

Table 1.8: Project well names, location and sample depth in Nappamerrie Trough South Australian part of Cooper Basin

Well name & shale formation	Location and sample depth
(1): Della4 PPL-15 Murteree shale core sample	Latitude: 28° 11' 56" Longitude: 140° 39' 33" Depth (range) in Well: 6,619.0 – 6,620.0 ft.
(2): Moomba 46 PPL-8 Roseneath shale core sample	Latitude: 28° 11' 11.72" Longitude: 140° 10' 20.53" Depth(range) in Well: 8096.0–8097 6 ft.

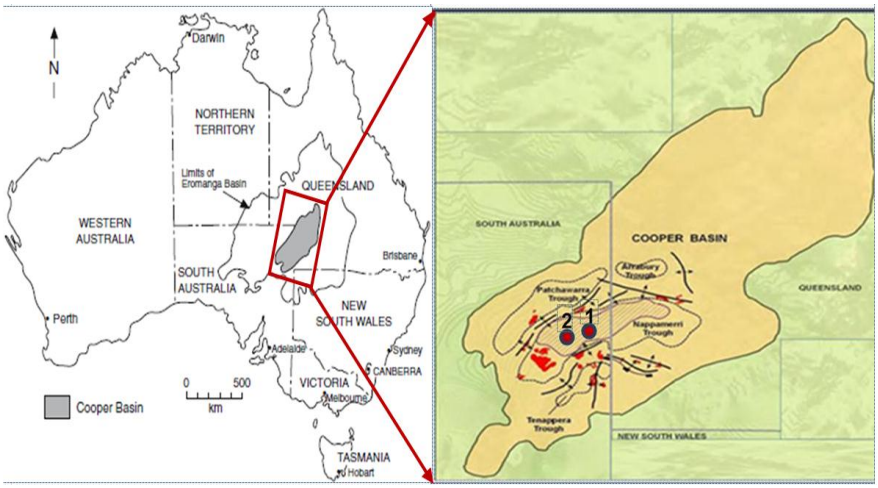

Figure 1.16: Study area location in Cooper Basin, South Australian (beachenergy.com.au)

Unconventional shale reservoirs could be part of conventional oil and gas plays or part of an incomplete petroleum system. In the latter case, there is no complete petroleum system and all the hydrocarbon charge is retained by the source rock. A schematic is given in figure 1.17.

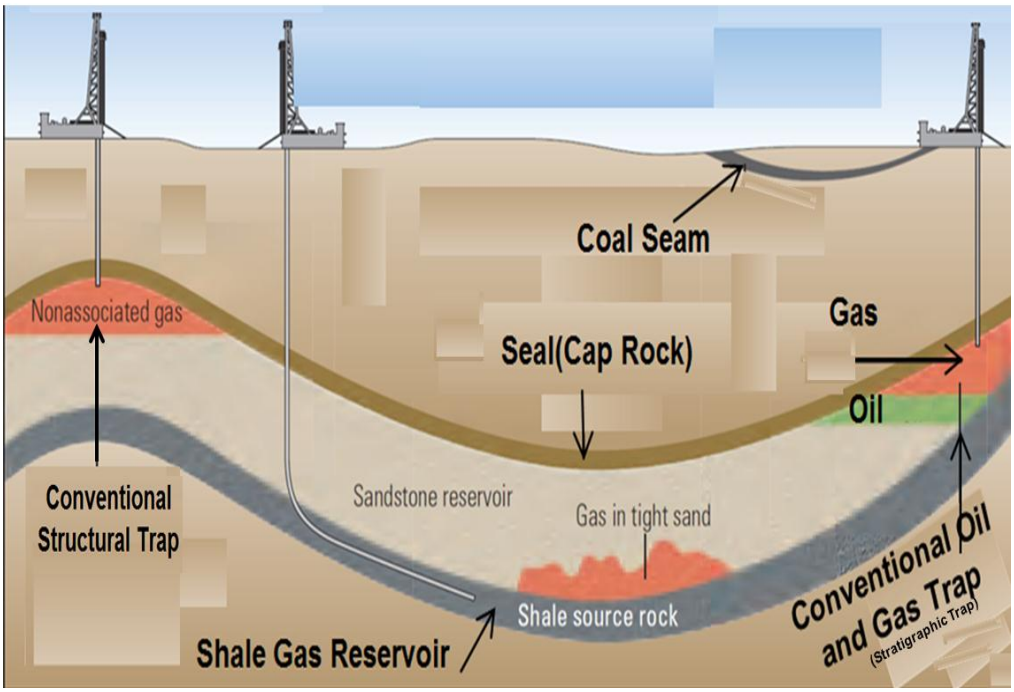

Figure 1.17: Schematic showing continuous hydrocarbon shale gas/source rock (shale gas reservoir), its relation to conventional oil and gas reservoirs in a petroleum system (with modification from Kevin McCarthy et. al., 2011)

1.10 Objectives

The objectives of proposed research methodology are to accurately and reliably build a datasets for reservoir characterization of gas shales, using recommended techniques and procedures. In the following parts of this chapter, the working of various convnentional and unconventional

techniques has been explained and their outcome has been correlated to make conclusive judgments about their application in shale gas reservoir characterisation.

Previous published research work was thoroughly reviewed to find and reach the current mineralogical and petrophysical understanding about these largely complex unconventional shale gas reservoirs. These gas reservoirs are still a challenge for both unconventional and conventional techniques. Conventional wireline logging had been tried and modified to achieve and make reliable assessment about the lithologies and petrophysical properties after correlation with results from cores. Core samples from representative shales in laboratories were investigated through fluids penetration methods to find out porosity and permeability we noted in previous published literature. Due to ultra-low permeability exposed during these methods, core samples were irradiated by X-rays to image and visualize nature of the microfabric and pores network to a nanoscale level almost stretching the limits of these tools. The previous published research work was thoroughly perused to improve understanding and find any analogy for mineralogical and rock characteristics of Roseneasth and Murteree shale gas formations.

Based on our extensive literature review and understanding about the used methodologies for research in these publications we have found that shale gas reservoir mineralogical and rock qualitative and quantitative evaluation level has been improved. Especially when logs are calibrated with core analyses data of same formation they can prove a source of help in formation evaluation. The outcome from QEMSCAN, XRD quantitative analysis is reliable as proved in this study. The issues raised about the modification of conventional wireline logs to identify source rocks in subsurface by Aguilera (1978) have been resolved by Fertl W.H. (1980), Passey et al. 1990 and Jacobi et al.,(2008).

Permeability and porosity assessments are most serious issues in petrophysical evaluation of shale gas reservoirs. The evaluation and assessment of permeability of Roseneath and Murteree shales is not in the scope of this research project. Porosity, both effective and total porosity, is part of this research work. It is found that effective porosity evaluation using helium porosimetry and mercury injection techniques is not worthy of application and consideration. Effective porosity and total porosity values from helium, mercury injections and pyknometry procedures are very doubtful when pores size and density in same samples are correlated with 2D images captured using FIB/SEM techniques.

We see there is plethora of information based on nanoscale 2D images taken using focused ion beam (FIB) milling for preparation of artefacts free surfaces of samples and imaging via SEM and TEM tools. The topography of these samples have been imaged by scanning electron microscope and pores throat size by transmission electron microscopy to enhance and improve judgement about pores types, pores morphology, fracture system and their interconnectivity. These 2D images later on have been used to build 3D volumetric shale gas reservoirs but have lost the

credibility due to their upscaling application on a reservoir level. An elaborate research and findings about porous nature of shale gas rocks have been done (Bustin et al. 2008, Loucks et al. 2009 and 2012, Wang et al. 2009, Rokosh et al. 2009, Schieber 2009, Curtis 2010, Passey et al. 2010, Milner et al 2010, Kale et al. 2010, Sondergeld et al. 2010, Houben et al. 2013, Fishman et al. 2012, Curtis et al. 2012, Milliken et al 2013 and Pearce et al. 2013) using SEM on mechanically polished as well as ion milled samples. These researchers have minutely imaged the shale 2D topography revealing details of the microfabric on nanoscale level. In some cases these 2D images were used for building 3D volumetric model to understand the connectivity of the micro pores and fractures system using BSE signals which are density and atomic number sensitive of scanned material (Sondergeld et al. 2010, Curtis et al 2010, Elgmati et al 2011, Curtis et al. 2012). The application of these details 3D models using FIB/SEM in shale plays still suffer from reluctance to be applied on reservoir scale.

Radiations techniques are able to recognize sillicates (authigenic and detrital silica and clays), heavy minerals (authigenic siderite and ankerite, pyrite, sphalerite, titanium and rutile), detailed properties of pores and organic matter spongy/porous morphology by SE signals with confidence. These observations made through the use of FIB/SEM/TEM on shale samples confirm presence of pores, high porosity concentration domains and fracture system. Also they reveal the distribution of various heavy minerals, their origin and the role in fraccability and help in selection of well completion site for better production which can be verified by correlation with results from XRD, QEMSCAN and other geochemical analytical techniques. Therefore, it has been overwhelmingly documented that organically mature and over mature source rocks have high isolated intergranular, intragranular porosity and intracrystalline porosity which cannot be assessed using inert helium molecules or using extremely high pressure non wetting mercury injection techniques. Identification of pores at nanoscale has contributed a lot in understanding microfabric porous nature of many shale gas formations, mostly marine in North America. These techniques also have helped us to understand and minutely examined Roseneath and Murteree shales.

Micro and nano computerized tomography (µ-CT and Nano-CT) is a non-destructive technique which have been largely employed with confidence in conventional sandstones, carbonates and shales reservoirs (Wellington and Vinegar 1987, Castanier and Reid, 1989, Lu et al. 1992, Duliu 1999, Ghous et al. 2008, Knackstedtt et al. 2010, Ketcham and Carlson 2001, Coenen et al.2004, Riepe et al. 2011, Gelb et al. 2011) to image pores morphology, connectivity and fracture system to have better understanding about the storage mechanism, flow paths and wettability of these systems. These tools have the power to reveal the fabric of the scanned materials without losing original arrangement and contact of grains, porosity and permeability to build 2D and 3D model. They work well for conventional reservoirs due to larger grain size, pore size, connectivity and fractures interconnectivity but when applied to image internal structure of shales they face problems like all other conventional tools. There are still number of issue with the use of

microtomography and nanotomography. X-Rays penetrating the shale fabric are sensitive to material density and atomic number. Gray scale threshold is used to identify various phases based on their density and atomic number which overlaps resulting in serious doubts about the integrity of identification of various clays, heavy minerals pores and organic matter. Also magnification and resolution powers FIB/SEM/TEM radiation systems enjoy is not achievable in both microtomography and nanotomography. We think there are some important characteristics of potential shale gas formations which have come across during literature review whose knowledge of existence can enhance understanding about the reason of very low effective porosity.

We found dolomitizartion of siderite to increase the occluded porosity in over mature Roseneath and Murteree shales, for example. The interaction between brine, clays, organic matter and methane has also been not investigated. The impact and interaction on water saturation has not been reported as post maturation micro porous system development has been ignored and overlooked during total porosity consideration in previous research work. These observations and issues are described in the following paragraphs under subheadings of microlamination, siderite dolomitizartion, brines, clays organic matter and methane interaction, and finally organic matter over maturation role in secondary fracture system development in shale gas reservoirs.

1.10.1 Microlamination

We found that pore types, size and morphology in a shale gas reservoir vary on a large scale, from micrometre to nanometre scales. Every selected potential shale reservoir will exhibit a unique porous and fracture system based on diagenetic level achieved by inorganic matrix and organic content laterally and vertically. The pore system in one shale play will thoroughly differed with other. These variable pore systems have been verified in previous study. We do not find the reasons mentioned in reviewed literature behind large inaccessible bound pore volumes in overmature source rocks when helium and MICP are applied to check effective porosity. We believe this critical property of source rock, microlamination has been overlooked and is the major cause of very low effective porosity when conventional helium porosimetry and even ultra-high pressure mercury injection techniques are used.

1.10.2 Siderite and Dolomitization

Siderite ($FeCO_3$ iron carbonate), can have number of impurity ions like Calcium(Ca), Manganese(Mn), Zinc(Zn) and Cobalt(Co) ions. When these ions are replaced by Magnesium ions, secondary porosity in the sporadic grains of siderite is developed which can increase occluded porosity which is not accessible through helium and Mercury injection techniques. This is a late diagenesis process in overmature source rocks. Siderite dolomitization role has not been mentioned in overmature source rocks. This secondary porosity not just improves fraccability but also increase total porosity to accommodate compressed gas. We found that contribution of

heavy minerals like siderite Iron carbonate Fe $Mg(CO3)_2$, ankerite (Fe Mg Mn (CO_3) in total porosity must be reassessed and included in reservoir evaluation phase.

1.10.3 Brine, Clays, Organic matter and Methane Interaction

Understanding of some post depositional changes in physical and chemical properties of mineralogy and organic matter are essential when formation evaluation of shale gas is done. These changes directly influence rock texture which plays a key role in porosity and permeability of the reservoir. For example generation of fresh and less saline brine during diagenesis of smectite, and chemical reactions between clays and organic matter will lower conductivity and increase resistivity making the use of second Archie equation option for water saturation calculation in shale reservoirs.

1.10.4 Organic Matter Over maturation and Graphitization

Biogenic methane gas generation starts after the deposition of the organic matter even before degradation of organic matter into kerogen which is the precursor of oil and gas in a source rock. There is sequential change in physical and chemical properties taking place in kerogen, and progressive irreversible chemical reactions due to gradual increase in temperature, pressure and overburden whose ultimate hydrocarbon product is methane, graphite and release of large quantities of nonhydrocarbon gases like CO_2 and H_2S. The generation of excessive amount of these gases will develop secondary porosity and secondary fracture system. At this stage of post-over maturation of source rock, most of the organic matter is in the form of graphite which is equivalent to anthracite along with large quantities of methane and carbon dioxide.

1.11 Research Problem Statement and Scope

A shale gas formation acting as a potential unconventional gas reservoir exhibits the most complex, heterogeneous and anisotropic character. Each gas shale formation has unique geological, geomechanical, geochemical and petrophysical properties. Consequently it develops multi-component storage mechanisms and production behaviour. This ultra-complex storage and production behaviour is the result of diverse micro-constituent minerals, organic matter and its maturity, interstitial fluids and the interaction between the solid and fluids. Knowledge about sedimentologic and stratigraphic nature of such rocks, their volume, TOC wt.%, kerogen type and maturity level, inorganic mineralogy are missing in databases of many sedimentary basins which are likely to become shale gas play in future, except a few, in South Australia, and Western Australia. Parameters having important role in hydrocarbons deliverability such as Young’s modulus, Poisson’s ratio, stress, and shear modulus have not been estimated as well. The existing petrophysical databases containing information literature and cored reservoirs samples show that likely shale gas formations mineralogical and rock characterization, porosity and water saturation are also remiss, which play a vital role in the estimation of initial economic value of any

shale gas reservoir. Australian shale gas potential is very huge and extensive according to some initial independent reports.

In this research study a systematic scientific and concerted approach was used to characterize the Murteree and Roseneath shales as potential unconventional shale gas reservoirs in Cooper Basin. Our major objectives set in this research dissertation are as follows

1. Rock and mineral characterization of carbonaceous shales
2. Investigation of very low effective porosity and ultra-low permeability
3. Assessment and identification of total porosity
4. Fluids, inorganic and organic contents interaction impact on water saturation estimation

In next chapter, entitled literature review we have described chronologically experimental work done by various researchers. Their observations and findings have been summarized pointing towards areas where some work is required to improve the understanding about source rock characterization. The research literature was mainly selected from lower North American states, shale plays which have been developed successfully in the last decade. Our methodology applied in this research try to follow the same guidelines used by these researchers.

CHAPTER 2

Literature Review

The history of potential source rocks evaluation as viable successful unconventional shale gas reservoirs can be divided into two phases, conventional techniques and unconventional techniques. The early and first phase during which gas rich shale was presumed just as another conventional natural gas accumulation with very low permeability and was tried to produce using conventional techniques. This phase is based on the gradual realization of characterizing it with modified conventional techniques like detecting organically rich shale intervals by the use of logs and calibrating results from core analyses in the laboratories with logs to improve production. The second phase is mainly involved with the use of much advanced level radiation technology to quantify the minerals, visualize and image nature of the void spaces and connecting flow paths probed through the use of radiation techniques, like QEMSCAN, FIB/SEM, FIB/TEM, Ultra Small Angle Neutron Scattering (USANS), Small Angle Neutron Scattering (SANS) and Small Angle X-Ray Scattering (SAXR) Scattering, Micro and Nano Computerized Tomography and X-Ray Diffraction techniques as well. These ultra-high level capabilities to magnify and resolve microfabric of shale rock, to image and visualize storage mechanism and flow pathways on submicron level have improved manyfold the understanding in characterizing and producing gas from shale gas reservoirs. These two phases of shale gas industry development are discussed in the following part of this chapter after USA map showing some of the most successful shale gas plays in the region especially Devonian and Barentt shale plays in figure 2.1 below.

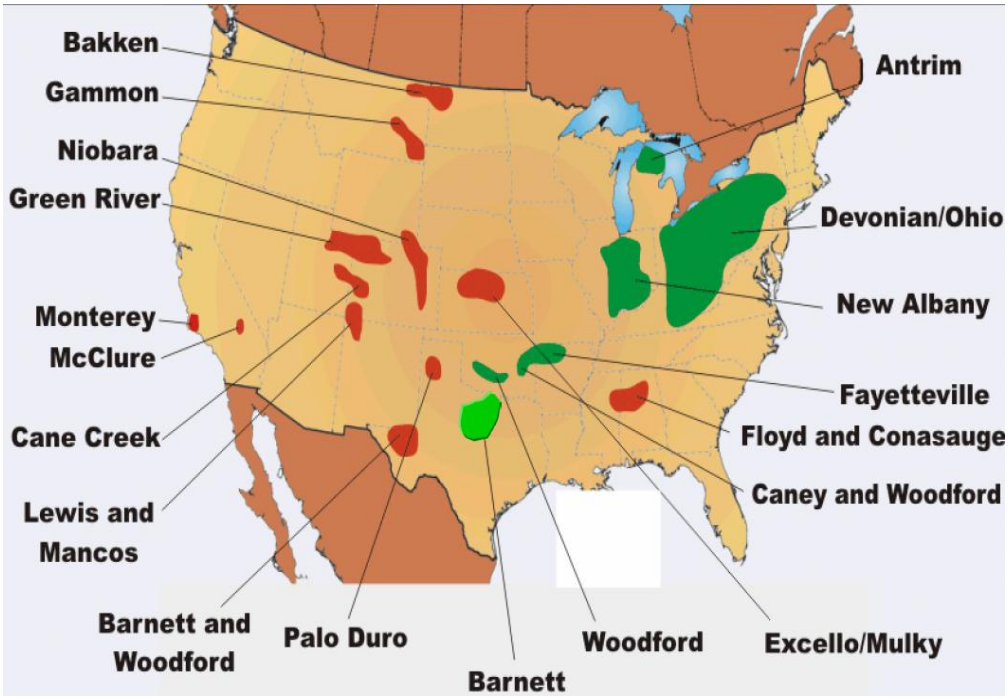

Figure 2.1: Location map of shale gas systems in North America (http://geology.com/energy/shale-gas/)

2.1 Conventional Wireline and Core Analyses - Evaluation Techniques

Production of natural gas methane from carbonaceous source shales is reported from Devonian Dunkirk Shale in New York in 1821, which later paved the way of drilling more shale gas wells in New York and Ohio states (Peebles 1980). After that, there is very sporadic record of interest taken by 19th century upstream petroleum industry operators till 1930 when we find the commencement of natural gas supply for consumption in local markets through pipelines in USA. It is believed that search, planned development and production of natural gas from source rocks obtained serious attention in 20th century and record of most relevant research work is briefly mentioned in paragraphs below.

Browning (1935) and Lafferty (1935) investigated rock and mineral characteristics, role of the matrix and any natural fracture system in the storage and flow of gas in organically rich clastic rocks. Devonian Shales. Foster (1975), Komar (1976) and Schrider et al. (1977), have unanimously reported that Energy Research and Development known as Bureau of Mines in 60's, took special interest in characterizing these shales with reference to storage and flow capacity by funding Eastern Gas Shales Project in 1976. The major objectives of this project were to estimate original gas in place, rock and mineral characterization, permeability, development and improvement of any artificial methods to increase production.

Later on, Aguilera (1978) raised the issue of compatibility of conventional logs for shale gas reservoir evaluation and recommended the amendments to detect and evaluate the source rock in situ. He found that evaluation of fractured shale gas reservoirs using logs is not reliable; some modifications are required to current wireline logging techniques, which must be suitable and fit to detect the lithology, fluids saturation and rock strength for stimulation purpose in shale gas reservoirs. Importance of wireline logging cannot be overlooked in conventional/unconventional sector, he concluded. Similarly extensive gas wells drilling activity in Devonian shales by Chesapeake Energy, then known as Columbia Gas System Service Corp, to produce large quantities of gas for local consumption has been reported by Smith (1978). Fertl W.H. (1980) applied spectral gamma ray logs for Eagle Ford, Niobrara and Pierre Woodford and Devonian shales, for identification of source rocks, fractured system identification and their reservoir properties. He found source rocks have natural isolated /impermeableb fracture system. Further he noticed that source rocks have complicated storage and production mechanism which can be identified by the use of spectral gamma ray logs and improved gamma ray log application in source rock identification and fractured system.

Steward and Paniszczyn (1981) reported the search for new shale gas reservoirs away from Appalachian Devonian Shales which started later after drilling first shale gas well in 1977 in Barnett Shale of Fort Worth Basin in North Texas by Michell Energy Corporation. Campbell and Truman (1986) investigated the petrophysical properties of Devonian shale to check resource potential as future potential natural gas resources using conventional techniques. Soeder (1988)

took special interest in investigation of reservoir characteristics of Ohio and Marcellus shale samples from Appalachian Basin using computer operated rock analysis laboratory techniques for porosity and permeability evaluation, rock and mineral characterization, fabric and grain size, shape and natural fracture system identification. The correlation of these results with the outcome from other resources was also done. He reported a gas filled porosity 10% in Marcellus shales, higher gas adsorbed content and bimodal pores size distribution. He noticed that gas flow capacity can be hindered by the mobile oil phase in shale which are not over mature and in that case they can perform and act as a good cap rock and seal for a conventional petroleum reservoir.

Luffel and Guidray (1989) applied wireline logging and core analysis techniques in Appalachian Basin, for Devonian Shales (USA) to evaluate total and effective porosity, gas saturation, water saturation by Dean Stark method, clays identification and their properties, capillary pressure and permeability. They observed that shale have higher total porosity than assumed previous low total porosity estimation and emphasized on core and log analysis results correlation and found it reliable. But they also reported doubts and concerns about Dean Stark method application for fluid saturation as well as high effective porosity in the presence of clays in Devonian shales. Again Guidry et al. (1990) in the same shale plays using wireline logging data, core analyses reports and production tests data, developed a wireline logging model to evaluate porosity, hydrocarbon saturation, kerogen content, rock and mineral identification and conventional formation evaluation procedure for evaluation of initial gas in place in Devonian shales. They probed and identified differences between a conventional gas and shale gas reservoir characteristics and emphasized on improvement of conventional methodology for unconventional shale gas reservoirs characterization using logs and cores results correlation.

Passey et al. (1990) used wireline logging data available from developed oil and gas fields with special interest in the use of sonic and resistivity logs. Sonic, resistivity and gamma ray logs are the core component of a wireline logging operation and using wireline data can be excellent aid in the identification of the potential shale reservoir and in shale gas reservoir characterization he reported. But these logs were not able to evaluate total gas content apart from identification of intervals of potential source rocks and improvement in identification of mature source rocks. Howard (1991) investigated the impact of the smectite/Illite diagenetic conversion on porosity in noncarbonaceous shale which was an appreciable step to understand the impact of these essential clays on porosity in shale gas reservoirs.

Davies et al (1991) have reported pores and fractures in Devonian shales which can be only identified, using high magnification and resolutions instruments like scanning electron microscope and transmission electron microscope which gradually developed the geoscientists and petroleum engineers interest in the use of scanning and transmission electron microscopy as an aid in characterizing source rocks. Similarly Bennett et.al., (1991) tried to predicted depositional environment and sedimentation, role of various process in sedimentation, diagenesis and fabric

signatures, microfabric of sediments, organic matter and grains arrangement and attachment in Bedford Shale and Bituminous Shale (USA and UK Mississippian Delta Yorkshire) by the use of SEM and TEM high magnification and resolution radiation techniques. These powerful probes can reveal the petrophyiscal characteristics of shale gas. These tools are very helpful to expose storage and flow mechanism and can help in developing a strategy for artificial stimulations well. But these observations are not from a real shale gas reservoir it is found in this study.

Lu et al., (1992) used Devonian shale samples. He tried to identify different zones of gas storage, and fracture system through krypton gas injection. The results were correlated and validated using micro CT scanning and thin section observations prepared from the same samples later on. They showed some concerns about the validity of the conventional techniques for shale gas due to ultra-low effective porosity and permeability. They found that krypton was the best alternative for porosity and porous zone identification and spatial distribution of the gas and can help to identify the fractures in core samples. The study expressed the concerns and lack of techniques how to improve the current methodology and to find any alternative method for the evaluation of total porosity and permeability in these ultra-complex clastic self-sourced and self-reservoired natural gas accumulations.

Katsube et al. (1992) conducted a detailed experimental work on Scotia, Shelf Shales, and Beaufor-Mackenzie Basin in Canada. Core samples were irradiated using XRD, SEM and Petrographic thin section were prepared for visual analyses. The analyses were performed to investigate changes in porosity with gradual increasing depth of burial and pore size classification. They found that organically rich shale gas have a range of porosities. Consequently the range of various pores size will express various effective and total porosity values. The formation factor, electrical resistivity, mercury porosimetry, permeability measurement techniques vary considerably in shale gas reservoirs. How to measure and evaluate these properties reliably by any technique needs improvement in the conventional techniques to evaluate petrophysical properties of shale gas reservoirs, they reported after the conclusion of this research project.

Lancaster et al., (1992) did mineral and rock characterization by X-Ray diffraction and wireline logging techniques using core samples of Devonian and Barnett shales, from Fort Worth Basin USA. The results from these two shale samples were correlated with each other to check and investigate any differences in lithology and petrophysical properties of these two shales. The results were found useful to locate free and compressed gas zones, adsorbed gas, and identification of fractured zones for well completion targets. The rock and minerals qualitative and quantitative assessment was not correlated with any other methods. The assessed porosity and permeability values have not been reported to be correlated with results prepared using same samples, it is found in this study.

Considering the complex and multicomponent natural gas storage mechanisms in shale matrix and organic matter, a wireline logging methodology was conceived and put forward by Decker et

al., (1993). They used wireline data and shales samples from wells drilled in Antrim shales, Michigan Basin. The cross plot between TOC content and sorbed gas content, as well as TOC content and shale bulk density were used to get reliable values for sorbed content. Later on these values based on the correlation coefficient, were used to calculate the total gas in place in the whole Michigan Basin. This method was low cost and less time consuming, and did not demand the rigorous rock and mineral characterization, estimation of free porosity and water saturation. The procedure was very simple for resource evaluation especially in coals where organic content was always more than 50%, and had very high adsorbed gas content compared to free and compressed gas in organically rich overmature potential shale gas reservoirs. The reservoir characterization, mineral and rock character, pore size, classification and distribution, natural fracture system or fraccability assessment were not thought to be necessary in this resource evaluation procedure. It can estimate the total gas in place in a potential shale gas reservoir. But this methodology did not address the valid issue of the adsorption of gas content on the clay, as well as when TOC and sorbed gas content are cross-plotted, the correlation coefficient is not reliable for other shale plays. Therefore, it is very simple method of resource evaluation which works well in coal seam gas but is not free of doubts when applied in shale gas resource evaluation.

Zuber et al., (1994) used wireline logging data, core analyses reports and production data prepared for Antrim Shale in Michigan Basin. The previous published data was screened and re-examined for petrophysical evaluation and resource evaluation, based on available petrophysical properties values reassessed in these reports. They concluded that conventional technique generate erroneous figures and are not free of doubts when applied for resource evaluation in shale gas reservoirs, especially when NMR and density logs in mature and overmature source rocks are used, they impact and influence the resource evaluation and production strategy.

Watson and Mudra (1994) used xenon gas for injection into Devonian shale samples and later scanned those using micro XR-CT scanning techniques to identify and differentiate zones of gas storage, microfracture systems and their interconnectivity. The results were correlated and validated by the use of thin section studies as well. The effective porous zones, higher storage zones, natural fracture system and pyrites nodules surrounded by the higher concentration of gas were identified. Xenon gas application to trace movement of methane and ethane in shales was documented but fracture system and its interconnectivity is doubtful because it is not clear whether imaged fracture system is not induced fracture system or a consequence of stress release during sample preparation.

We found that it is appropriate to acknowledge as mentioned in the preceding paragraphs, the pioneer work, how to compute total free porosity, identify rock types and organic content and develop a petrophysical model for a shale reservoir was initiated by Luffel and Guidry (1989; 1990; 1992), Guidray and Luffel (1995) and Guidry et al (1995) using core samples from the biggest shale gas region in USA, Devonian Shales of Appalachian Basin. The research project

was funded by Gas Research Institute (GRI) to characterize the carbonaceous shale as future unconventional gas reservoirs. The objective of this experimental work using core samples from selected wells was to design a method using logs for the identification of prolific gas intervals. They applied conventional methods for total pore volumes, free gas porosity, and water content, using helium for grain volume and bulk volume, Dean Stark method (using boiling toluene) for water saturation (S_w), to calculate gas filled porosity. Using values computed from logs, geochemical analysis, and using the correlation coefficient and line of best fit concept, they were able to design a petrophysical model for in situ calculation of free porosity, water saturation, pyrite, clay, quartz and kerogen content for Devonian shales. The core samples were immersed in mercury to compute the bulk volume and bulk density and applied Archie's equation for estimation of water saturation in Devonian shales.

Hill and Nelson (2000) reported about petrophyiscal properties of Antrim (Michigan Basin), Ohio (Appalachian Basin), New Albany (Illinois Basin), Barnett (Fort Worth Basin) and Lewis (San Juan Basin) shales and the probable resources held by these shales. The estimated resources in these organically rich shales were determined using five key parameters, like thermal maturity, sorbed gas fraction, reservoir thickness, TOC wt. % and prospective shale formation area. These estimates about the initial gas in place were based on values of parameters, evaluated using conventional techniques, wireline logging and core analyses.

Kawata and Fujita (2001) wrote about consequences of depletion of conventional oil and gas resources in 21st century and presented a report giving some figures about the total unconventional gas resources like coal seam gas, gas hydrates and shale gas in world with an insight about the alternative cheap source of energy in future. He presented shale gas data from various reports about world total natural gas resources available included Australia. He stressed on consequences of escalating future energy demand and how in future high energy demands will be fulfilled from the unconventional resources using improved shale gas characterization and production techniques, with some environmental pollution issues.

Shale gas reservoirs are continuous natural gas reservoirs, with a very complex storage, trapping and sealing mechanism and with a limited gas migration distance in a petroleum system, Curtis (2002) emphasized. The five key parameters which make these gas reservoirs unique from one another are thermal maturation of the organic matter, sorbed and free gas content, total organic carbon, and volume of gas in place and there is no analogy for any shale gas reservoir Curtis (2002) argued. Therefore he stressed on the need for separate and independent characterization of each shale gas formation, even possessing optimal geological and geochemical attributes. The reservoir characterization of shale gas reservoirs till late 90s in 20th century was absolutely focused on improvements of applied standards prevailing in the conventional petroleum sector and borrowed standards from coal industry. The application of gas canister desorption analysis technique in shale gas reservoir is one of these standards borrowed from coal industry. The major area of focus was on evaluation of the rock and mineral density, rock and constituent minerals

classification, effective and total porosity, water saturation, permeability and wettability of the reservoir grains using core samples. The researchers mentioned above, heavily relied on methodology and techniques, like helium porosimetry, mercury injection and liquid/gas pyknometry, x-ray diffraction and wireline logging techniques with some possible appreciable improvements. For pore size distribution, classification, BET (Brunauer-Emmette–Teller Theory) equation, mercury injection capillary pressure (Washburn Equation) techniques were recommended and favoured.

We also found that Lewis Rick et al. (2004) showed special interest in shale gas reservoirs. Characterization using wireline logs and core analyses. Rock and mineralogy, kerogen identification and quantification through logs while adsorbed gas content using Langmuir Isotherm. The producibility was tried to predict using logs and later calibration with cores data as well. Their main focus of project was on improvement of logs after calibration with core analysis data. Though recommended the use of SpectroLith and ELANPlus logging tools but have not confirmed results by actual field data, when applied for petrophysical characterization of any shale play.

Montgomery et al. (2005) took special interest in evaluation of hydrocarbon generation potential of Mississipian Barnett shales of Forth Worth Basin. They used geochemical laboratory analysis techniques for TOC wt. %, vitrinite reflectance, free and adsorbed gas content using Langmuir isotherm method, transformation ratio and remaining potentials of the reservoir. They tried to make assessment through simulation of geochemical parameters changes and how they are related to check the hydrocarbon generation potential in a potential hydrocarbon gas plays and reported total gas in place based on adsorbed and free gas content. They presented an example how an organically rich source is evaluated as a future potential source rocks without before initiation of investigation of its reservoir characteristics. Zhao et al. (2007) also investigated thermal maturity and hydrocarbon phases using wireline logs. They found that increase in thermal maturity is strongly related to decrease of hydrocarbons, source rock bulk density as well as water saturation decrease in potential source rocks. Ross and Bustin (2007) report that when helium gas is used to evaluate the total void space in a shale gas core sample, under very high and low pressured, it can affect the total void space estimation. Helium also adsorbs, at higher pressure is followed by increased calibration time, which needs consideration because internal surface measurements are controlled by the pore throat size, diameter of the pores and kinetic diameter of the molecules used for assessment especially the use of helium for shale gas reservoirs which have ultra-high heterogeneity and pore throat diameters.

Jacobi et al. (2009) developed a wireline logging model based on density, neutron, acoustic, nuclear magnetic resonance logging tools responses recorded in exploratory and production wells in Barnett shales of Fort Worth Basin. The model was designed to assess geochemical properties/data, lithology, mineralogy and stratigraphy, total organic carbon content, and depositional facies identification, and selection of zones for hydraulic fracturing. Shale gas

formations are unique, in geological, geomechanical and geochemical characteristics they argued. This model was developed specifically for Barnett shale with a hope of application in other shale gas formations, found in other parts of the globe. The strength of logging tools and model have not been verified in any other shale gas play and we do not find any example where this wireline logging tool with how much success have been applied and recommended for others shale gas play. It is reported by Jacobi et al. (2009) that this model was used and wireline logs were run in wells drilled in Caney and Woodford shales of Arkoma basin in USA. They tried to characterize these shales using the properties like density, porosity, sonic velocities pores pressure, overburden stress poisson's ratio and horizontal stress found in the wireline logs records. Wireline logging tools can help to locate fraccable intervals after calibration with core laboratory analysis. In this study FIB/SEM results and outcomes of wireline logs have not been correlated which we think is an essential part to check the validity and integrity of this technique in the field. They are time saving tools but NMR application is still under investigation due to its sensitivity to organic matter which is always present in the potential shale gas reservoirs.

Worthington P.F. (2011) described these unconventional shale gas reservoirs as the most complex petroleum gas reservoirs. Lithology, mineralogy and rocks, pore types and morphology, fluids and matrix interaction and application of second Archie equation for water saturation estimation when wireline logging tools are used for in situ characterization of these complex gas reservoirs are challenging, he reports. He has expressed concerns about the impact of high volumes of clays/shale and porous nature of shales acting as unconventional natural gas reservoir on outcome when Archie second formula is applied for water saturation. Complexity of the shale gas reservoirs reasons and needs for crucial amendments in standards to characterize these problematic unconventional gas reservoirs, when petrophysical evaluation techniques are applied, were highlighted by him.

Yu and Aguilera (2011) investigated validity of Passey et al. (1990) method for the identification of source rocks using sonic and resistivity logs in oil and gas wells, with focus on estimating TOC wt. %, water saturation fracture intensity and diffusion. They recommended the use of Archie equation for water saturation in shale gas reservoirs without giving any reason of its application except that there is no another universal model for this purpose.

These reservoir characterization techniques mentioned in the preceding paragraphs for gas shales are indirect reservoir characterization techniques. The major stress was on tools improvement, wireline logging and core analysis in laboratories, with major focus on calibration and correlation of predicted results. The use of radiation techniques was very limited due to limited access to these tools, expensive and very time consuming procedure only available in a very few laboratories in North America. This early phase about shale plays characterization was more about understanding nature of these rocks through conventional methods and gradually updating accordingly as needs arise during characterization, development and production phases.

In summary we find that the foremost prerequisite for source rock to be considered a shale play is the type, amount and maturity of organic matter and was investigated using resistivity, gamma ray and sonic logs as Fertl W.H 1980 and Passey 1990 reported about their successful use. The worthy work of Luffel and Guidray in 90'^{S} led to more detailed investigation of organically rich mature source rocks as potential natural gas reservoirs. They laid down the guidelines for shale gas characterization. The petrophyiscal model built was based on real core samples description done in laboratory experimental work. The outcome based on laboratories work observations and later calibration with logs results made these tools suitable for field application. Some of the researchers in 90^{S} evaluated effective porosity using helium gas and mercury injection procedures and results were calibrated with NMR logging probe results, sonic and density logs response in these intervals with some concerns about size of the molecule of helium and mercury used for this purpose. Liquid pyknometry method was applied on rock powder samples to find the grains volume and consequently to estimate the total pore volume in shale samples. There have been always discrepancies among results about same formation porosity, permeability and water saturation which are most important parameters in the results received from various service providers. Core analyses in laboratories play an important role to build petrophysical models for conventional in the past and same concepts have been applied for shale gas formation evaluation as mentioned in aforementioned paragraphs above.

The history of previous work and research mentioned above was mainly focused on improvement of conventional techniques. Amendments and changes were made to conventional standards. They were applied in laboratory core analysis and wireline logging techniques for evaluation of porosity, permeability mineralogy and rock classification, and fluids saturations. The objective of this phase of research was to improve understanding, detection and evaluation of natural gas resources in potential mature, gas rich source rocks in shale gas systems. Very little effort is found in this reviewed literature mainly concerned with cores analyses and wireline logging about exploring microfabric and multimodal porous nature, complex storage and flow mechanisms existing in shale gas reservoirs.

To characterize and analyses these ultra-fine-grained sedimentary rocks as viable future economic potential natural gas rich rocks was a formidable task, until the breakthrough by the application of focused ion beam milling, scanning electron microscopy and transmission electron microscopy. The maturity of organic matter/kerogen, inorganic and organic pores, identification, classification density and their interconnectivity was manifold improved by the use of FIB/SEM and FIB/TEM techniques as these properties have critical role in unconventional reservoir characterization. In the next part of this chapter application of FIB/SEM/TEM, Micro-CT Scanning radiation techniques and their importance in improving the understanding of shale gas reservoir have been reviewed in publications found in various journals and conference papers.

2.2 Unconventional Evaluation Techniques – Radiation Probes

Shale with sedimentary organic matter have Kaolinite, Illite and chlorite clay components which have flakes/needles like structures with size less than 4.00µm and silica (Quartz, Opal), particles in range of 31.25 to 7.812 µm. Carbonates (Calcite and Dolomite) and other heavy minerals like siderite, pyrite rutile and sphalerite all have their own morphology, size and shapes. After deposition in a lake or marine basin, the initial clast, inorganic debris and organic matter undergoes through a collective physical and chemical change due to gradual increase in overburden, pressure and temperature in subsurface developing into a very complex porous media. Pores and pores density, morphology, location and relation to inorganic and organic matrix, inetrconnecetivity and fractures system all need ultra-high magnification and resolution power to understand morphology, texture and fabric, storage and flow properties. The porous nature of this medium whose understanding is so crucial and play a key role in reservoir characterization and its economic value cannot be probed, understood and classified just by using fluids penetration methods and application of wireline logging techniques. Results obtained from BET theory, helium and mercury, and porosity from logs raise some valid concerns when correlated with FIB/SEM images. Therefore Bennett et al. (1991) recommended the use of SEM and TEM radiation techniques to enhance the understanding of the microfabric of organic and inorganic shale. But due to limited access, very time consuming procedure and high cost of FIB/SEM/TEM radiation techniques application in shale gas reservoir was not possible in the last decade of 20^{th} century. As consequence radiation technology to image and visualize microfabric of shale rocks has emerged as an essential tool for investigation of petrophysical and geological properties of shale gas reservoir. As mentioned below due to number of reasons radiation probes are being used globally in petroleum unconventional sector. FIB/SEM application in characterizing shale plays intensified in the last five years and literature review in the next part of this chapter mainly covers FIB/SEM work of those researchers which is mostly related to North American active shale plays emerging as modern success of shale plays.

The understanding of shales porous system through FIB/SEM is important for two reasons, firstly to determine the initial gas in place and then ascertain the flow characteristics which are not possible without the use of probing radiation system like FIB/SEM/TEM. These instruments are equipped with ultra-high magnification and resolution power which can image pores and flow paths at submicron level. Conventional sandstone and carbonates porous media and gas shale vary considerably in number of petrophysical properties especially in the way the gas is stored and flow during production. Gas is stored as adsorbed gas on clays and organic matter, stored as free compressed gas like conventional. Davies et al (1991) recommended that identification of pores and fractures in Devonian shales, is only possible by using high magnification and resolutions instruments like scanning electron microscope and transmission electron microscope which gradually developed the geoscientists and petroleum engineers interest in the use of scanning and transmission electron microscopy as an aid in characterizing source rocks. This

early record about the use of SEM and TEM was only for better understanding of the microfabric nature of these rocks to check their sealing capacity and sealing integrity for conventional petroleum system and for nuclear repository surveys. The most relevant part of research work and totally committed to characterize shale reservoirs applying radiation techniques commenced in 2008.

Bustin et al. (2008) and Jacobi et al. (2008) have reported that very low effective porosity, micro to nano Darcy permeability, large surface area of clays and organic matter to adsorb gas will challenge the limits of the techniques applied on molecular size levels when different fluid penetration techniques are used for pore volumes measurements. The amount of organic content, particle size, pore size and pore size distribution and the mechanism of the storage and flow altogether vary in conventional oil and gas reservoirs, coal and shale formations. The characterization of shale gas reservoirs without taking the advantage of radiation techniques always leave some doubts about the petrophysical parameters values derived from conventional techniques. Rokosh et al. (2009) have emphasized for SEM application when evaluating sealing capacity for a petroleum reservoir. Shales possess submicron level silt laminae, which cannot be detected by wireline logging tool but SEM; they observed, emphasizing on the use of SEM in shales petrophysical characterization. FIB/SEM and TEM can help to point out this property which can affect production of gas.

Loucks et al (2009) probed pore network system in Mississippian Barnet Shales using FIB/SEM. Argon-ion milled samples were scanned to identify pore size, pores distribution and morphology, origin and location of the various porous zones. Mature organic matter, kerogen as a consequence of the conversion into oil and gas generates more porous mass, hosting nanoscale pores, compared to immature organic matter. When kerogen/organic matter making thin laminae along the bedding plane of the deposited clast, conversion of thin organic matter laminae into porous mass can generate porous laminae which can provide higher adsorption area as well as conduit for production of gas from these areas. The level of continuity of the mature organic matter, kerogen, deposited like thin laminae along the bedding plane can provide space for storage of compressed gas and later facilitate the flow of the gas towards the production wells, they reported. Although they have used the state of the art technology to probe and estimate the pores and their size at high level of resolution and magnification, there is a sense of reluctance not to measure the free porosity even though having access to core samples and instruments. The major concern is the amount of information and up scaling to laterally very extensive and vertically very heterogeneous reservoirs.

Rokosh et al. (2009) scanned and imaged Upper Colorado Group, Banff and Exshaw shales core samples from Western Canadian Sedimentary Basin using field emission scanning electron. Microscope. Applying Energy Dispersive X-ray spectroscopy (SDXS) embedded in the radiation system, semi-qualitative elemental maps of various minerals phases were prepared for minerals identification along with pores type, size, morphology and relation of these pores to inorganic

matrix and organic matter. They found that many characteristics of shale gas reservoirs cannot be viewed without the aid of FE-SEM which is essential part of formation evaluation in this scenario.

Barnett shale has nanoscale intraorganic pores ranging between 5 and 1000nm. These pores are sites of higher gas storage, possessing very high fractions of the retrievable natural gas, both adsorbed and free gas compared to the nonorganic matrix part of the shale gas reservoir, Wang et al. (2009) reported. This intraorganic porosity (pores) is hydrocarbon wet, support the single phase flow, gas and exhibit higher permeability as well. The interconnectivity of these porous zones can facilitate higher gas production when these natural porous system and natural fractures in the reservoir are connected through the hydraulic fracturing operations. Therefore importance of organic porous zones and pores size and morphology cannot be overlooked when characterising these shales, but evaluation of total free porosity and the determination of interconnectivity of natural fractures are still speculative, Wang et al. (2009) have stated.

Nelson P.H. (2009) reviewed previous published data, generating using mercury injection; gas flow and small angle neutron scattering (SANS), scanning electron microscopy (SEM) applied to sandstone reservoirs and organically mature source rocks acting as self-sourced gas reservoirs in USA, Canada and few other examples worldwide. Nelson (2009) reported range of porosities, 5.1% to 12.6% in Pliocene shales of Beaufort-Mackenzie Basin Canada and pore throat size range 0.009 µm to 0.044 µm respectively. Porosity in source rocks of USA; Bakken 4.3 %, Cherokee 5.2%; Monterey 8.5% and Monterey 12.7% with median pore diameters, 0.005 µm; 0.007 µm 0.010 µm and 0.016 µm respectively have been reported. Also he found that Devonian shales also have a range of porosities 3.2%, 3.9%, 6.0% and 8.5% for pore diameters 0.007 µm; 0.008 µm, 0.024 µm and 0.019 µm respectively. Jurassic and Cretaceous shales of Scotian shelf in Canada, porosity ranges from 1.5% to 8.4% Nelson reported. He concluded that pore throat sizes are directly related to porosity and permeability values, but when effective porosity measured 8% or more raised some issues in shale gas reservoirs, needs revaluation to check the contribution of some induced fractures when using very high mercury injection techniques.

Kale et al., (2010) applied number of conventional and unconventional techniques to investigate hydrocarbon generation potential of Barnett shales using LECO-pyrolysis techniques, MICP, Helium Porosimetry, Fourier Transform Infrared Spectrometry (FTIS) for core description and environmental scanning electron microscopy for pores size and morphological classification of the pores. They investigated how varying lithologies/ mineralogies can change porosity, but does not mention how to measure porosity and no correlation of pore size classification between ESEM and MICP is mentioned in this study.

Schieber (2010) have found and classified the shale gas pores into phyllosilicate framework pores (PF-Pores) defined and related to clay minerals, carbonate dissolution pores (CD-Pores) related to carbonates content (CD-Pores) and organic matter pores (OM Pores) hosted by residual kerogen after its metamorphism. These PF, CD and OM pores range in size from 5 to 1000, 50-

1000 and 10-100 nanometre respectively. These samples were taken from various locations, from core library, personal laboratory collection and from the cliff exposures in the field. Mechanical and ion millings procedures were followed to prepare the samples for scanning electron microscopy (SEM) and transmission electron microscopy (TEM) to investigate the location, origin, morphology and distribution of all these pores. Aided by combination of very high resolution, magnification of SEM and TEM techniques and ion milling technology can reveal some intrinsic characteristics of porous media. Using morphology of these diversified pores, Schieber (2010) managed to predict pre and post-depositional changes in these sediments which can have a role in the storage capacity and flow capacity, using the interconnecting channels among these pores of various shape and size. Also prediction of organic matter maturity level of these shales based on level of metamorphism of kerogen leaving behind a porous mass is possible, when a considerable portion of kerogen has been transformed into oil and gas, Schieber (2010) stated.

Milner et al. (2010) used ion beam milled and SEM scanned samples from four organically rich shales, namely Barnett, Haynesville, Horn River and Marcellus, to investigated porosity system. There are four types of pores rather three as previously identified by Schieber (2010). They are identified as matrix intercrystalline, organic (kerogen hosted) and organic (masses and particles), dissolution and the fourth type, intraparticle pores, having various dimensions. They are interconnected to the rest of three pores type and must be considered for pore size classification in fine grained conventional and non-conventional reservoirs. The nano to micro size of these pores in a shale reservoir is largely dependent on the microfabric and microtexture, type of organic matter and level of organic matter maturity, Milner et al., (2010) maintained.

Potential shale gas formations whether marine or lacustrine like Roseneath and Murteree shales are over mature source rocks having negligible oil and mainly comprising thermogenic gas. Using key controlling parameters like TOC W%, its type and maturity, mineralogy, thermogenic gas generation and production can be predicted applying various conventional and non-conventional techniques like X-ray diffraction, vitrinite reflectance, TOC wt.%, FIB/SEM and FIB/TEM, MICP and helium porosimetry Passey et al (2010) said. Shale has very small pores, in submicron scale in a multiple systems of porosity and contains large surface area due to the presence of clays. FIB/SEM is capable of imaging and identifying these pores. Using the serial sectioning and imaging of the ion milled samples to build 3D volumetric model is possible. But considering the level of heterogeneity and pores size distribution, 3D volumetric model cannot represent a shale gas reservoir, free of doubts when up scaled to apply in the Initial gas in place estimation, Passey et al. (2010) suggested.

According to Sondergeld et al., (2010), porous system in a shale formation has direct control on porosity and permeability, which in turns has impact on the deliverability and economic potential of the reservoir. Classification, location and connectivity of such porous domains using FIB/SEM dual system and building a 3D-volume to observe connectivity in the shale samples can help to improve shale gas play modelling for future fraccing operations. The results from this study were

later correlated with helium and NMR outcomes from the same core sample (Sondergeld et al. 2010). They have reported that a large contribution of this pore volume is from nanoscale pores, some of them could be the result of soft kerogen removal during milling operation before scanning operation known as pull-outs. Also the total porosity based on the visual quantification of the nine Barnett shale images is equal to helium, which is actual effective porosity not total porosity raises some concerns. The total thickness of each slice milled has 10 nm in 3D volume, there are some concerns that pores whose thickness is less than 10 nm are likely not to be included in the final total pore volume, while using dual FIB/SEM system to explore the pore system and the connectivity of these pores in the used sample.

Similarly Curtis et al. (2010) selected nine shales samples from active shale gas plays, namely, Barnett, Eagle Ford, Fayetteville, Floyd, Haynesville, Horn River, Kimmeridge, Marcellus, and Woodford shales. Focused ion beam (FIB) milling and scanning electron microscopy (SEM) were used to prepare 3-dimensional volumes to visualize individual pores, total pore volumes, pores connectivity and amount of kerogen in selected nine carbonaceous shales. They used energy dispersive x-ray spectroscopy technique (EDXS) embedded in the system, to identify the pores, kerogen, inorganic minerals like clays, quartz, carbonates and pyrites based on the spectra produced. The matrix was divided into four phases based on the grey scale intensity, pores are black, kerogen, grey black, while clays, carbonate, quartz are light grey and white, heavy minerals like pyrite. Kerogen volume in 3D does not represent the actual volume when compared to the remaining volume of matrix in rendered 3D Horn River model. It is also worth noticed that helium porosimetry reflects effective porosity, should be less than total SEM imaged porosity, which actual is greater than SEM values. The results and models actually demand to check the applicability and reliability of FIB/SEM 3D volumetric results before incorporating into evaluation of initial gas in place, which is one of the ultimate goals of these research endeavours.

Adsorption of natural gas on clays and organic matter surface will occupy some space, in the micro, meso and macropores in a shale gas reservoir. The pore volume measured before desorption and after desorption in a shale sample will have different figures (Ambrose et al. 2010). Initial reservoir pressure, temperature, and pore size will define the fraction of total pore taken by adsorbed gas and by the free compressed gas content. To determine the fraction of total free porosity taken by adsorbed gas is much problematic when simulating at initial reservoir pressure and temperature. They derived a constant for estimation of the volume taken by the 1lb. Mole of adsorbed gas content (Ambrose et al. 2010). This constant at standard condition of temperature and pressure is used to estimate the fraction of total free porosity taken by adsorbed gas content, needs to be evaluated at reservoir temperature and pressure when using volumetric methods to evaluate initial gas in place.

Passey et al. (2010) used a composite of valid geological, geochemical and petrophysical concepts in the description about the origin of source rocks, Cretaceous Mowry, Barnett Wood

Ford shales and Exshaw type section Alberta, in USA and Canadian Sedimentary Basins. They have given a detailed idea about source rocks depositional environment, concepts of sedimentation, use of wireline logging and FIB/SEM application advantages in shale gas reservoir mineralogical and petrophysical evaluation. The found disparities in the porosity, permeability and water saturation results from various laboratories, when evaluated on exactly same sample and reported role of clay minerals in water saturation and porosity determination in overmature source rocks.

Milner et al., (2010) used secondary electron and back scattered electron detectors of FIB/SEM for minerals identification, pores classification and connectivity. It is observed that these shales have pores range from nanoscale to micron scale and are function, which is related to the microtexture, grain size mineralogy organic matter and maturity. The core samples were selected from Haynesville, Horn River, Barnett and Marcellus Shales of USA. While geochemical analysis for TOC wt. % and vitrinite reflectance were also incorporated in this study to check the maturity of the source rock. Milner et al. (2011) have expressed their concerns as before by other authors that use of 3D cubes as representative of total porosity in shale gas reservoirs is not free of doubts when applied in real shale gas play resource assessment and consequently in production models.

Loucks et al., (2011) re-examined and reviewed the already published data mainly in 2010, found in mud rock systems research laboratory of Austin University. An extensive pores classification, relation to a particular matrix constituent was performed. Pores, cracks and fractures classification into interparticle, intraparticle, intercrystalline and intracrystalline and microfracture system based on their morphology and significance in porosity, permeability and role of natural fracture system on stimulation was investigated. The mechanical and chemical stability of constituent microfabric of shales and their role in developing secondary porosity due to dissolution at higher temperature was probed. They have reported role of depth of burial in both storage and flow capacity of these reservoirs. But there is no mention of how reliably we can evaluate total porosity and water saturation in shale gas reservoirs except the worthy work about the 2D identification and classification of void spaces and micro cracks.

Handwerger et al., (2011) did a comparative study on the application of Dean Stark and Retort methods for fluids saturations estimates in shale gas reservoirs. They reported advantages of retort method for fluid saturation, (water and oil) determination when using crushed shale gas reservoirs samples and improvement in reducing the extraction time compared to procedure by Luffel et al., 1993. They observed that free, clay bound and clay structural water can be extracted to check the water saturation (S_w). They powder sample was continuously heated in a controlled succession of three characteristic retort temperature, later used in calculation of various porosity values, clay bound, free and adsorbed water.

Free porosity in organic shales can be divided into, porosity related to clay matrix, to non-clayey content as well as to the organic part (kerogen), which hosts most of the free porosity fraction according to some authors. The academic and commercial laboratories are in initial stages of developing standards for free porosity assessment and evaluation. The use of helium, mercury, water, nitrogen and rock matrix independent NMR tool, and outcome regarding free porosity is not free of concerns and doubts when applied in initial gas in place final formula (Glorioso and Rattia 2012) have raised some concerns. These issues are the result of very low effective porosity and permeability, due to ultra-fine grained fabric of the shale gas reservoirs and their very heterogeneous nature. The ultra-high magnification power and super resolution strength to observe the microfabric of shale gas reservoirs have offer an outstanding contribution. In reservoir shales characterization, rock and minerals identification and quantification, natural fractures identification, pores, pore size classification and interconnectivity can augmented many fold by FIB/SEM dual system application. Later when outcome correlated with the results from QEMSCAN, NMR, MICP, Pyknometry and Helium Porosimetry, it can provide reliable petrophysical properties and features of a potential reservoir essential to establish its economic viability.

Curtis et al. (2012) reviewed previous FIB/SEM published research work since 1996, mainly related to Barnett Woodford Eagle Ford, Haynesville Marcellus Kimmeridge (UK), and Floyd, Fayetteville and Horn River (Canada) shales and mudstones. They investigated the origin and relation to inorganic matrix or organic content, shape size and morphology of pores, and total pore volume. They found each shale or mudstone is unique in its pores types, size and classification. Based on the relationship and location in matrix and organic matter, pores can be identified as interparticles, intraparticles, and intercrystalline and organic matter dominant pores. This extensive visualization of 2D images taken from mudstones and shale samples using FIB/SEM proves that these organic rich source rocks have high occluded porosity which is not accessible by helium and mercury injection techniques and 3D volumetric model built based on FIB/SEM techniques cannot be taken as representative for whole shale gas reservoir. Finding a true representative porosity for any shale gas reservoir in the field by any standard available is still a challenge for researchers, they argued.

Kimmeridge formation organic source richness, maturity, generation potential and pore classification was performed by Fishman et al. (2012) by applying XRD, Rock Evaluation Pyrolysis geochemical method, use of transmitted, reflected light and SEM equipped with EDXS capabilities. Rock and mineralogical qualitative and quantitative analysis was achieved by XRD while Rock Evaluation Pyrolysis was used for TOC wt. %. Identification of macerals and maturation level of organic matter was also confirmed by SEM. EDXS was mainly used for semi-qualitative analysis of minerals. Pores identification and major areas of free porosity were located. No pore size classification and total porosity evaluation are reported in this study.

Wu and Aguilera (2012) investigated the implication of porosity exponent (m) used in Archie's second formula for water saturation. They used SEM, TEM and AFM (Atomic Force Microscope) for imaging samples on nanoscale, sonic porosity from logs and applied Pickett plots to evaluate the water saturation for Muskrat and Nordegg shales, in Western Canada Sedimentary Basin. Water saturation is more sensitive to resistivity changes and not to porosity changes in shale gas formation they have reported.

Houben et al (2013) found that broad ion milling (BIM) and scanning electron microscopy (SEM) is equivalent to FIB/SEM in application and objectives when shales and other fine grained rock samples are scanned. Opalinus clay from Mont Terri, Switzerland, have been investigated and imaged to better understand and evaluate the porosity by pores counting, pores classification and connectivity, morphology, orientation, pore size distribution as well as fracture system. There is no mention of reasons for fractures origin in samples and porosity evaluation is based on pores counting in 2D images taken using BIM/SEM. Houben et al. (2013) have not reported total porosity which could be considered as representative porosity in Opalinus clay.

Milliken et al. (2013) have reported that TOC wt. % varies strongly in shales universally, even in exactly same shale formations and the effect of higher and lower TOC wt. % is always visible in the form of concentration of pores in organic matter. Using field emission–scanning electron microscopy (FE-SEM) for imaging ion milled surfaces of Marcellus formations (Devonian) of Appalachian Basin they have investigated and classified pores, pores morphology and connectivity. The pores were manually counted first and software was used to facilitate counting speed later. The total porosity determination from this method could not be considered as a standard for any shale gas formation, as the TOC wt. %, can vary in the same formations and the observations are based on submicron level in 2D image, not a representative of the whole shale formations.

Achaean Junction Gold Deposit of Kambalda in Western Australia has been targeted for identification of magnesium, iron, and calcium carbonates and their impact on the porosity by Pearce et al. (2013). They used SEM and EDXS to prepare semi-qualitative elemental maps for identification of simultaneous magnesium, iron and calcium ions replacement in siderite, calcite and dolomite resulting into generation of secondary porosity in these rocks. These simultaneous replacement generate porous siderite and dolomite, increasing the porosity which was correlated to porous siderite in Murteree and Roseneath shales imaged via FIB/SEM techniques. We found that porous siderite and dolomites intermingled with each other and identified as siderite can develop secondary porosity like conventional carbonate reservoirs which have dolomite as a replacement for calcite.

The application of radiation techniques to explore the fabric, pores size distribution and to trace the interconnectivity between various porous domains in a shale formation characterization is of critical importance as recommended by many authors in the preceding paragraphs. Helium measures more free porosity while using mercury for size classification does not seem to be

working due to ultra-low permeability in these formations some researcher in published work argued. Similarly, use of canister gas adsorption techniques is not appropriate and needs milling of shale samples which actually increase the surface area for adsorption leading to overestimate adsorbed content. The application of nitrogen, methane and carbon dioxide for free porosity and pore volume determination have raise doubts about the results, if correction are not made to their adsorption effects in shale gas reservoirs (Bustin et al. 2008). Therefore the application of these coal and petroleum industry standards for reservoir characterisation, formation evaluation, and recovery factor, ultimate enhanced recovery, cannot be is not satisfactorily used in shale reservoirs. All conventional and nonconventional reservoirs evaluation techniques whether they are fluid based or particles based radiation procedures, have advantages, disadvantages and limitations to determine any petrophysical property. Therefore a collective approach based on number of methods and techniques is required to understand the petrophysical nature of unconventional shale gas reservoir in which QEMSCAN can also play a role.

2.3 Unconventional Rock and Mineral Analysis Techniques - QEMSCAN

QEMSCAN technology is used in mining, oil and gas industry due to fast, quick and balanced response for mineralogical identification and quantification evaluation based analyses and outcome. This technique can classify the rocks into shales, carbonates and sandstones leading to make a quick decision about nature of sedimentary interval penetrated during drilling operations. Mineral identification and quantification of shale gas reservoirs is an essential phase of shale reservoir characterization for number of reasons, as mentioned in chapter 1. Pores and porosity for free gas content, clays and residual organics for sorbed gas content, quartz, carbonates and clays content for fraccability test must be investigated and are strongly recommended for any potential shale gas reservoirs. The knowledge of these properties have role in storage, fraccing operations both and in creating artificial pathways for gas production. QEMSCAN capabilities to analyse rock samples in mining have been highly acknowledged while application in conventional reservoirs are far better than unconventional shale gas reservoirs. Rock and mineral qualitative and quantitative by QEMSCAN techniques for petrophysical characterization of shale gas reservoirs have recently been introduced in this area and research work related to this project is follows in next paragraphs.

QEMSCAN identifies various crystalline and noncrystalline mineral phases at much higher speed with quite reliable accuracy, quantify these phases, and later on prepare a digital map for the identification and location of organics sillicates and heavy minerals. From these maps adsorption and compressed gas zones (Lui et al. 2007; Trudgill and Abuckle 2009; Lemmens and Butcher 2011; David and Garrick 2011) can easily be marked. Based on the type and amount of the mineral, QEMSCAN will not only help in giving some insight about the rock fraccability but also will help correlating the values with the wireline logging results as well. It also reveals complex geological depositional environments of unconventional plays from samples.

The false coloured maps generated using QEMSCAN are useful to understand shale mineral characteristics, fissility and lamination, distribution of minerals and zones of high clay and organic concentration, giving invaluable insight about the texture of the sample (Sliwinski et al 2010), without losing the in situ texture and grains arrangement in the scanned sample. But QEMSCAN technique does not provide reliable and useful information about the total porosity and total organic carbon (TOC wt. %). It does help in predicting the brittleness which can help in planning the fraccing operations later on. Therefore it has its own limitation when used to characterize shales as gas reservoirs.

Lemmens et al., (2010) have reported the correlation of FIB/SEM and QEMSCAN results when carbonates reservoir samples from Middle East and shale were irradiated. With ultrafast speed to identify the various minerals, their concentration through 2D false colored maps is prepared using ultra-high resolution and magnification of FIB/SEM. This visual information about formation petrophysical and petrographic characteristics enhance understanding many folds and are helpful in 3D modelling of complex shale reservoirs. When FIB/SEM dual system aided by EDXS and QEMSCAN Automated Mineralogy for mineral identification and quantification mineralogy applied to single sample will further improve and can expose most important variables related directly to storage and flow qualities of any petroleum reservoir. The ultrafast identification and quantification minerals with reliable accuracy have been universally acclaimed when QEMSCAN and FIB/SEM results are compared and total porosity evaluation through QEMSCAN is evolving like FIB/SEM 3D models prepared for shale gas reservoirs.

Knackstedt et al (2010) have tried to integrate QEMSCAN SEM and µ CT Scanning to investigate the rock properties, pore size classification and connectivity and the fluids interaction with the rock matrix in sandstones sample. The major objective of this study was to investigate the wettability and fluids distribution in the rock sample. But they have used sandstones cores plugs and there is a single wetting phase unlike carbonaceous shale where we have dual wettability, organic matter and grains and pore size and distribution vary very much compared to the sandstones. This technique of integrating and incorporating the results from various techniques does not seem to be working in shales.

Armitage P.J. et al., (2010) selected fine grained siliciclastic lithologies from Krechba Field, Algeria (North Africa). These rocks have acted as cap and seal rock for oil and gas petroleum system. The objectives of this research program was to check the strength of SEM and EDXS; X-Ray Diffraction and Fourier Transform Radiation Spectroscopy, MICP, QEMSCAN and Gamma ray log use for fine grained lithologies. The petrogrpahical and petrophysical techniques helped in mineral identification and quantification, pore size classification, porosity evaluation, rock and mineral diagenesis as well as pore zones identification. They reported correlation of porosity between QEMSCAN and MICP results giving very high porosity values in these lithologies. The higher pore sizes documented are questionable and higher porosity values have not been correlated and verified from other experimental work results using same sample.

Lemmens and Butcher (2011a) applied QEMSCAN and FIB/SEM for petrophysical and petrogrpahical evaluation of Marcellus shale samples from Appalachian Basin in USA. They prepared high magnification and resolution mineral and texture map of the Marcellus shale to reveal distribution of inorganic and organic matter pores, their identification and quantification into total pore volume. Determination of total porosity is in doubt and this technology needs more improvement to give a reliable way of evaluating representative total porosity which can be used in initial resource evaluation.

Kanitpanyacharoen et al. (2012) have reported problems about the use of Micro X-Ray Tomographic Microscopy for calculation of porosity when it was compared with MICP results from the same samples. Kimmeridge-aged North Sea shale (UK) and Barnett Shale (USA) were irradiated and scanned applying different Synchrotron Facilities in USA and Switzerland. They differentiated between high and low x-ray signals absorbing areas like pyrite, and pores; fractures and organic/kerogen; their average volumes, and correlation of the results from same samples, scanned at various synchrotron facilities. Minerals average % in both shale samples scanned at three synchrotron facilities were also correlated. They reported that quartz, clays and feldspars distinct identification was problematic. While pores, fractures and kerogen/organic matter can be readily identified. The source of problem was assigned to resolution of these facilities which was less than 3 µm. Kanitpanyacharoen et al. (2012) agreed to extend capabilities of these techniques for petrophysical and mineralogical evaluation of unconventional shale gas reservoirs free of any concerns especially about identification and quantification of porosity and mineral phases.

Quantitative results from QEMSCAN can be correlated with X-ray diffraction results from the same core samples for further verification about the mineralogy of carbonaceous shale. The false coloured digital maps prepared are very useful quick source of rock characterization. The system cannot detect macro, meso and nanopores and presence of organic matter dispersed in the clast is another source of doubt in total porosity evaluation (M. Ahmad and M. Haghighi, 2012). The detail description how this ultra-fast automated technology, QEMSCAN works and results obtained are given in next chapter and later correlation with the XRD and gamma ray log derived clay results for Murteree shales.

The most relevant already published literature to our research project has been perused to enhance the understanding of the petrophysical and mineralogical characteristics of shale gas reservoirs. The selected reviewed research publications have improved understanding about the various methodologies and techniques used, results achieved and outcome found in these publications have highlighted the area where more work is needed to characterize these shales as future unconventional reservoirs more reliably. We have come to know that shale gas reservoir mineralogical and rock qualitative and quantitative evaluation level has been improved. Especially when logs are calibrated with core analyses data of same formation they can prove a source of help and build confidence in formation evaluation. The outcome from QEMSCAN, XRD

quantitative analysis is reliable as proved in this study as well. The issues raised about the modification of conventional wireline logs to identify source rocks in subsurface by Aguilera (1978) have been resolved by Fertl W.H. 1980, Passey et al. 1990 and Jacobi et al. 2008.

Permeability and porosity assessments are most serious issues in petrophysical evaluation of shale gas reservoirs. The evaluation and assessment of permeability of Roseneath and Murteree shales is not in the scope of this research project. Porosity, both effective and total porosity, is part of this research work. It is found that effective porosity evaluation using helium porosimetry and mercury injection techniques is not worthy of application and consideration. Effective porosity values from helium and mercury injections procedures are very doubtful when pores size and density in same samples used for helium and mercury are correlated with 2D images captured using FIB/SEM techniques.

As we see there is plethora of information based on nanoscale 2D images taken using focused ion beam (FIB) milling for preparation of artefacts free surfaces of samples and imaging via SEM and TEM tools. The topography of these samples have been imaged by scanning electron microscope and pores throat size by transmission electron microscopy to enhance and improve pores types, pores morphology, fracture system and their interconnectivity. These 2D images later on have been used to build 3D volumetric shale gas reservoirs but have lost the credibility due to their upscaling application on a reservoir level. An elaborate research and findings about porous nature of shale gas rocks have been done (Bustin et al., 2008, Loucks et al. 2009 and 2011 Wanget al. 2009, Rokosh et al. 2009, Schieber 2009, Wirth, 2009, Curtis, 2010, Passey et al., 2010, Milner et al., 2010, Kale et al., 2010, Sondergeld et al., 2010, Houben et al., 2011, Walls and Diaz., 2011, Fishman et al., 2012, Curtis et al., 2012, Miliken et al., 2013 and Pearce et al., 2013) using SEM on mechanically polished as well as ion milled samples. They have minutely imaged the shale 2D topography revealing details of the microfabric on nanoscale level. In some cases 3D sectioned slices were used for building 3D volumetric model to understand the connectivity of the micro pores and fractures system using BSE signals which are density and atomic number sensitive of scanned material (Sondergeld et al. 2010, Curtis et al 2010, Elgmati et al 2011, Curtis et al. 2012). The application of these details 3D models using FIB/SEM in shale plays still suffer from reluctance to be applied on reservoir scale.

In radiation techniques X-rays have been used, whether they are reflected from the surface to image 2D surface area using SE and BSE signals (FIB/SEM), penetrating rock samples to image pore throat size and porosity (FIB/TEM) and Micro X-ray tomography to expose any detail about pores and fracture system in the irradiated shale sample. Radiations techniques are able to recognize sillicates (authigenic and detrital silica and clays), heavy minerals (authigenic siderite and ankerite, pyrite, sphalerite, titanium and rutile), detailed properties of pores and organic matter spongy/porous morphology by SE signals with confidence. These observations made through the use of FIB/SEM/TEM on shale samples confirm presence of pores, high porosity

concentration domains and fracture system. Also they reveal the distribution of various heavy minerals, their origin and the role in fraccability and selection of well completion site for better production which can be verified by correlation with results from XRD, QEMSCAN and other geochemical analytical techniques. Therefore, it has been overwhelmingly documented, as we found during this literature review, that organically mature and over mature source rocks have high isolated intergranular, intragranular porosity and intracrystalline porosity which cannot be assessed using helium molecule or using extremely high pressure non wetting mercury injection techniques. Identification of pores at nanoscale have contributed a lot in understanding microfabric porous nature of many shale gas formations, mostly marine in North America and lacustrine shales like Roseneath and Murteree shales conducted in this study, first time in Cooper Basin.

Micro and nano computerized tomography (μ-CT and Nano-CT) is a non-destructive technique which have been largely employed with confidence in conventional sandstones, carbonates and shales reservoirs (Welllington and Vinegar 1987, Castanier and Reid, 1989, Lu et al. 1992, Duliu 1999, Ghous et al. 2008, Knackstedtt et al. 2010, Ketcham and Carlson 2001, Coenen et al.2004 Riepe et al. 2011, Gelb et al. 2011) to image pores morphology, connectivity and fracture system to have better understanding about the storage mechanism, flow paths and wettability of these systems. These tools have the power to reveal the fabric of the scanned materials without losing original arrangement and contact of grains, porosity and permeability to build 2D and 3D model. These tools work well for conventional reservoirs due to larger grain size, pore size, connectivity and fractures interconnectivity but when applied to image internal structure of shales they face problems like all other conventional tools. There are still number of issue with the use of microtomography and nanotomography. X-Rays penetrating the shale fabric are sensitive to material density and atomic number. Gray scale threshold is used to identify various phases based on their density and atomic number which overlaps resulting in serious doubts about the integrity of identification of various clays, heavy minerals, pores and organic matter. Also magnification and resolution powers of FIB/SEM/TEM radiation systems are possessing is not achievable in both microtomography and nanotomography.

We think there are some important petrophysical properties whose knowledge of existence can enhance understanding about the reason of very low effective porosity found during helium and mercury use in the experimental results. Also we found evidence of dolomitizartion of siderite to increase the occluded porosity. The interaction between brine, clays and methane has not been investigated. The over maturation of organic matter and its influence on the secondary porosity and late isolated microfracture system development need to be addressed in more details as well.

We found in reviewed research work that pores types, size and morphology in shale gas reservoirs vary on a large scale, from micrometre to nanometre scales. Every selected potential shale reservoir exhibits a unique porous and fracture system based on diagenetic level achieved by inorganic matrix and organic content laterally and vertically. The pore system in one shale play

thoroughly differs with other. These variable pore systems have been heavily verified in previous study. We do not find the reasons mentioned in reviewed literature behind large inaccessible bound pore volumes in overmature source rocks when helium and MICP are applied to check effective porosity. We believe this critical property microlamination in source rock have been overlooked and is the major cause of very low effective porosity when conventional helium porosimetry and even ultra-high pressure mercury injection techniques are used and they fail to indicate the reasons of very low effective porosity.

Siderite ($FeCO_3$ iron carbonate), can have number of ions like Calcium (Ca), Manganese (Mn) and Zinc (Zn) Cobalt, (Co) ions. When these ions are replaced by Magnesium ions, secondary porosity in the sporadic grains of siderite is developed which can increase occluded porosity which is not accessible through helium and mercury injection techniques and through micro and nano-computerized tomography as well. This is a late diagenesis process in overmature source rocks. Siderite dolomitization role has not been mentioned in overmature source rocks. This secondary porosity not just improves fraccability but also increase total porosity to accommodate compressed gas. We found that contribution of heavy minerals like siderite Iron carbonate Fe Mg $(CO3)_2$, ankerite (Fe Mg Mn (CO_3) in total porosity which must be revaluated and included in reservoir evaluation phase.

Understanding of some post depositional changes in physical and chemical properties of mineralogy and organic matter are essential and critical. These changes directly influence rock texture which plays a key role in porosity and permeability of the reservoir. For example generation of fresh and less saline brine during diagenesis, as a consequence of chemical reactions between smectite and potassium ions will lower conductivity and increase resistivity making the use of second Archie's equation valid for water saturation calculation in shale reservoirs.

Biogenic methane gas generation starts after the deposition of the organic matter even before degradation of organic matter into kerogen which is the precursor of oil and gas in a source rock. There is sequential change in physical and chemical properties taking place in kerogen. These progressive irreversible chemical reactions continue due to gradual increase in temperature, pressure and overburden whose ultimate hydrocarbon product is methane, graphite and release of large quantities of nonhydrocarbon gases like CO_2 and H_2S. The generation of excessive amount hydrocarbon and nonhydrocarbon gases will develop secondary porosity and secondary micro fracture system. At this stage of post-over maturation of source rock, most of the organic matter is in the form of graphite which is equivalent to anthracite along with large quantities of methane and carbon dioxide.

We applied QEMSCAN and XRD for minerals and rock characterization. Occasionally the EDXS techniques were used for identification of various mineralogical phases in Roseneath and Murteree shale for elemental maps preparation during FIB/SEM use. Pores types, their

morphology, density and location in matrix, connectivity and microfracture systems were mainly investigated using FIB/SEM and Micro computerized tomography. Helium porosimetry and MICP conventional laboratory techniques to check the effective porosity and pores throat size. For water saturation wireline logs were used. These techniques application with detailed methodology, results discussion and conclusions are given in next chapters.

CHAPTER 3

Mineralogy and Petrophysical Evaluation Using QEMSCAN, Micro and Nano CT-Scanning, FIB/SEM and XR-Diffraction Techniques

3.1 Introduction

In this chapter radiation techniques applied for petrophysical and mineralogical evaluation of Murteree and Roseneath shales are described in detail to have better understanding of the goals achieved at the end and mentioned in the conclusion part of this dissertation as well. It also highlights the needs for necessity of various techniques to check the reliability of the information and data correlation.

Every shale gas play has different reservoir properties because each shale gas formation has unique provenance from where the clast was derived, transporting agent and depositional environment and later due to post depositional biological, physical and chemical changes undergone by the sediments (Halliburton 2008). The amount of gas stored and its producibility depend on many factors in selected organically rich source rocks like preserved amount of organic matter, its maturity, reservoir temperature, pressure, porosity, mineralogy, permeability, rock brittleness and success of fraccing operations (Josh et. al., 2012). To estimate the total free porosity in shale samples, different conventional and unconventional evaluation techniques need to be integrated for correlation to check the integrity of the evaluated parameters. We have integrated QEMSCAN, Computerized Tomography (micro and nano CT scanning), FIB/SEM and XRD techniques to characterize Murteree and Roseneath shales to identify and quantify mineral contents for rock classification. The foremost objective of QEMSCAN was identification and quantification of constituent minerals and used these results to classify core sample as a rock type. Results from QEMSCAN were correlated with X-Ray diffraction outcome to check the accuracy of the results from both methods. The second objective was to investigate total porosity based on constituent minerals, organic matter content and its maturity, pore types, their interconnectivity and fracture system using FIB/SEM and Computerized Tomography based on visualization of 2D high magnification and resolution slices/images of these samples. The samples scanned and investigated were taken from same depth in the project wells for all these four techniques. In the following sections, core samples preparation procedures are presented followed by reviewing different scanning and imaging methods in detail using schematics and illustrations. Then the visualization and quantitative results are presented and discussed. Some conclusive remarks are mentioned in the last section of this chapter.

3.2 Mineral and Rock Evaluation (QEMSCAN)

The Murteree shale sample was crushed into small chunks ranging 1-2 cm in length. The two selected samples were mounted into epoxy resin first; surfaces were mechanically ground,

polished and carbon-coated later, before performing analysis as shown in figure 3.1 below (Swierczek 2012).

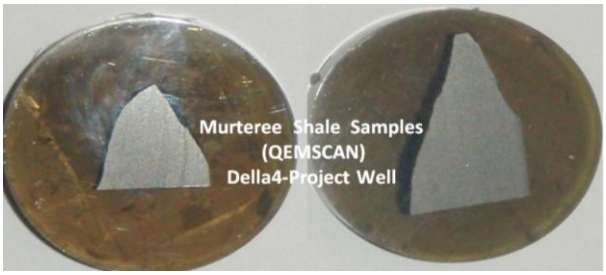

Figure 3.1: Murteree Shale resin embedded two samples used for QEMSCAN techniques and SEM Imaging.

Samples were scanned using field scan mode of automated mineralogy system. A schematic of the working of the automated QEMSCAN system first to generate characteristic x-rays to identify minerals in the prepared samples and later how the energy and wavelength can be applied to quantify minerals into rocks is explained. Steps **A1 –A5** in figure 3.2 have been illustrated **how** estimated energy and wavelength for identification and quantification of minerals and rock classification in QEMSCAN techniques was applied to Roseneath and Murteree shales samples. Red circles surrounding nucleus marked as **I, 2** and **3** shows electrons while $\mathbf{E_0}$, $\mathbf{E_1}$ and $\mathbf{E_2}$ are bound energies of **K, L** and **M** shells around the nucleus (**n**) of the atom and **ΔE** is the energy released when an electron drops from lower energy level to higher energy level and **λ** is the wavelength of signal emitted (French D. et al. 2008).

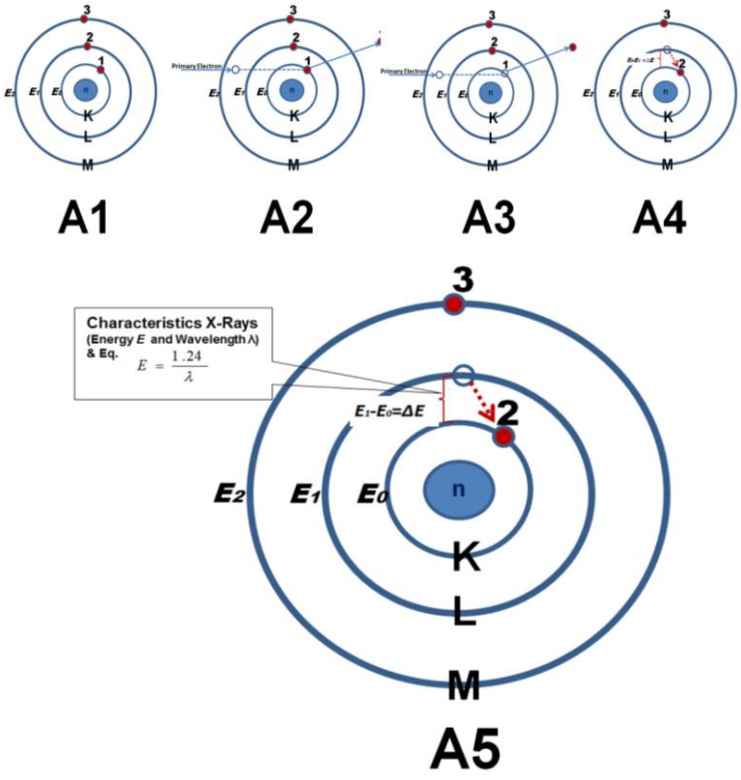

Figure 3.2: Schematic of production and estimation of characteristics x-rays

In table 3.1 below how estimated characteristics x-rays energy (*E*) and wavelength(*λ*) as shown in figure 3.2 in the preceding page is used for identification and quantification of minerals in rock samples by QEMSCAN techniques (French D. et al. 2008).

Table 3.1: Identification and quantification of minerals in rock samples by QEMSCAN techniques (French D. et al. 2008).

Element	Atomic Number(A)	K_α – X-ray Line	
		Energy (*E*) (KeV)	Wavelength (λ) (Angstroms)
Sodium	11	1.041	11.19
Magnesium	12	1.254	9.89
Aluminium	13	1.487	8.339
Silicon	14	1.740	7.125
Phosphorous	15	2.014	6.157
Sulphur	16	2.308	5.372
Chlorine	17	2.622	4.728
Potassium	19	3.314	3.741
Calcium	20	3.692	3.358
Titanium	22	4.511	2.749
Manganese	25	5.899	2.102
Iron	26	6.404	1.936

The polished and carbon coated Murteree shale sample was split into a number of grids as shown in figure 3.3 part A. The analysed fields were then stitched into a single composite image allowing mineral associations and distribution to be visually represented for interpretation as shown in figure 3.3, part B. Preliminary scans of the sample indicated that the cuttings mounted in the resin gave better results in terms of the phase identification compared to those without the resin. The observations made on sample without resin and inappropriate polishing can generate result with some concerns about minerals identification and consequently in the quantification which is mainly related to uneven scanned surface. The data presented here is based on the analysis of the resin embedded sample being measured with 5 µm spacing resolution. A total of 64 fields were collected, each 1000 µm in size, as shown in figure 3.3 part A. Low count (1000) X-ray spectra were collected from each analytical point. Major phases such as quartz, muscovite/illite, kaolinite, siderite as well as the organic carbon were virtually extracted using software embedded in the QEMSCAN system [to] highlight their distribution.

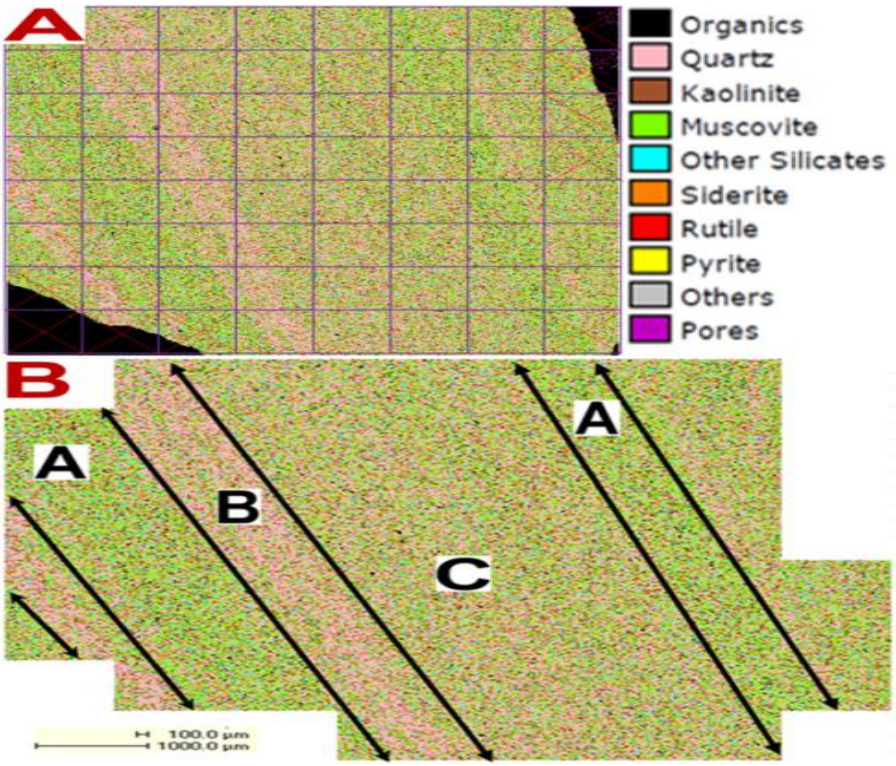

Figure 3.3: **(A)** Murteree shale false coloured digital map **(B)** Identification of laminations/streaks labelled as A and B prepared using QEMSCAN.

The identified and quantified minerals phases were expressed in volume (%) and mass (%) as given in table 3.2 while the digital bar map of scanned Murteree shale showing mass percentage of each mineral content are given in Figure 3.4 as well.

Table 3.2: Mineral constituents distribution (volume% and mass %, grain and pore size) in Murteree shale sample presented in figure 3.3.

Organics & Inorganics Phases	Phase Volume (%)	Phase Mass %	Phase Grain & Pore Size (Avg. µm)
Organics	**02.49**	**01.91**	**9**
Quartz	**44.02**	**42.78**	**18**
Kaolinite	**14.32**	**14.09**	**10**
Muscovite/Illite	**28.37**	**28.96**	**12**
Other Silicate	**04.54**	**04.36**	**9**
Siderite	**05.35**	**06.75**	**12**
Rutile	**00.79**	**01.03**	**9**
Pyrite	**00.02**	**00.04**	**15**
Others	**00.07**	**00.08**	**8**
Pores	**00.02**	**N/A**	**7-pore size**

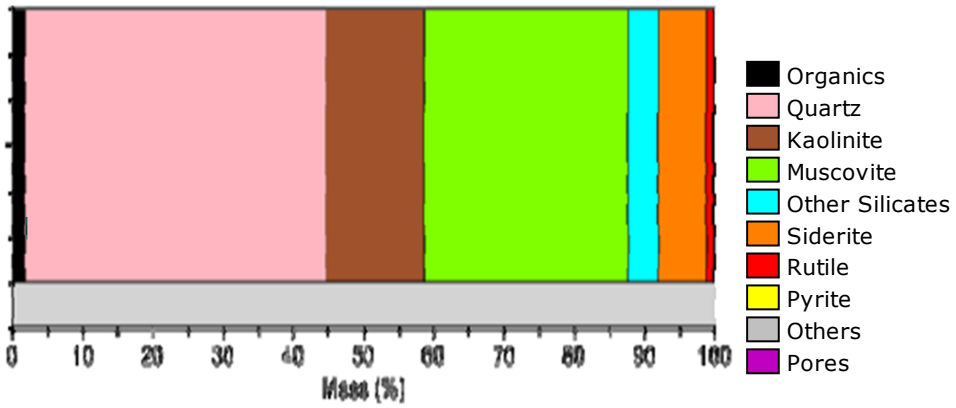

Figure 3.4: Bar map showing mass % of constituent inorganic and organic phases using QEMSCAN automated system.

The same Murteree shale sample prepared for QUEMSCAN analysis was compatible for Scanning Electron Microscopy (SEM) imaging to capture micro and nanoscale 2D images. QEMSCAN and SEM both have built-in system called energy dispersive x-ray spectroscopy (EDXS). A detail description how a SEM system works is given in more detail in section 3.4. Both QEMSCAN and SEM use backscattered and secondary electrons reflected from the sample surface for imaging and identification of mineral phases, using x-rays characteristics analysis techniques, except the latter (SEM) cannot quantify the constituent mineral phases identified in the sample. The inelastic collision of primary beam with sample's atoms, generate secondary electrons following a complex path when returning back to EDS (Volkert and Minor 2007). From SEM electron beam and sample atoms interaction, three types of signals are produced namely: secondary electrons; back scattered electrons; and characteristic X-rays. These signals generated by the bombardment of the electron beam are used to characterize a sample (David and Butcher 2008). To image the topography of the sample, secondary electrons are used. Back scattered electrons are used to identify the different types of material based on density variation, while characteristic x-rays are used for the identification and quantification of elements in minerals in the samples. The sample is coated with carbon to make it conductive for electron beam before imaging the surface using returned secondary electrons from sample surface. EDXS techniques give quick semi-qualitative elemental map to aid the mineral phase identification and are not powerful as QEMSCAN. SEM-Quanta450 with high vacuum can also be applied to image and analyse surface topography and morphology using secondary electrons emitted after interaction of the sample atoms with focused electron beam. The later SEM-Quanta450 system was used for the validation of identified minerals in QEMSCAN technology. For example siderite mineral presence was validated and checked using EDXS in SEM-Quanta450 and later all other mineral phases presence was also checked using the same procedure. In QEMSCAN techniques X-rays from SEM system are used to produced Characteristics X-rays from sample under investigation for analyses, while in micro and nano CT-Scanning, X-rays from an external source are used to strike and penetrate the sample to record changes in the strength of the x-ray signal on a detector for characterization of shale samples petrophysical properties.

3.3 Micro and Nano CT-Scanning Techniques

Samples from same core chips, used for QEMSCAN were cut for CT-Scanning analysis. In CT-Scanning analysis samples do not require very special preparation method. A specific width and length of the sample is required to make sure that it fits into the CT Scanning sample holder as shown in figure 3.5. Actually the sample holder is mounted on a rotating motor in front of continuously penetrating x-rays monochromatic collimated beam, in a 360° manner as illustrated in figure 3.5 part A. The x-rays are partially absorbed by rock grains and partially pass through sample to be detected on the detector screen finally. The recorded intensity of the penetrated x-rays is used to make multiple images of the internal structure of the scanned sample and the data recorded on the detector is converted into digital data file.

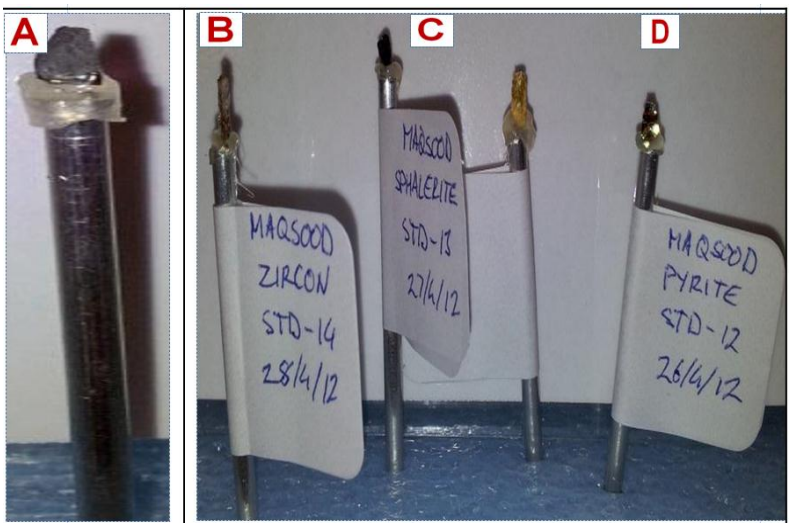

Figure 3.5: (A). Murteree shale sample mounted on aluminium tube with glue to be scanned by Micro - Computerized Tomography and (B) (C) and (D) are zircon, sphalerite and pyrite mineral standards.

Murteree shale sample was placed between the x-ray source and 2D detector screen on which the various intensities of the transmitted x-rays were recorded. While rotating in front of the x-ray beam, digital images mapping numerical value of the attenuation coefficient (attenuation profile data) was continuously recoded before sending to processor for reconstruction of 2D (XY-slices) and later used for 3D modelling (Coenen et al. 2004; Diaz 2009). The linear attenuation coefficient is converted into signal, passing through each point of 2D-XY slice and is expressed by CT-Number, whose numerical value represents the density and the chemical composition of the point. The focal spot diameter of x-ray source, detector resolution, distance between the focal spot and centre of object scanned are crucial parameters which are considered important to achieve desired resolution and information about scanned sample (Coenen et al. 2004; Long et al. 2009). Although there are some concerns about porosity estimation using X-Ray computed tomography (Taud et al., 2005), it is widely used as scientific research in geosciences and material sciences. For micro and nano CT scanners a low energy laser ablation system was used to avoid any stress. Any stress can develop some artificial fissures, porosity or micro-cracks in the

investigated sample leading to any erroneous judgement about the internal intrinsic petrophysical properties (Coenen et al. 2004; Diaz 2009). The size and diameter of the sample and pixel size of the images obtained vary in micro and nano CT-scanning analysis (Diaz, 2009). A 1.0 mm long and 0.5 mm wide chip was selected for microtomography to fit into 6.00 cm long sample holder to investigate any internal micro fracture system, pores size distributions, interconnectivity and classification. For nanotomography a fragment of sample was glued on the tip of pen, inserted into the sample holder of XRCT system. An illustration is given in figure 3.6 below to express graphically how x-rays are applied to penetrate the sample to obtain digital data/files and later converted into useful information about the internal structure of the scanned reservoir rock sample as shown in figure 3.7.

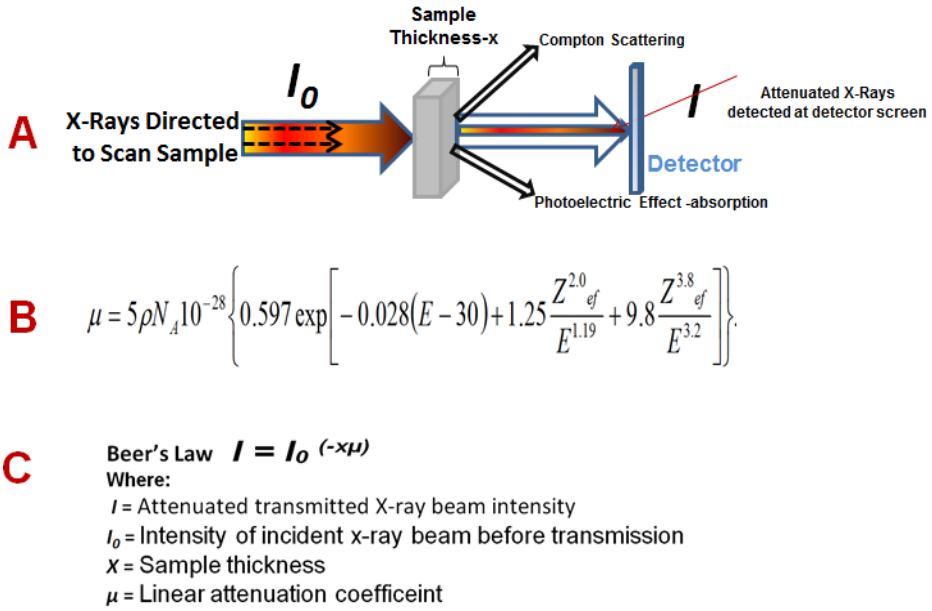

Figure 3.6: Schematic illustrating x-rays application (A) for detection of attenuated x-rays (***I***) and (B) mathematical expression used for linear attenuation coefficient estimation, ***μ*** using (C) Beer's law (Curry et al., 1990; Duliu 1999).

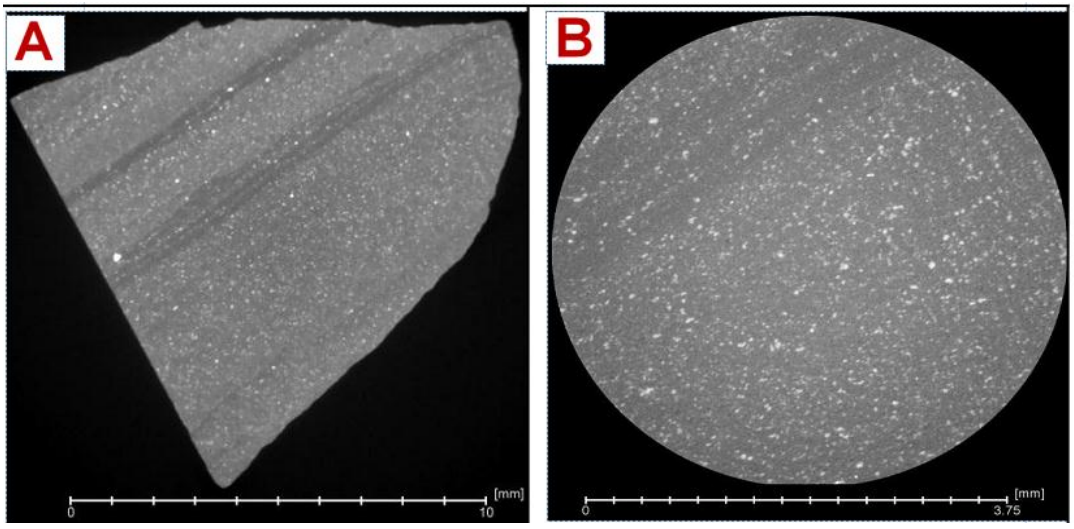

Figure 3.7 Slices of Murteree shale sample embedded in resin in X-Y plane imaged by Micro X-Ray CT technique (A) and (B)**.**

3.4 FIB/SEM (Focused Ion Beam Milling/Scanning Electron Microscopy)

Integrated focused ion beam (FIB) milling and scanning electron microscope is referred as dual beam system and is capable of cutting away specified area followed by imaging surface of the sample after sectioned volume of sample. Focused ion beam (FIB) systems have been in use for more than twenty years and operate in a way similar to a scanning electron microscope (SEM). In FIB a gallium ion (Ga^+) or Argon ion (Ar^+) beam is focused by FIB column in system at low beam currents for imaging or high beam ion current for site sputtering or milling to prepare samples free of any artefacts to have better understanding about the desired properties of the milled surface. A detail description, how this technology works is not in the scope of this research but a schematic showing all the components of a focused ion beam column is given in figure 3.8 below and samples used are shown in figure 3.9.

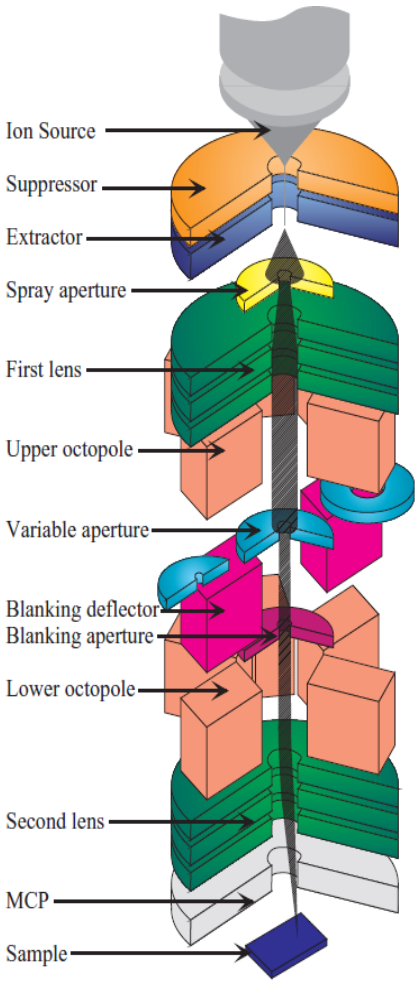

Figure 3.8: Schematic diagram of a FIB (Focused Ion Beam) column **(**Reyntjens and Puers 2001)

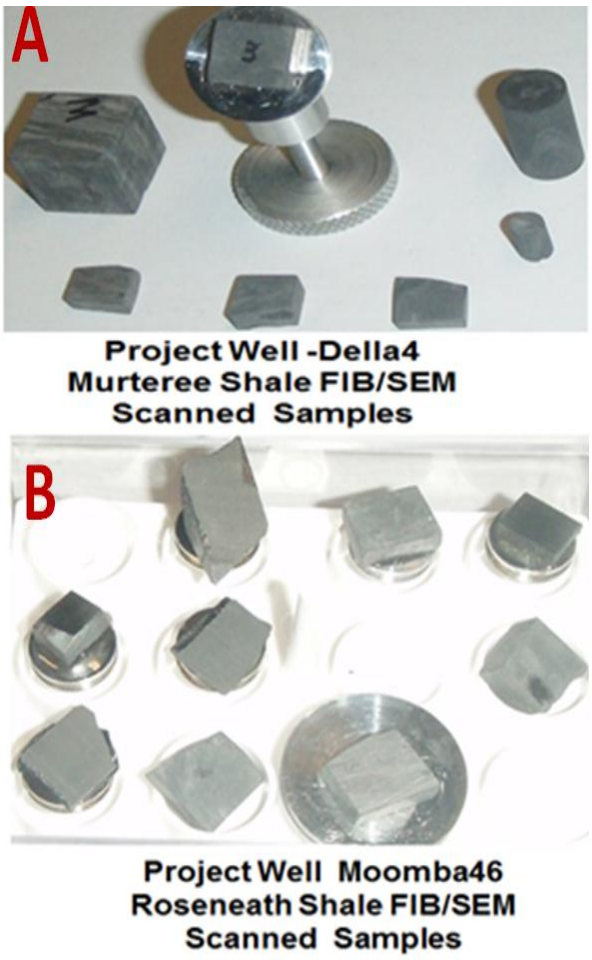

Figure 3.9: Murteree Shale (A) and Roseneath Shale (B) samples prepared using focused ion beam milling and later imaged using secondary and back scattered electron signals in Scanning Electron Microscopy.

Samples prepared using traditional mechanical methods of grinding and polishing rock samples are not suitable to image various types of pores, their interconnectivity, any fracture system and interconnectivity which have key role in reservoir characterization of shale gas reservoirs especially in ultra-fine grain shale formations. The most favourable and strongly recommended technique used for these shales is the use of focused ion beam milling procedure. There are a number of different types of liquid metal ion sources (LMIS) and most widely used is Ga^+ (Gallium) based blunt needle source. Ga^+ has decided advantages over other LMIS metals such as In (Indium), Bi (Bismuth), Sn (Tin), and Au (Gold) because of its combination of low melting temperature (30°C), low volatility and low vapour pressure. The low melting temperature makes the source easy to design and operate. Ga^+ ion does not react with the material defining the needle (typically W Tungsten) and evaporation is negligible. Also Ga^+-based LMISs are typically more stable than other LMIS metals. During operation, Ga^+ flows from a reservoir to the needle tip (with an end radius of about 10 mm, where it is extracted by field emission, a large negative potential between the needle and an extraction electrode, generating an electric field of magnitude 10^{10} V/m at the needle tip. The balance between the electrostatic forces and the Ga^+ surface tension wetting the tapered W (Tungsten) needle geometry results in the formation of a single taylor cone at the needle tip. For typical emission currents used in FIB microscopes (~2 mA), a cusp forms at the tip of the taylor cone (Bolinger and Fink 1980; Reyntjens and Puers 2001; Volkert and Minor, 2007). The ion milled samples of Roseneath and Murteree shales used in this research project are shown in figure 3.9 on preceding page.

A scanning electron microscope (SEM) images a sample by scanning it with a high energy beam of electron in raster scan pattern and the resolution to see distinctly submicron size particles and fabric. The images at such resolution are achieved by very small electrons beam wavelength and power of electrical lenses in SEM system. The electrons interact with the atoms that make up the sample producing signals that contain information about the sample's surface topography, composition and crystallographic details about the material. In electron beam column of SEM microprobe, the FIB milled sample is bombarded with electrons using a focused electron beam generated by electron gun, and these electrons scatter after interacting with atoms in sample. These scattered electrons lose energy after colliding with atoms in sample, and they follow complex twisting paths as they return back to the scanning electron microscope (Volkert and Minor, 2007). From this electrons and atoms interaction phenomenon, three types of signals are produced namely: secondary electrons; back scattered electrons; and characteristic X-rays. After emerging and returning from scanned sample surface to the SEM they are collected using backscattered x-rays and secondary electron detectors. These signals generated by the bombardment of the electron beam are used to characterise a sample (French and Butcher, 2008). To image the topography of the sample, secondary electrons are used. Back scattered electrons are used to identify the different types of material based on density, while X-rays are used for the identification of elements in minerals present in the scanned sample. The sample is coated with carbon before imaging the surface using secondary electrons.

There are two types of electron scattering when a beam of electron hits the sample surface, namely elastic and inelastic. In elastic scattering electron changes direction through interaction with the sample but loses negligible energy. This process leads to spreading of the electron beam in the sample. While in inelastic electron scattering the electron loses energy through interaction with the sample and is considered to produce secondary electrons. X-rays, electromagnetic radiation have wavelengths ranging from 10 to 0.01 nm, much shorter than visible light. In the electron microscope, characteristic X-rays are used to analyse elemental composition with high spatial resolution. A wide range of magnifications is possible, from about 10 times (about equivalent to that of a powerful hand-lens) to more than 500,000 times, and about 250 times the magnification limit of the best light microscope. We can image surface and topography of the ion milled surface of sample on micron to nanoscale, classify and identify pores and their origin and relation to organic and inorganic matrix part. It is also possible to use this technique for pore size distribution and classification (Micro, Meso and Macro pores), quantify the pores and porosity by point counting in 2D-imaged slices. It is also possible to use the system capability of sequential sectioning and imaging of a predefined volume of the rock to build 3D representative volumetric model to see interconnectivity of the pores and fracture system. Figure 3.10 shows the various component of a Dual FIB/SEM system applied in this methodology.

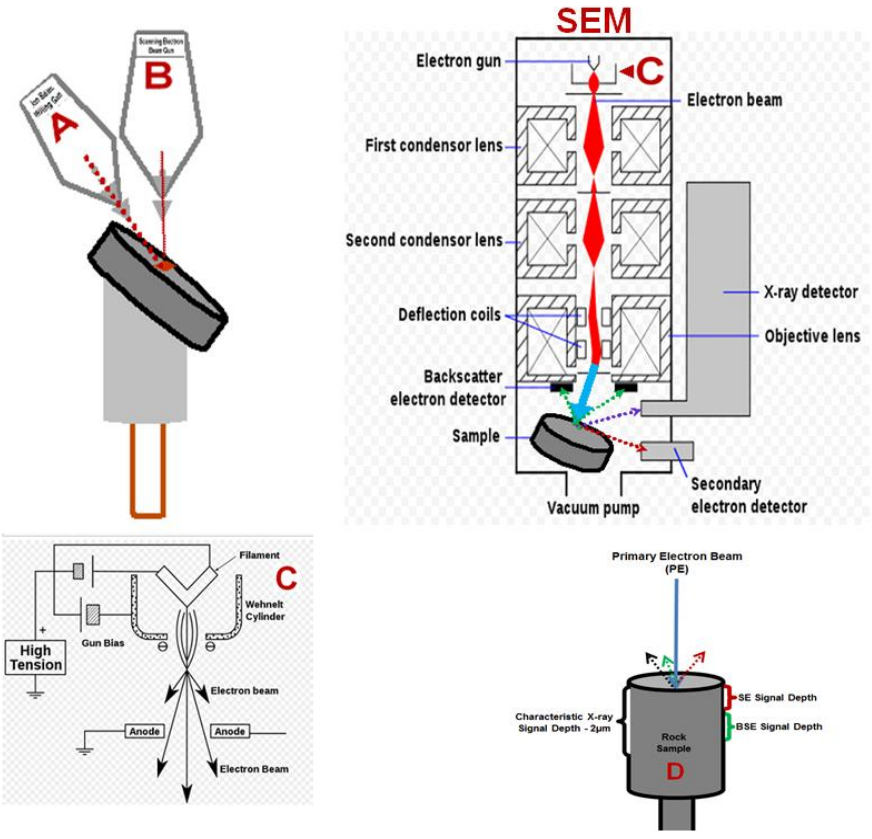

Figure 3.10: Schematics of Focused Ion Beam Gun (A), Scanning Electron Gun (B), Scanning Electron microscope (SEM-Column) with an angle 52° to each other, chambers with different internal components and Electron Beam Gun (C), used in FIB/SEM milling and imaging techniques. Schematic (D) showing penetration depth of secondary electron (SE) and backscattered electron (BSE) after the primary electron (PE) beam has hit sample surface (Silin 2010, Elgmati et al., 2011 and Curtis et al., 2012).

In the SEM microprobe, the sample is bombarded with electrons using a focused electron beam, and these electrons scatter after interacting with atoms from the sample. These scattered electrons lose energy after colliding with atoms from the sample, and they follow complex twisting paths as they return back to the scanning electron microscope (Volkert and Minor, 2007) resulting in the production of three types of signals, secondary electrons; back scattered electrons; and, X-rays. These signals generated by the bombardment of the electron beam are used to characterise a sample (French and Butcher, 2008). To image the topography of the sample, secondary electrons are used. Back scattered electrons are used to identify the different types of material based on density, while X-rays are used for the identification of elements in minerals in the samples. The sample is coated with carbon before imaging the surface using secondary electrons.

To check the morphology of pores and total void space, both connected and isolated, a combined system of FIB and SEM was the best option to image the polished surface of the Roseneath and Murteree shales The images taken using SEM expose overwhelming details and nature of the particles, pore size and morphology, and the contact between grains. The impact of these characteristics on permeability and porosity in these very fine grain sedimentary rocks is shown in figure 3.11 of Roseneath Shale image captured by FIB/SEM system. For example In figures 3.11 and 3.12 the arrangement of the grains is highly chaotic causing high total free porosity. Similar types of pores and morphology have also been presented in images of Roseneath and Murteree shale attached as appendices A and B at the end of dissertation. To check the reliability of FIB/SEM system output SEM-Quanta450 was also used. SEM-Quanta450 with high vacuum was applied to image and analyse surface topography and morphology using secondary electrons emitted after interaction of the sample atoms with focused electron beam. This system was also used for the validation of identified minerals using QEMSCAN technology. The inelastic collision of primary beam with sample's atoms, generate secondary electrons following a complex path when returning back to EDS (Volkert and Minor 2007, David and Butcher 2008). These signals generated by the bombardment of the electron beam are used to characterize a sample (David and Butcher 2008). To image the topography of the sample, secondary electrons are used. Back scattered electrons are used to identify the different types of material based on density variation, while characteristic x-rays are used for the identification of elements in minerals in the samples. The sample is coated with carbon to make it conductive for electron beam before imaging the surface using returned secondary electrons from sample surface. The advantages and quality of the images prepared using FIB milled samples are expressed by Roseneath and Murteree shales which have been labelled with types of minerals, organic matter, type of porosity and fractures in figure 3.11 and 3.12 below.

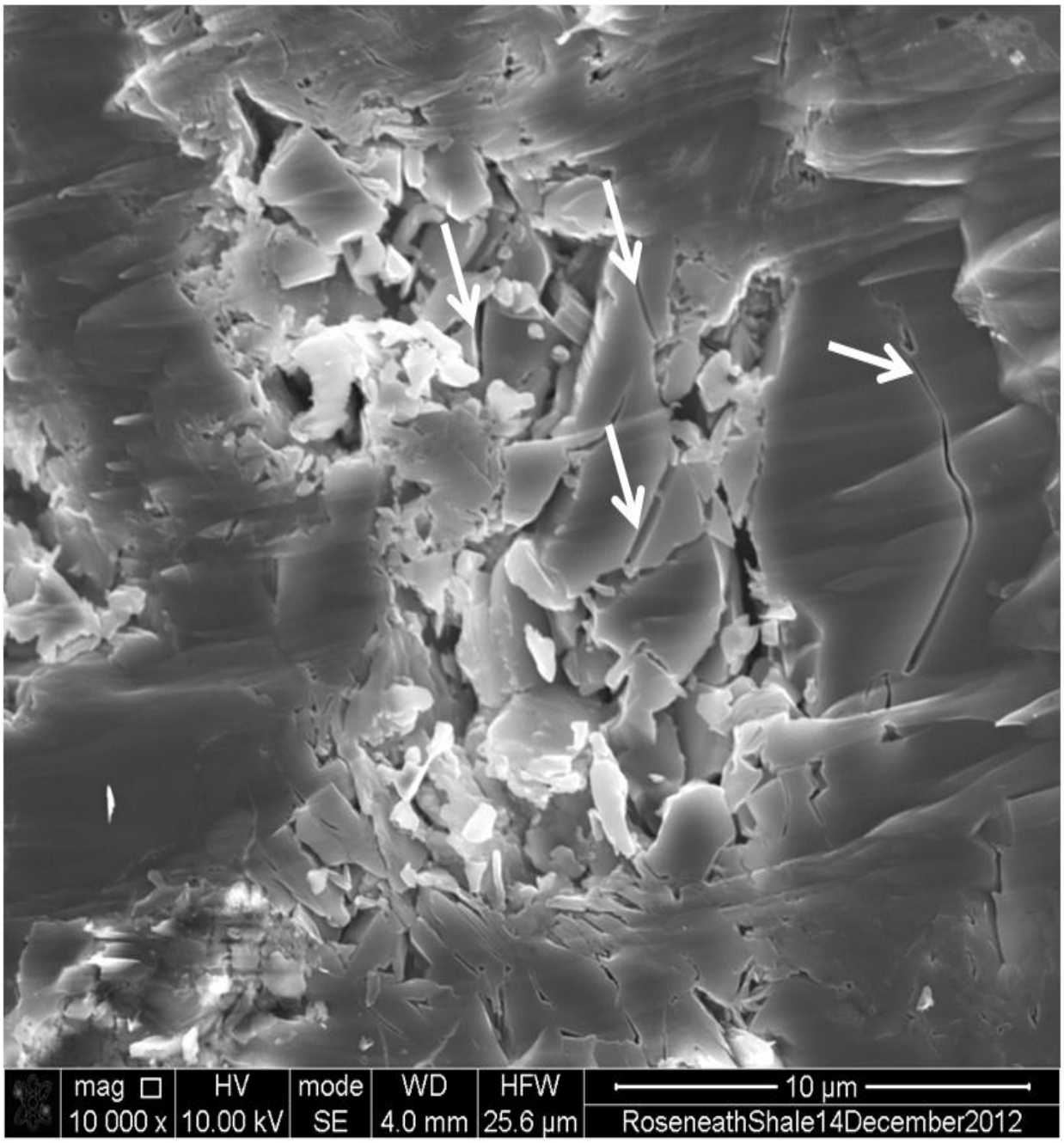

Figure 3.11: Roseneath shale sample prepared using FIB techniques showing the image quality to identify intergranular/interparticle/interstitial porosity, minerals, flocculation organic matter and fracture system marked by white arrows. The “Curtains” effect of FIB milling procedure is evident in this image.

Key/legend (FIB/SEM system generated 2D image):

(**mag** = Magnification; **HV** = High Voltage –Accelerating Voltage); **mode** = Back Scattered Electron Beam Detector or Secondary electron Beam Detector Usage); **WD** = Working Distance (distance from the bottom of the SEM column to the sample surface); **curr** = Current; **HFW** = Horizontal Frame Width.

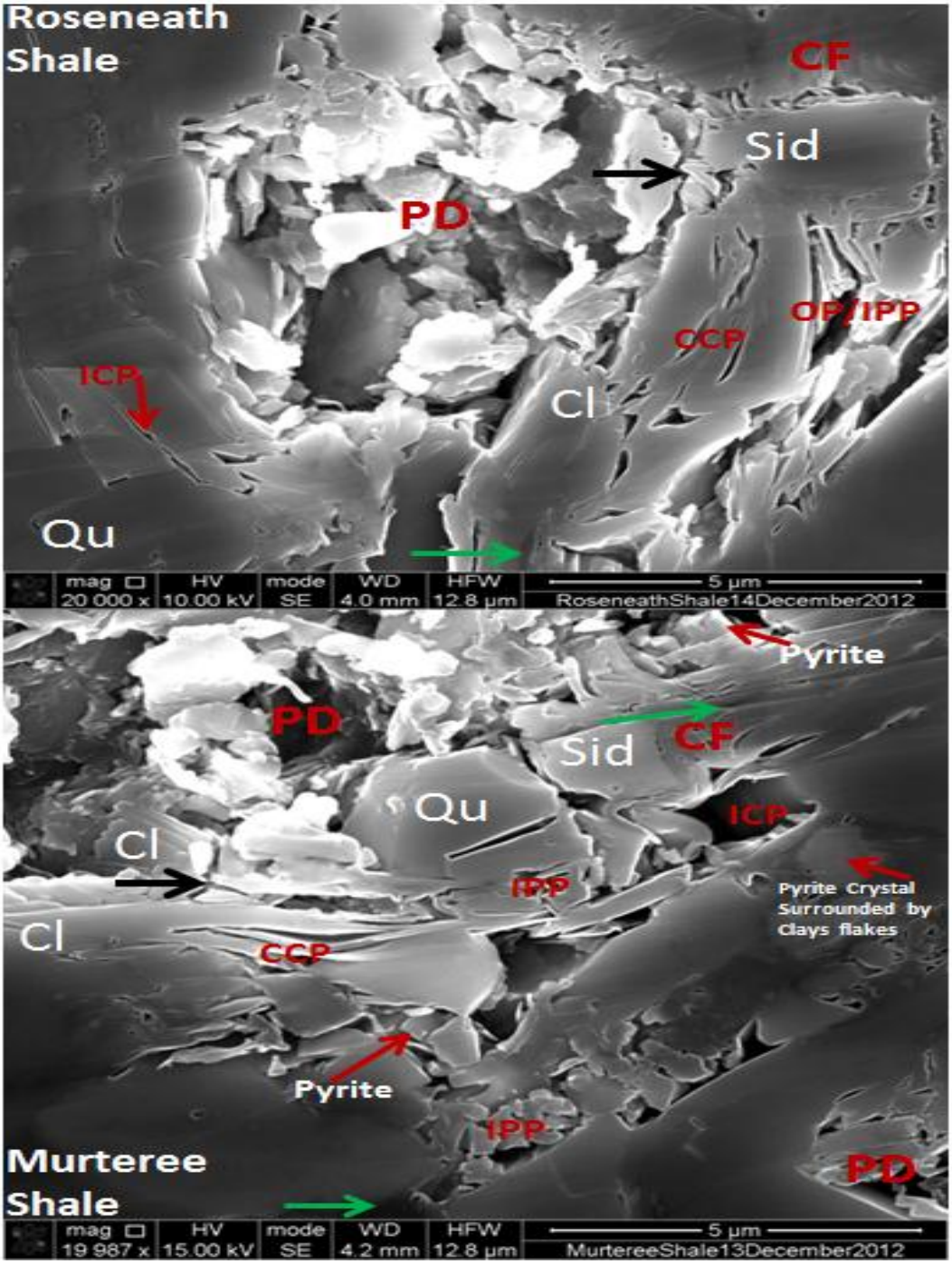

Figure 3.12: Roseneath and Murteree shale samples prepared using FIB techniques showing the image quality to identify intergranular/interparticle/interstitial porosity, minerals, flocculation organic matter and fracture system. (Green Arrows= Organic matter; Black Arrows= Fractures; IPP= Interparticle porosity; PD=Porous domains; ICP=Intercrystals porosity; CCP= Clay cleavage porosity; Cl= Clay; Qu= Quartz; Sid=Siderite and OP= Occluded porosity).

3.5 XRD Quantitative Techniques (Rietveld)

Small chips of Murteree shale were pulverised mechanically using Labtechnics vibrating grinder for Rietveld-based Quantitative XRD analyses to identify and quantify the various mineral phases.

Powder sample was later sieved before using in the X-ray diffractometer in laboratory. Samples used for XRD are given in figure 3.13.

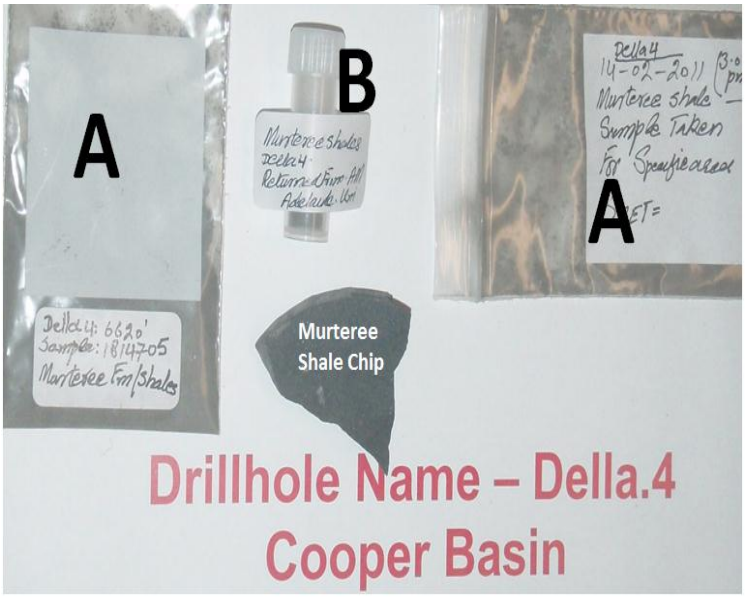

Figure 3.13: Murteree shale (A & B) powder samples in plastic bags used for XRD analyses and small chip before grinding the sample into powder.

A beam of X-rays strikes powder sample or crystals in a sample and diffracts into many beams in specific directions. The angles and intensities of these diffracted beams when collected after collimation make it possible to produce a three-dimensional picture of the electron density within the scanned sample. Therefore, using this output it is possible to locate the positions of the atoms and determine the structure of the molecule or molecules within the crystal and powder of rock sample. It provides information on structures, phases, preferred crystal orientations (texture), and other structural parameters, such as average grain size, crystallinity, strain, and crystal defects. X-ray diffraction peaks are produced by constructive interference of a monochromatic beam of x-rays scattered at specific angles from each set of lattice planes in a crystal sample. The peak intensities are determined by the distribution of atoms within the lattice. Consequently, the x-ray diffraction pattern is the fingerprint of periodic atomic arrangements in a given material. A standard database of x-ray diffraction patterns enables quick phase identification for a large variety of crystalline samples.

H.M. Rietveld (1969) introduced an improved X-ray diffraction technique for use of full XRD profile generated using x-ray diffractrometry which was later extended to evaluate the mineral percentages in a mixture or powder of a given rock sample. The same method was used for identification and quantification of minerals in powder sample of Murteree shale which we have already scanned using QEMSCAN to validate the accuracy of the results in the latter. The Extended Rietveld methodology uses the calculated XRD profile of each (phase) mineral in the sample to be generated from its refined crystal structure, and the sum of all calculated patterns to be fitted to the observed XRD profile of a multi-mineral mixture by least-squares analysis to find

the optimum phase scales. The phase scales are then used to determine the individual mineral percentages represented in the sample. The Shcematic in figure 3.14 showing how XRD techniques are used to quantify the mineral phases A), diffraction of X-rays from a set of atomic planes in sample crystals/powder and showing constructive interference at angles where the Bragg equation is satisfied (B), **ɵ** incident angle, **d** spacing between two atomic planes and **λ** is the wavelength of the incident ray and a diffractogram used for identification and quantification of various minerals in the sample expressed in (C) (Ward C. R. and French D. 2002) is given in figure 3.14.

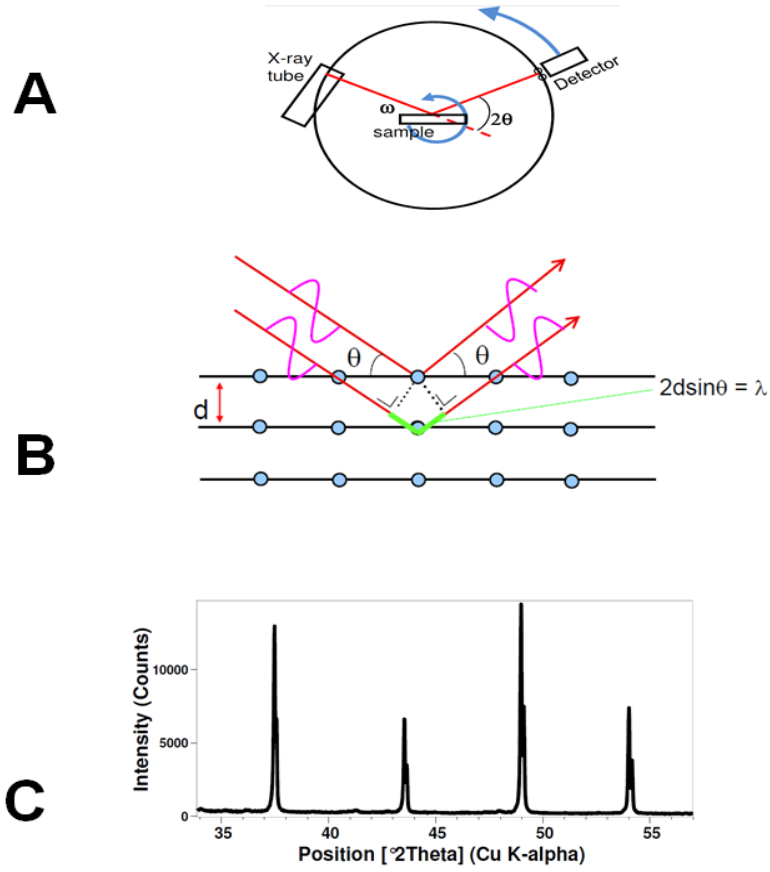

Figure 3.14: Schematic showing the working of the X-Ray diffractometer.

3.6 Results

QEMSCAN automated technology results were generated from wavelength and energy of the emitted photons as characteristic rays, for identification and quantification of minerals in scanned sample. QEMSCAN mineralogical data indicates that Murteree shale consists mainly of quartz (45%) and K-Aluminium silicates represented mostly by muscovite/illite (30%). The QEMSCAN technique provides quantitative measurements of both crystalline and non-crystalline phases with distinct elemental composition. SiO_2, for example, can be represented by either quartz (crystalline) or opal (amorphous). Any silica phase found in the sample was reported as quartz in this analysis. The mineral assay based on mass % of each constituent mineral is shown first in figure 3.4 and table 3.2. The clay minerals are also present with kaolinite dominating (15%).

Among the other silicates K-feldspar and assumed chlorite as well as smectite were found. Due to difficulties in differentiating the fine grained layered clays, XRD analysis was separately conducted on the standards constituent minerals for further verification and identification of the different phases. Among other minerals, siderite, rutile, pyrite, sphalerite, zircon and some unknown traces of mineral matter were also observed and reported. Apart from the inorganic minerals, organic carbon was calculated to be present at approximately 2%. The mass and volume of each phase identified using EDS-SEM are presented in table 3.2. The calculation of pores versus mineral matter is presented in volume % only (as pores have density of 0 g/cm^3). However, this number is underestimated due to the limit of the QEMSCAN resolution for this purpose. To investigate the pore size (micropores<2 nm; mesopores 2-50 nm while macropores > 50), pore size distribution and pore shape (cylindrical, slit, ink bottle, wedge shape) SEM images were used later.

Micro and Nano Computerized Tomographic Scanning was applied to investigate the internal arrangement of the micro fabric, fracture system, interconnectivity of the pores and the fracture system. Compton scattering (incident energy >>100 KeV) and photoelectric absorption (incident energy << 100 KeV) a dual scanning system was used in both Micro and Nano computerized tomography techniques to reveal internal petrophysical features and properties of the sample under investigation. Micro and nano CT Scanners uses a collimated X-ray beam received on the detector screen after passing through the sample. The X-ray attenuations takes a projection at each angular position, and from these projections, a cross-sectional slice as one shown in figure 3.15 for Murteree shale, is reconstructed by a computer algorithm. When attenuations from all planes, in scanned images, are superimposed, a CT image can express details about the internal structure of the sample in black, grey, white and bright areas as shown in figure 3.15. Later a 3D model based on these slices can be constructed as shown in figures 3.7 and 3.15. Using region of interest command, in the CT-scanning software, a series of cross-sectional slices are selected to identify the various zones of interest. These images showing silicates, heavy minerals, organic matter and pores, are colourized for identification of their morphology, based on their individual densities and chemical composition to enhance the understanding, as shown in figure 3.16.

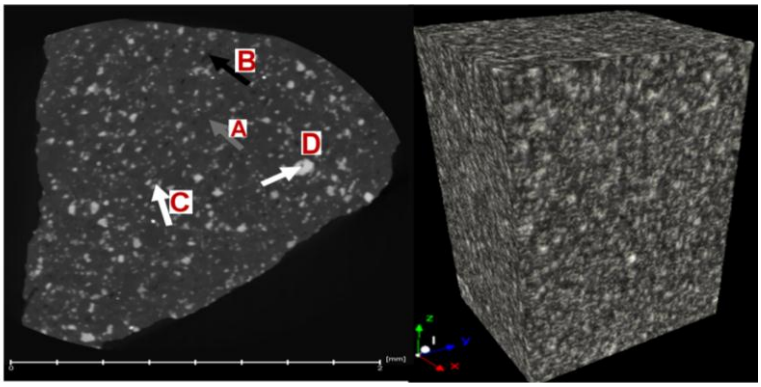

Figure 3.15: XY slice of microtomogram of Murteree shale using Micro-X-ray Computerized Tomography (black, gray, white and bright areas by A, B, C, and D).

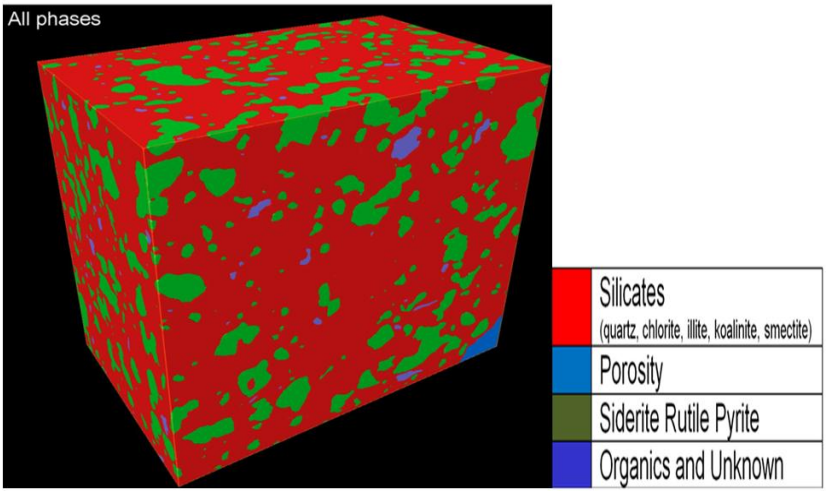

Figure 3.16: 3D Model of Murteree shales sample. Red = silicate phase, Green = Heavy minerals like siderite rutile, Light blue = Porosity; while Blue Colour = Represents the lowest density phase Organics and unidentified phase using Micro-X-Ray Computerized Tomography.

Signals generated and used for the characterization of shale sample are namely, secondary electrons, backscattered electrons, and characteristic X-rays. We used secondary electrons ejected from the near surface of the sample for imaging and to have better understanding of the topography, pores morphology and pores classification. The results and images in figures 3.17 and 3.18 show the use of secondary electrons. A vast majority of pores in figures 3.17 and 3.18, especially identified in clay rich zones are less than 1 µm, as documented by labelling with the dimensions in figure 3.17. These pores contribute a large quantity of intergranular porosity towards the total free porosity.

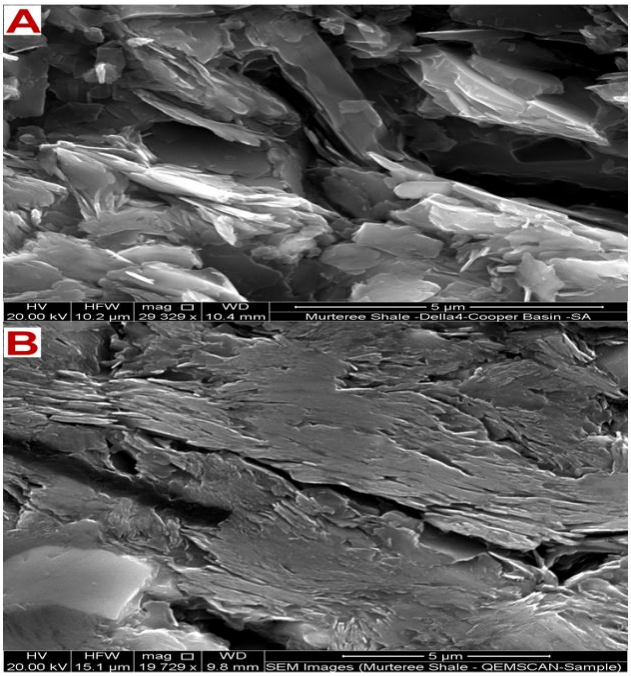

Figure 3.17: (A) Murteree shale images taken before and (B) after application of QEMSCAN using SEM and porosity loss by visual quantification is evident in B after grinding sample for QEMSCAN analyses.

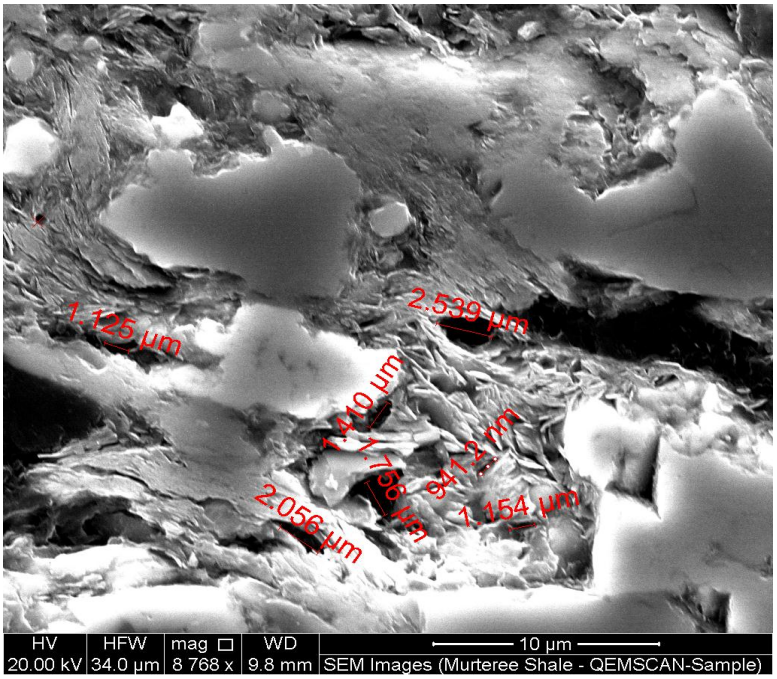

Figure 3.18: Porosity related to flocculated compacted clays in SEM Image of Murteree shale QEMSCAN results

To verify the result of QEMSCAN, and determine the elemental composition of the minerals, backscattered electrons were used by Quanta450 Energy Dispersive Spectroscope Detectors (EDS) and result as spectra are shown in figure 3.19 and 3.20 for siderite and organic matter respectively.

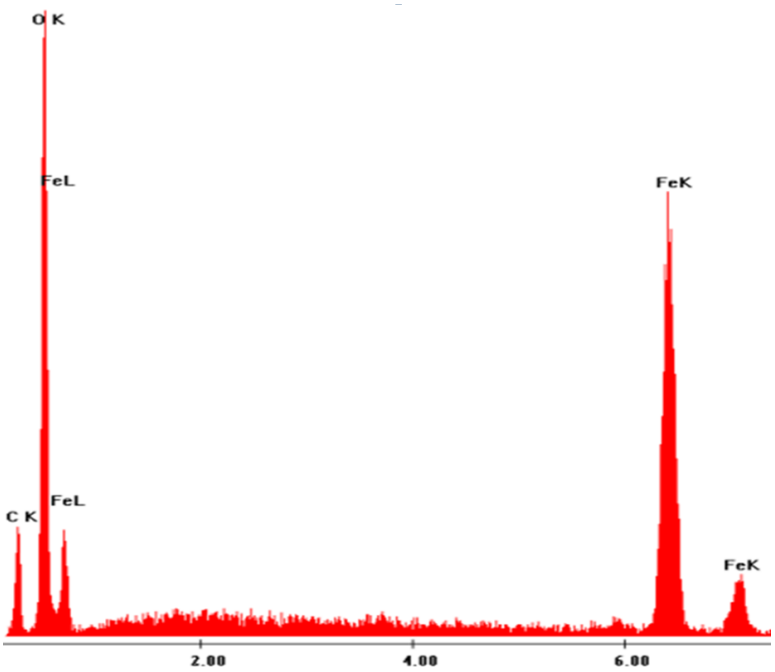

Figure 3.19: Siderite ($FeCO_3$) identification in Murteree shale sample by Characteristic X-rays using SEM-Quanta450 system.

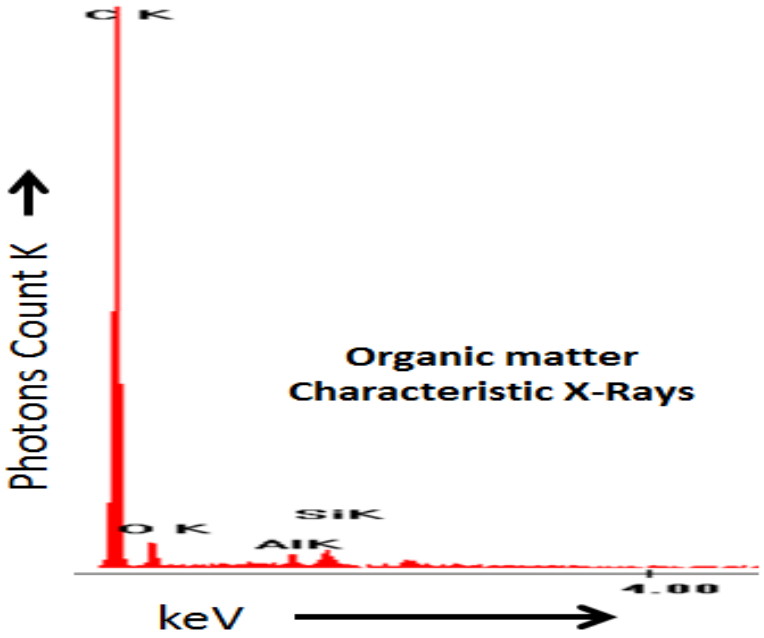

Figure 3.20: Organic matter (Residual Kerogen) identification in Murteree shale sample by Characteristic X-rays using SEM-Quanta450 system.

For the natural fractures and cracks identification, secondary electrons from sample surface were collected by SED (Secondary Electron Detector) to prepare micrograph as given in figure 3.21 and 3.22, where white area representing the heavy minerals after x-rays were detected and recorded on detector screen (Green arrow = Organics; Dark Blue arrow = Clays; and Red arrow= Quartz Thick big white arrow = Fracture/ Cracks, and whitish gray = Siderite), on the following pages. We believe this fracture system is consequence of overmaturity of the organic matter, graphitization, and a low grade metamorphism equivalent to anthracite (Abad 2007).

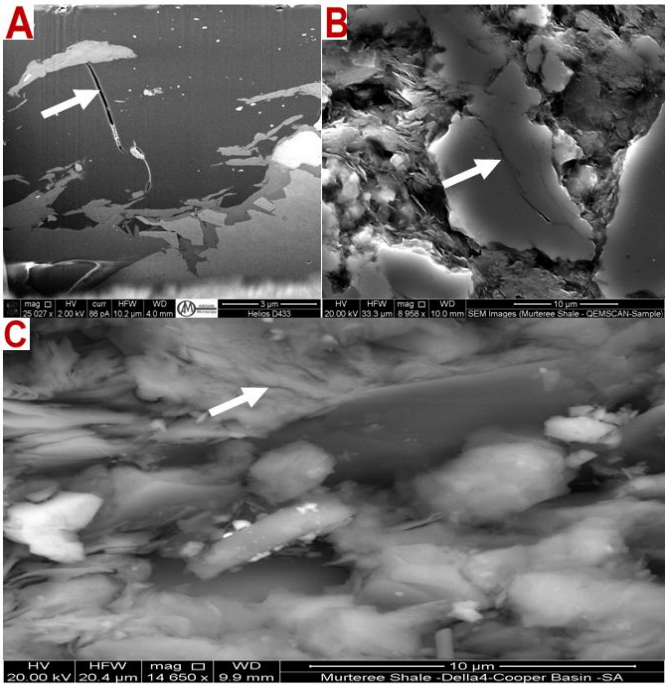

Figure 3.21: Images of Roseneath shale, and (A&B) and (C) Murteree shale using FIB/SEM with natural fracture system (white arrows).

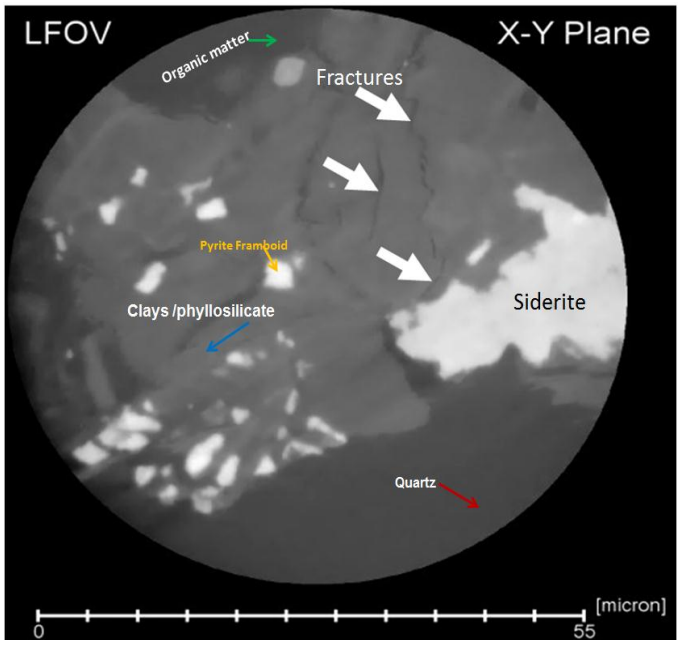

Figure 3.22: Microfracture system using X-Ray Nano-Computerized Tomography Scanning system (white arrows).

Table 3.3: Minerals, their EDXS % estimated and density used in QEMSCAN, SEM, Micro and Nanotomography Evaluation Techniques (Liu et al. 2005, David French et al., 2008).

Mineral Name & Chemical Formula	Typical EDXS & Percentage (%) Ratio	Mineral Density gm/cm^3
Quartz SiO_2	**Si>85**	**2.7 gm/cm^3**
Kaolinite-aluminosilicate $Al_2Si_2O_5$ $(OH)_4$	**Al:Si-45:55**	**2.79-2.80 gm/cm^3**
Illite K-Aluminosilicate $K(Al, Fe)_4$ $(Si, Al)_8O_{20}$ $(OH)_4$ $(Al\ Mg\ Fe)_2$ $(Si\ Al)_4O_{10}$ $(OH)_2$ (HO_2)	**Al:Si:K:-30:55:10**	**2.79-2.80 gm/cm^2 Measured 2.61 gm/cm^3 Calculated**
Muscovite K Al_2 $(AlSi_3O_{10})(OH)_4$ K $Al_2(Al\ Si_3O_{10})(F, OH)_2$ K $Al_2(Al\ Si_3O_{10})$ $(OH)_2$	**Al:Si:K:30:55:10**	**2.77-2.88 gm/cm^3 Measured 2.61 gm/cm^3 Calculated**
Chlorite (Chamosite), Fe Aluminosilicate $(Fe\ Mg\ Al)_6$ $(Si\ Al)_4$ $(Si\ Al)_8$ O_{20} $(OH)_4$	**Mg:Al:Si:Fe-5:20:35:40**	**2.8 gm/cm^3**
Montmorillonite $(Ca\ Na)(Al\ Mg)_4(Si\ Al)_8O_{20}(OH)_4$	**(Na Ca):Al:Si:-5:25:65**	**2.00-2.70 gm/cm^3**
Pyrite $FeSi_2$	**S:Fe-65:30**	**5.00 gm/cm^3**
Siderite $FeCO_3$	**Fe >70**	**3.90 gm/cm^3**
Rutile $FeCO_3$	**Ti >80**	**4.25 gm/cm^3**
Organic Carbon /Coal Macerals		**1.2-1.5 gm/cm^3 Density of TOC is about 0.94 to 0.98 gm/cm^3**

The XRD techniques are industry standards for a very long time in geological investigations. Murteree shale XRD results about various minerals phases were found in a very good agreement and on level of reliable consistency when correlated with QEMSCAN outcome. We found evaluated clay content using gamma ray log and applying Steiber formula free of major doubts when percentages were correlated with QEMSCAN and XRD outcomes as well. QEMSCAN and XRD techniques especially, Rietveld method is very helpful in qualitative and quantitative analysis for minerals and rocks classification. The XRD results for Murteree shale sample are presented in table 3.4 below.

Table 3.4: X-Ray Diffraction results of Murteree Shale

Constituent Mineral Name	Percentage (weight %)
Quartz	39.00%
Feldspar	0.91%
Muscovite 2M1	17.89%
Rutile	0.27%
Siderite	10.15%
Kaolinite	14.01%
Illite	17.78%
Organics	Not - detectable
Others	Pyrite, Sphalerite etc.

The diffractogram of Murteree shale powder based on scanned in X-Ray diffractometry is shown in figure 3.23 below.

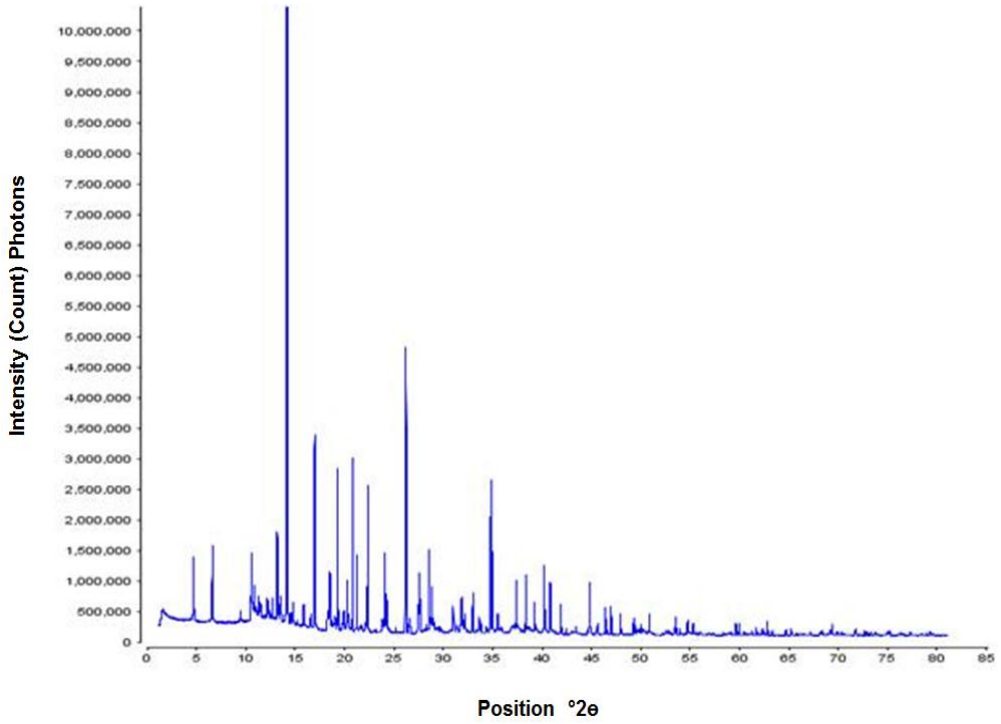

Figure 3.23: Murteree shale Diffractogram produced using XRD Quantitative Techniques (Rietveld).

3.7 Discussion

3.7.1 QEMSCAN

QEMSCAN with multiple silicon drift detectors and 1000 count spectra can achieve ultrafast analysis speed, 10 milli-seconds per pixel (Herman et al. 2010). Due to very high detection speed, automated mineralogy system has number of advantages. For example the false colour images and digital maps generated are quite helpful to investigate the topography, morphology and composition of the scanned core samples (Knackstedt et al. 2010). Digital images generated are used to reveal locations of particular interest like lamination, clays lamination, quartz lamination marked by A and B in Figure 3.3, Part B. Similarly zones of adsorbed, compressed gas or mixed zones holding both adsorbed and compressed gas can readily be identified in figure 2, part B, by the letters A, B and C. The insight gained from the type of minerals and grain size in the investigated sample, a particular depositional environment can be assigned to reservoir rocks as well. Also the type of minerals and their average grain sizes in the scanned sample of Murteree shale are proof of low energy lacustrine depositional environment due to high clayey content, organic matter, quartz, siderite and pyrite identified in the Murteree sample as it has been reported in the published literature about geological and stratigraphy of Cooper Basin (Stuart 1976, Thornton 1979, Hill and Gravestock 1995, Gravestock et al., 1998 and Lindsay 200).

Although, QEMSCAN technology is helping in a number of ways to characterize source rocks as potential unconventional gas reservoirs, still there are some shortcomings about its application in the selection of the potential shale gas reservoirs. The mass and weight % evaluation and density values are based on the chemical composition of the individual mineral species identified and later quantified in QEMSCAN procedure. Clay minerals (silicates) share a great deal of same chemical composition (polytpes) like muscovite (mica) and Illite (clay), chlorite (clay) and chamosite (mica) as given in table 3.3. They exhibit density, very close to each other. When these density values are used in evaluation of the various organic and inorganic weight %, mass %, they generate data and information which could be misleading in the assessment of fractions of adsorbed and free natural gas. Consequently, in the targeted shale gas reservoirs, the amount and type of clays and quartz will affect the judgment about the fraccability operation for a potential unconventional reservoir as well.

Oil and gas can be generated from different terrestrial and marine types of organic matter in a source rock. Murteree and Roseneath shale have terrestrial/lacustrine source of organic matter, which can be classified into number of macerals, like Vitrinite, Inertinite, and Exinite. They exhibit a range of density (Dyrkacz and Horwitz 1982). After maturation of organic matter, the residual organic matter can have different density values depending on its type and source of origin (Duliu 1999; Dyrkacz and Horwitz 1982). The use of wrong density value assigned to organic matter, identified in QEMSCAN can affect the total hydrocarbon generation potential assessment of a shale gas play when applied using QEMSCAN quantified TOC wt. % results.

Similarly there are some doubts about the total porosity (2%) evaluated in QEMSCAN. When QEMSCAN total porosity correlated with the imaged pores and their concentration in the SEM micrographs, they do not corroborate each other as shown in figure 3.15. The average pore size evaluated ~7 µm by QEMSCAN, is much higher than the majority of the pores imaged using SEM. Therefore, evaluated total free porosity is unreliable assessment, raising some valid concerns about pores size, pores classification and total porosity in this evaluation technique. QEMSCAN system has a resolution limitation of 2 µm. Pores less than 2 µm, cannot be visualized and quantified, resulting in loss of actual total porosity assessment, which is dominant porous characteristic of all shale gas reservoirs as shown in figure 3.15 and more images attached in the appendices A and B as well. The total free porosity in Murteree and Roseneath shale gas reservoirs, comprised pores of various dimensions, mainly found in inorganic and organic matrix whose dimensions have been documented are well below 1 µm scale as seen in figure 3.15.

3.7.2 Micro and Nano-CT Scanning

Due to almost equal attenuation coefficient value of the constituent minerals at this level of incident x-rays energy, the discrimination of the various solid mineral phases and voids is very challenging in shale gas reservoir samples. High energy incident X-rays (above, 100 KeV, Compton Effect) passing through sample, reflect blurred internal features, due to very low attenuation in the medium. While the low energy x-rays (below 100 KeV, Photoelectric Absorption) are absorbed most by sample medium and reveal the internal characteristics of the sample in better details. By using this dual x-ray system, heavy minerals with high atomic number absorb most of the x-rays, displaying the highest attenuation coefficient values and appear very bright, while organic matter and pores show gray and black areas in the tomogram as expressed in figures 3.15 and 3.16. Low energy absorption is the best option to image and scan the internal features of minerals.

As a consequence of this very small density difference and using very limited range of incident x-rays only four different phases have been identified using computerized tomography techniques in model figure 3.15 and 3.16. After a careful look at the table 3.15, the different phases can be categorized into four groups, based on QEMSCAN results: (1) silicates like quartz, muscovite, illite, kaolinite, chlorite having an average density 2.8 gm/c^3, (2) with very high atomic number like pyrite, siderite and rutile (5.0, 3.9, 4.5) with an average density 4.47 gm/c^3 and (3) organics and rest of the phases possessing very low density, having average density 1.2 gm/c^3 while (4) the voids/pores do not have density (0 gm/c^3) respectively. 3D models given in figures 3.15 and 3.16 are based on interpretation of the CT-scanning data consisting of xy-slices from the Murteree shale sample.

Based on range of applicable incident radiation energy, therefore the identification of all the individual solid, liquid and gaseous phases using micro and nana tomography is very challenging

indeed. Similarly the pore size in micron or below micron scale in inorganic matrix and organic matter offers a formidable task in discrimination of a pore or a kerogen particle and later use in the quantification of the total free porosity. As seen in SEM images, pores in submicron scale are not even counted towards the total porosity in QEMSCAN. Due to very small size and lack of resolution to identify these submicron's pores in carbonaceous shale is still an area and micro and nantomography is struggling to achieve reliable total porosity estimation. Although the microfracture system in scanned Roseneath and Murteree shale samples can conspicuously be visualized as one shown in figure 3.22 but the interconnectivity and density of microfracture system is a challenge.

3.7.3: FIB/SEM

Shale gas reservoirs due to ultra-fine fabric possess very low effective porosity and ultra-low permeability. Pores origin and types, pore size and pore size distribution vary from phase to phase in the matrix of potential shale gas reservoir. There is strong heterogeneity and anisotropy represented by the petrophysical parameters related to storage and flow capacity. Based on ultra-high magnification strength and very high resolution capabilities, scanning electron microscope is capable to divulge shale reservoirs micro, meso and macroporosity to enhance the understanding of the storage mechanism and flow capacities. There is strong evidence of missing pores and fractures of all dimensions like macro, meso, and micro porosity fractions which have not been quantified in results from QEMSCAN and Computerized Tomography scanning techniques. There is considerable information through ultra-high magnification and resolution in 2D images of Murteree and Roseneath shales samples scanned by FIB/SEM dual beam system that there is vast number of pores, whose dimensions are much smaller than 7µm as identified by QEMSCAN and are extensively populating these shale samples as shown in figures 3.11, 3.12, 3.17 and 3.18 in the preceding pages. In QEMSCAN techniques the identification and evaluation of the total free porosity after polishing sample for digital mapping and quantification can create serious concerns about the total free porosity assessment and pores size distribution when correlated between figures 3.17, 3.18 and 3.21. QUANTA450 SEM embedded with XRD facility was also used to confirm the various mineral phases identified in QEMSCAN analysis as shown in figure 3.19 and 3.20 for identification of siderite and organic matter using energy vs. no. of photons counted. Consequently, the necessity of the application of FIB/SEM techniques is vital part of evaluation techniques when embarking on the unconventional reservoir petrophysical characterization.

3.7.4 X Ray Diffraction

Shale gas reservoirs have large number of constituents as seen in scanned samples of Murteree shale using QEMSCAN and XRD. XRD methods were applied to confirm the various minerals identification and quantification in order to have confidence in the results and better understanding about petrophysical properties like porosity, permeability and water saturation estimation in carbonaceous Roseneath and Murteree shale formations. We found that XRD techniques can be reliably used and applied in qualitative and quantitative analyses for potential

shale reservoirs in parallel to QEMSCAN radiation techniques. These radiation techniques have number of advantages and disadvantages for example in FIB/SEM as given in the table 3.5, below.

Table 3.5: Petrographic Techniques – Advantages and Disadvantages

FIB/SEM: (Focused Ion Beam Milling & Scanning Ecletron Microcopy)	
Advantages	Disadvantages
1: Submicron level pores identification, interconnectivity & pores classification 2: 3D volumetric model building 3: Micro rock texture – Organic and inorganic mineral constituents relationship and distribution 4: Source rock maturity and organic matter morphology	1: Problem with upscaling of outcome 2: Time consumimg and expensive 3: Need large volumes to be scanned

Based on these observations inferred from the outcomes of QEMSCAN, FIB/SEM, XRD and Micro and Nano-Computerized Tomography we reached the following conclusions.

3.8 Conclusions

1. After QEMSCAN and CT – Scanning analyses, FIB/SEM imaging has cogently proved Roseneath and Murteree shales lack in cylindrical pores. Linear/elongated, wedge-shaped, and triangular void spaces are the dominant type of intergranular porosity heavily populating clay dominant zones in 2D images of core samples from these shales.
2. Possessing large quantity of quartz, and moderate amount of evenly distributed siderite, these shales are brittle enough and highly prone to fraccing operations.
3. Intergranular and interstitial heavy mineral grains presence can play a role in maintaining the initial pores open in the matrix.
4. QEMSCAN is not very accurate to identify type of kerogens and correct density values. This can underestimate or overestimate the absolute hydrocarbon generation potential of shale gas reservoir (TOC wt. %).
5. High clay content, organic matter, detrital and authigenic quartz, fine grained nature of mineral grains identification and quantification, confirm that Murteree and Roseneath shales are lacustrine type shales.
6. Murteree and Rosenreath shales have natural fracture system like coal but its connectivity and concentration is low due to low organic content.
7. FIB/SEM application confirms that low resolution of QEMSCAN and CT-Scanning cannot capture micro and meso porosity which constitute major part of intergranular and interstitial storage capacity. Therefore, only FIB/SEM is reliable technique for free porosity visual evaluation in shale gas reservoirs.
8. Murteree shale results from QEMSCAN and XRD were in good agreement and presence of each phase was also reconfirmed using EDXS technique available in SEM Quanta450 system.

CHAPTER 4

Evaluation of Porosity Using Core Analysis

4.1 Introduction

In chapter 3, qualitative and quantitative mineralogy, rock classification and characteristics, 2D images visualization of pores, microfracture systems nature and interconnectivity were investigated using radiation techniques QEMSCAN, XRD, FIB/SEM, Micro and Nano Computerized Tomography to evaluate these source rocks as potential unconventional shale gas reservoirs. In the outcome of these techniques we found exceptionally large porous domains, pores of various sizes and shapes whose interconnectivity was not clear in the FIB/SEM high resolution 2D images at all. Also we identified the presence of the heavy minerals grains in between the matrix grains whose role in maintaining communication channels/apertures open between the porous domains was found doubtful also as shown in 2D image of Roseneath shale in figure 4.1 below.

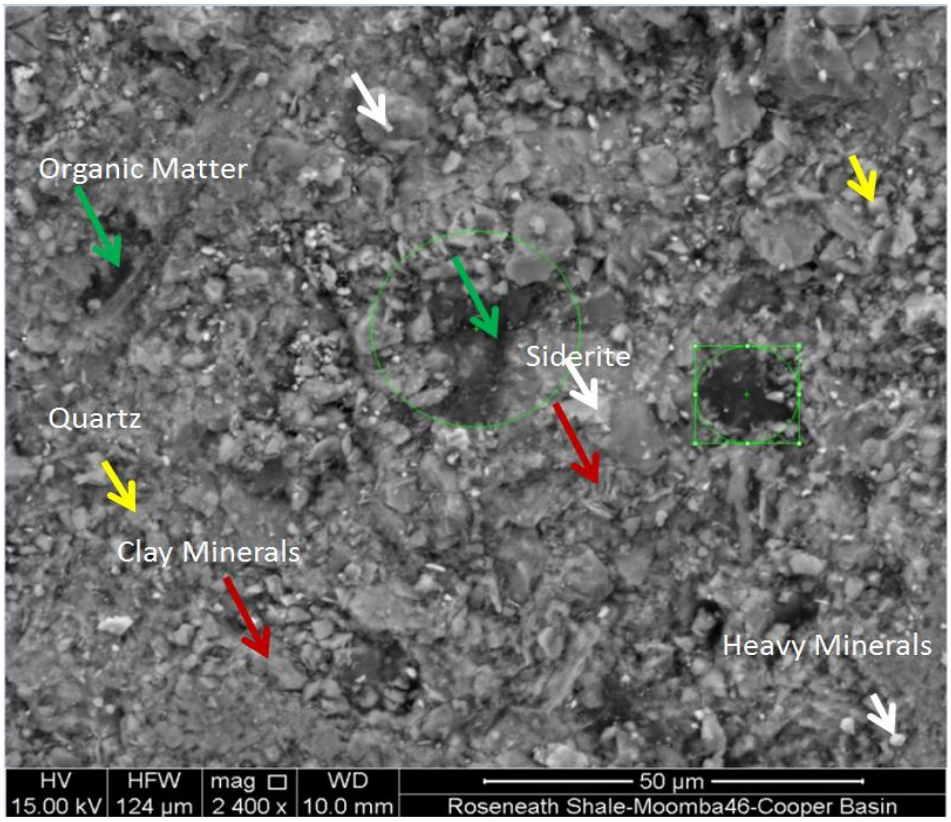

Figure 4.1: Mechanically prepared Roseneath shale sample to observe the distribution of clay (Red arrows), quartz (Yellow arrows) heavy minerals (Whites arrows pointing pyrite siderite rutile) and organics (Green arrows) using BSE signal detector, while green circles representing area of higher organics concentration.

The objective of this chapter is using conventional techniques like helium porosimetry, mercury injection capillary pressure techniques (MICP) and liquid pyknometry to find out the

interconnectivity of large porous zones/domains, estimate of effective porosity and total porosity. Furthermore the size of the interconnecting pore throats among very broad range of pores of various origin, forms, sizes, and shapes of Roseneath and Murteree shales has been investigated, as shown in 2D FIB/SEM images of Roseneath Shale in figures 4.2 and 4.3.

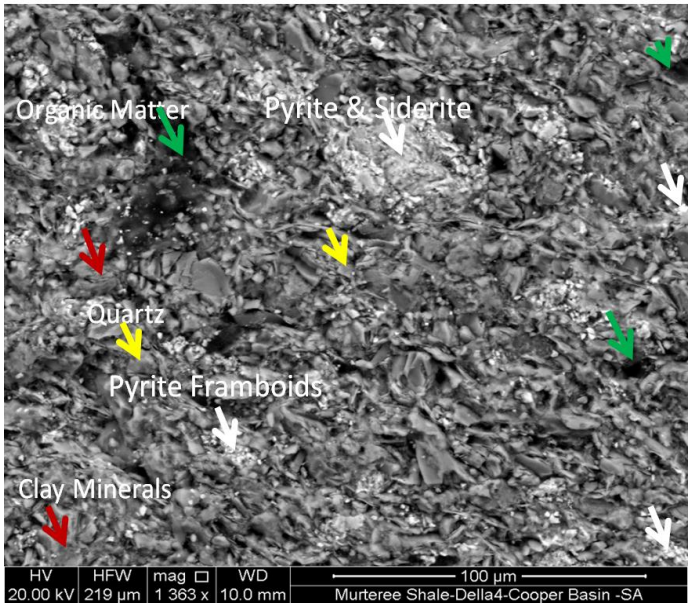

Figure 4.2: Mechanically prepared Murteree shale sample to observe the distribution of quartz (Yellow arrows), clays (Red arrows) heavy minerals (Whites arrows) and organics (Green arrows) using BSE signal detector.

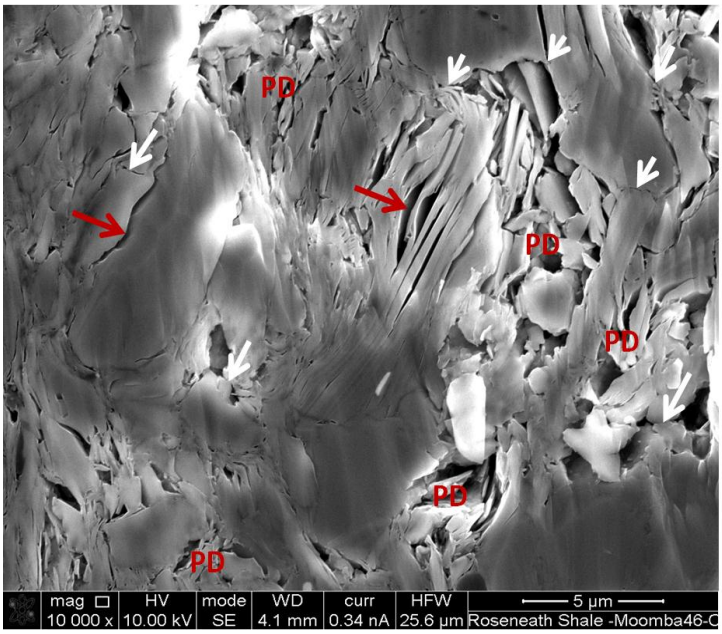

Figure 4.3: FIB/SEM prepared Roseneath shale sample labelled for pore throat, porous domains, intergranular and interstitial pores identified using SE signal detector (Red arrows= Intergranular/Interstitial pores; PD= Porous domains and White arrows= Pore throats or apertures connecting pores in domains).

Estimation of total free porosity in shale gas reservoir remains a challenge for both direct and indirect techniques which has a crucial role in the total initial gas in place estimation. For example porosity evaluation using wireline logging for prospective shale gas reservoirs is the subject of

controversy because of organic matter (kerogen) and very high density minerals like iron carbonates and pyrite response to logging tools in these shales. The doubts and uncertainties are based on the presence of low density organic matter with high hydrogen nuclei concentration and the response of heavy minerals (such as pyrite and siderite) to resistivity, sonic, neutron, and nuclear magnetic resonance (NMR) logging tools. This results in very high or very low total porosity. Similarly, due to very low effective porosity and permeability, the use of helium and mercury injection techniques will give erroneous results about the actual storage capacity and producibility from these unconventional reservoirs. The reason behind the dubious resource evaluation of shale gas reservoirs using conventional methods is due to the ultra-complex nature and variety of microfabric, lateral and vertical anisotropy and heterogeneity found in these sedimentary rocks. Acting as a source and reservoir simultaneously, shale gas reservoirs develop a complicated gas storage mechanism. Natural gas is held in the parent rock as free compressed gas and adsorbed gas in the micropores in kerogen and on clay's charged surfaces (Cheng and Huang, 2004; Gault and Stotts, 2007; Hartman et al, 2008; Ross and Bustin, 2007). The micropores range from nano to macropores in kerogen organic matter and among the shale particles, apart from the natural fractures and porous domains found in the shale gas reservoir. The dual storage mechanism and dual porosity (compressed and adsorbed gas) in the shale gas reservoir demand two different evaluation procedures to calculate the total storage capacity. Shaw et al (2006) have reported very low effective free porosity results found in potential carbonaceous shales using helium porosimetry and mercury injection capillary pressure (MICP) techniques due to very low permeability, ranging from micro to nano darcies.

For the measurement of total and effective porosity, two methods direct and indirect are applied. One of the direct methods is dual FIB/SEM system (focused ion beam milling and scanning electron microscopy). SEM images of a freshly broken/polished core sample's surface are used to identify the pores in the shale sample and are a direct way of investigating the total free porosity. Similarly, FIB/SEM is used to build a 3D volumetric model to probe the connectivity of the pores. Identification and quantification of the minerals, and rock classification are also part of the direct visual techniques (Sondergeld et al, 2010a). However these techniques and methods are expensive and time consuming and are not readily available for research compared to indirect methods.

Mercury injection capillary pressure (MICP), helium porosimetry, and pyknometry are indirect methods and are widely used to probe the total and effective porosity in reservoir rocks. But Sondergeld et al (2010b) stated that there are many factors that can affect the accuracy and the precision of the gas shale porosity measurements such as: adsorption effects; sample size and crushed sample weight; the effect of pore pressure and net over-burden stress on micro fractures; pore access problems to gas (helium, nitrogen, methane) and liquid (mercury, water) due to the low permeability of shales. But still these methods are cheap source of initial investigation to have some understanding about the petrophysical characteristics of shale gas reservoirs. And when

aided by FIB/SEM results from the same cores they can help in the selection of other techniques to improve the understanding of the shale reservoirs. To investigate the reliability of results gained through indirect methods like MICP technique, helium porosimetry, liquid pyknometry and later correlation of these results with SEM direct method can give a better understanding of pores size, density and porous domains, pores interconnectivity forecast and estimate of reserves in a shale gas reservoir. How indirect methods outcome for shale gas rocks can be improved through the aid of the direct method is described in the next pages starting with subheading methodology.

4.2 METHODOLOGY

Murteree and Roseneath shales cores from wells, Della4, located at a depth range of 6,619–6,620 ft., and Moomba46 at a depth range of 8096–8097.6' ft., were collected from PIRSA's (Primary Industries and Resources South Australia) core library. The samples were cut and polished carefully using a diamond saw and iron files, two core plugs and later were grinded for pyknometry as shown in figures 4.4 and 4.5 for Murteree and Roseneath shales. Each core sample was divided into four parts for mercury injection capillary pressure technique, helium porosimetry, and liquid pyknometry and for imaging core samples using focused ion beam milling and scanning electron microscope as mentioned in detail in the preceding chapter for very high magnification and resolution 2D images. The effective porosity and range of pore throat sizes was checked using MICP, and verified by helium porosimetry later on in preliminary part of this phase of our research. In the second phase FIB/SEM 2D images observations revealed isolated highly porous domains in cores samples followed by liquid pyknometry on crushed samples to determine the total porosity. A detail description of application of these four techniques, results discussion and conclusions respectively are given in the following pages.

Figure 4.4: Murteree shale samples from project well Della4 used for MICP, Helium Porosimetry, Pyknometry and FIB/SEM Analyses

Figure 4.5: Roseneath shale samples from project well Moomba46 used for MICP, Helium Porosimetry, Pyknometry and FIB/SEM Analyses

4.2.1 MICP-Mercury Injection Capillary Pressure Techniques

Less than 1 cm^2 irregular shaped block of Roseneath and Murteree shales were cut using a diamond saw. After being cleaned and dried, these samples were loaded into penetrometer, which was installed into the Micromeritics AutoPore-III Model for effective porosity and pore throat size classification analysis. At the initial low applied pressure, rock sample surface artefacts, imperfections and open surface pores are not saturated with surrounding mercury in the sample holder of AutoPore-III porosimeter. Later, as the pressure is increased, these open pores and artificial cracks on the sample's surface are filled, and mercury volume, which enters into these surface pores and cracks, is not counted into total mercury intrusion. This deduction from the total final mercury intrusion is called the conformance value (Vavra et al, 1992). Washburn Equation (1921) assumes that the pore size is cylindrical and the opening (pore throat) is circular in cross-section as well. Net force tends to resist entry of mercury into pore and this force is applied along the line of contact of the mercury, solid, and mercury vapour. The line of contact has a length of 2Pr; where r is radius of the pore throat and the component of force pushing the mercury out of the capillary acts in the direction cosɵ, where ɵ (theta) is the liquid-solid contact angle. A schematic illustrating the concept and application of Washburn equation in porous media is given in figure 4.6 after the mathematically expression of Washburn equation (1921) below:

$$D = -4\frac{\gamma \cos\theta}{P}$$

Equation 4.1

Where:
D = Diameter of the Pore (2r, and r pore throat radius μm)
P = Pressure required for mercury intrusion into pore (N/m)
γ = Interfacial tension/Surface tension (dynes/cm)
Cosɵ = Contact angle between solid and Mercury (degree).

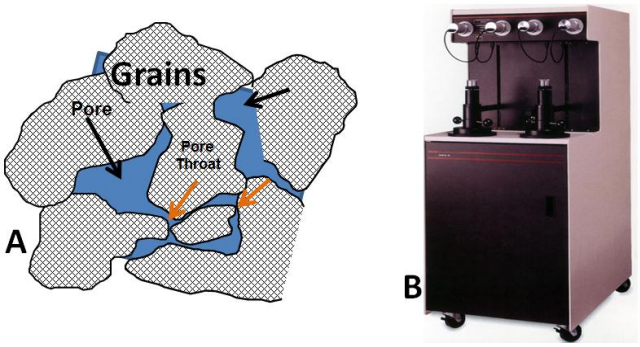

Figure 4.6: Schematic illustrating concept of pores and pore throat used in Washburn equation (Black arrows pointing to pores while yellow arrows pointing the communication channels/pore throats between pores, blue colour represents the fluid in pores in figure part **A** and state of the art high pressure Micromeritics AutoPore-III porosimeter used for Pore throat classification as shown in figure part **B**.

4.2.2 Core Crushing Method/Liquid Pyknometry

After identifying a large number of isolated pores whose dimensions were in a range much higher than the mesopores identified in the MICP results, it was desirable to use pyknometry to calculate the total free porosity in the samples to check the validity of the porosity in FIBM/SEM images and observations before making final conclusions. Core crushing procedure was first introduced by Luffel et al (1992) to investigate porosity in available pore networks for various Eastern Devonian gas shales. They suggested the pores were all connected, but the connections were so small that even helium required substantial amounts of time to equilibrate and reach all the pore space, documenting the idea of possessing very low permeability.

For over-mature organic shales, the chances of clay hydration are very low and there is no oil in these shales at this level of source rock maturation, when all the oil has been cracked into gas or the source organic matter is simply gas prone. The total free porosity was evaluated using this technique, not the absolute total free porosity, which is porosity when water molecules are still adsorbed by the clays. It was assumed that due to smectite-illite conversion, the amount of the adsorbed water by the illite is very low and negligible in this case. Consequently, there is no loss of porosity when measuring total porosity in samples from the Roseneath and Murteree shales using the crushed sample in the pyknometry method. The pyknometry apparatus used in this experimental work is shown in figure 4.7 below.

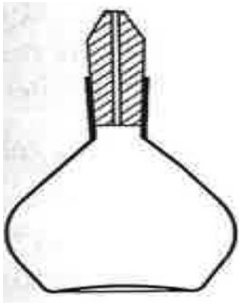

Figure 4.7: Capillary-Stoppered Pyknometery

A detailed mathematical procedure how mass and volume of pyknometry, grains and distilled water used, are evaluated is described here. Buoyancy is the loss of weight by the rock grains when they are immersed in water and correction value corresponds to the difference of weights between the pyknometer filled with water and the pyknometer with the shale sample divided by the weight of pyknometer filled with water as shown in equation 4.2 below;

$$Buoyancy\ Correction\ Value = \left(\frac{(M3-M0)}{M3}\right). \qquad \text{Equation 4.2}$$

$$\rho g = \frac{(M1-M0)\rho w}{(M3-M0-M2+M1)1000} + C \qquad \text{Equation 4.3}$$

ρ_g= Grains density in sample

$$Vg = \frac{(M2-M3)}{\rho g} \qquad \text{Equation 4.4}$$

Where:

ρg: Grain density, in g/cm^3
M0: Apparent mass in air (weight in air) (g) of the empty pyknometer.
M1: Apparent mass in air (g) of the pyknometer plus solid.
M2: Apparent mass in air (g) of the pyknometer plus solid plus water.
M3: Apparent mass in air (g) of the pyknometer filled with water.
C: Correction of air buoyancy in gm/ml
ρ_w: Density of water in g/m^3 at the temperature of calibration

$$\boldsymbol{\phi} = \frac{\mathbf{Vb-Vg}}{\mathbf{Vb}} * 100 \qquad \text{Equation 4.5}$$

V_b: Bulk volume of Core Sample
V_g: Grains Volume in sample
Ø (%): Total Porosity in sample

Parts of core samples from the Roseneath and Murteree shales were cut, pulverised and ground separately, first by using a mortar and pestle, and then by a vibrating grinder, to prepare a suitable amount of powder for pyknometry tests. The powder was sieved using a 40 μm sieve. The size of microfabric of shales and carbonaceous shale is less than 40 μm. Distilled water in the pyknometry method was used to find the most reliable volume of shale grains/matrix in the samples for the calculation of total interstitial free porosity.

To calculate total free porosity in the core sample the estimation of bulk volume with utmost accuracy before crushing sample was an essential part of this experiment. Mercury immersion for bulk-volume measurements failed due to a density difference in the rock shales and mercury liquid. The immersion of shale samples in mercury to measure the bulk volume was replaced by cutting a rectangular core block equal to the weight of the powder used in the pyknometer from the exact same core interval and depth of the well. To achieve a very high accuracy in bulk-volume measurements, extraordinary care was taken during sample dimension measurements, detailing the width, length and height of the sample block for bulk-volume calculations. Later on,

by taking multiple readings and using the standard deviation method to remove any possible error, the bulk volume of these rectangular blocks were estimated.

4.2.3 Helium Porosimetry

Helium porosimetry is being used continuously for effective porosity measurement of conventional reservoirs for a long time in the petroleum industry. Due to its inert nature and very small molecular diameter 0.260 nanometres (Sondergeld et al, 2010b) a helium molecule can penetrate pores with very small pore openings in the rock samples. This technique is reliable and insensitive to mineralogy with the lowest adsorption trend on the grain and pore surfaces, especially when having organic matter and adsorbent clays in the sample. Issler and Katsube (1994) claimed that helium porosimetry values are more reflective of the total interconnected pore space (effective porosity) than values obtained by mercury porosimetry because of the molecular diameter difference between helium and mercury. Due to extremely low permeability and micro-porosity, helium needs extra time to equilibrate in the porous media by diffusion. Neglecting to allocate sufficient time for total diffusion of helium may yield higher calculated grain volumes and lower porosities in shale samples. The equilibrium pressure allows the computer software to calculate the porosity by applying Boyle's Law to calculate the grain volume, and subtracting it from the bulk volume to obtain the pore volume. The experimental apparatus used for effective porosity is shown below in figure 4.8 below.

Figure 4.8: Software and TEMCO HP-401 Helium Porosimeter

The mathematical derivation for calculation of effective porosity (Ø), volume of the reference chamber and lines (V_1,cm^2), volume of the sample chamber and lines to the air valve (V_2 cm^2), and grain volume of the core sample (V_{gr}) are given below in equations 4.6, 4.7, 4.8, and 4.9 respectively, while a detailed variables definitions are given in the appendices part of this dissertation.

$$V_1 = \frac{\frac{V_{ref}(P_{eqr} - P_1)}{(P_{2r} - P_{eqr})}}{\frac{(P_{eq} - P_1)}{(P_2 - P_{eq})} - \frac{(P_{eq} - P_1)}{(P_2 - P_{eq})}}$$ Equation 4.6 where:

V_{ref} = Volume of the reference core, cc
V_1 = Volume of the reference chamber and lines, cc
P_1 = Initial system pressure, atm
P_2 = Pressure of reference chamber and lines with air valve closed, atm
P_{eq} = Equalization pressure of the system air valve open, atm

P_{1r} = Initial system pressure with reference core in the sample chamber, atm
P_{2r} = Pressure of reference chamber and lines with air valve closed (with reference core in the sample chamber), atm
P_{eqr} = Equalization pressure of the system (with reference core in the reference chamber) with air valve open, atm

$$V_2 = \frac{V_1(P_{eq} - P_1)}{(P_2 - P_{eq})}$$ Equation 4.7 where:

V_2 = Volume of the sample chamber and lines to the air valve, cc
V_1 = Volume of the reference chamber and lines, cc
P_1 = Initial system pressure, atm
P_2 = Pressure of the reference chamber and lines with air valve closed, atm
P_{eq} = Equalization pressure of the system air valve open, atm

$$V_{gr} = (V_1 \text{ x } (P_{1s} - P_{eqs}) + \frac{V_2(P_{2s} - P_{eqs})}{(P_{1s} - P_{eqs})}$$ Equation 4.8 where:
where V_{gr} = Grain Volume

$$\text{Porosity}(Ø) = \frac{V_b - V_{gr}}{V_b} \text{ x } 100$$ Equation 4.9
Where
Ø = Effective porosity)
V_b = Core bulk volume

After finding contradictory results about the pore sizes and their morphology, visualised directly in the FIB/SEM images and indirectly from MICP, helium porosimetry was the next method used to probe the effective porosity in the samples.

4.3 RESULTS AND DISCUSSION

4.3.1 MICP Techniques

While using mercury injection techniques, three variables are recorded: the applied pressure; the diameter and/or width of the pore apertures intruded and the amount of the volume intruded into the pores. In Figure 4.9 a graph of mercury saturation versus pressure to calculate the effective porosity is shown. In Figure 4.10, when pore volume percentage is plotted against the calculated diameter, a range of the pores throat size is obtained. In this case, a range of pores throat between nano-porosity and macro-porosity is represented by the black brace where maximum mercury intrusion has taken place. Similar graphs have been presented for Roseneath Shale samples in figures 4.11 and 4.12 respectively.

An interface is established between the pores and mercury between 2–8 psi, as expressed in Figure 4.10, where the mercury saturation in the sample is almost 20%. The pressure is increased gradually, in an incremental steps, and at every step of increased pressure, the intruded volume of mercury into the sample pores is allowed to stabilise, is measured and recorded until a pressure of 60,000 psi is finally achieved in the instrument. Mercury can enter into pores with an opening of 36 Angstrom at 60 kpsi, while a methane molecule has a diameter of 2.16 Angstrom (Oslon and Grigg, 2008). Later, the applied pressure is gradually reduced to

atmospheric pressure, allowing partial withdrawal of the mercury from the sample pores as expressed by drainage and imbibition curves (Vavra et al, 1992) as shown in Figure 4.9 for Murteree shale. These two curves show the presence of pores of various throat sizes. It also shows that after withdrawal of the applied pressure, part of the intruded mercury remains in the sample due to an absence of pressure in these pores where the mercury has entered previously. The exact measurement of the pore opening size or pore throat size using the mercury injection techniques is impossible, except estimating a range of pore throats where some intrusion has taken place.

Gradual mercury intrusion into the sample from 0 to 20% shows the filling of the surface fractures and pores which represent the conformance, followed by an interface established between the nonwetting mercury and sample in the penetometer without further intrusion untill pressure is reached to 1000 psi. Later when pressure is increased in steps using Micromeritics AutoPore-III porosimeter, the gradual increase in pressure represents the decreasing pore throat size in the sample. The volume of mercury entered at every pressure step applied and diamter range of pore throats estimated make the application of this technique for estimation of density, pore throat range estimation as well as effective porosity in the investigated sample as shown in this figure 4.9 and in the following figures from 4.10 to 4.12 on the next pages.

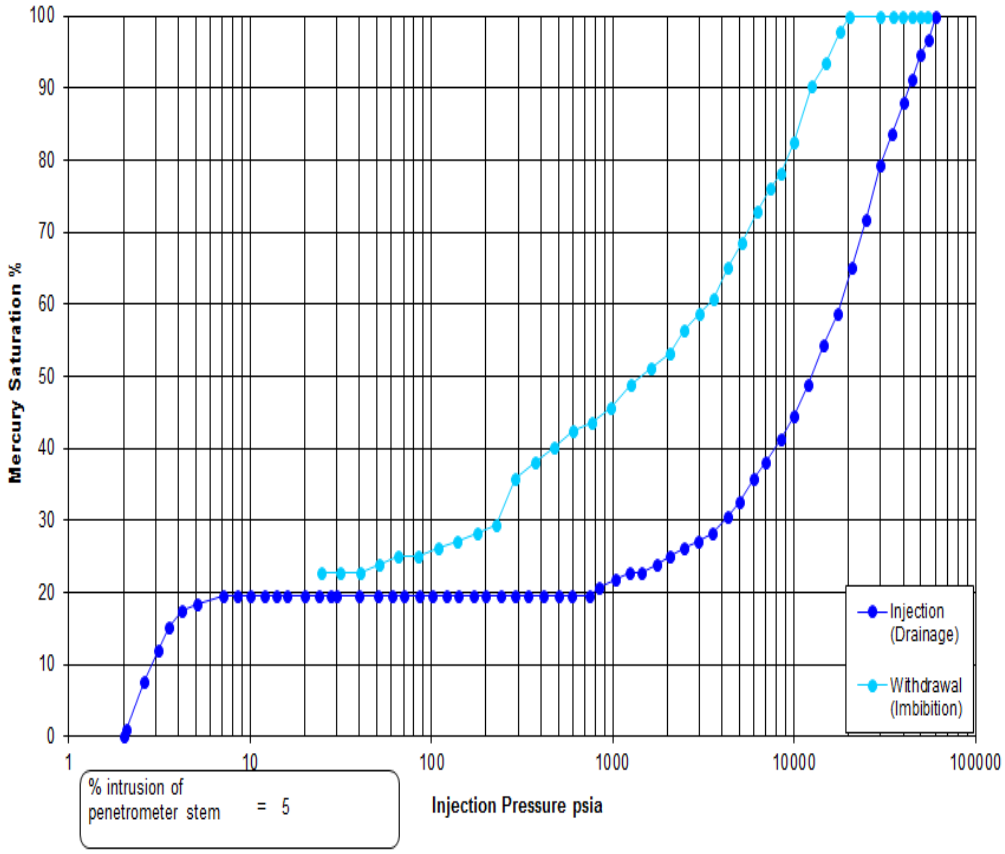

Figure 4.9: Imbibition and Drainage curves of Murteree shale samples using MICP technique, Della4 Project Well, Porosity % = 2.5221; Grain density gm/cc = 2.6876.

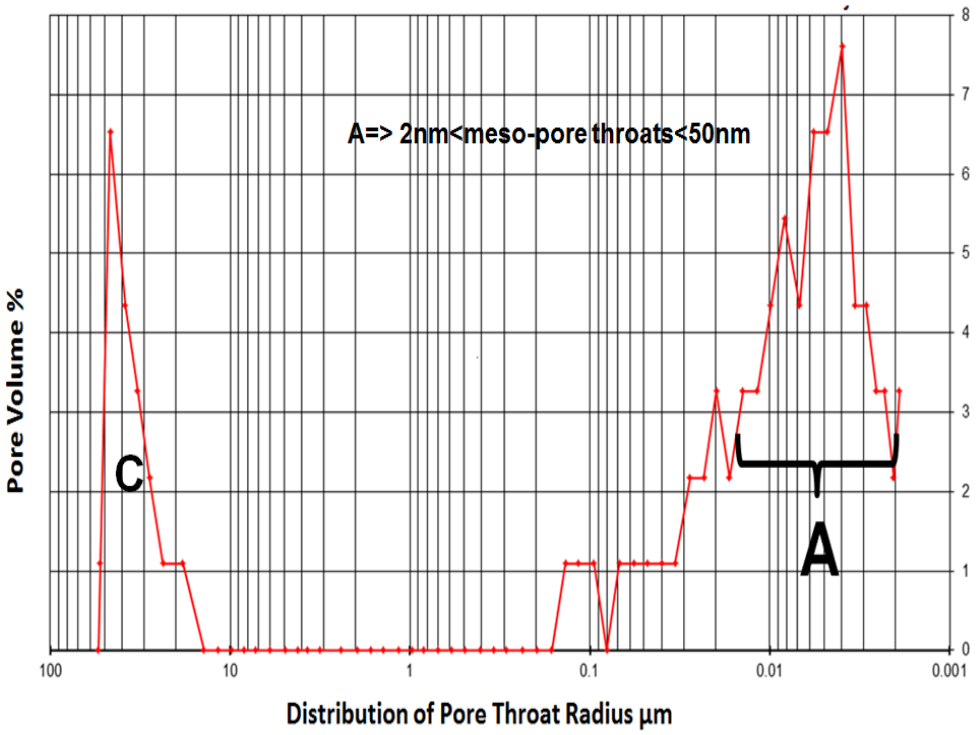

Figure 4.10: Pore throat size range distribution illustrated by black bracket (A) in Murteree shale samples using MICP technique results and C= Conformance.

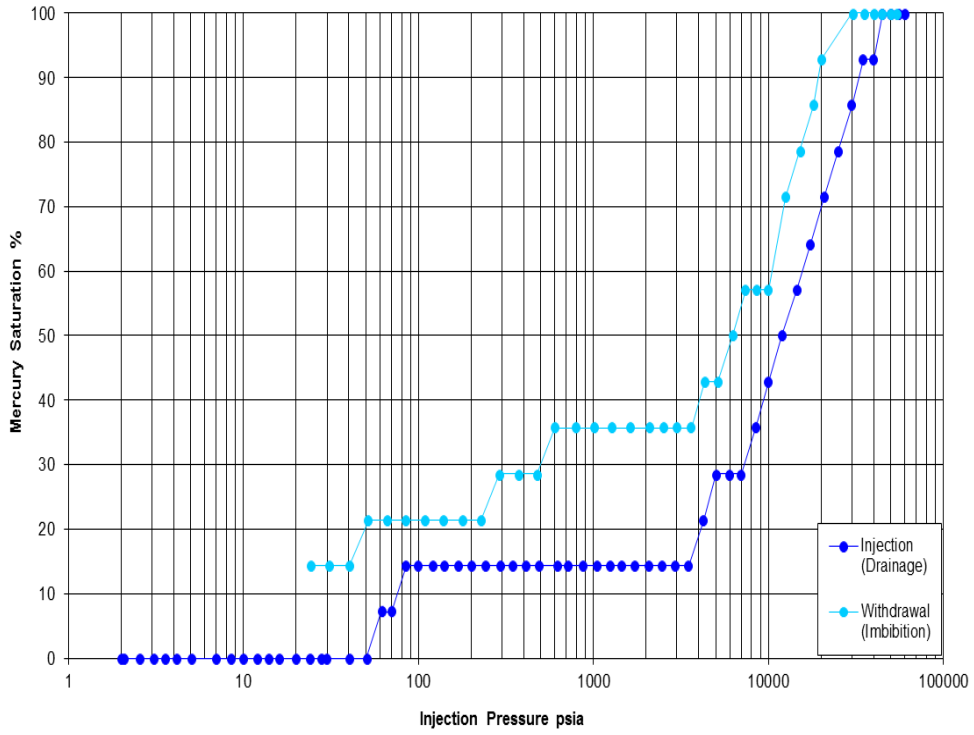

Figure 4.11: Imbibition and Drainage curves in Roseneath Shale sample using MICP technique, Project Well Moomba#46, Porosity % = 0.9066; Grain density gm/cc = 2.5686.

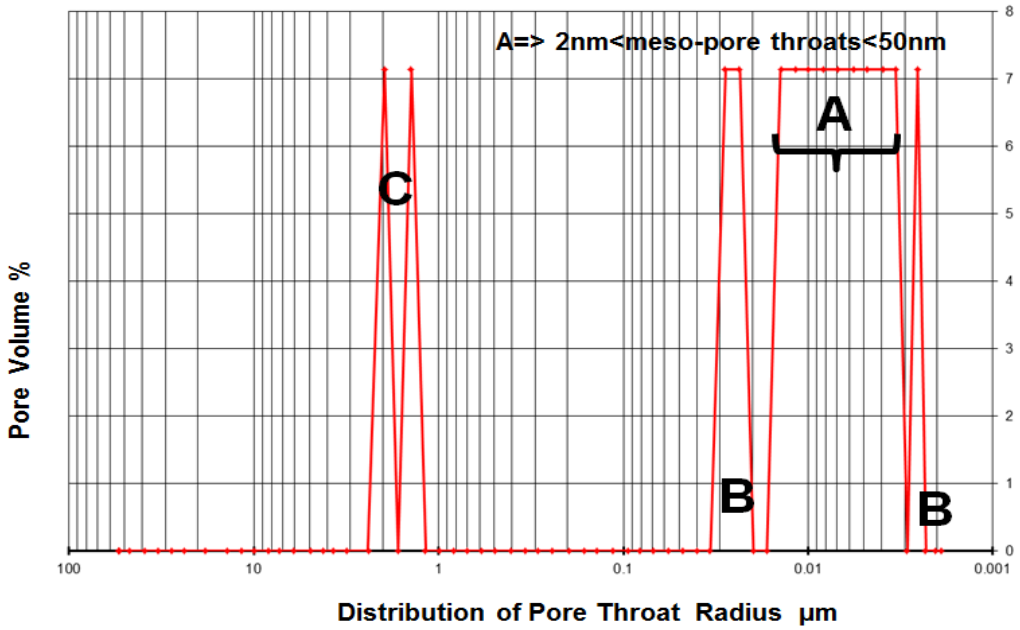

Figure 4.12: Pore throat size distribution in Roseneath shale samples using MICP technique results (A= meso-pore throat size range, B = Porous/Fracture zones, C=Conformance).

4.3.2 Liquid Pyknometry /Core Crushing Method

The core crushing method was conducted for each powder sample taken from the Roseneath and Murteree shales. Each measurement of weight for the empty pyknometer, powder sample, pyknometer with distilled water, and with powder and distilled water was repeated five times to achieve the maximum possible accuracy in the final results for the total porosity given in Table 4.1. The average total porosity is 30.43% in the Roseneath shale, and 35.39% in the Murteree shale. The amount of uncertainty, based on repeating the measurements, is 13.5% and 7.5% for the Roseneath and Murteree shales, respectively.

Table 4.1: Porosity values of Roseneath and Murteree shale using the core crushing method (Liquid Pyknometry)

Number of Measurements	Total Porosity (%) Murteree Shale	Total Porosity (%) Roseneath Shale
1	25.49	33.34
2	27.15	37.42
3	31.26	33.78
4	32.60	39.12
5	35.64	33.31
Average	**30.43**	**35.39**

4.3.3: Helium Porosimetry

Due to the carbonaceous nature of the shale samples, the preparation of cylindrical plugs for helium porosimetry failed. Therefore, rectangular blocks were prepared and the dimensions of the rectangular blocks were used to calculate the equivalent cylindrical diameter to enter into the porosimeter software to find out the porosity after each experiment was run.

The main limitation of the helium porosimetry was very low pressure against very low porosity and permeability of the shale samples. The helium porosimeter has about 100 psi available for use,

out of which only 90 psi is recommended to be applied during these experiments. Therefore, injection of the helium gas into the core sample is very slow and takes a long time to saturate and equilibrate in the samples. It is also worth mentioning the effect of the applied 60 kpsi while measuring bulk density, effective porosity and pore throat size distribution during the MICP techniques. There is possibility of incorporating some mercury volume entered into induced fractures in during this experimental operation as there are chances of reducing the pore throat size during this enormous application. There is a problem, however, when correlating the results of mercury and helium due to the difference in the molecular diameter of the inert liquid and inert helium gas used in these experiments. It is likely that due to the applied pressure difference, this is not a very reliable correlation between these two techniques in this case. There is also chance of losing water during crushing and grinding the rock sample, but due to the strong ionic bond between clay particles, water loss from the shale particles was assumed to be negligible.

The largest porosity result from helium porosimetry is 2.80%, whereas the lowest porosity measured using the crushing method is 26.32% revealing a tremendous difference between these two methods. These two results challenge the accuracy of each other. Therefore, further investigations of the reliability of both methods necessitate investigation of the actual pores and voids volume available in the samples. The results obtained from the Roseneath and Murteree shales using helium porosimetry are shown in table 4.2.

It is evident from the data that the effective porosity results using helium porosimetry are between 3–10% of the total porosity from the core crushing method. As discussed before, the non-effective pores may not be 100% isolated, the openings connecting these micropores might be inaccessible due to nano scale openings through which helium gas or mercury cannot move into to saturate these pores and porous domains with much higher porosity.

Table 4.2: Comparison of Roseneath and Murteree shale formations porosity (%) using helium porosimetry

Number of Measurements	Murteree Shales Porosity Values (%)	Roseneath Shales Porosity Values (%)
1	2.80%	0.58%
2	1.49%	0.58%
3	0.60%	1.30%
4	0.06%	1.47%
5	1.50%	1.46%
6	0.88%	0.52%
7	1.40%	1.36%
8	0.98%	1.03%
9	0.15%	0.46%
Average	**1.09%**	**0.87%**

4.3.4 Total Free Porosity and FIB/SEM

A detailed description of focused ion beam milling and scanning electron microscopy methodology and secondary electron, backscattered electron and characteristic x-rays production and their application in mineral identification and rock classification has been given in previous chapter. In this chapter ultra-high magnification power and resolution was applied to extensively image the core samples to identify pores and porosity on submicron scale to investigate the reasons of very high total porosity estimated in liquid pyknometry procedure after having very low effective porosity and ultra-low permeability in both Roseneath and Murteree shale samples. Roseneath and Murteree shales are organic rich and overmature carbonaceous shales. They have attained over maturation at level, where natural gas methane gas has been cracked down into carbon dioxide (CO_2) (Encounter#1) and a secondary natural fracture system due to natural gas decomposition has developed we assume. Due to large quantities of available carbon dioxide, magnesium rich siderite as a consequence of its secondary dissolution and exhibit sporadic porous nature as identified in figure 4.13 using characteristic x-rays. These pores are comprised of siderite but they are part of the chaotic arrangement of the clays platelets creating large voids in these very porous zones. Rossi et al., 2001 Bell M. S., 2007; Estupiñán et al., 2007; and Pearce et al 2013 have reported the creation of secondary porosity in sedimentary rocks based on their observations. Secondary origin has been ascribed to feldspar and carboantes cements dissolution and the presence of siderite plays a very critical role in the retention of the primary intergranular porosoty by becoming load bearing mineral in clay rich shale like Roseneath and Murteree Shales (Fisher et al., 1998, Estupiñán et al., 2007). Siderite, the iron carbonate (Fe CO_3) is a common ore of iron, and mostly found in oraganic shales with higher clay content and coal seams in sedimentary rocks. Its common impurities are Manganese (Mn), Cobalt (Co), Calcium (Ca) Magnesium (Mg) and Zinc (Zn). Therefore a more general formula with these impurities can be written for siderite is as follows, (Fe, Mg, Ca, Mn, Zn, Co)CO_3 and hence give a number of different varieties which can coexist in the same sedimentary rock. The iron atom (Fe) in siderite can readily be replaced by these impurities to convert original siderite into Oligonite (Mn CO_3) and Sideroplesite (Fe Mg) CO_3. These varieties are not permenent and become unstable under various combinations of temperature and pressure and fluids intrusion and are prone to convert into other siderite avrieties as mentioned above. The interface between the two minerals graind become porous and porosity consolidates when Calcium ion(Ca^{++}) is replaced by the Iron ion (Fe^{++}, Ferrous) present in the intergranular fluids in the matrix followed by a change in volume as well (Pearce et al., 2013) by following chemical reaction:

$$\mathbf{3CaCO_3}(\text{Cacite}) + \mathbf{Fe^{2+}} + \mathbf{Mg^{2+}} = \mathbf{FeCO_3}(\text{Siderite}) + \mathbf{MgCa(CO_3)_2}(\text{Dolomite}) + \mathbf{2Ca^{2+}}(\text{Calcium Ion})$$

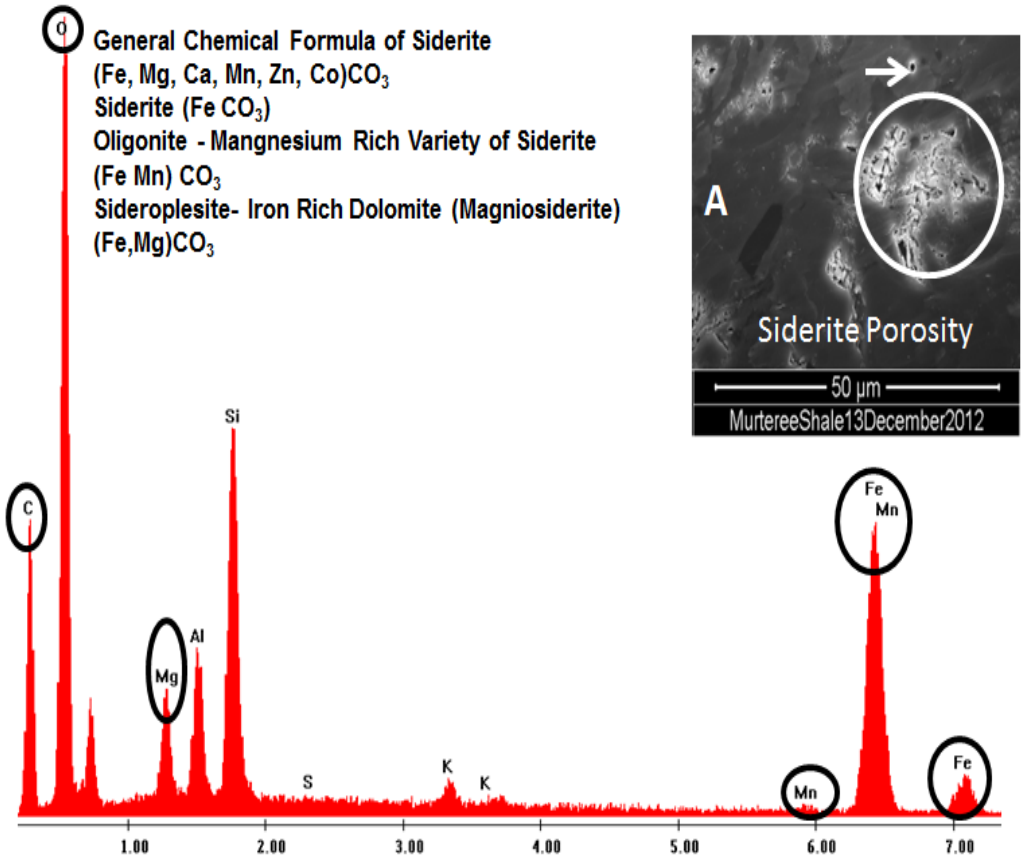

Figure 4.13: Characteristic x-rays of siderite grains for identification of oligonite and Sideroplesite surrounded by the clay platelets in FIB/SEM 2D image of Murteree shale labelled as A. A white arrow pointing to a cylindrical pore in siderite rich area over the ellipse surrounding a porous domain in Panel A is given as a proof of high density in this FIB/SEM scanned image of Murteree Shale.

Roseneath and Murteree shale samples were imaged at submicron level to ascertain the reasons of very high total porosity as labelled in 2D images using very high magnification and resolution power of FIB/SEM system. These core samples of Murteree and Roseneath were found having dispersed porous siderite rich zones surrounded by microlamination mainly build by mica/clay minerals platelets. The stacks of these platy minerals have strong role in impeding the flow of fluids across these porous zones and consequently giving very low effective porosity and permeability when helium porosimetry and MICP techniques are applied. Dense porous zones identified using FIB/SEM system is core requisite to explore free porosity as shown and documented in figures from 4.14 to 4.20 in the following pages.

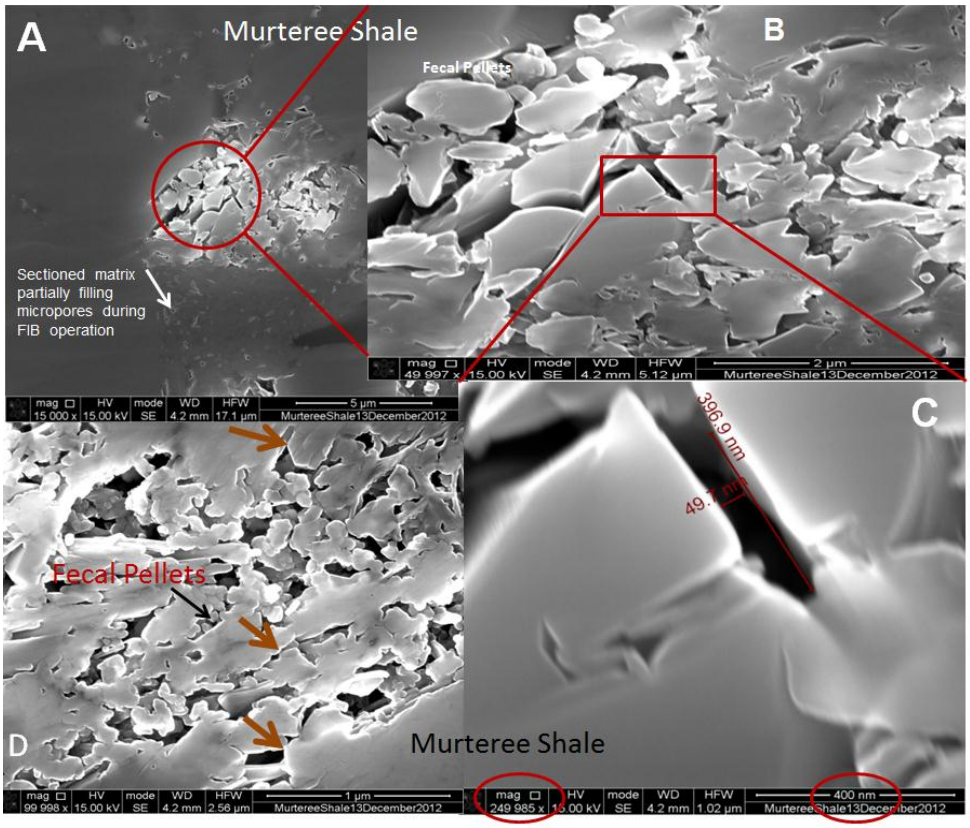

Figure 4.14: 2D images of highly porous isolated siderite rich domains in Murteree shale core sample labelled A, B and C from Project well Della4 at depth 6619.00 – 6620.00 ft., identified using SE detector of FIB/SEM system, inaccessible by helium porosimetry and MICP techniques, and pore throats labelled by brown arrows in 2D image labelled D.

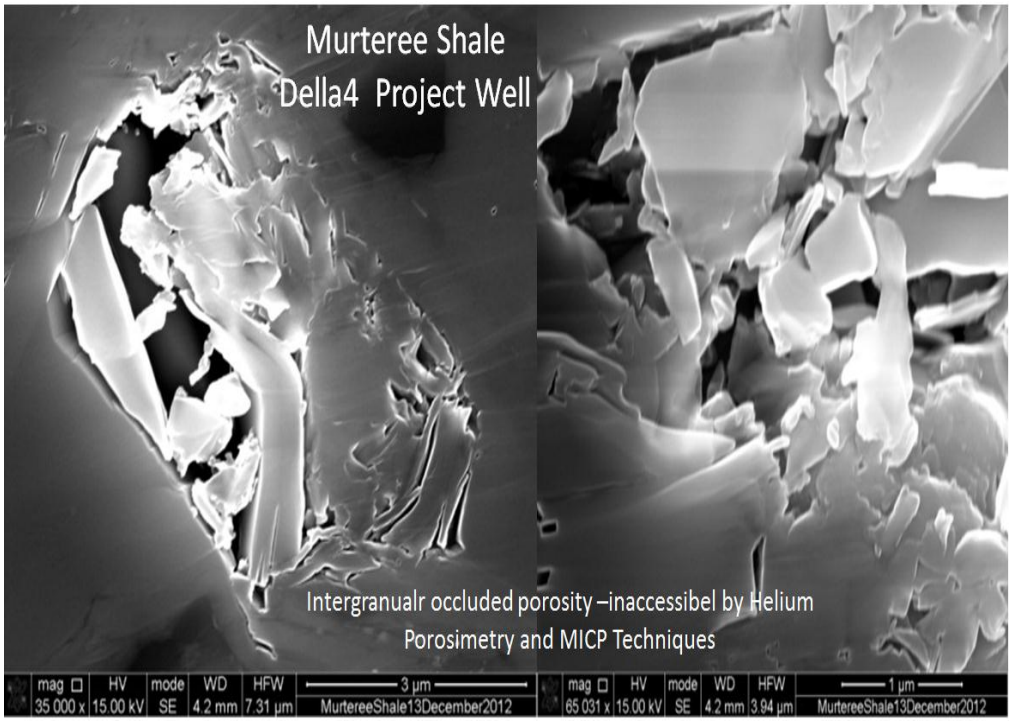

Figure 4.15: Occluded intergranular porosity in FIB/SEM 2D images of Murteree Shale.

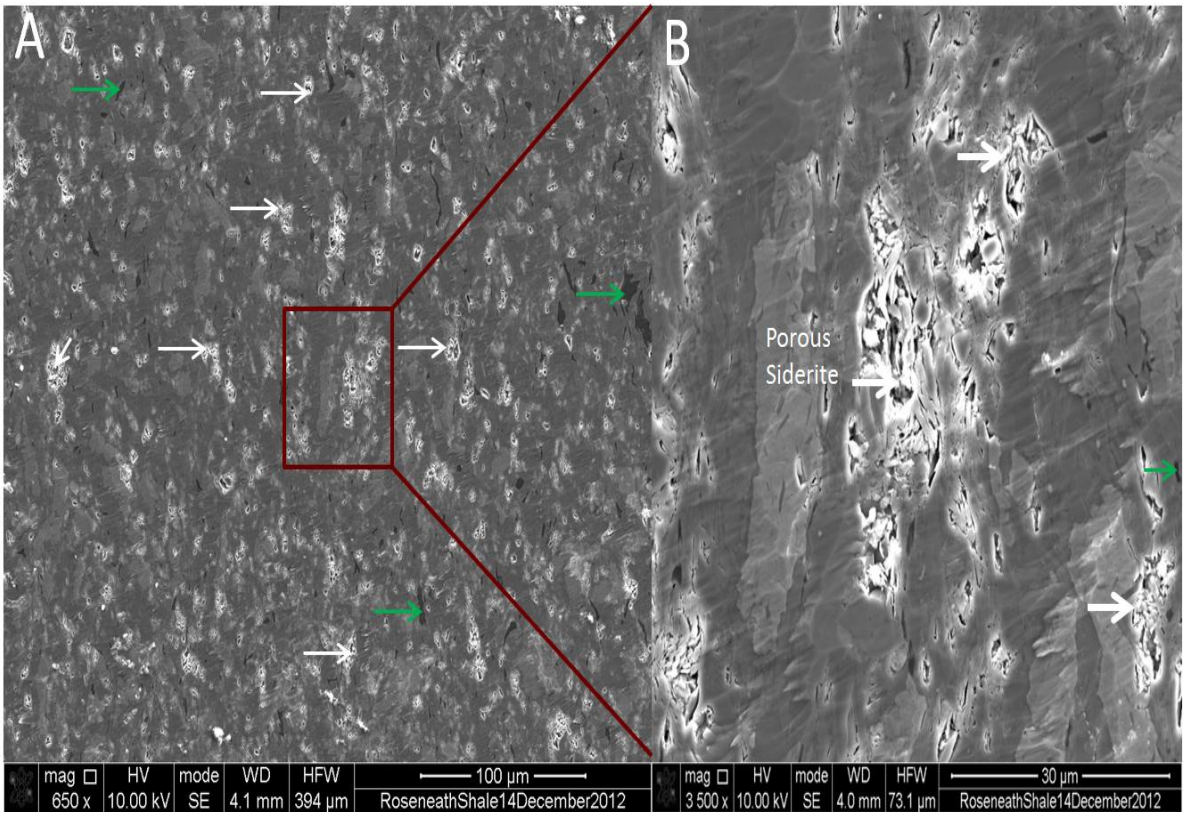

Figure 4.16: FIB/SEM prepared Roseneath Shale sample image with isolated highly porous domains, siderite grains marked by white arrows and green arrows showing the organics in panel A and red rectangle in A and enlarged (increased magnification & resolution) to show the strength of the intergranular porosity of siderite grains in panel B.

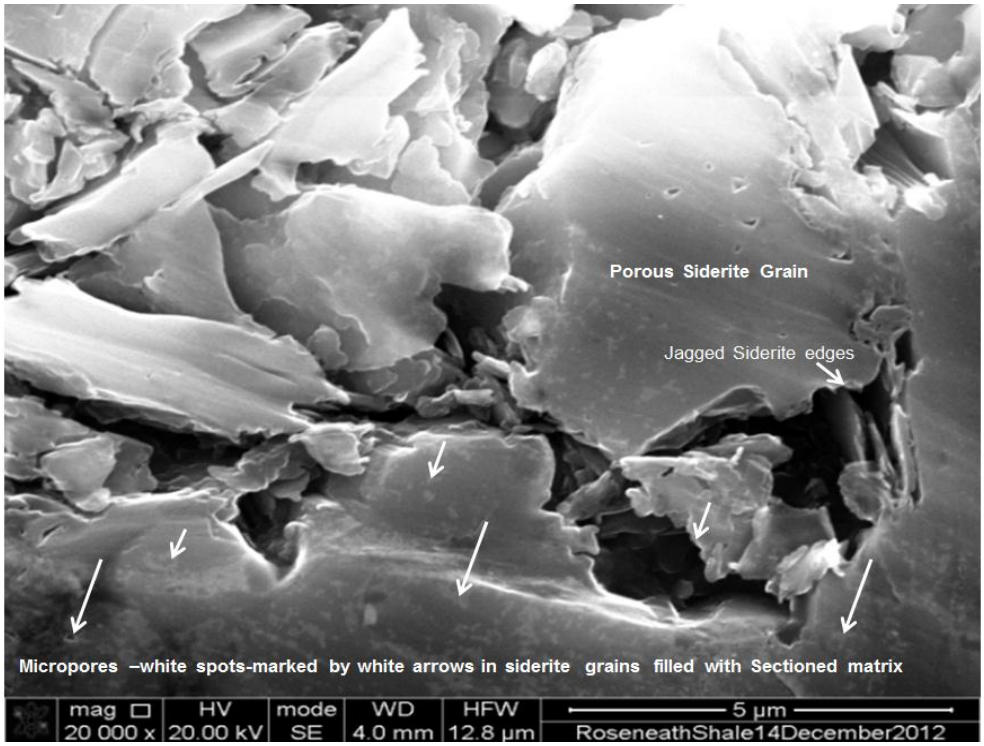

Figure 4.17: Roseneath shale FIB/SEM sample showing porous siderite grain with intragranular microporosity and surrounded by intergranular porosity as well.

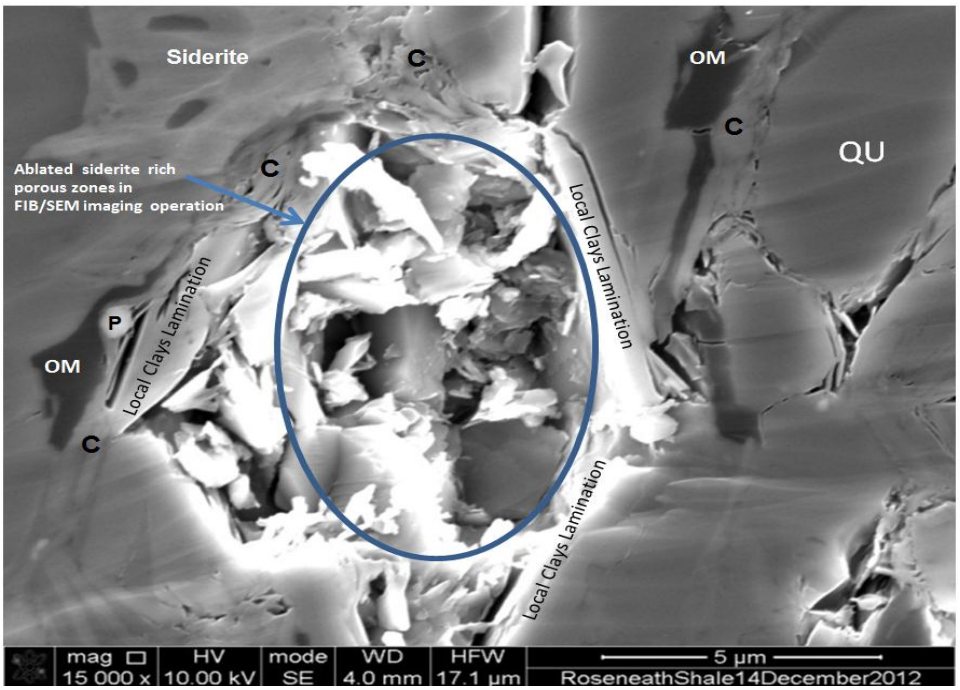

Figure 4.18: Roseneath shale (FIB/SEM) image depicting the role of local clays lamination in the inaccessible porous zones mainly dominated by siderite and clay platelets and role of pyrite (marked by P) and other heavy mineral in keeping the intergranular pores open during fraccing operations (OM =organic matter, QU=quartz; and C=clays).

There were some problems confronted during the 3D pore model building using FIB/SEM automatic sectioning techniques and Avizo® software. Due to very rich in clay zones as shown in figure 4.22 below labelled A, B and C, large amount of serially sectioned material was found redeposited in front of sectioned face of the sample. Higher contents of clays found in this sample were verified later by SEM as one shown in figure 4.20 on next page.

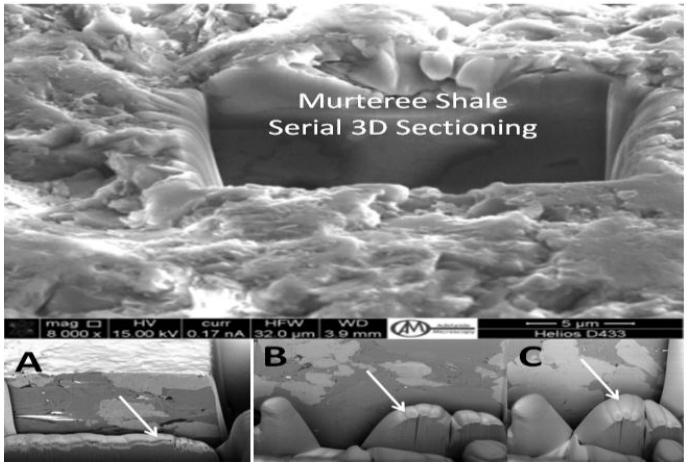

Figure 4.19: Serial Sectioning of Murteree Shale using FIB/SEM for 3D volumetric Model, depicting the problem faced during milling operations, redeposition of the sectioned material in front of ablated faces of the sample labelled by white arrows in panels A, B and C, leading to failure of 3D model construction for identification/guess of interconnectivity of the pores and total porous zone in sample.

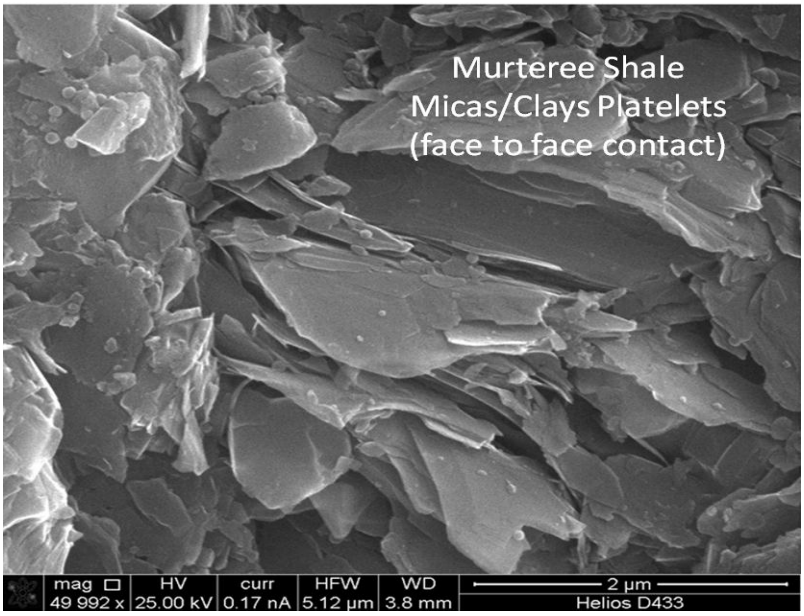

Figure 4.20: Murteree shale sample mechanically prepared and imaged without carbon coating using SE detector of SEM, showing stacked clays/micas platelets representing challenge for fraccing operation.

Organic rich sedimentary rocks can be divided into bitumen impregnated rocks, humic coals and oil shales. Oil shales or source rocks as an essential part of a petroleum system have various sedimentray environment and origin as lacustrine, deep marine and deltaic locations but to define oil shale precisely is yet a matter of controversy apart from that any organically rich sedimentray rock which yields in commercial quantities of oil on pyrolysis (Cane 1976; Hutton 1987; Magoon and Dow , 1994). Also black shale and carbonaceous shale are two different orgaic rich source rocks. The former is mudrock containing silt and clay size minerala grains and clastic material impregnated with organic matter (Swanson, 1961) and most often defined as argillaceous, argillaceous pelitic, argillaceous siliceous and argillaceous –carbonate sediments with transformed organic matter. Carbonaceous shales possess type III kerogen (Terrestrial organic matter) representiong a transition of one organic matter, humov coals into coaly shale, and with a fine stratification, hard and compact and dull in colour (Suárez-Ruiz I., 2012).

4.4: CONCLUSIONS

Based on helium, mercury porosimetry and liquid pyknometry results correlation with extensive very high magnification and resolution 2D-iamges we reached the following conclusions:

- The Roseneath and Murteree carbonaceous shale samples have very high isolated intergranular porosity to accommodate large quantities of natural gas, which is not accessible by mercury and helium injection.
- The very low permeability and effective porosity are due to the micro-fabric and local microlamination documented in FIB/SEM images of the Roseneath and Murteree shales.

- The effective porosity measured using helium porosimetry is not worth consideration in carbonaceous shale acting a source and reservoir simultaneously because it measures the porosity from where stored methane molecules cannot escape or cannot enter to be stored. Helium's molecular diameter is less than methane's molecular diameter.
- Similarly, free effective porosity and pore throat size classification using MICP seems to be in quite good agreement with helium porosimetry. Pores comprising of effective porosity estimated less than 2.00% have pore throat size in range of 2nm to 50nm (mesopores throats).
- Helium and mercury effective porosities are not exactly the same, and the result in each case is an average representation of a range of effective porosities evaluated in these two techniques. These two results simply corroborate that the shales have very low effective porosities.
- The isolated highly porous domains are surrounded by an inorganic and organic minerals matrix. There are no pores in this surrounding matrix, or communication channels and apertures of these surrounding porous zones through which helium and mercury molecules cannot penetrate. The diameter of apertures leading to these porous zones is smaller than the molecular diameter of both helium and mercury consequently and is not able to quantify this porosity.
- Porous Fe (iron) rich magnesium carbonate, (Fe Mg)CO_3 and Fe (iron) rich manganese siderite (Fe Mn)CO_3 cannot be detected even by Micro and Nano Computerized Tomography, because porous mass is surrounded by heavy minerals, atoms of iron and it will absorbs all the X-rays leaving very bright spot in the scanned samples of Murteree and Roseneath shales, making pores within these iron rich grains hard to be identified and quantified in the final values of the total porosity.
- Highly porous matrix consisting of siderite and clays confirmed in FIB/SEM images of both Roseneath and Murteree shale has contributed toward high total porosity values when liquid pyknometry methodology was conducted.
- The average density of various siderite forms and pyrite is around 4.00 gm/cm^2 and 5.00 gm/cm^2 respectively in the presence of some other heavy minerals like sphalerite and rutile, which makes wireline logs especially density log application/readings very sceptical along organic matter having average density 1.10 gm/cm^2.
- It is believed that initially estimated very low effective porosity by helium porosimetry and mercury injection techniques is acceptable whilst presumed very high total porosity estimated by liquid pyknometry and later visualised in 2D Murteree and Roseneath shale FIB/SEM images confirmation is formidable task using available experimental techniques.

CHAPTER 5

Water Saturation Evaluation using Wireline Logs, Focused Ion Beam Milling and Scanning Electron Microscopy

5.1 Introduction

The objective of this chapter is to investigate the validation of various resistivity water saturation models application in Roseneath and Murteree shales. FIB/SEM visualized total porosity of Murteree shale scanned samples and clays volumes content from logs data was incorporated as well. Since Archie's formula in 1942 a number of models were derived for water saturation determination for shaly sand such as Simandoux (1963); Total Shale Schlumberger (1969); Simandoux (1969); Fertl and Hammack (1971); Indonesian Poupon and Leveaux (1971); Dispersed Clay Schlumberger (1972); Modified Total Shale Schlumberger (1972); Dual Water Model (1978); Schlumberger (1989). There are two groups of models to determine water saturation, namely shale volume fraction (V_{sh}) models and cation exchange capacity (CEC) models. Roseneath and Murteree carbonaceous shales have sourced natural gas which is being held as compressed free gas in interstitial pores and adsorbed on organics and clay minerals. These source rocks and reservoir rocks exhibit very heterogeneous rock, mineral, organic and fluid content spatially as found and reported in the last two chapters, 3 and 4. The knowledge of mineralogy and organic content is core requisite for water saturation estimation for shale gas reservoirs like conventional reservoirs. Therefore the amount and type of salt dissolved in the brine along with the knowledge of fraction, structure and types of constituent clay minerals like illite, kaolinite, and chlorite have controlling effects in water saturation calculation (Serra Oberto 1984). Also the evaluation of porosity is an essential part of resource evaluation although its evaluation is a formidable task due to ultra-fined grained argillaceous, arenaceous and carbonaceous nature of clastic material (Ahmad M. et al. 2011). As a consequence, the knowledge about the diversity in type and amount of minerals and fluids, and interaction among rock solid grains and fluids affecting the storage capacity as well as production of gas, is a fundamental requirement. Organic shale can also has some conductive heavy minerals like pyrite, hematite, siderite, and very rarely found, glauconite, an iron rich dioctahedral clay mineral, but more often they lack in providing continuous phase to conduct electric current through sampled reservoir (Pirson, 1963). These minerals can have reasonable impact on the wireline logging outcome and ultimately can lead to an erroneous error in initial resource evaluation.

Wireline logging has been used for petrophysical and geomechanical rock properties of shale gas reservoirs (Passey et al., 1990; Zuber et al. 1994; Kundert and Mullen 2009; Quirein et al., 2010; Amiri et al. 2012. Wu and Aguilera (2011) favoured the application of Archie's equation for water saturation estimation in Barnett shale based on the experimental observations. They believe that Barnet shale is water wet, although Clarkson et al. (2011) have expressed some concerns about the application of the Archie's formula in unconventional gas reservoirs. In Marcellus shale, the

water saturation was estimated using Archie's formula but Boyce and Carr (2009) have recommended the use of Simandoux model in Marcellus shale. Popielski et al. (2012) and Torres-Verdin (2010) have reported Archie's equation use for water saturation determination. Miller and Shanley (2010) also believed that as long as industry lacks in any global standard for water saturation estimate in shale gas reservoirs, the Archie's formula is the only option available. In Cooper Basin, Archie's equation was applied to determine the water saturation in Epsilon formation bearing a clay content of 22% and Indonesian formula in Roseneath and Murteree shales with clay content more 50% (PIRSA, 2011). Water saturation determination in Cooper Basin was found problematic when gamma ray for shale volume calculation was tried as well as Indonesian equation (Poupon and Leveaux, 1971) and Fertl formula (Fertl, 1987) with some adjustments (Gravestock et al. 1988). Worthington (1985) pointed out some uncertainties when Simandoux equation was applied to estimate water saturation in these fresh water shaly reservoirs and the rest of reservoir rocks as well. Similarly, Morton (1990) evaluated the clay conductivity values based on the clays cation exchange capacity (CEC) to estimate water saturation in sampled reservoirs from Cooper Basin. It was found that all these empirical models failed in predicting the accurate water saturation in Cooper Basin. The reasons of this unreliable water saturation estimates were assigned to variable brine salinity (R_w), high clay content (V_{cl}), variable gas and oil saturation (S_h) as well as high reservoir temperatures prone to affect the wettability of the both conventional and unconventional reservoirs in Cooper Basin (Gravestock et al. 1988). Similarly, Wyllie formula application to evaluate sonic porosity in these reservoirs was recommended to be reinvestigated on some valid grounds observed by Khaksar (1994) and Khaksar and Griffith (1996) leaving Roseneath and Murteree shales porosity subject untouched. In any shaley model to calculate water saturation, shale volume estimation is essential.

The direct evaluation and assessment of shale is not possible from wire-line logs like conventional reservoirs and if it is estimated by logs, it is essential that logs estimated values be calibrated with other data such as Quantitative Evaluation of Minerals using Scanning Electron Microscopy (QEMSCAN), XRD analysis, and Focused Ion Beam Milling and Scanning Electron Microscopy (FIB/SEM). In the following sections we have discussed our methodology used to determine different parameters for water saturation evaluation and then results are presented followed by the discussion on sensitivity study of different parameters. Some conclusive results are given at the end.

5.2 Methodology-Wireline Logs and FIB/SEM - Application for Water Saturation

In order to check and investigate scope of Archie Indonesian, Simandoux and Total shale models application in Roseneath and Murteree shales for water saturation the completion reports of some selected wells were retrieved from South Australian Resources Information Geoserver (SARIG web site). These well completion reports have geochemical and log data for Archie's parameters, like tortousity factor (a), cementation exponent (m), saturation exponent (n) and brine salinity R_w.

Archie's parameters a, m and n are prone to exhibit a range of values especially the cementation exponent m (Salem and Chillingarian 1999) and there is no direct relationship between these variables (Rezaee et al. 2006; Haghighi et al. 2008) consequently sensitivity analysis was only solution to find the most appropriate values for these variables in logged Murteree shale interval in project well Della4. Porosity (ø) and formation true resistivity R_t, shale volume V_{sh} and shale resistivity R_{cl} values were retrieved and correlated among these different wells. The selected wells whose completion well reports from South Australian Resource Information Geoserver web site (SARIG) have been used and data applied in the Archie's model are as follow:

1. Della004 Well (SARIG WCR 02047)
2. Encounter 001 Well (SARIG WCR 2010/000389)
3. Middleton 001 Well (SARIG WCR 08131/000)
4. Moomba 46 Well (PIRSA WCR-Open File Env.- 04893)

These completion reports have data for correlation to make judgment about the lithology, mineralogy organic content, as well as reservoir properties like porosity, permeability, a, m, n, true resistivity, brine resistivity (R_w). These parameters values were correlated between wells to check the validity of their application later in water saturation estimation, using any resistivity model of choice. Project well Della#4 composite logs was digitized to find true resistivity, gamma ray, bulk density, and sonic velocity and caliper data, in Murteree shale zone as shown in figure 5.1. These digitized values of required parameters were used to derive various values for shale/clay volumes, porosity and later applied in four saturation models.

Porosity evaluation using wireline logging for prospective shale gas reservoirs is subject of controversy like by any other industry standards. The doubts and uncertainties are consequence of low density organic matter with high hydrogen nuclei concentration and heavy minerals impact on resistivity, sonic, neutron, and nuclear magnetic resonance (NMR) logging tools. The micropores making free porosity, range from nano to macropores in shale particles, apart from the natural fractures found in the shale gas reservoir. Shaw et al (2006) have emphasised that very low effective free porosity results usually found in potential carbonaceous shales, using helium porosimetry and mercury injection capillary pressure (MICP) techniques have very low permeability, ranging from micro to nano darcies and Rezaee et al (2012) also reported submicron range of pores throat size in shales. Although there is dual storage mechanism (compressed and adsorbed gas) in the shale gas reservoir we have only tried to estimate the total free porosity available for compressed free gas using logs data and FIB/SEM high magnification and resolution images.

We used wireline log and core samples in well Della4 for this study. Composite log of Della4 (PIRSA1972) was digitized to find caliper, gamma ray, sonic velocity, true resistivity and bulk density in Murteree shale zone as shown in figure 5.1. These digitized values were used to estimate various properties as given in table 5.1.

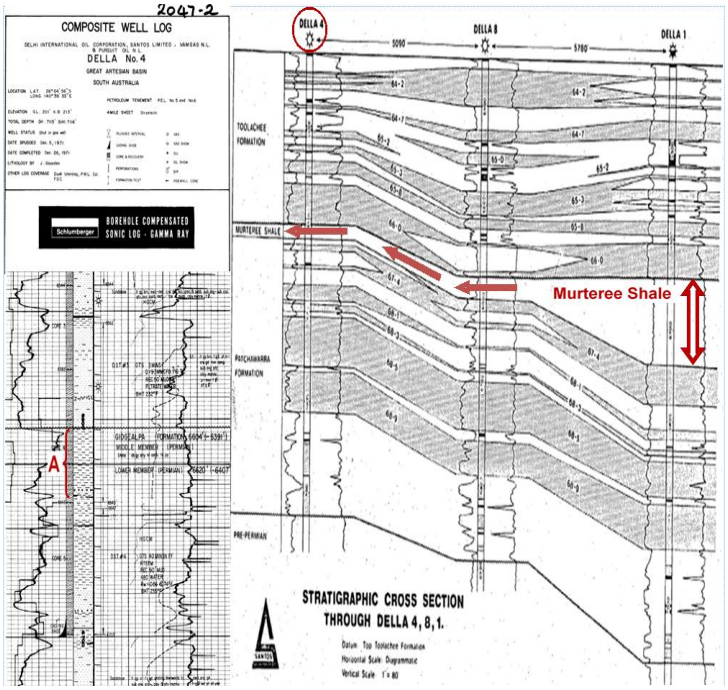

Figure 5.1: Stratigraphic cross section and composite well log from project well Della4

Table 5.1: Digital log data of Murteree shale in project well Della4					
Sample Depth in Project well Della4 (ft.)	Caliper (in.)	Gamma Ray (API)	Δt Sonic Velocity (µs/ft.)	Rt True Resistivity Ohm.m	Rho-b Bulk Density gm/cc
6620.00@	9.50	132.30	71.67	64.80	2.62
6619.50@	9.48	138.00	71.28	67.56	2.60
6619.00@	9.47	142.40	70.81	70.70	2.59

Legend:	
6620.00ft @ 6619.50 ft.@ 6619.00ft @	Derived log based values from exact location of Murteree Shale Core sample in Della#4 Project well

The core samples from the same depths were used to estimate porosity, brine resistivity, and Archie's parameters (*a*, *m* and *n)*. Focused ion beam milling and scanning electron microscopy (FIB/SEM) results were used for mineralogical and petrophysical evaluation. Considering the ultra-complex nature of Mureteree and Roseneath shale formations and sensitivity of estimated water saturation on initial resources, four models were selected and results were correlated to improve the understanding of water content evaluation. Although we have not used any samples from Roseneath formation except FIB/SEM images, early Permian Roseneath and Murteree organic shales have similar lithological, mineralogical and geochemical characteristics as they were sourced from same provenance and were laid down in same type of depositional environment in Cooper Basin (Gravestock 1988). The post depositional changes in shale organic matter and inorganic sediments are believed to be as follows:

1. Smectite to illite conversion reducing clay surface area (Illite has less surface area than Smectite)

2. Authigenic quartz formation increasing tortousity and cementation
3. Water production followed by decrease in salinity
4. Mixed wettability of reservoir rock, the attachment of organic matter, kerogen, brine and natural gas to clays grains/platelets

We believe that the collective impact of these post depositional physical and chemical reactions in shale sediments especially with reference to organic matter, clays conversion and fresh water production tend to lessen the effect of low conductivity on the estimation of water saturation which makes Archie formula and other resistivity shaly models vulnerable in source shale rocks.

5.3 Results

The core samples of Murteree shale from well Della4 have been extensively analysed using FIB/SEM, QEMSCAN and XRD for mineralogy identification and quantification of minerals and rock classification. Total porosity estimated in QEMSCAN, total porosity from pyknometry method and total porosity from density logs were correlated with FIB/SEM visual estimation of total porosity in 2D images of Murteree shale. Effective porosity from helium porosimetry and effective porosity from mercury injection capillary pressure (MICP) techniques compared to check ultra-low permeability correlated using cores from Murteree shale in Della4 well. The detailed results have been discussed in (Ahmad et al. 2011) and (Ahmad and Haghighi 2012). To document characteristic response of organic matter, heavy mineral and sillicates content and their distribution pattern has been shown in figure 5.2 to understand the their collective resistant and conductive shale constituents response on wireline logging tools in Murteree shale gas reservoir.

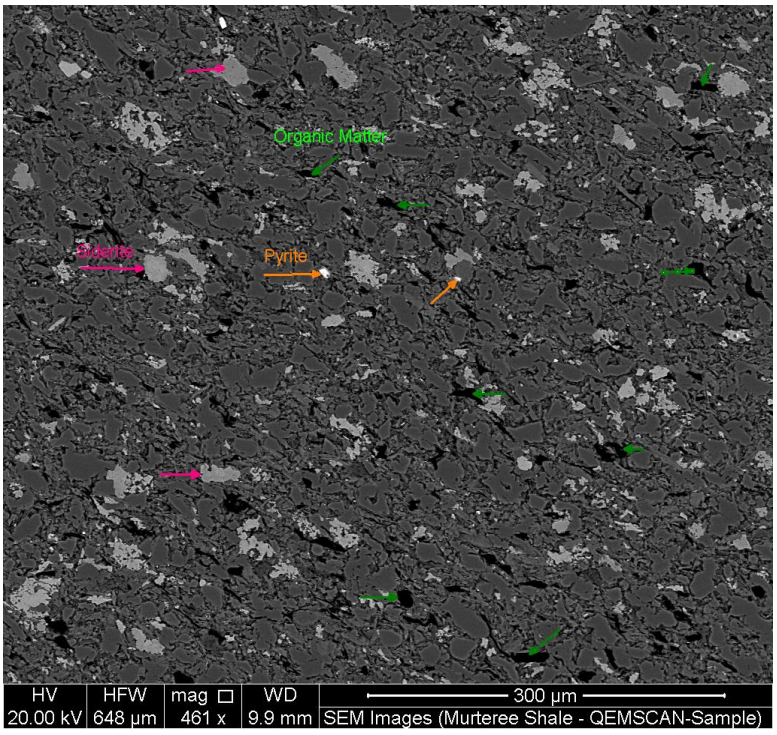

Figure 5.2: Backscattered electron beam image showing the distribution of organic matter, pyrite, siderite and silicate content of a scanned Murteree shale sample during QEMSCAN analyses

The clay content using QEMSCAN and XRD were evaluated to be 47.30% and 52.3% respectively. This is in quite good agreement with the results from gamma ray log using Steiber formula in well Della#4 (PIRSA 1972) as shown in table 5.2.

Table 5.2: Total clay content% in Murteree shale Well Completion Report Della#4 Project Well	
XRD Results	50.59% (Avg.)
QEMSCAN Results	47.30% (Avg.)
Della#4 wireline Log using Steiber formula	52.3 % (Avg.)
Encounter#1 XRD Results	Avg. 53.4%

A number of authors have recommended the use of various empirical formulas for derivation of shale volume using gamma ray log values depending on the nature of shale interval (Rider 1996). In addition to Steiber formula, five other correlations have been used and the results are shown in Table 5.3. The linear laminated IGR equivalent to V_{sh} was derived as given in appendix. Other radioactive minerals can cause higher IGR readings. Therefore, IGR is not recommended. The other nonlinear relationships are tertiary unconsolidated rocks, consolidated and high shale content, older consolidated and Mesozoic rocks, Steiber and Super Steiber (see appendix, C and mathematical expression C1-C6) and are graphically shown in figure 5.3. As we can see in table 5.3 compare to other correlations, Steiber formula estimates the shale content closer to the results from QEMSCAN and XRD. Non-carbonaceous shale resistivity value, R_{cl} (25.00 Ohm.m) was taken from Encounter#1 due to strong correlation of Murteree shale mineralogy in Della4 and Encounter1 as shown in table 5.2.

Table 5.3: Shale/Clays Volume (Total Clay Fraction) Derived

Depth (ft.)	Shale Volume=Gamma Ray Index(GRI) (Fraction)	Tertiary Rocks Unconsolidated Formula (Fraction)	Tertiary Rocks Consolidated Formula (Fraction)	Older Rocks (Mesozoic) Consolidated High Shale Content Formula (Fraction)	Steiber Formula (Fraction)	Super Steiber Formula (Fraction)
6620.00 @	0.7300	0.4570	0.5780	0.7250	0.4740	0.3110
6619.50@	0.7690	0.5130	0.6280	0.7440	0.5260	0.3560
6619.00@	0.7990	0.5610	0.6680	0.7590	0.5690	0.3980

Legend:	
6620.00ft @ 6619.50 ft.@ 6619.00ft @	Derived log based values from exact location of Murteree Shale Core sample in Della#4 Project well

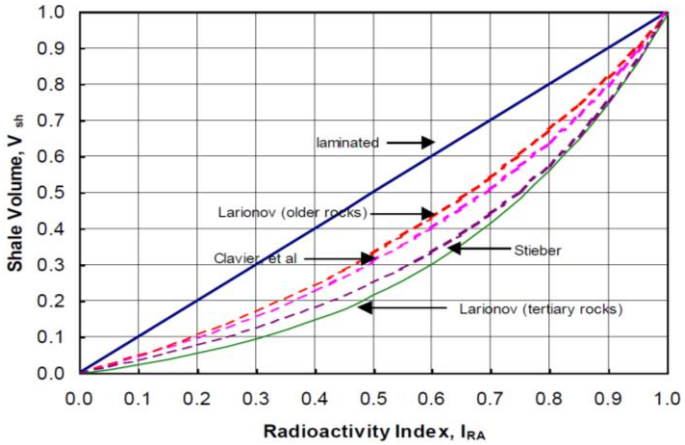

Figure 5.3: Graphical expression of various formulas used to derive shale/clays volume (Engler 2012).

We found a very high total isolated porosity of 30.43% based on pkynometery for Murteree shale. Therefore, the value of porosity in Roseneath and Murteree shale is controversial. Using Wireline log data, the porosity was calculated from six different correlations (see appendix C and mathematical expressions, C7 – C12)). We found Wyllie formula with Hilchie's correction factor estimate the porosity to be the closest value to effective porosity from MICP and total porosity to QEMSCAN. Density/sonic cross-plot also determine the total porosity close to QEMSCAN and when density of clays and matrix is very close to each other, density porosity can be used without correction as reported by Asquith, 1990. We found a range of density porosity from 1.00% to 9.00% which seems dependent on varying amounts of total clay volume in Murteree Shale in Della#4 project well.

Table 5.4: Porosity evaluated using various formulas

Depth(ft.)	Sonic Porosity Wyllie Formula (Fraction)	Hilchie's Correction Factor (Sonic Porosity*0.7) (Fraction)	Sonic Porosity using B Correction Factor (Fraction)	Sonic Porosity using BBc Correction Factor (Fraction)	Density Porosity (Fraction)	Sonic-Density Cross Plot Porosity (Fraction)
6620.00@	0.0363	0.0254	0.0171	0.0073	0.0212	0.0321
6619.50@	0.0325	0.0228	0.0153	0.0066	0.0361	0.0284
6619.00@	0.0278	0.0195	0.0131	0.0056	0.0446	0.0240

Legend:	
6620.00ft @	Derived log based values from exact location of Murteree Shale Core sample in Della#4 Project well
6619.50 ft.@	
6619.00ft @	

Our results on porosity evaluation show that Murteree shale has very low effective porosity. Using MICP and helium porosity, we found effective porosity to be 2.0 % in average and QEMSCAN

results give total porosity around 2% in Murteree shale. FIB/SEM 2D images of Murteree shale given in figures 5.4, 5.5 and 5.6 present some examples showing very high intergranular and matrix fractured porosity with chaotic clay platelets arrangement creating some concerns about reliability of total porosity we found in liquid pyknometry and effective porosity in helium and MICP techniques.

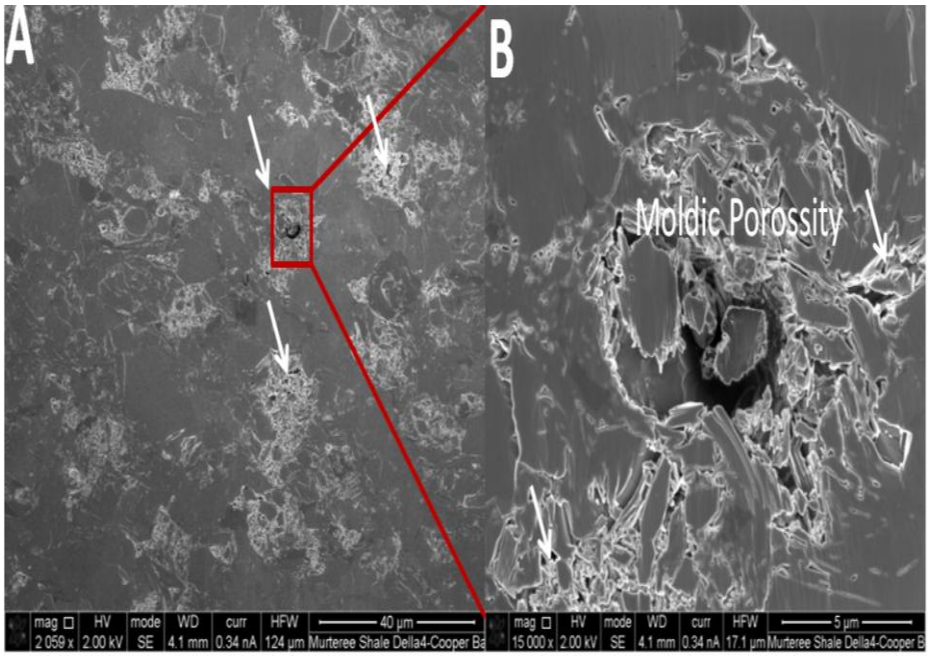

Figure 5.4: Two FIB/SEM images showing moldic and intergranular porosity, from Murteree shale (A) and enlarged rectangle in panel B project well Della4, depth 6619.00-6620.00ft.

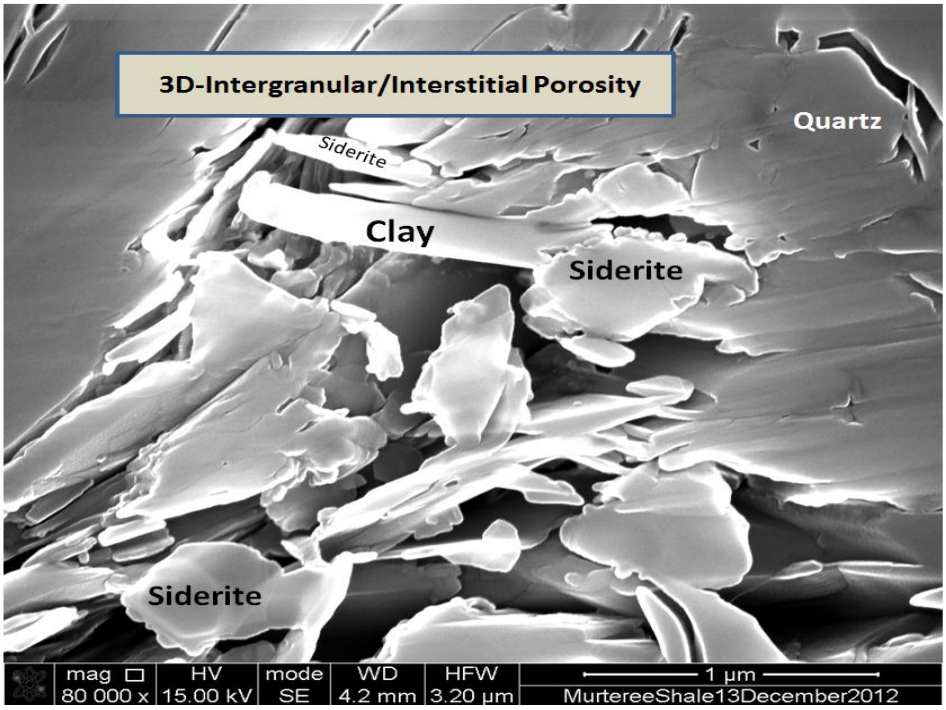

Figure 5.5: One of FIB/SEM images showing intergranular/fractured submicron porosity and chaotic clay platelets arrangement from Murteree shale.

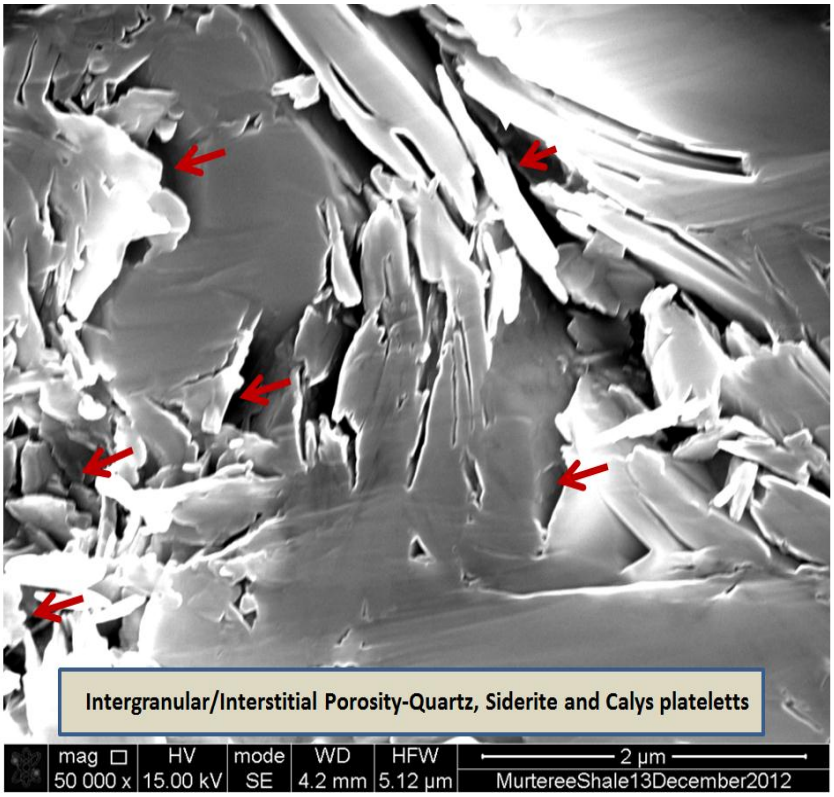

Figure 5.6: One of FIB/SEM images showing intergranular/fractured submicron porosity by red arrows and chaotic clay platelets, both detrital and authigenic minerals arrangement in this 2D image Murteree shale with from Project well Della4.

We used four different saturation models (Archie, Indonesian, Simandoux, and Total Shale (see appendix C and mathematical expressions C13 – C16), using shale volume from Steiber formula and density porosity from density log (see appendix D and TableD4). As we can see from the results in table 5.5, Archie and total shale model give false results of higher than 100% water saturation. Only Indonesian and Simandoux estimate water saturation with reasonable values when total porosity is very low (2%-4%).

Table 5.5: Four water saturation models results

Type of Porosity		Sw Archie Model (Fraction)	Sw Indonesian Model (Fraction)	Sw Simandoux Model (Fraction)	Sw Total Shale Model (Fraction)
Density Log Porosity (Project well Della4)	0.0212	4.306	0.875	0.878	5.529
	0.0361	2.477	0.700	0.725	2.228
	0.0446	1.960	0.612	0.628	1.545

A sensitivity analysis was performed on the impact of true resistivity on Indonesian and Simandoux models. In table 5.6, when the resistivity is less than 50-40 Ohm.m, the water saturation becomes more than 100% and unreasonable results are created.

Table 5.6: Sensitivity analysis results using assumed true resistivity values in Indonesian and Simandoux models

True Resistivity (Ohm.m)	Sw Indonesian Model (Fraction)	Sw Simandoux Model (Fraction)
10.00	1.985	3.969
20.00	1.310	2.153
30.00	1.016	1.434
40.00	1.062	1.347
50.00	0.882	1.002
60.00	0.762	0.785
64.80	0.834	0.860
67.56	0.759	0.753
70.70	0.702	0.671
80.00	0.702	0.683
90.00	0.618	0.559
100.00	0.556	0.471
150.00	0.513	0.378
200.00	0.414	0.260
250.00	0.352	0.194
300.00	0.362	0.193
350.00	0.313	0.150
400.00	0.278	0.122

Legend:
True resistivity at exact location of Murteree Shale Core sample in Della#4 Project well

In order to study the effect of porosity we assumed the porosity to be 10% in those four different saturation models using the same shale volume from Steiber formula. In this scenario assuming higher porosity based on pyknometry doubtful estimates and FIB/SEM images, we found that all four saturation models give reasonable results as it is shown in table 5.7, however Archie and total shale model calculate the water saturation higher than Indonesian and Simandoux models. Also we examined the sensitivity of Archie formula for porosity (a=1, m=2, n=2) versus Humble formula (a=0.62, m=2.15, n=2) and the results are also given in table 5.7below.

Table 5.7: Sensitivity analysis for assumed porosity =0.1(fraction) in Murteree shale

Porosity Ø (Fraction)	Shale Volume-Steiber Formula (Fraction)	a	m	n	Sw Archie's Model (Fraction)	Sw Indonesian Model (Fraction)	Sw Simandoux Model (Fraction)	Sw Total Shale Model (Fraction)
0.1000	0.474	1.00	2.00	2.00	0.894	0.488	0.550	0.600
0.1000	0.526	1.00	2.00	2.00	0.894	0.467	0.523	0.570
0.1000	0.569	1.00	2.00	2.00	0.894	0.451	0.503	0.543
0.1000	0.474	0.62	2.15	2.00	0.837	0.534	0.601	0.734
0.1000	0.526	0.62	2.15	2.00	0.837	0.509	0.568	0.701
0.1000	0.569	0.62	2.15	2.00	0.837	0.490	0.543	0.669

Also in another sensitivity study, we studied the effect of different porosity on four saturation models. As it is shown in table 5.8, when the porosity is less than 9 percent, Archie is not valid correlation; however, at high porosity, Archie model may be used for water saturation calculation.

Table 5.8: Sensitivity analysis results using different porosity in water saturation models

Density Porosity Ø (Fraction)	Archie's Model Sw(Fraction)	Indonesian Model Sw(Fraction)	Simandoux Model Sw(Fraction)	Total Shale Model (Schlumberger) (Fraction)
0.0850	1.052	0.532	0.598	0.726
0.0900	0.993	0.492	0.551	0.646
0.0950	0.941	0.463	0.515	0.578
0.1000	0.894	0.488	0.550	0.600
0.1050	0.851	0.455	0.510	0.539
0.1100	0.813	0.429	0.480	0.486
0.1150	0.777	0.451	0.508	0.511
0.1200	0.745	0.423	0.474	0.462
0.1250	0.715	0.401	0.448	0.419
0.1300	0.688	0.419	0.471	0.445

5.4 Discussion

The direct evaluation and assessment of porosity in shale is not possible from wireline logs and some special algorithms are needed (Worthington 2011), because density, sonic and neutron logs do not measure porosity directly. Well logs in shale gas reservoirs can help in reservoir strata classification, their fluids content and saturation, porosity, their thickness and depth. But to check the economic value of a conventional and unconventional reservoir with confidence, it is essential that logs based estimations about original gas in place must be correlated with laboratory geochemical analysis of cores taken from the same depth of the same exploratory well.

Application of Archie's formula for water saturation in shale gas reservoirs is controversial when clay content is higher than 50%. There are negatively and positively charged surfaces and edges of clays platelets, adsorb alkaline ions like Na^{+}, Ca^{++}, K^{+} through brine while there is also attraction between surface of a clay particle or platelet to the edge of the other clay platelet. This natural affinity of the brine alkali ions and clay flakes in reservoir matrix is the fundamental theme which makes Archie's formula vulnerable in shaly petroleum reservoirs. Sapropelic organic matter also has charged surface and is attached to the clay grains during depositional phase of sediments in a lake or marine depositional environment. This chemical interaction and attachment of the alkali ions in brine and organic matter to clays is known as flocculation and results in formation of larger flake particles and aggregates called flocs or floccules (Horseman et al. 1996;

Rieke et al 1974, Wolf and Chilingarian 1975; Yu and Aguilera 2012) as shown in figures 5.7 to 5.10. on following pages.

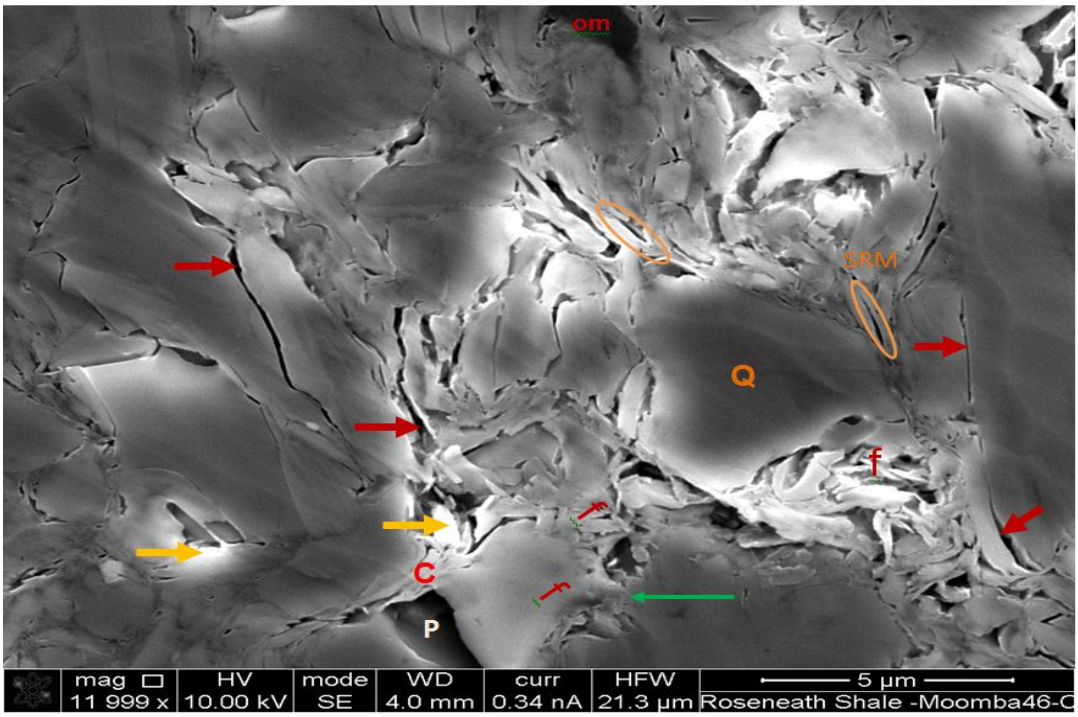

Figure 5.7: Ion Milled Roseneath Shale sample surface: Red arrows pointing the electric current paths/gas flow paths and tortousity in sample, Q quartz, C clays, f, floccules, om, organic matter; yellow arrows showing heavy minerals; green arrow pointing to the attachment of the clay particles edges with face of the clay particles, shale resistivity model concept (SRM, organics, clays and adsorbed gas - yellow ellipses) and P (white) showing a large pore just above window task bar at the bottom.

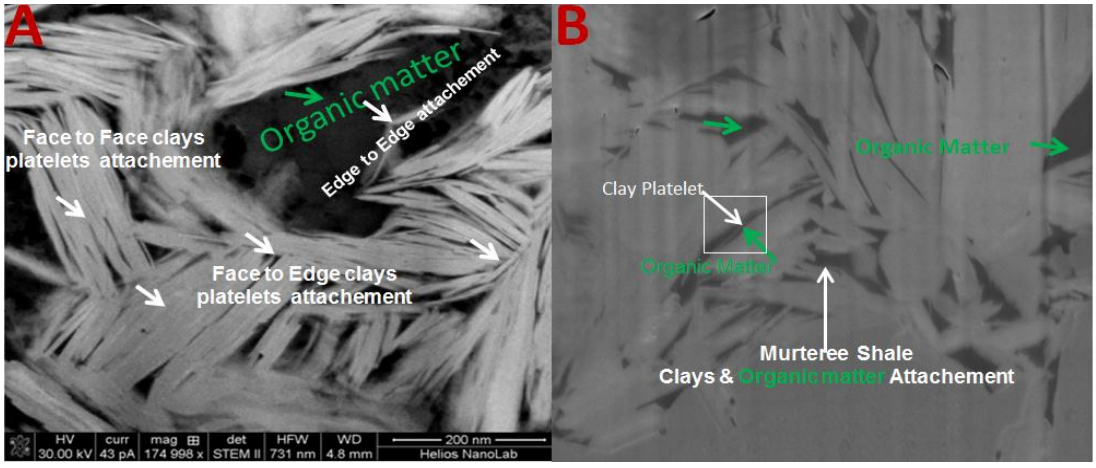

Figure 5.8: STEM (Scanning Transmission Electron Microscopy) image (A) showing clay platelets attachment, in panel A (Face to Face red arrow, Face to Edge white arrow, and Edge to Edge green arrow) with dark coloured organic matter (green arrow), inter-clay platelets porosity – flocculation (from Sondergeld et al. 2010 with modification), and Murteree shale SE images with clays (white arrows) attachment to organic matter (green arrow) image in panel B by white arrow. In panel B, white rectangle, represents a clay platelet pointed by white arrow is embedded in organic matter pointed by green arrow.

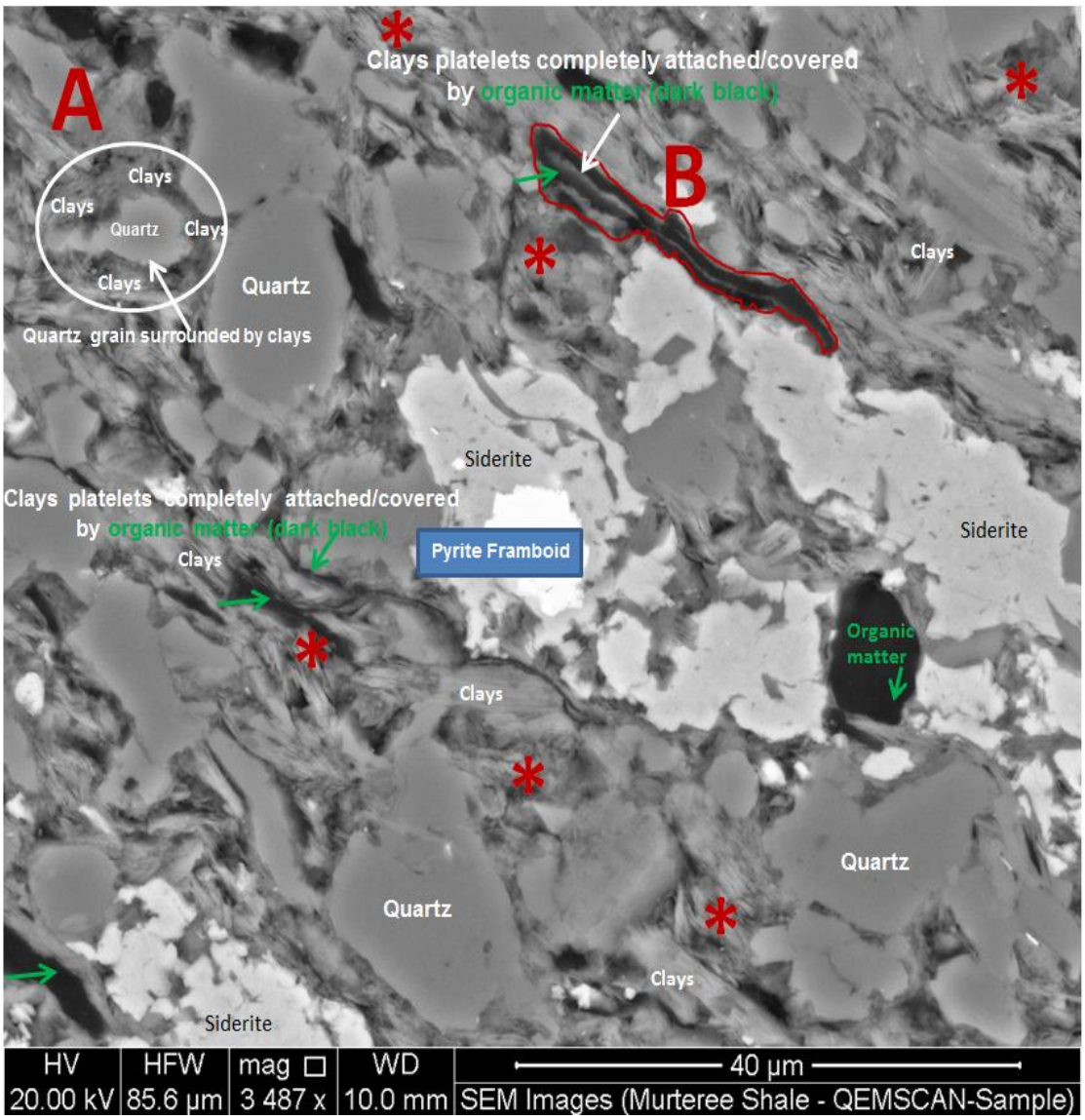

Figure: 5.9: Mechanically prepared and resin embedded Murteree shale sample imaged using backscattered electrons detector of SEM system to identify distribution and morphology of the microfabric comprising chaotic attachments of clays plateletts - (a) face to face, (b) face to edge and (c) edge to edge, siderite, quartz, organic matter, pyrite. Red asterisk showing flocculation areas, zone A showing a mechanically and chemically resistant quartz grain surrounded by clays and zone B showing clays fully covered and attached to the organic matter.

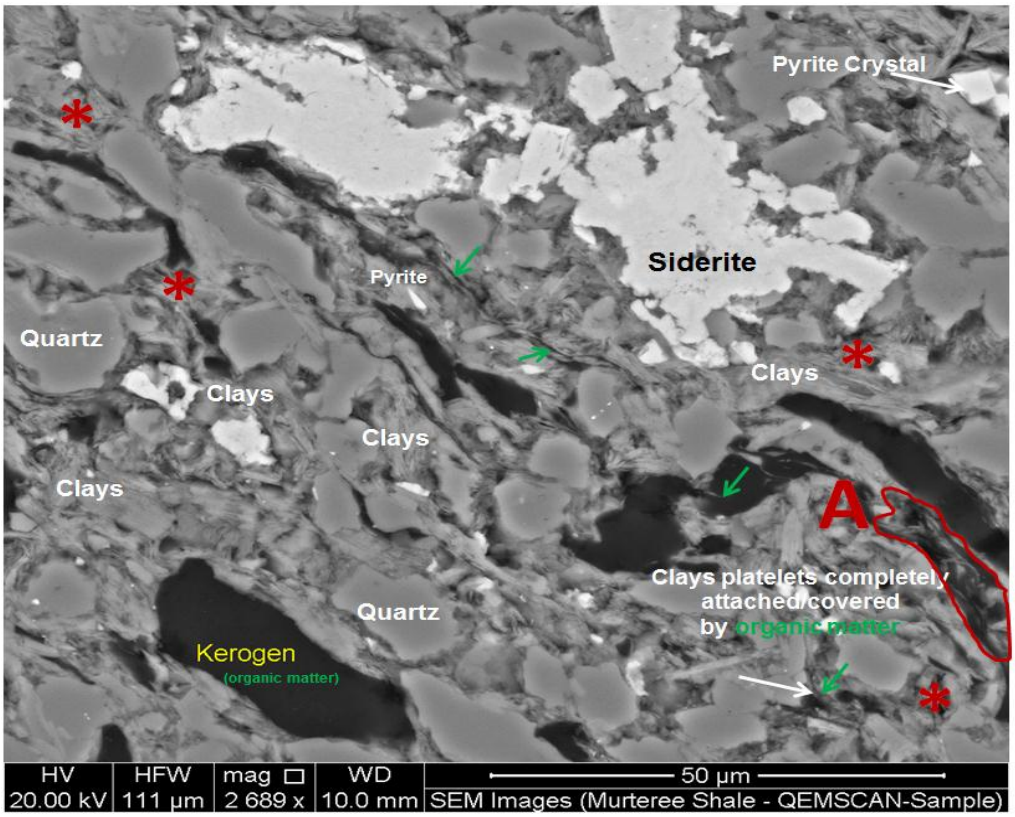

Figure: 5.10: Mechanically prepared and resin embedded Murteree shale sample imaged using backscattered electrons detector of SEM system to identify distribution and morphology of the microfabric comprising chaotic attachments of clays plateletts - (a) face to face, (b) face to edge and (c) edge to edge, siderite, quartz, organic matter pyrite, red asterisk showing flocculation, zone A showing and zone A showing clays fully covered and attached to the organic matter. Kerogen labelled with yellow text colour was identified as carbon rich using characteristic X-rays during SEM analysis.

In these images of Roseneath and Murteree shale images captured at very high resolution and ultra-high magnification we can readily identify clay platelets attached and totally surrounded by organic matter especially in figure 5.9 marked by B and in figure 5.10 marked by A. Therefore study of physical and chemical properties of these floccules/flocs and identification through FIB/SEM after deposition is essential to check the application of any water saturation model when characterizing a shale formation as potential reservoir. Flocculation provides insight about the clays, organic matter and brine attachment to one another after the deposition of source rocks sediments and estimated conductivity and resistivity. Carbonates, quartz, and all other non-clay content in shale do not adsorb organic matter or gas after kerogen conversion into gas. Only clays can attract organic matter during deposition and retain it attached to the clays platelets after deposition as seen in figures 5.9 and 5.10. Later, after the conversion of organic matter into kerogen and release of oil and gas, organic matter acts as adsorbent for the natural gas. We believe these major pre and post depositional physical and chemical events in shale sediments mentioned above play a vital role in the values of the true resistivity (R_t) in logged data. Further it has been observed that during the digenesis of clays known as shale dehydration/loss of water from clays, large quantities of fresh water are released when smectite is converted into illite,

quartz and water (Wolf and Chilingarian 1975; Foscolos, 1990; Sam Boggs Jr., 2006; Thyberg et al. 2009; Handwerger, et al. 2011). Consequently, these reactions will change the pore fluids chemistry, and will lower the salinity level of the original brine in the sediments. Similarly it will increase brine resistivity and bulk density of the formation (Fitts and Summa 2002, Sondergeld et al. 2010). Therefore authigenic quartz as a by-product of this chemical reaction will reduce the clays content surface available for attachment of the cations and ultimately creating more tortousity for electric current and increase sediments resistivity. These concepts about the diagenesis of organic matter, clays conversion and release of fresh water, authigenic silica formation, adsorption of gas and organic matter(bitumen) on clays are summarized in figures 5.11 and 5.12.

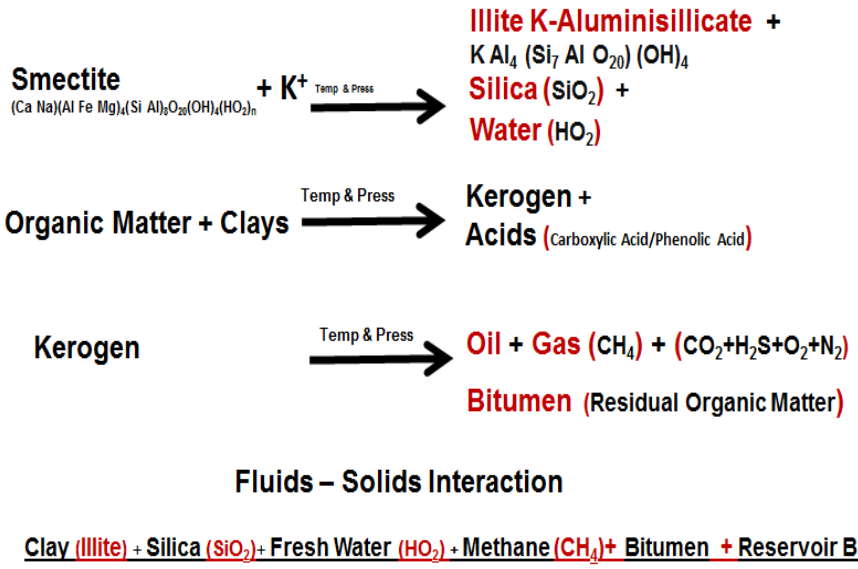

Figure 5.11: Clays and Organic matter postdeposition diagenetic process and consequent products (Boles and Franks 1979, Hunnur 2006, Thyburg et al., 2009, Passey et al., 2010 and Schieber 2010)

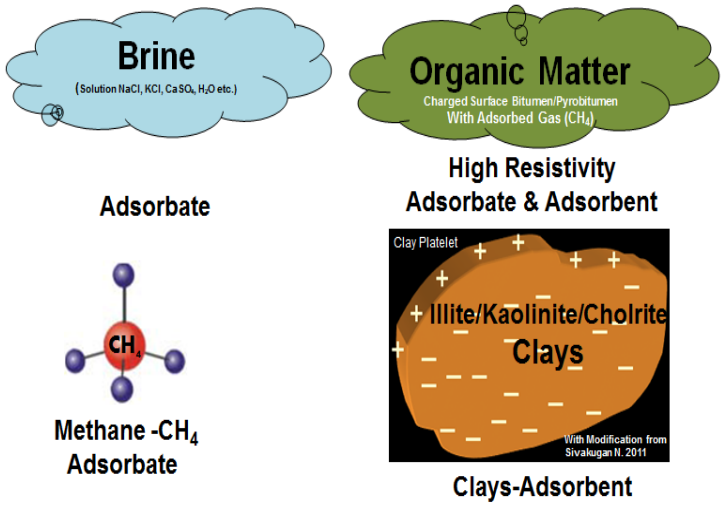

Figure 5.12: New Fluids (fresh water and methane gas along with brine), organic matter and clays as a postdeposition diagenetic process which has impact on true resistivity and conductivity estimated using wireline logging techniques as well as on water saturation.

Based on observations inferred from figures 5.11 and 5.12 we came up with two conceptual resistivity models which gave some insight about how clays in shale gas reservoir can affect water saturation estimation as labelled in figure 5.13 by A and B, showing conventional shaly model in shaly reservoirs and shale gas reservoir model respectively.

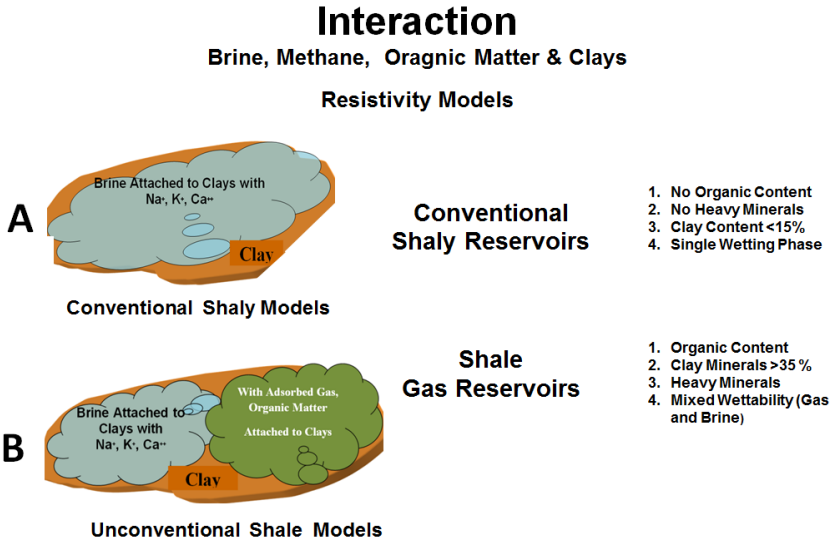

Figure 5.13: Correlation between conventional shaley model (A) and conceptual resistivity model (B) in Murteree shale gas reservoir.

Cheng and Huang (2004) and Ramirez et al. (2011) have reported that kerogen is saturated by the evolved hydrocarbon gases first leaving the remaining gas to be adsorbed by clays in the system and increase the resistivity of the formation. Kerogen will increase the formation true resistivity (R_t), but its effect on R_t (Uninvaded Formation Resistivity) has been overlooked. Sundberg (1980) argued that resistivity of the rocks depends on the arrangement of the gas and liquids and the estimated true resistivity must be investigated before application to calculate water saturation. Shale gas reservoirs are over mature source rocks as there are no liquid hydrocarbons as a consequence of oil cracking down into thermogenic gas (Passey et al. 2010). Worthington (2011), Handwerger et al., (2011) and Sondergeld et al (2010) have reported mixed wettability in shale gas reservoirs and some questions about the use of the Archie equation for water saturation have been related to variable salinity domains in shale gas reservoirs. Therefore, it is envisaged that connate water with reduced salinity by fresh water generation and natural gas are the only wetting phase in over mature shale gas reservoirs like Roseneath and Murteree shales.

Based on FIB/SEM images figures 5.7 to 5.10 and liquid pyknometry for total porosity , as well as sedimentologic and post depositional diagenetic chemical, physical processes as shown in 5.11 to 5.13, we have come up with following Murteree shale gas resistivity model to illustrate the effect of the gas, fresh water generation, organic matter and clays interaction on water saturation, as shown in the figure 5.14 below.

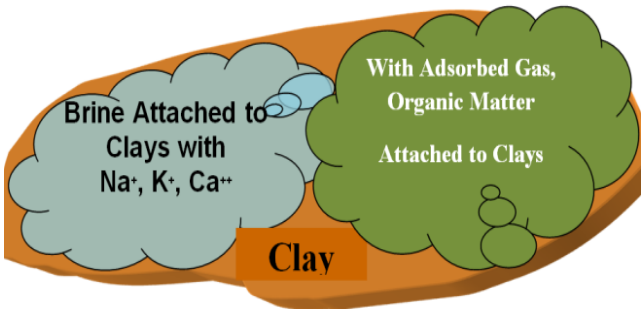

Figure 5.14: Unconventional resistivity model of Murteree shale gas reservoir.

Similarly we have used extensive FIB/SEM images of Murteree shale as shown in figures 5.4 to 5.10 to justify the higher values for porosity, (higher than 9.00%) to apply for this model to estimate water saturation in Murteree Shale based on model given in figure 5.14 above while Archie, Indonesian, Simandoux and Total shale models correlated results based on these concepts are given in table 5.9 below

Table 5.9: Correlation of four water saturation models results for Murteree shale gas reservoir

Total Porosity (Fraction)	Tortousity Factor (a)	Cementation Exponent (m)	Saturation Exponent (n)	S_w Archie's Model (Fraction)	S_w Indonesian Model (Fraction)	S_w Simandoux Model (Fraction)	S_w Total Shale Model (Fraction)
0.100	1.00	2.00	2.00	0.894	0.468	0.525	0.571
0.100	0.62	2.15	2.00	0.837	0.511	0.570	0.701
Humble Values for Tortousity factor (a = 0.62) and cementation Exponent (m = 2.15)							
Shale Volume-Steiber Formula (Fraction)			0.474	Shale Resistivity Rcl (Ohm)**			25.00
Brine Resistivity Rw (Ohm.m)**			0.540	Tortousity factor (a)			1.00
Cementation Exponent (m)			2.00	Saturation Exponent (n)			2.00
Density Log Porosity Project Well Della4 (Fraction)			0.0212	(** Encounter 1 - DMITRE SA)			

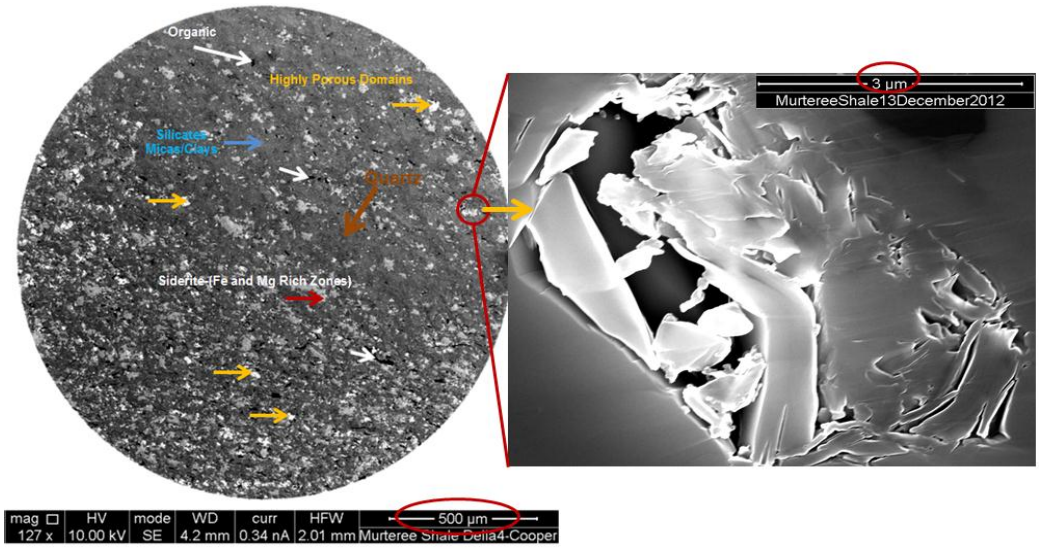

Figure 5.15: Murteree Shale FIB/SEM Sample and size of the porous domains. (Keys/legend for SEM Terms on FIB/SEM: (mag = Magnification; HV = High Voltage –Accelerating Voltage); mode = Back Scattered Electron Beam Detector or Secondary Electron Beam Detector Usage); WD = Working Distance (distance from the bottom of the SEM column to the sample); curr = Current; HFW = Horizontal Frame Width)

We believe these observations based on geochemical and organic chemical behaviour are worth considering when evaluating the brine content. Consequently we made the following conclusions including the application of Archie's formula.

5.5 Conclusions

1. Stieber formula was selected as the proper correlation to estimate shale content for Murteree formation when using gamma ray log.
2. Wyllie formula with Hilchie's correction factor was found to be the appropriate correlation for density log porosity calculation in Murteree shale.
3. For water saturation, both Simandoux and Indonesian correlations gave reasonable results.
4. Effect of adsorbed gas, generation of fresh water during smectite to illite conversion and silica, and presence of organic matter attached to the clays platelets surface were found to have stronger impact than assumed brine higher conductivity.
5. Using the original true resistivity values in Murteree shale, it was found that Humble's formula is more appropriate model for tortuosity and cementation factors.
6. From our FIB/SEM visual experimental work and results, Roseneath and Murteree formations showed very high level of heterogeneity, and total porosity which was not possible to be evaluated using any available means and standards, and definitely are much higher than 2%.
7. It is found that when total porosity is in the range of $0 < \emptyset \leq 2\%$, both Indonesian and Simandoux formula are applicable, while, for total porosity higher than 9%, Archie's and Total Shale formula can also produce reasonable and acceptable results.

CHAPTER 6

6.1 Conclusions

In summary, preliminary insight was built on extensive review of published literature for selection of scientific methods and techniques to investigate the Roseneath and Murteree shales character as potential shale gas reservoirs. QEMSCAN, XRD, Micro and nano CT Scanning was applied for a reliable mineral and rock characterization (identification and quantification) while FIB/SEM for pores identification, classification and quantification in these shales. Later considering TOC wt.%, maturity level, temperature and pressure of Roseneath and Murteree shales, Helium Porosimetry, MICP, Pyknometry, Micro and Nano-Computerized Tomography were used to identify and quantify effective porosity, total porosity, pore network and interconnectivity. As a last part aided by FIB/SEM images and wireline logging digital data, Archie, Indonesian, Simandoux and Total shale models were applied for estimation of water saturation in Murteree shale. The results obtained from these applied scientific techniques and methods were correlated with one another in this research and were used to make following conclusive observations:

1. Based on QEMSCAN analysis, it is found that Murteree shale has, quartz 42.78%, siderite 6.75%, illite 28.96%, koalinite 14.09%, Total Organic Content (TOC) 1.91 wt.%, and pyrite 0.04%, while rutile and some other silicates minerals were identified as accessory minerals.
2. QEMSCAN results when correlated with XR-diffraction quantitative analyses are found in good agreement with each other for Murteree shale samples.
3. Stieber formula was used to estimate clay/shale content for Murteree formation using gamma ray log data from Della#4 well completion report and is in good agreement with QEMSCAN and XRD results as well.
4. Identification and quantification of high clay content, organic matter, quartz, fine grained nature of mineral grains, and presence of high level flocculation confirm that Murteree and Roseneath shales are lacustrine type shales.
5. To build 3D volumetric model for porosity, micro fractures and their inetrconnecetivity was halted many times due to very high clay content (48.00%) in Murteree shales during FIB/SEM operations. In sectioned faces of 2D slices later viewed, micro pores were partially filled by the ablated materials removed from other parts of the sectioned sample surface.
6. Possessing large quantity of quartz, and moderate amount of evenly distributed siderite, these shales are brittle enough and prone to fraccing operations.
7. QEMSCAN is not very accurate to identify type of kerogens and their correct density values. This can underestimate or overestimate the absolute hydrocarbon generation potential of shale gas reservoir (TOC wt. %), when total organic content from QEMSCAN was correlated with Murteree shale published literature
8. FIB/SEM images show more organic content in Murteree shale than Roseneath shales.

9. After QEMSCAN and CT – Scanning analyses, extensive FIB/SEM imaging of these carbonaceous shales has proved that Roseneath and Murteree shales lack in cylindrical pores. Linear/elongated, wedge-shaped, and triangular void spaces are the dominant type of intergranular porosity heavily populating clay dominant matrix zones as viewed in FIB/SEM scanned samples.
10. Siderite grains have secondary porosity as a consequence of dolomitization. This secondary porosity cannot be detected by helium, MICP and even by micro and nano CT scanning techniques except by the use of FIB/SEM images visualized at very high magnification and resolution.
11. The Roseneath and Murteree carbonaceous shale samples have very high isolated intergranular porosity to accommodate large quantities of natural gas, which is inaccessible by very high pressure nonwetting mercury and inert helium gas injection techniques as a consequence of microlamination due to localized stacking platelets of high clay content.
12. FIB/SEM application confirms that low resolution of QEMSCAN and CT-Scanning cannot capture micro and meso porosity which constitute major part of intergranular and interstitial storage capacity. Therefore, only FIB/SEM is reliable technique for free porosity visual evaluation in shale gas reservoirs.
13. The effective porosity measured using helium porosimetry is not worth consideration in carbonaceous shale acting a source and a reservoir simultaneously because it measures the pores where stored methane molecules cannot escape or cannot enter to be stored. The reason behind this conclusion is that helium's molecular diameter is less than methane's molecular diameter.
14. Similarly effective porosity and pore throat size classification using MICP seems to be invalid, except it role in verification of ultra-low permeability in these source rocks.
15. Helium and mercury effective porosities are not exactly the same, and the result in each case is an average representation of a range of effective porosities evaluated in these two techniques. These two results simply corroborate that the shales have very low effective porosities and ultra-low permeability as well.
16. Highly porous domains are surrounded by an inorganic and organic minerals matrix. There are no pores in this surrounding matrix, or apertures of pores leading to these highly porous pockets are smaller than the molecular diameter of both helium and mercury impeding the fluid communication.
17. Murteree and Roseneath shales have natural fracture system, whose interconnectivity is very much localized by the presence of microlamination and ultra-low aperture throats estimated using MICP techniques.
18. Identification of graphite through FIB/SEM images and EDXS elemental maps as a result of very high reservoir temperature, radioactive granitic base and pressure, these shales are overmature and organic matter is in low grade metamorphism phase equivalent to anthracite.

19. Roseneath and Murteree shales have secondary natural microfracture system brought about by cracking of natural gas nearly in metagenesis stage of organic matter maturation followed by the large quantities of natural hydrocarbon gas and carbon dioxide generation.
20. The origin of secondary and late microfracture system development is not free of doubts and concerns, because micro cracks and fractures lack in cementation and not even partially filled with authigenic minerals. The origin can be related to stress released during full core withdrawal from exploratory well or during Focused Ion Beam milling procedure.
21. Microlamination is property developed by clays flakes and platelets stacked on top of one other identified by the ultra-powerful imaging strength of FIB/SEM. This is major source of very low effective porosity and ultra-low permeability in overmature source rocks.
22. Wyllie formula with Hilchie's correction factor was found to be appropriate for porosity calculation in Murteree shale when sonic log response was used and it correlated well with porosity estimated using helium and mercury injection techniques.
23. For water saturation, both Simandoux and Indonesian resistivity models are applicable in shale gas reservoirs.
24. We concluded that effect of adsorbed gas, generation of fresh water during smectite to illite conversion and silica, and presence of organic matter attached to the clays platelets surface are found to have stronger impact than assumed brine higher conductivity.
25. Using the original true resistivity values in Murteree shale we found that Humble's formula is more appropriate model for tortuosity and cementation factors.
26. From our FIB/SEM experimental work, Roseneath and Murteree formations were found to have high level of heterogeneity, and possess natural macro and micro-level natural fracture systems; therefore, we believe the total porosity of these formations are much higher than 2%.
27. We also concluded that when total porosity is in the range of $0< \emptyset \leq 2\%$, both Indonesian and Simandoux formula are applicable, while using total porosity higher than 9%, Archie's and Total Shale formula can be applied as well.
28. When total porosity is greater than 9.00% the evaluation of clays volumes, required in Indonesian, Simandoux and Total shale model are not required for water saturation determination.
29. Based on visual total free porosity assessment, Archie's formula can deliver results to correlate with other water saturation models to facilitate the understanding of water saturation in shale gas reservoirs like Roseneath and Murteree shales.

6. 2 Recommendations

Based on extensive experimental work leading to conclusive observations we recommend that:

1. QEMSCAN and XRD for minerals quantitative analysis are reliable techniques and Steiber formula based on gamma ray log readings is worth believing for shale/clay volume estimation in shales like Murteree shale gas reservoirs.
2. Helium porosimetry, mercury injection capillary pressure (MICP) and liquid pyknometry results about pore volume in resource evaluation are not recommended for potential shale gas reservoirs.
3. Due to interaction between organic matter, clays, natural gas and brine, water saturation estimation using Archie, Indonesian, Simandoux and Total shale model is possible in Shale formations like Murteree shale.
4. Documented by extensive FIB/SEM 2D(two dimensional) images it is found that shales with organic geochemical and mineralogical characteristics of Roseneath and Murteree shales have porosity more than 10.00 %. The estimation and evaluation of total pore volume by applied techniques in this research is controversial although there is enough proof of identification and existence in FIB/SEM 2D images to believe. Therefore as a consequence it warrants a very concerted scientific effort to improve these techniques and/or any other standard method for total porosity estimation which have a key role in economic value of a potential shale gas reservoir.

APPENDIX – A
Murteree Shale FIB/SEM 2D Images

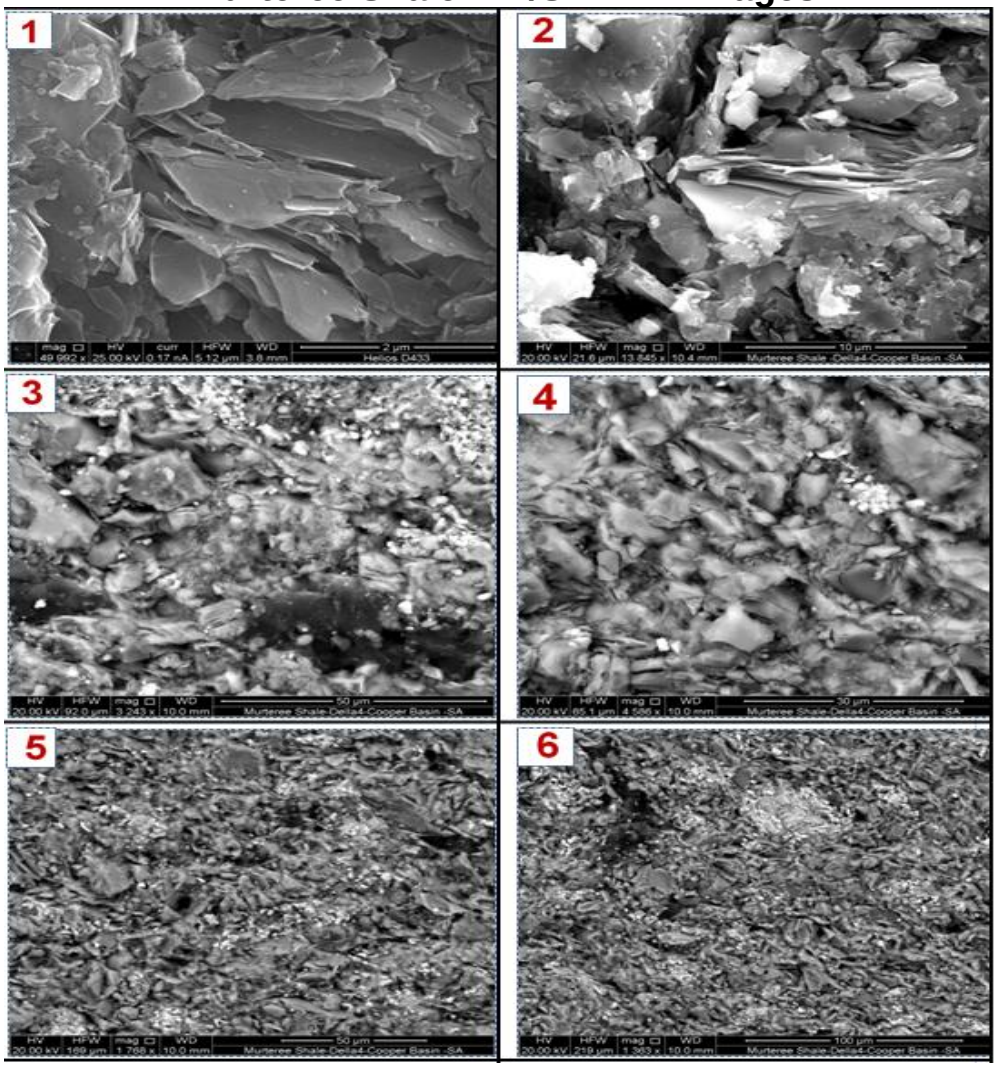

Figure A1: Mechanically Prepared Murteree Shale samples and images taken using secondary electron signals (SE) in panel 1 and 2, and back scattered electron (BSE) signals were used in panels 3, 4, 5 and 6. In (1) clay platelets are conspicuous, but the identification of the pores is very uncertain in this imaged sample and same problem was verified using Murteree shale sample in panel (2). Images 3 and 4 are also mechanically prepared, and images were captured using BSE to check the mineralogy of the sample, where bright spots are heavy minerals, gray colour particles are silicate minerals while black spots represent the pores and organic matter with varying shades of gray and black shades. Images 5 and 6, by using BSE signals detector representing a better and even distribution of heavy minerals, like pyrite, siderite rutile and sphalerite in Murteree shale sample from Della#4 project well. Identification and quantification of porosity in these mechanically prepared and images using both SE and BSE are very challenging.

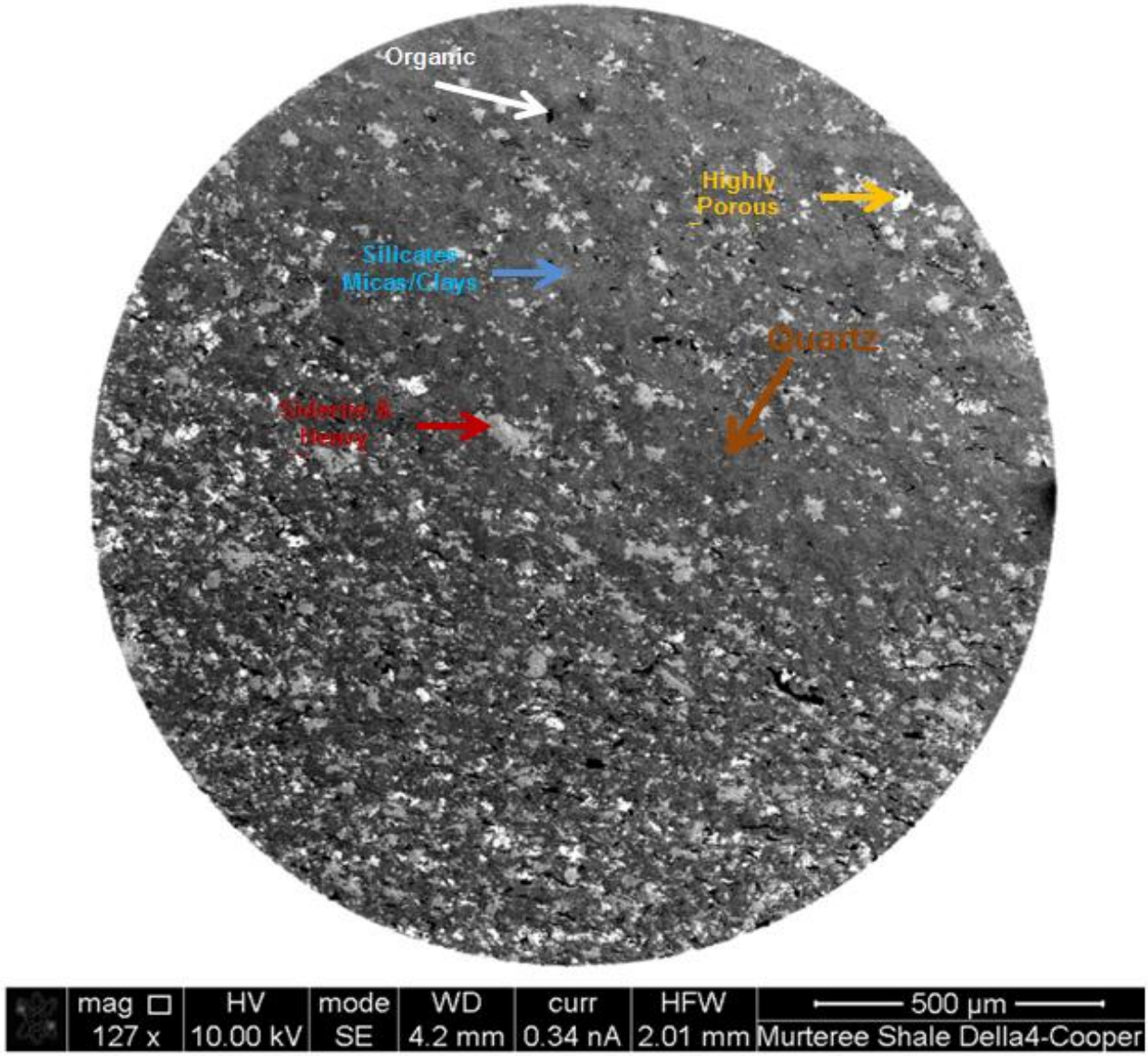

Figure A2: Argon ion milled Murteree Shale 2D image sample using (FIB/SEM), using backscattered electron beam signal detector in Focused Ion Beam Milling and Scanning Electron Microscope (FIB/SEM) system, in Adelaide Microscopy facility, in University of Adelaide. Organic matter (kerogen) marked by white arrow, porous zones by yellow, silicates (micas/clays) by blue, heavy minerals by marron and quartz by brown colour arrows.

Key/legend (FIB/SEM system generated 2D image):

mag = Magnification; **HV** = High Voltage –Accelerating Voltage); **mode** = Back Scattered Electron Beam Detector or Secondary Electrum Beam Detector Usage); **WD** = Working Distance (distance from the bottom of the SEM column to the sample); **curr** = Current; **HFW** = Horizontal Frame Width

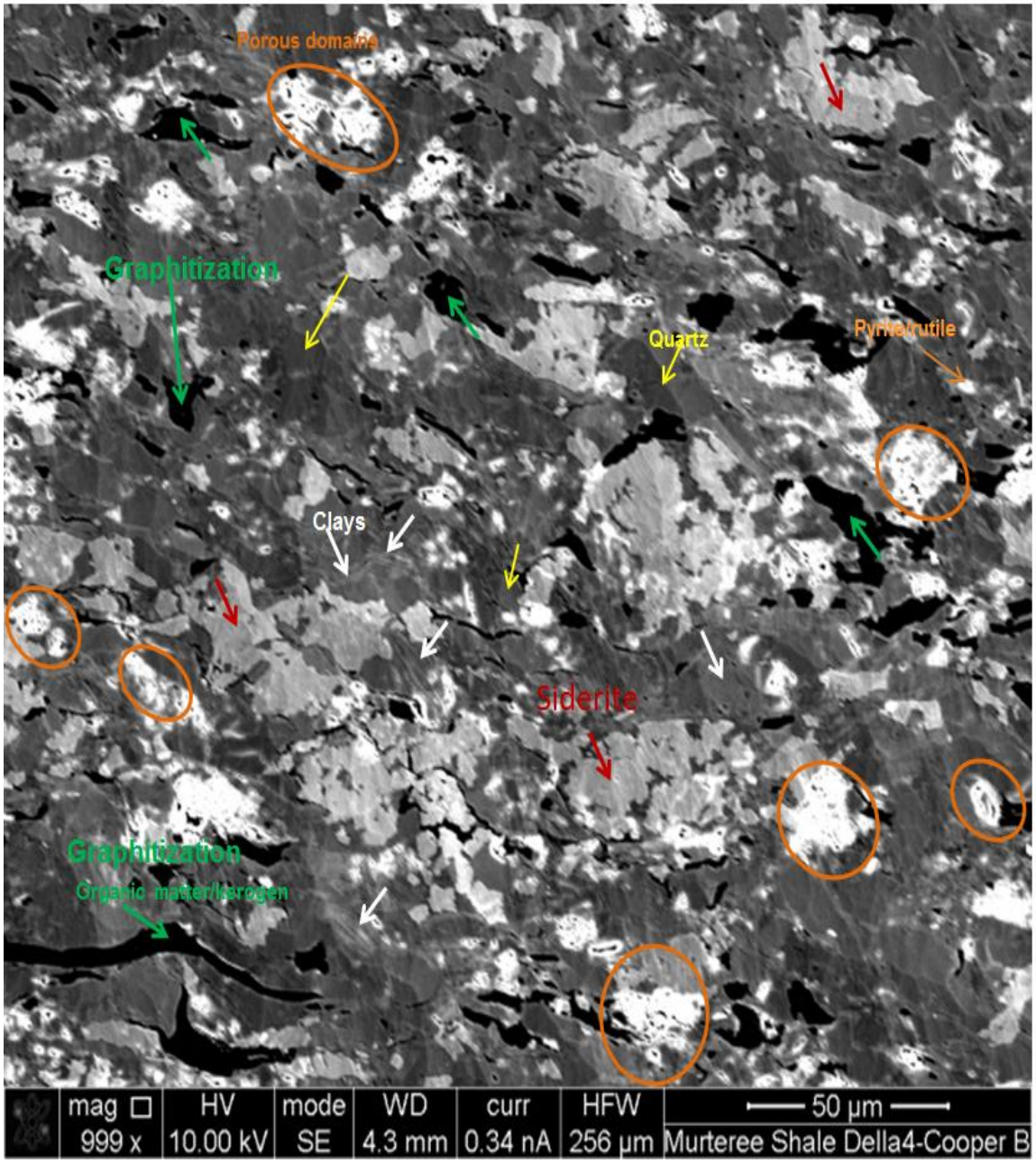

Figure A3: Organically rich Murteree shale sample polished and prepared using ion beam milling (FIB) and identification of various mineral phases. Sillicates (white arrow Clays and Micas), heavy minerals (chrome orange arrow, Pyrite and Rutile) quartz (orange arrow), thick organic matter bands (green arrow pointing graphitization), siderite (red arrow) highly porous zones using secondary electron beam, while pore identification and classification at this scale of magnification and resolution is not possible as seen in this FIB/SEM 2D image. Identification of various phases is based on their morphology. Porous zones are magnesium rich siderite area, where calcium ion in siderite has been replaced by magnesium ion (Dolomitization), and leaving porous siderite rich in iron.

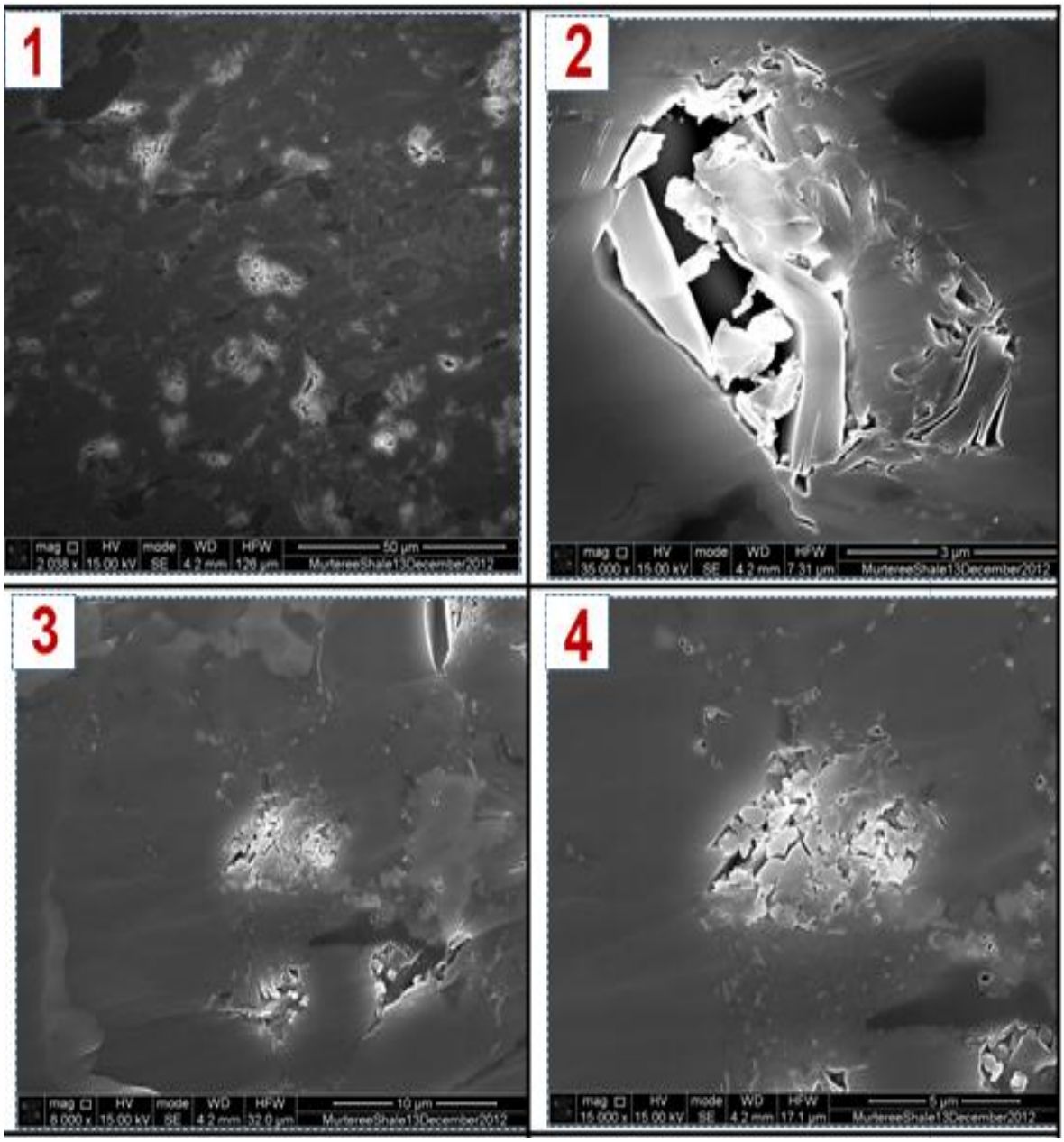

Figure A4 : Highly porous isolated zones in panels 1, 2, 3, and 4, are common features in this image prepared by FIB/SEM at high magnification and resolution to check their morphology, size shape density and relation to sediments/matrix/ organic matter. The porous zones like vugs have charge effect of the electron beam, making these areas very bright. Organic matter clays, quartz and siderite are easily identifiable in this image by their respective grains morphology and boundaries, although there is sectioned material deposition between grains making boundaries not very sharp and closing partially or fully especially in panel 4. Organic matter is very compacted between rigid grains of quartz, clays, siderite and pores in organic matter are not visible / not possible to be located at such resolution and magnification of FIB/SEM system.

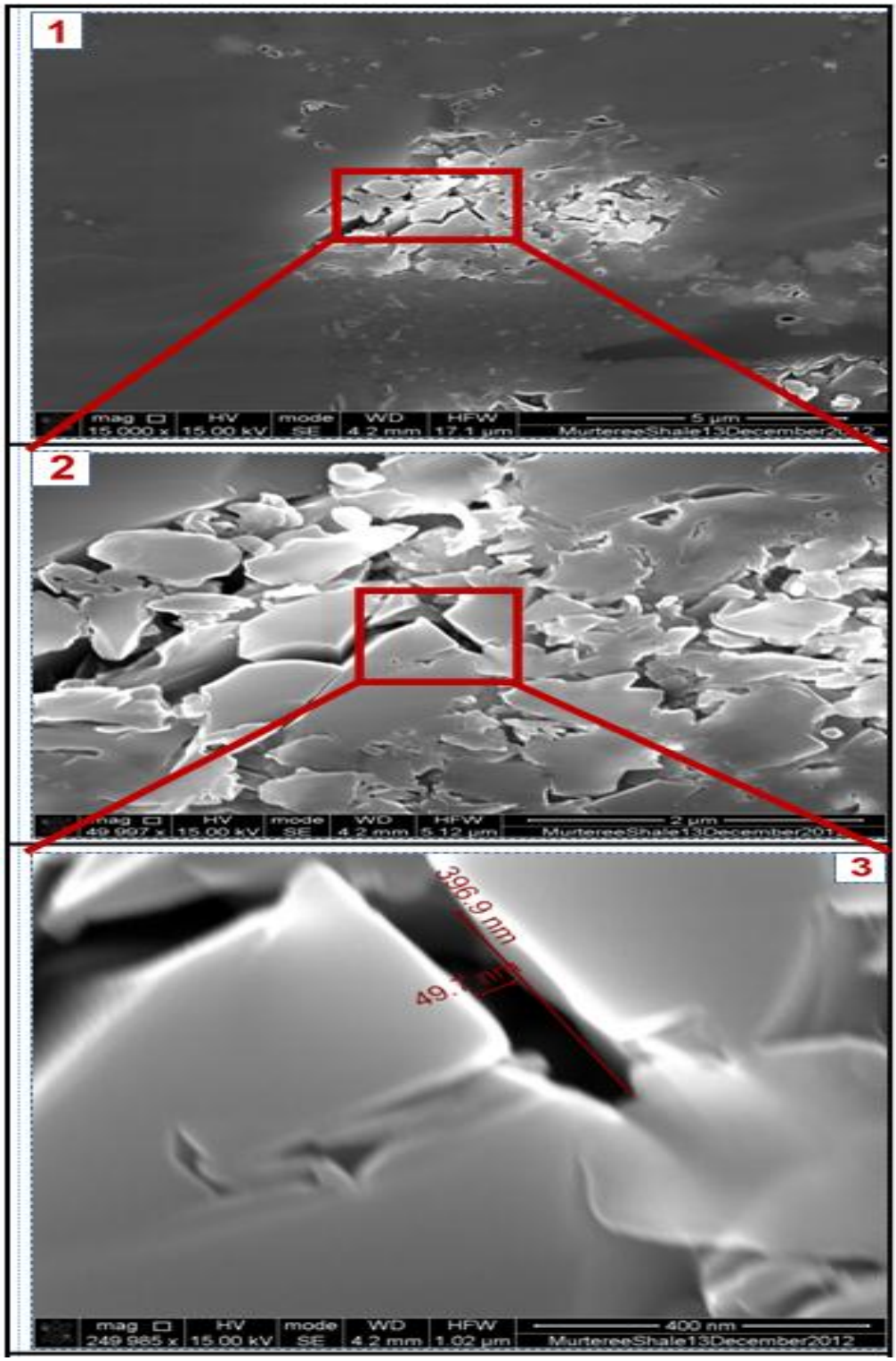

Figure A5: Image in previous figure4A, in panel 4 on previous page, have been magnified from 15,000 to 250, 000 while resolution increased from 5 µm to 400 nm gradually in above three images labelled 1, 2 and 3 to capture pore width and length and fracture size. Almost 400 nm long and 50 nm wide fractures have been identified naturally open without any cementation and compaction effect.

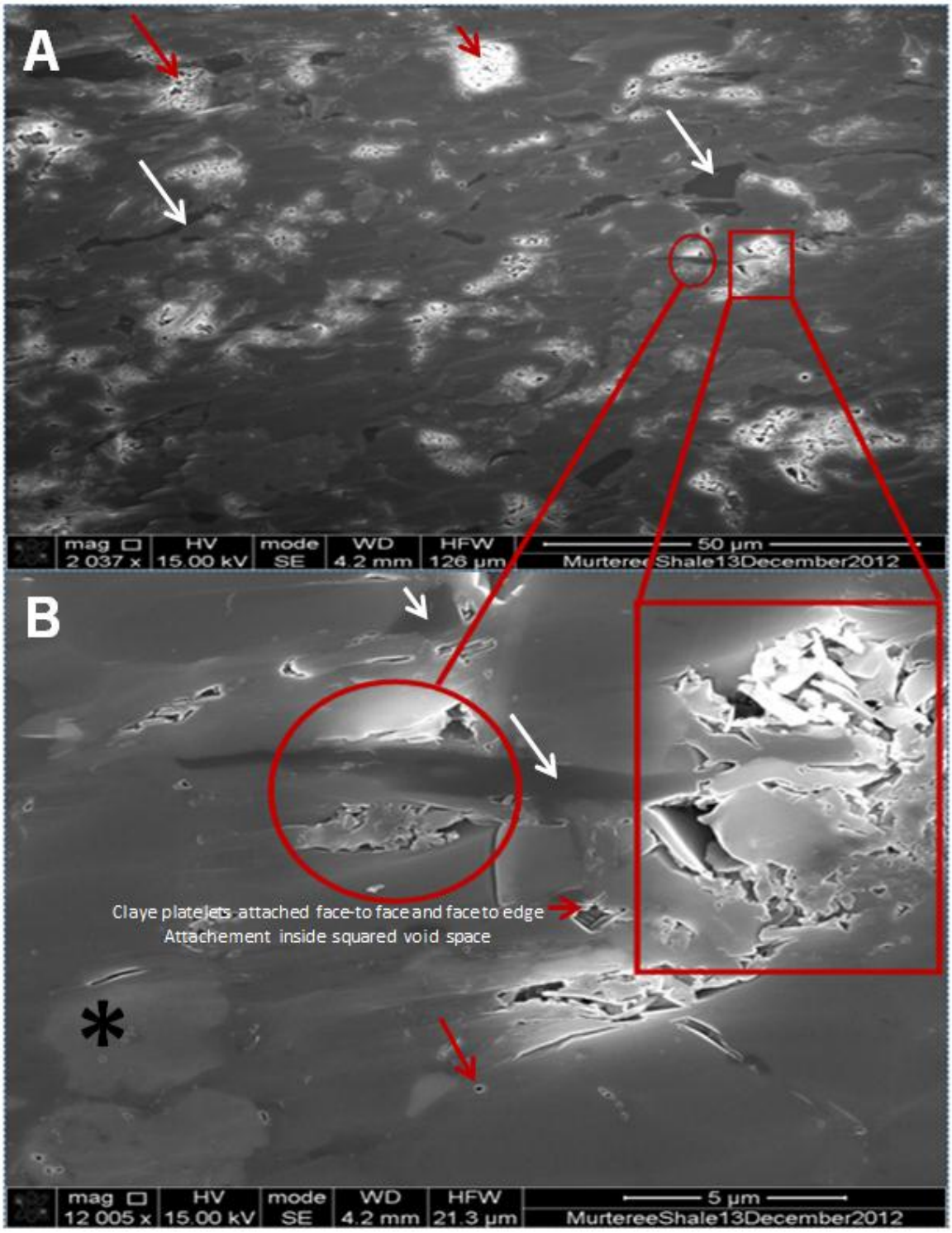

Figure A6: Isolated and occluded porosity marked by red colour rectangle and ellipse identified in (A) and later magnified and seen at high resolution in (B), presence of organic matter (graphitization) pointed by white arrows while micropores and porous vuggy zones are shown by the red arrows as well in both images (A) and (B). This is FIB polished sample and SE detector signals were used to image surface. A large black asterisk in panel B, at bottom of far left shows a large grain of siderite with cylindrical pores in it.

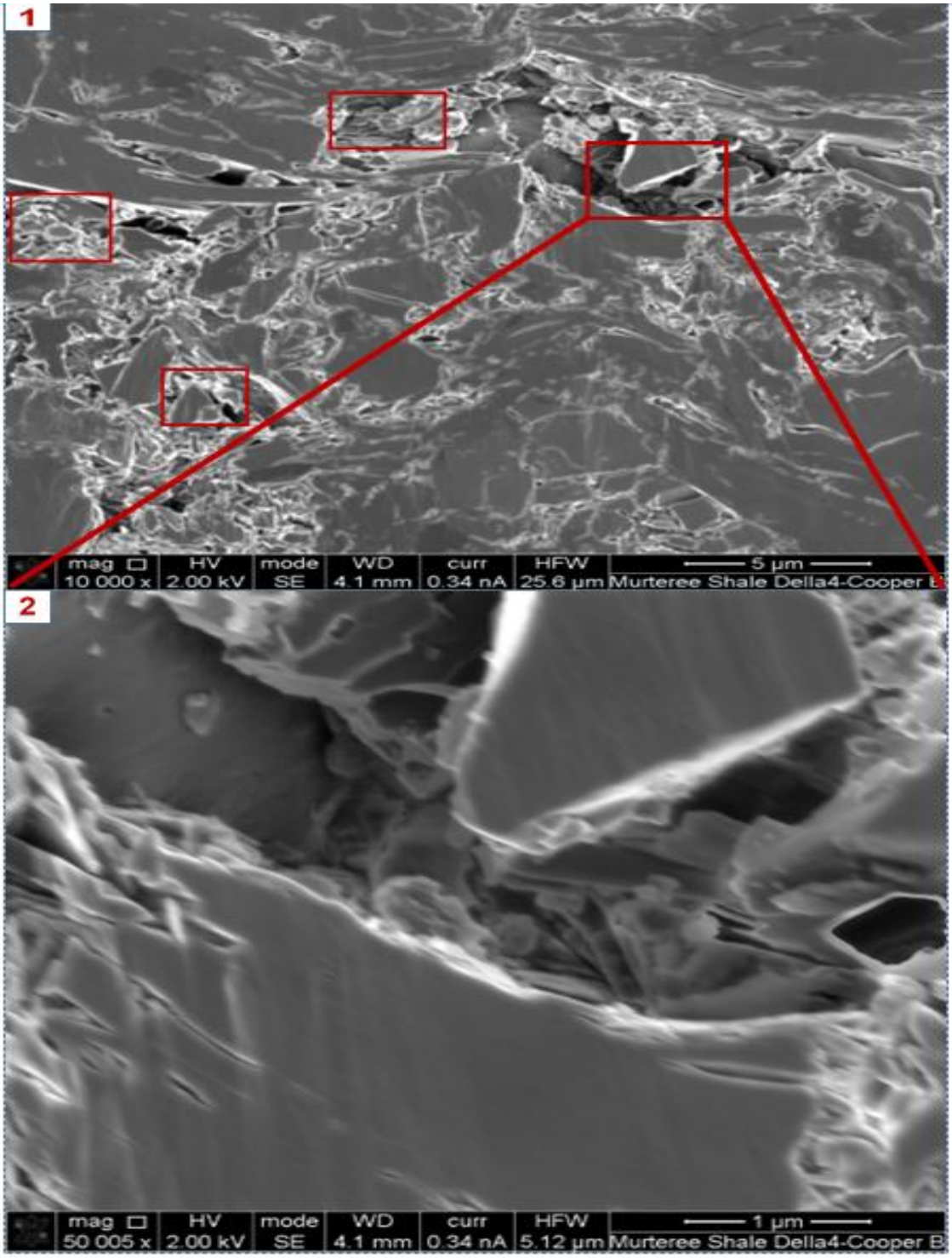

Figure A7: Moldic pores/vugs are very common (1) in feldspar grains formed by partial grains dissolution along the grains boundaries creating large cavities and irregular porous mass in Murteree shale, which can accommodate large quantities of compressed gas (2) and later will facilitate the flow of gas to production wells once these porous zones are connected through fraccing operation.

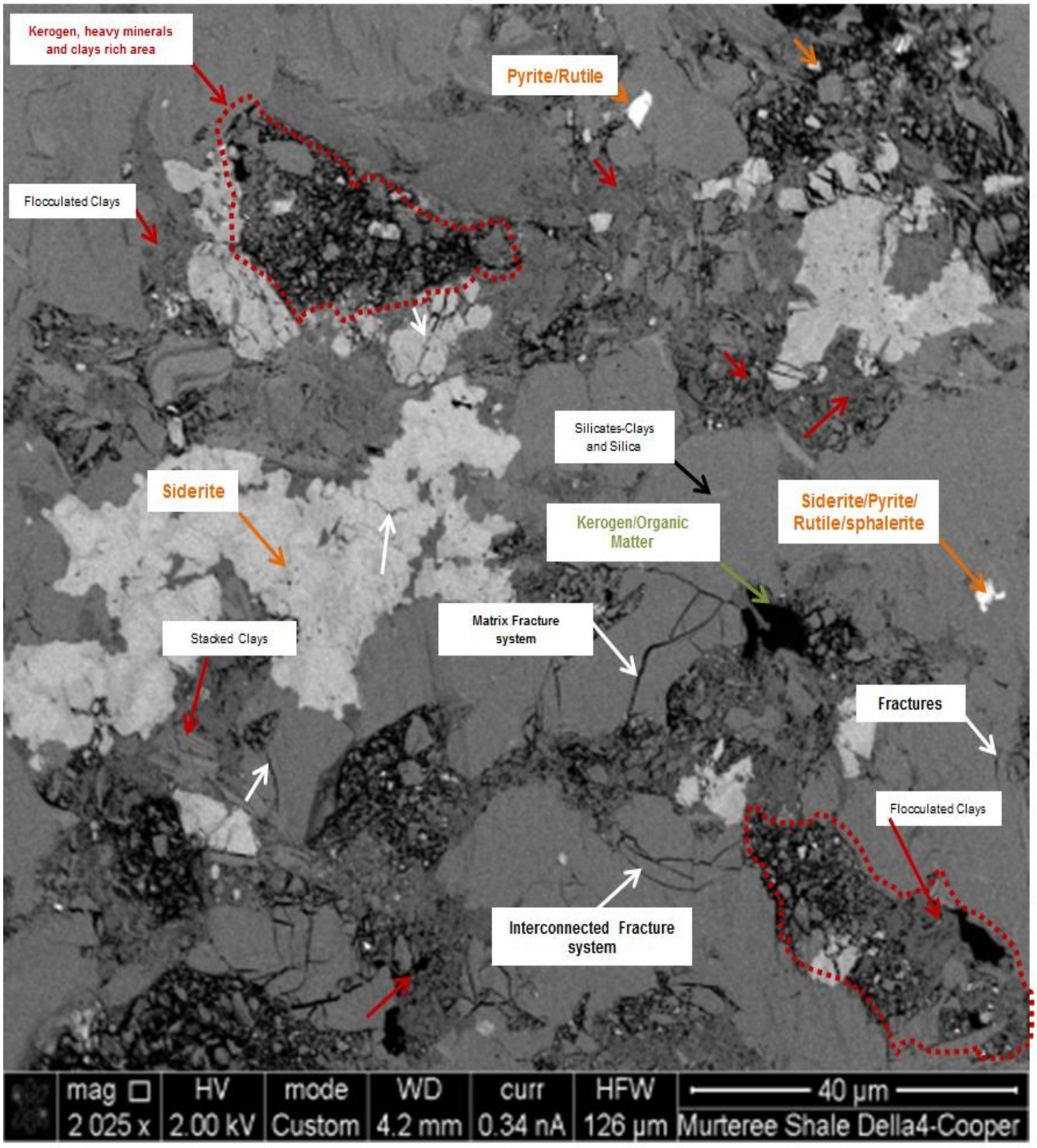

Figure A8: Interconnected natural fracture system running through the matrix of Murteree shale sample, as a consequence of cracking of methane natural gas in overmature Murteree shale can generate large volumes of carbon dioxide and hydrogen sulphide gas. Identification of interconnectivity of fracture system is still challenge. Flocculated clays, heavy minerals, kerogen and silica seems like connected through this fracture system, if connected through fraccing operation can have great impact on gas production.

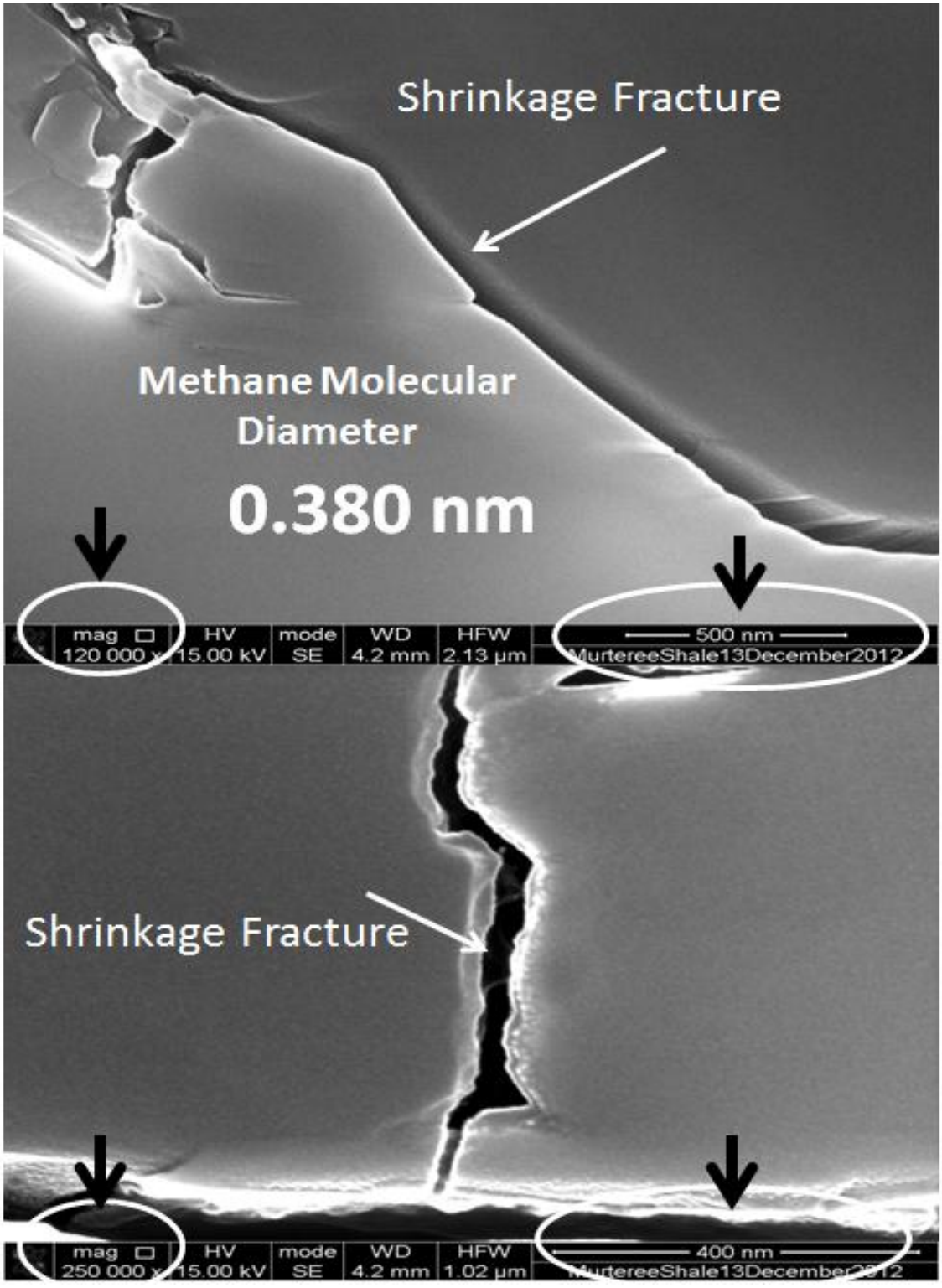

Figure A9: Murteree Shale sample at 500 nm resolutions in top image and 400 nm, in image below. These natural fractures are open, even at nanoscale level and are not closed by cement or any other diagenesis or dissolution process. a naturally opened fracture system tendency marks contribution in storage and later in production phase of the field development (FIB/SEM and SE detector was used for this image).

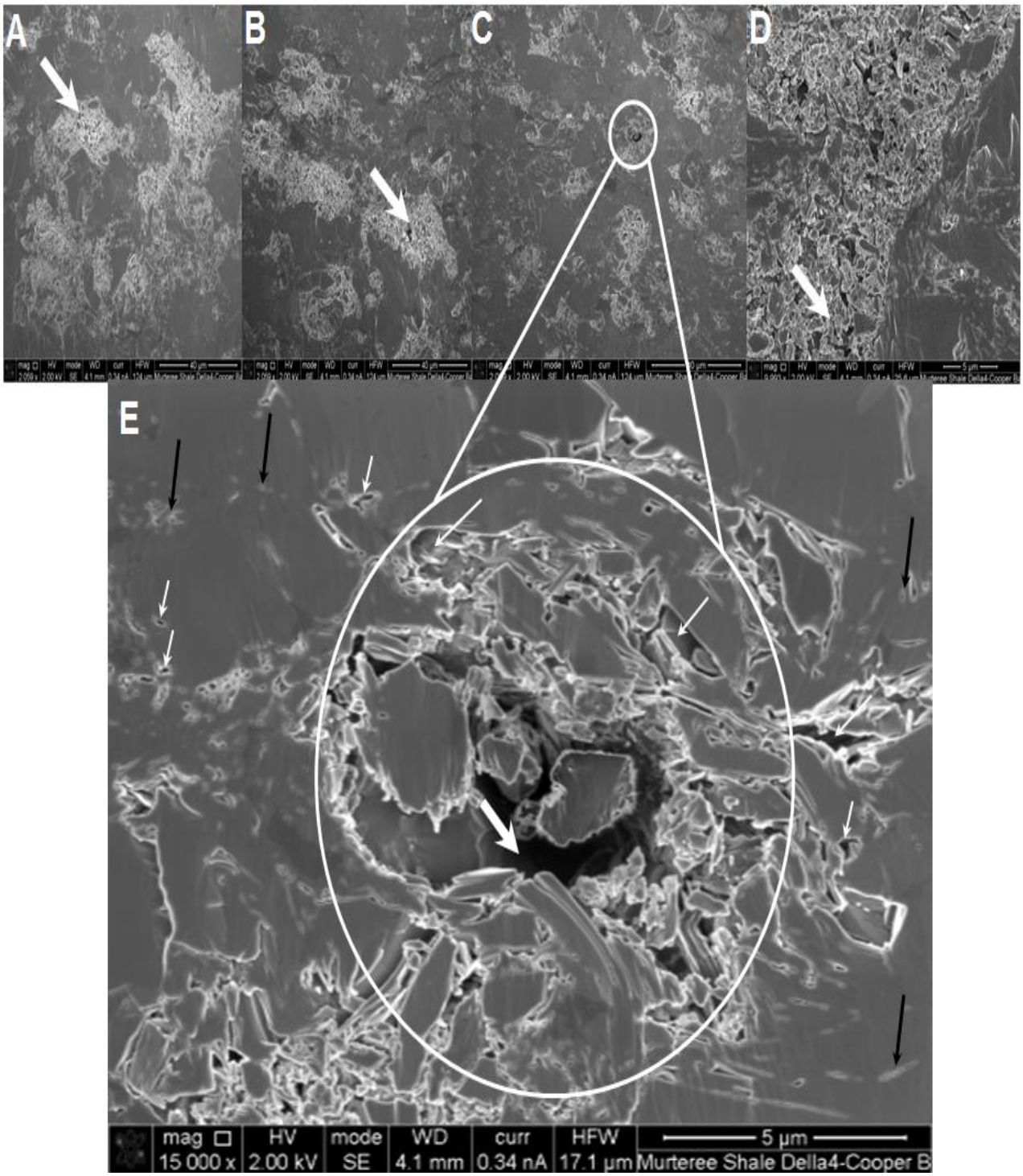

Figure A10: Dissolution of feldspar creating vugs in Murteree shale samples marked by large white arrows in images (A), (B), (C), and (D). as well as intergranular pores marked by the small white arrows in image E below. A part from large vuggy porosity represented by large white arrow in middle of ellipse in image E, there are large number of intergranular pores and microporosity, while some of these pores are completely closed by ablated material redeposit ion marked by black arrows in image (E), during ion milling procedure.

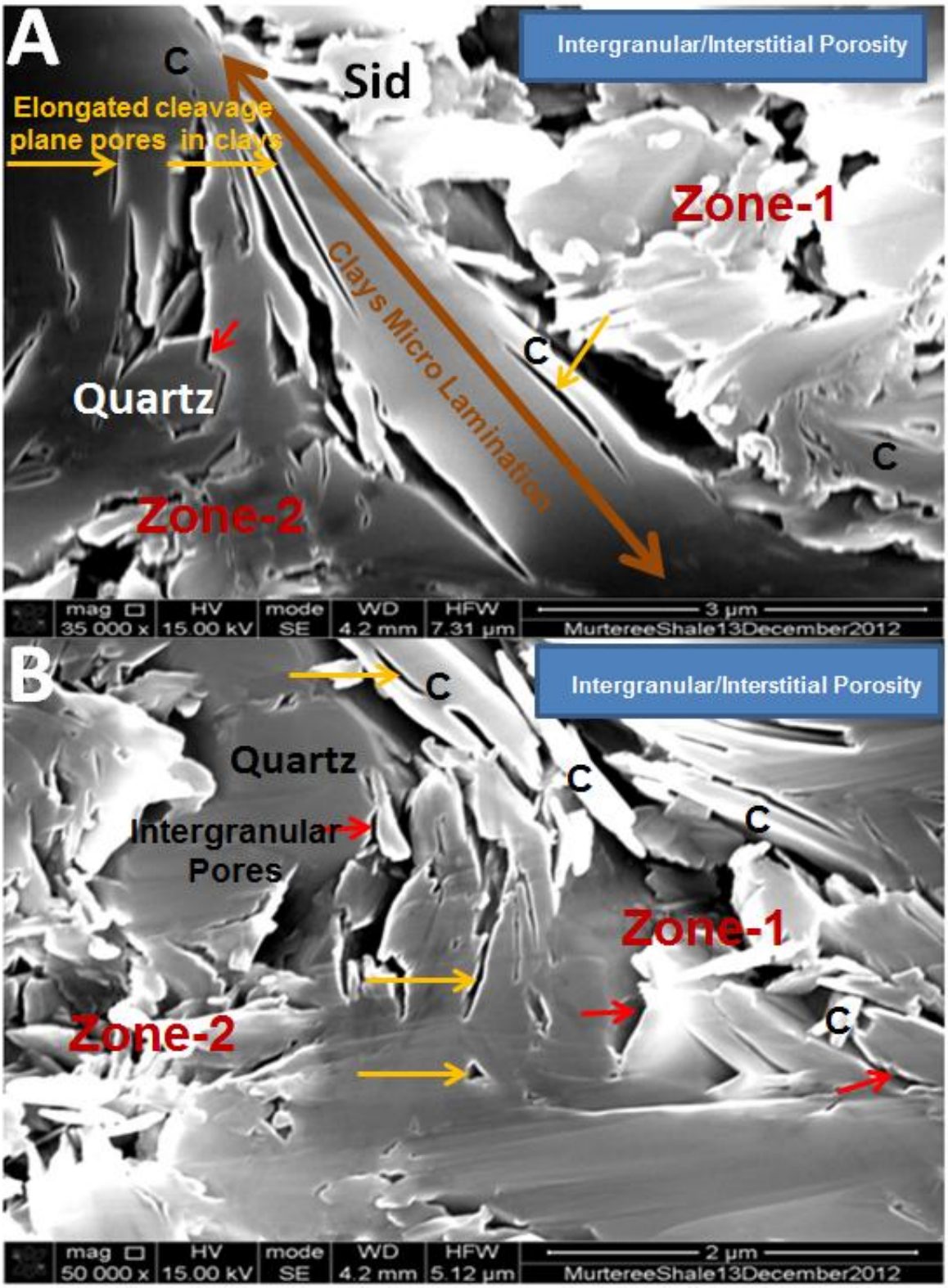

Figure A11: Two highly porous zones, Zone-1 and Zone-2, separated by submicron scale clays stacked structures in panels 1 and 2 FIB/SEM scanned Murteree shales. Interconnectivity of these zones is not known. C=Clays; Red Arrow=Intergranular Porosity; Yellow Arrows = Cleavage plane pores in clays ; Sid=siderite grains.

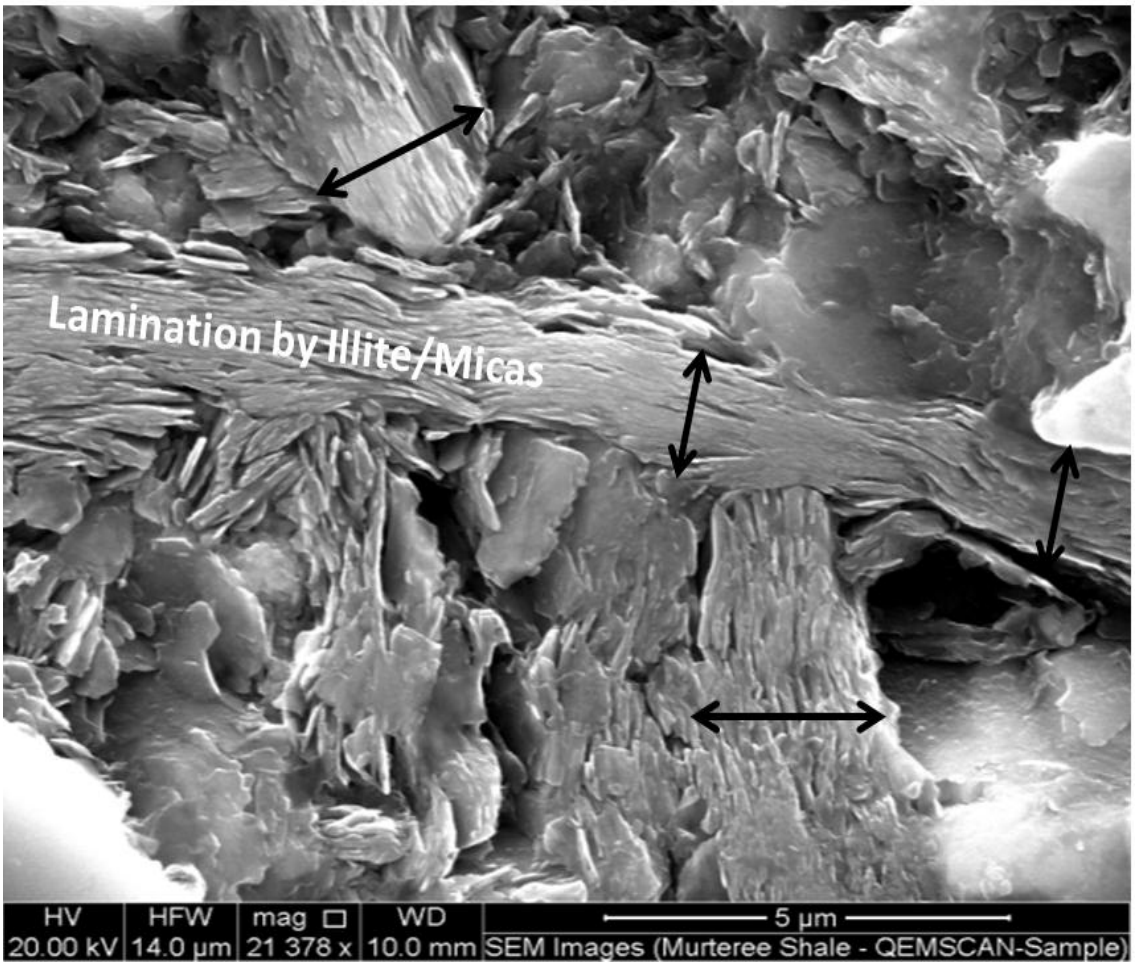

Figure A12: Resin imbedded, mechanically polished, Murteree shale sample scanned for QEMSCAN analyses, and later imaged using SEM, illustrating lamination phenomenon, which can retard the fluids communication between the neighbouring porous zones in a clay rich porous and siderite matrix. A number of local laminae almost 1 to 2 µm in thickness have been identified and marked by black arrows in this image. Black arrows showing local random clays platelets lamination, which impedes local communication and flow of fluids.

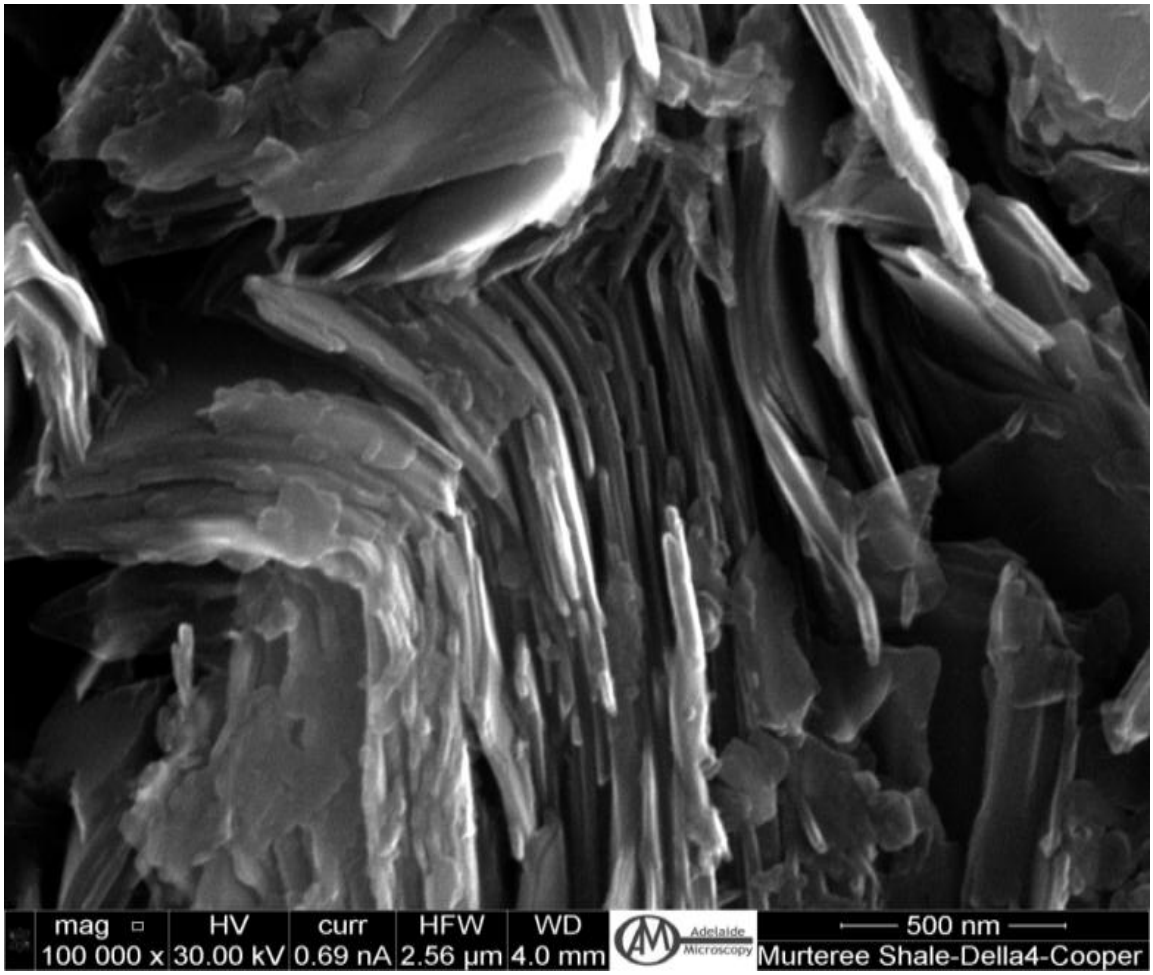

Figure: A13: Mechanically polished and prepared Murteree shale sample showing submicron folding due to post depositional compaction of Illite platelets, (ductility of clays) under very high stress and depicting the behaviour of clays when fraccing operations are carried out in clay rich matrix shale. (image taken using secondary electron detector).

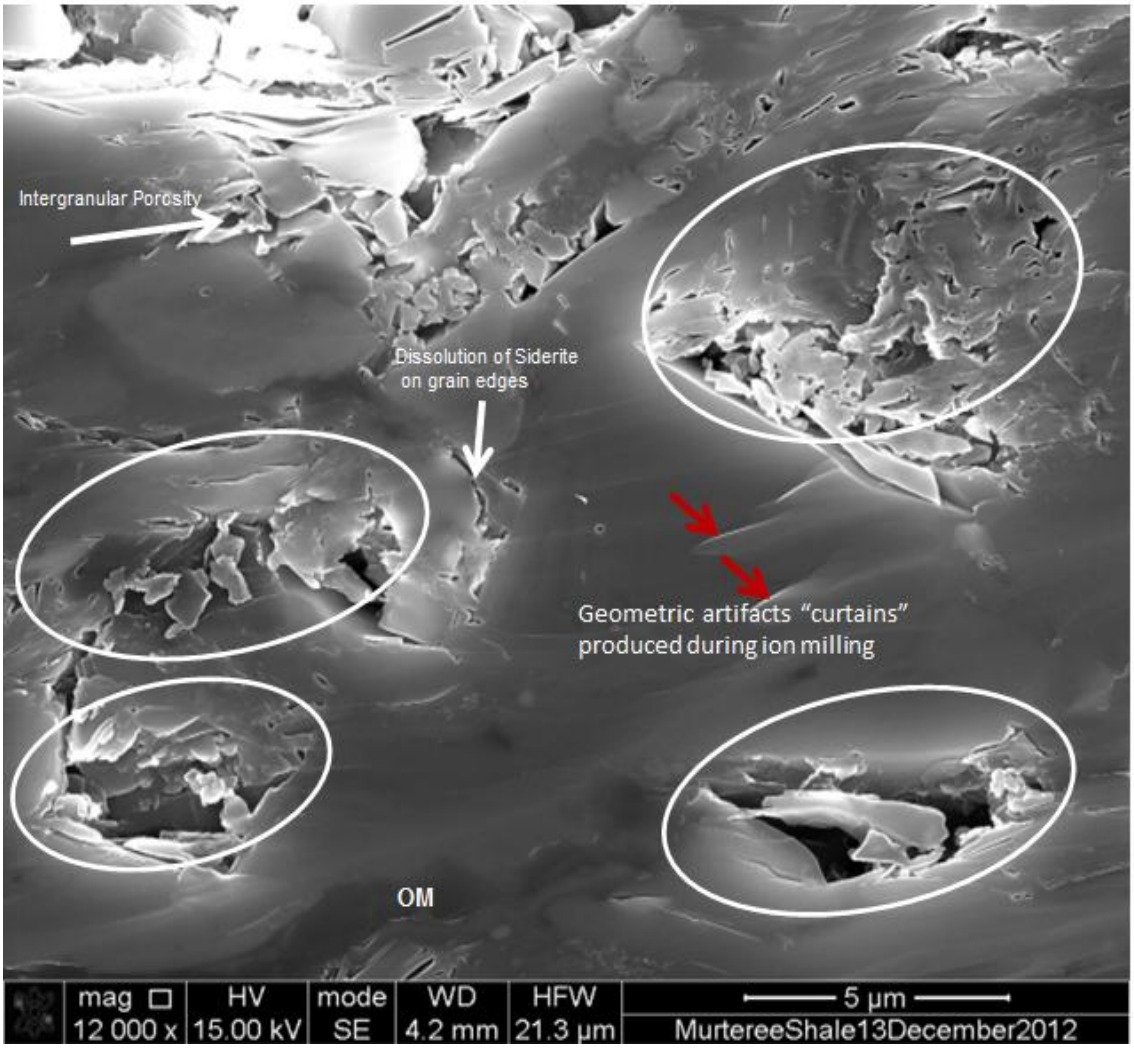

Figure A14: FIB/SEM image using secondary electrons detector for the identification of intergranular pores surrounding grains (white arrows) organic matter (OM) porous area (white ellipses) and pore morphology, curtains on image surface (red arrows) in Murteree Shale, Della4 Project Well, Depth 6619.00-6620.00 ft.

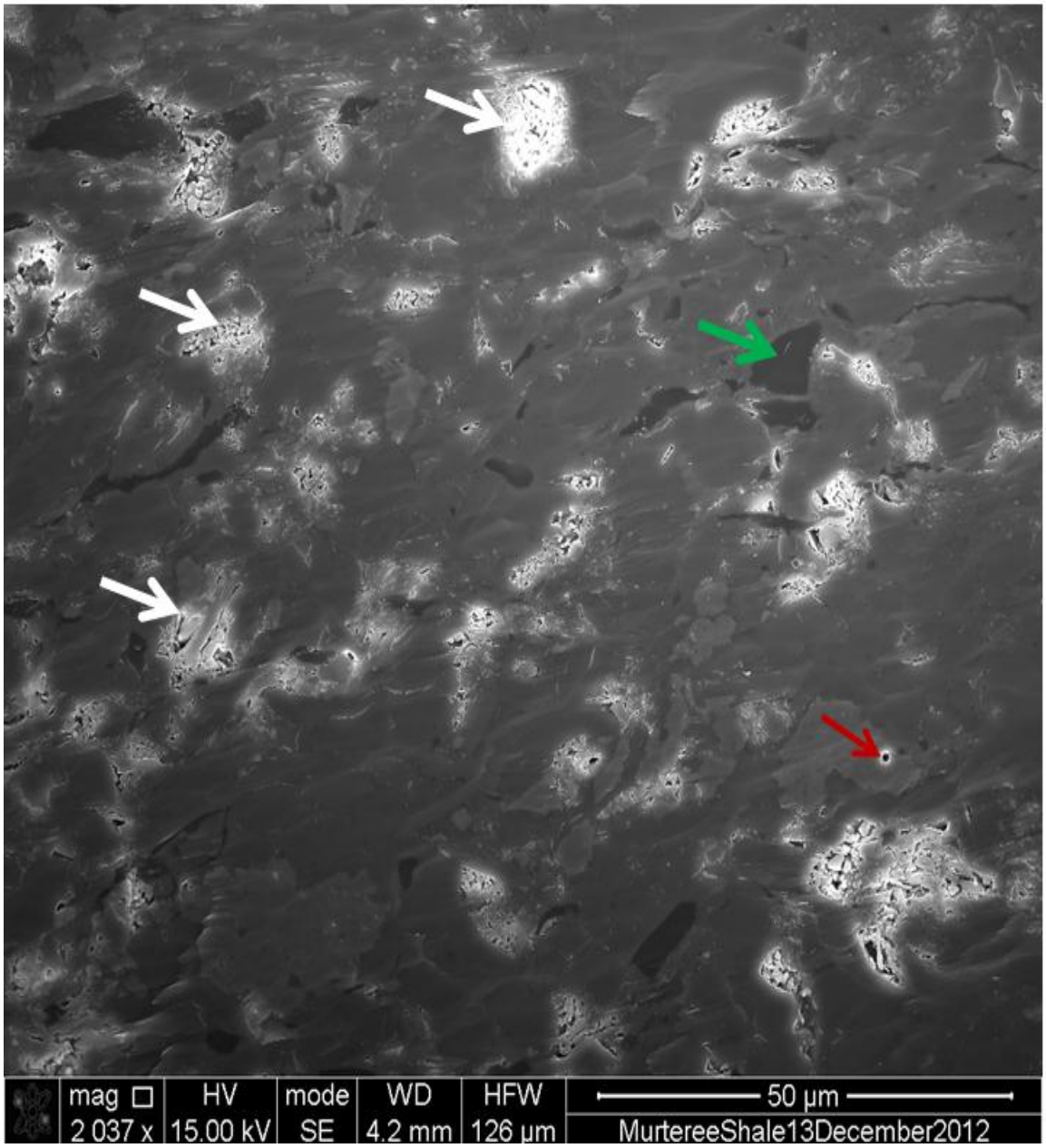

Figure 3.24: Murteree Shale image with highly porous siderite domains marked by white arrows, a red arrow showing a pore in a siderite grain while green arrow representing organic matter.

APPENDIX – B

Roseneath Shale FIB/SEM 2D images

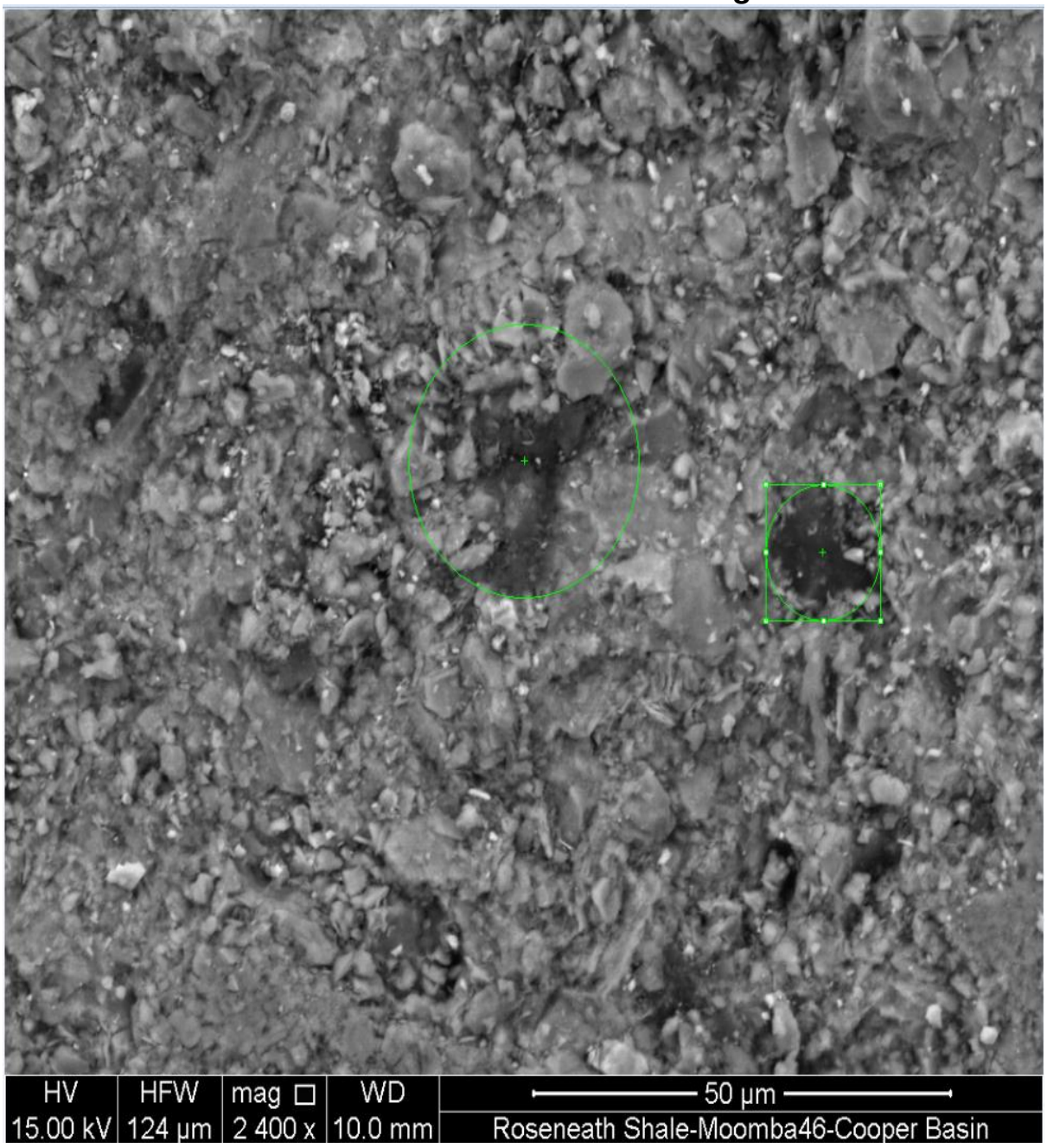

Figure B1: Mechanically Prepared Roseneath Shale sample and imaged using back scattered electron beam (BSE) detector. Clay platelets are conspicuous, but the identification of the pores is very uncertain in this sample, same problem we faced in Murteree shale sample in **figureA1** panels (2). (3), (4), (5) and (6). This sample was scanned using back BSE to check the mineralogy of the sample, bright spots are heavy minerals, gray colour are phyllosilicate/silicate minerals while black spots represent the pores and organic matter with varying shades of gray and black shades.

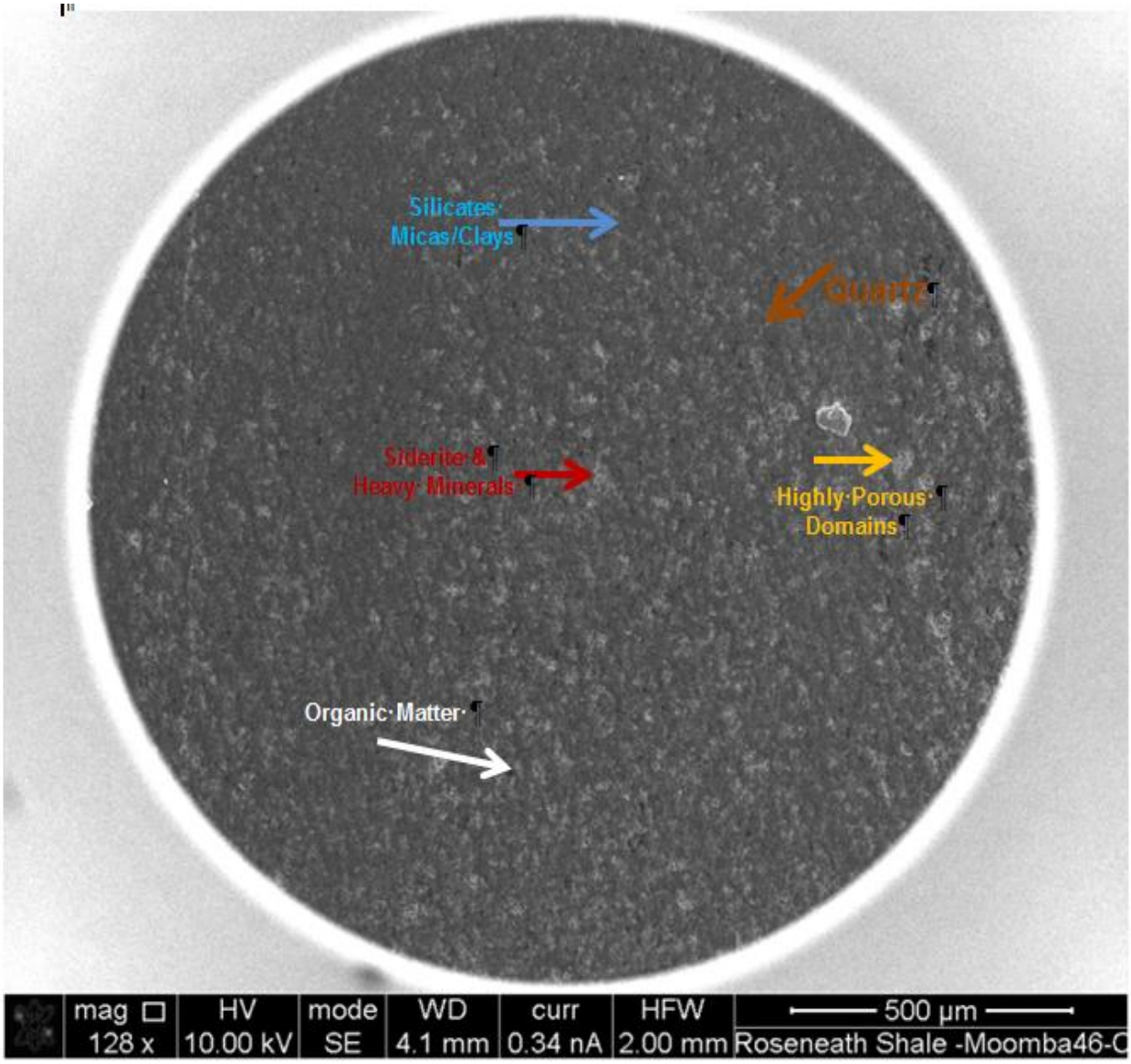

Figure B2 : Argon—ion milled Roseneath Shale sample, prepared for 2D images using secondary electron beam in a dual focused Ion beam milling and scanning electron microscope system in Adelaide Microscopy facility, University of Adelaide. Organic matter (kerogen) marked by white arrow, porous zones by yellow, silicates (micas/clays) by blue, heavy minerals by marron and quartz by brown colour arrows

Key/legend (FIB/SEM system generated 2D image):

mag = Magnification; **HV** = High Voltage – Accelerating Voltage; **mode** = Back Scattered Electron Beam Detector or Secondary electron Beam Detector Usage); **WD** = Working Distance (distance from the bottom of the SEM column to the sample); **curr** = Current; **HFW** = Horizontal Frame Width

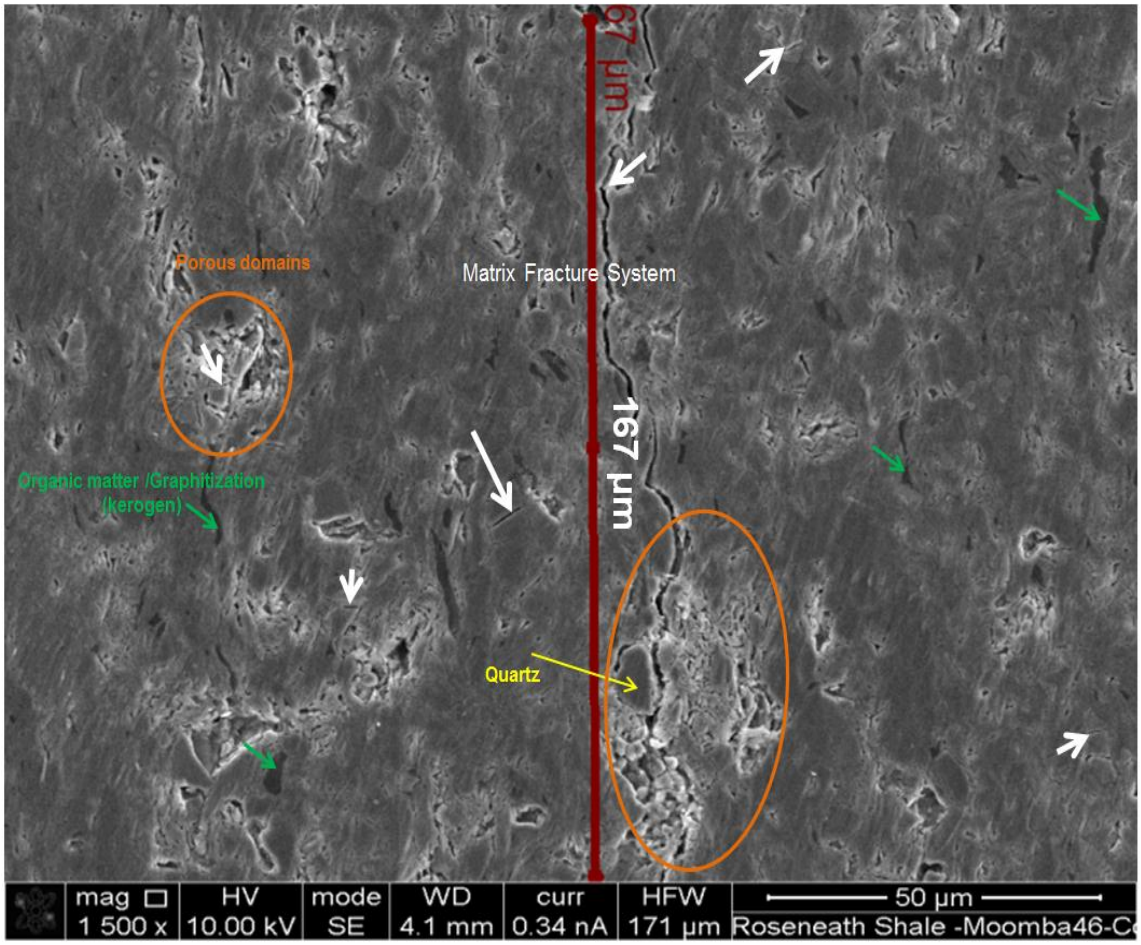

Figure B3: Roseneath FIB/SEM imaged sample with almost 170µm long vertical fracture and some local fractures identified as well, marked by white arrows showing the fraccability of matrix and highly dense porous zones marked by yellow ellipses. These highly porous zones are clay rich areas, where platelets are randomly attached to each other, a face to edge, attachment leaving void spaces and accommodating large isolated occluded porosity. Interconnected natural fracture system running through the matrix of Murteree shale sample, as a consequence of cracking of methane natural gas in overmature Roseneath shale can generate large volumes of carbon dioxide and hydrogen sulphide gas. Identification and authenticity as a natural phenomenon of such fracture system is not free of doubts as interconnectivity is still challenge.

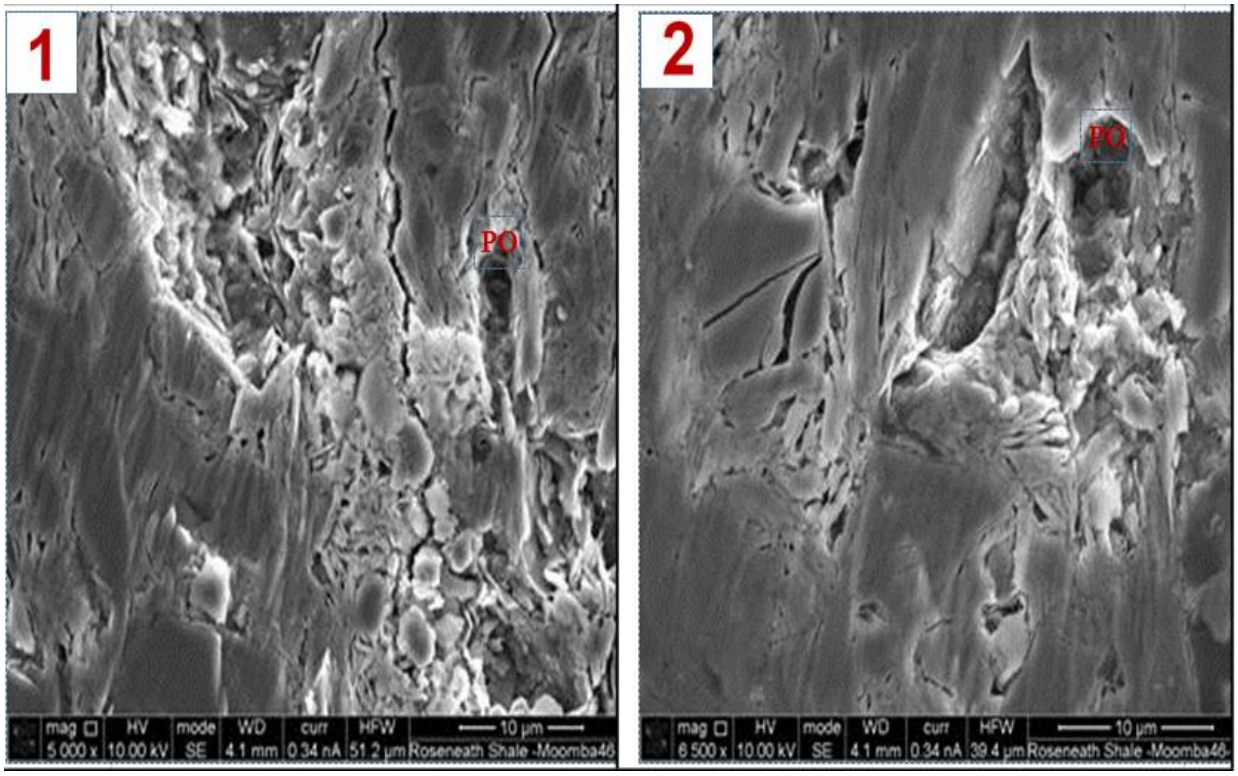

Figure B4: FIB/SEM Roseneath sample imaged. Rich in intergranular porosity and natural fracture system in panel (1) and (2). There are pull-outs in both panels marked by PO and artefacts called “Curtains” are dominant in both panels as a consequence of focused ion beam milling and ablation operations. Interconnected natural fracture system running through the matrix of sample, as a consequence of cracking of methane natural gas in Roseneath shale is clear in this image. Authenticity about origin as natural and identification of interconnectivity of fracture system is still challenge.

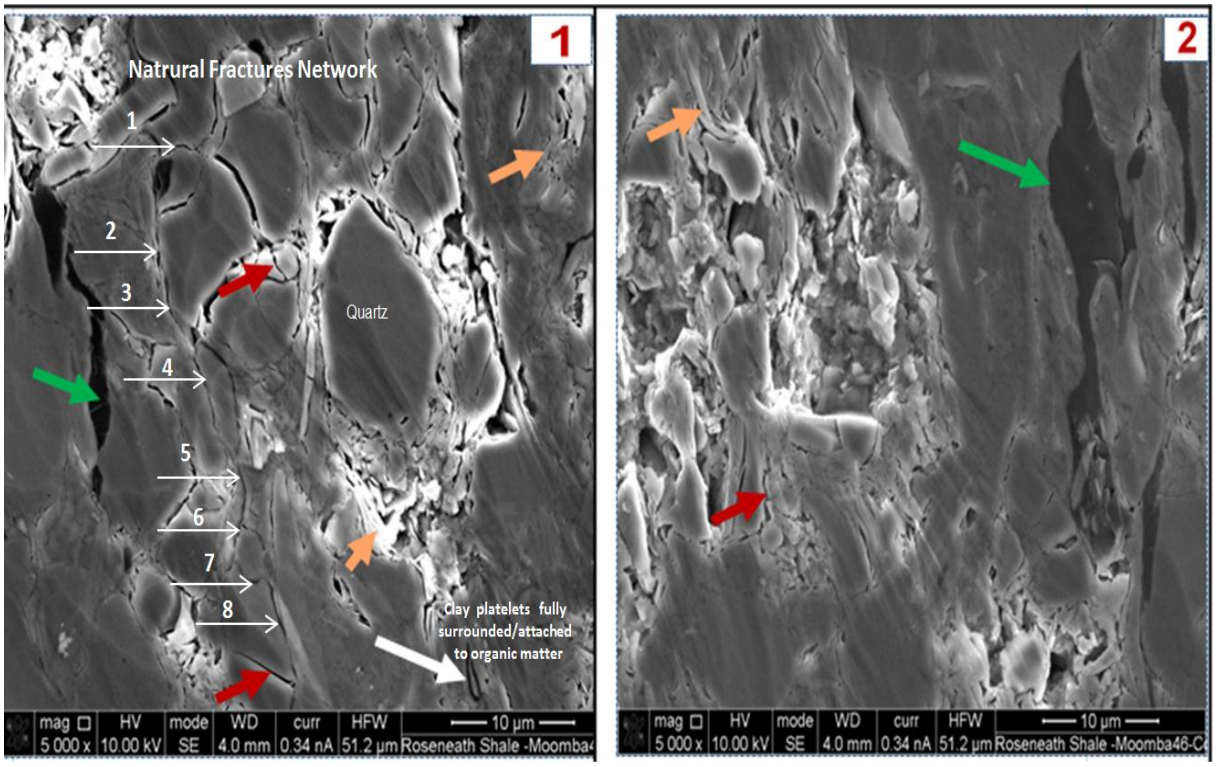

Figure B5: Large porous area surrounding the rigid grains quartz in panel 1. Kerogen and organic matter is not showing any pull-out labelled with green arrows, the matrix fracture porosity is also very common in both images labelled 1 and 2 marked by red arrows, while yellow arrows pointing towards the clay platelets compacted between hard grains of siderite, quartz and other heavy minerals. Natural Fracture system progressively marked by white arrows in image 1, from 1 to 8 and similarly others fractures networks can be traced as well in both images. Samples were prepared using Argon ion milling procedure (FIB) while secondary electron beam was applied to image at same magnification and resolution power of SEM. Impact of ion milling curtains artefact is clearly visible in these two images.

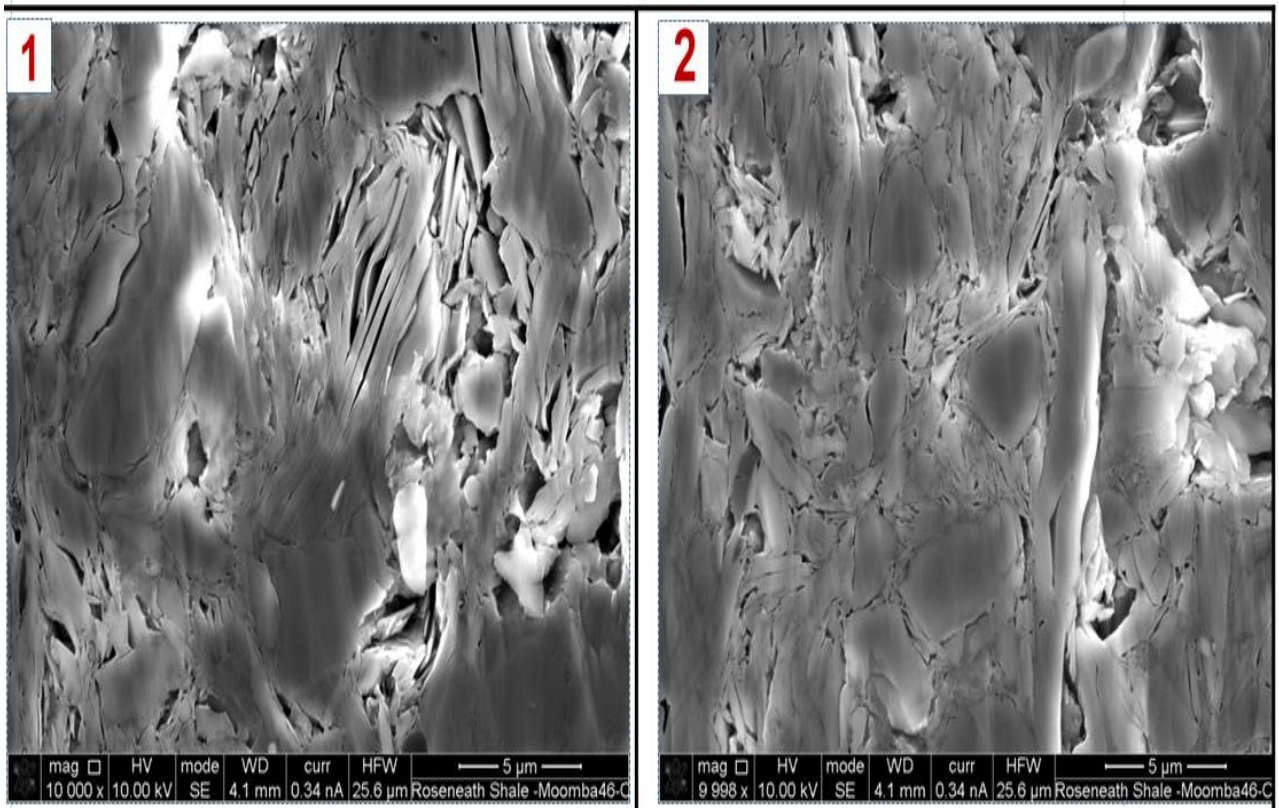

Figure B6: Intergranular, grain rim porosity, fracture cleavage plane, ductile clay flocculates compacted around hard grains of quartz, siderite, pyrite, representing a very complex permeable network in images 1 and 2. Pores are open and level of tortousity in these both panels is ultra-complex in both images.

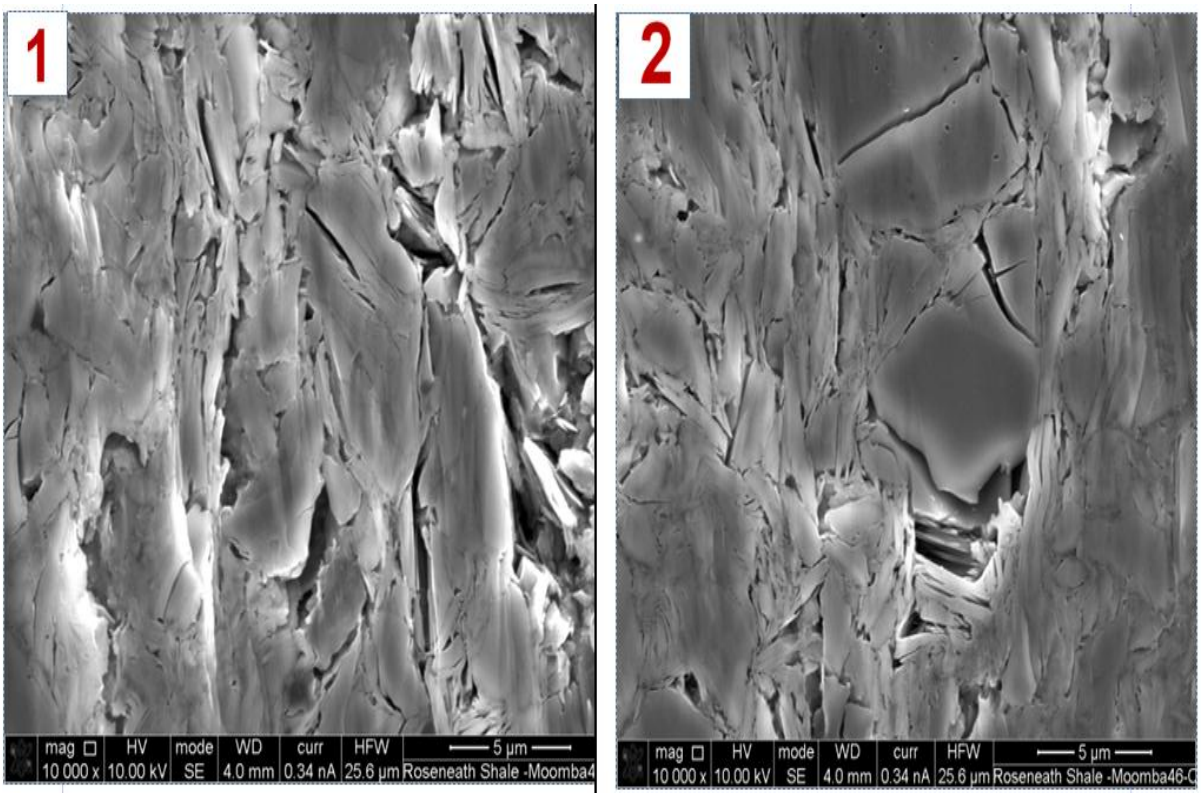

Figure B7: Elongated pores around the grains (grain edge pores) are connected and there is matrix fracture porosity/system in 1 and 2 images as well. Most of these pores are interparticle pores. The geometries of these pores are in large range, from nanoscale to larger than few microns and they are primary in origin and the bending around the grains is impact of compaction. There is clear evidence of loss of porosity which cannot be quantified by even FIB/SEM serial sectioning and 3D modelling seen here around the grains by filling the void spaces between the grains by the sectioned material.

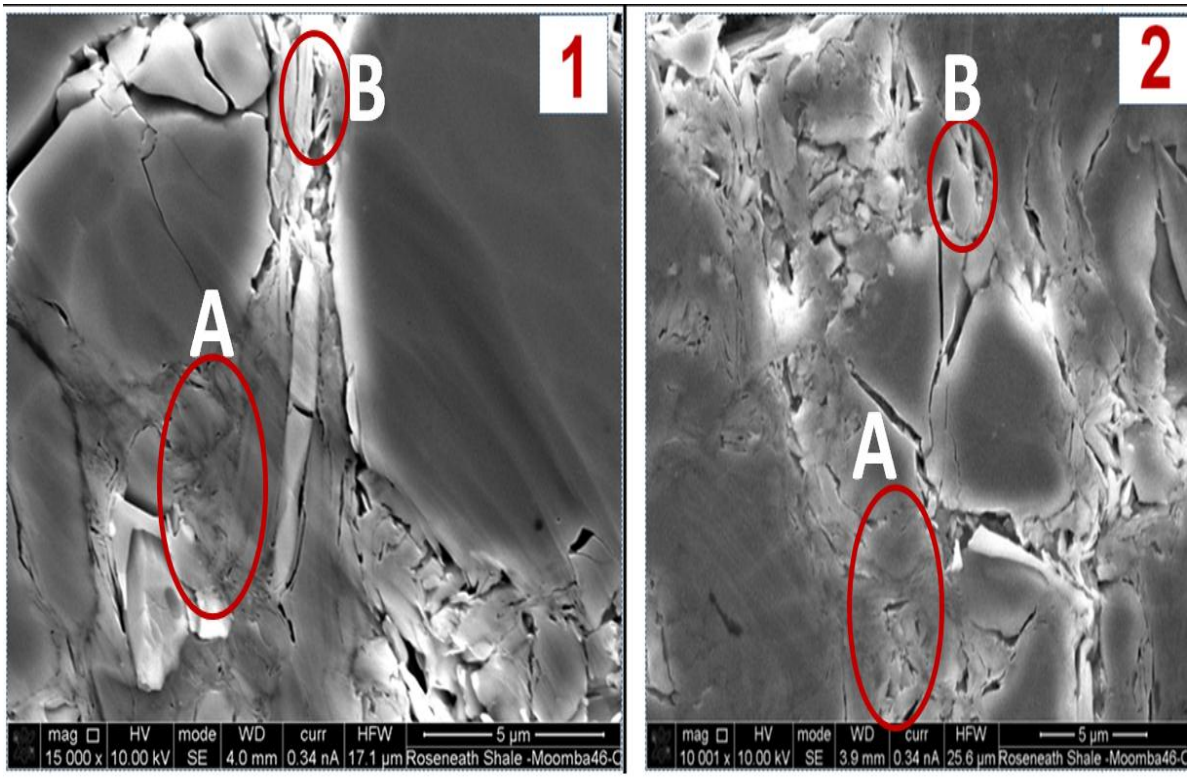

Figure B8: Irregular shape pores around the grains and matrix fracture porosity/system in 1 and 2 images as well is evident. Most of these pores are interparticle pores. The geometries of these pores are in large range, from nanoscale to larger than few microns, as particles bending around the rigid grains as a consequence of compaction with some various shapes of pores and voids is evident. During ion milling procedure there is loss of porosity by redeposition of ablated material from other parts of the sample as marked by ellipse A and some open pores marked by ellipse B in both panels 1 and 2 in this image.

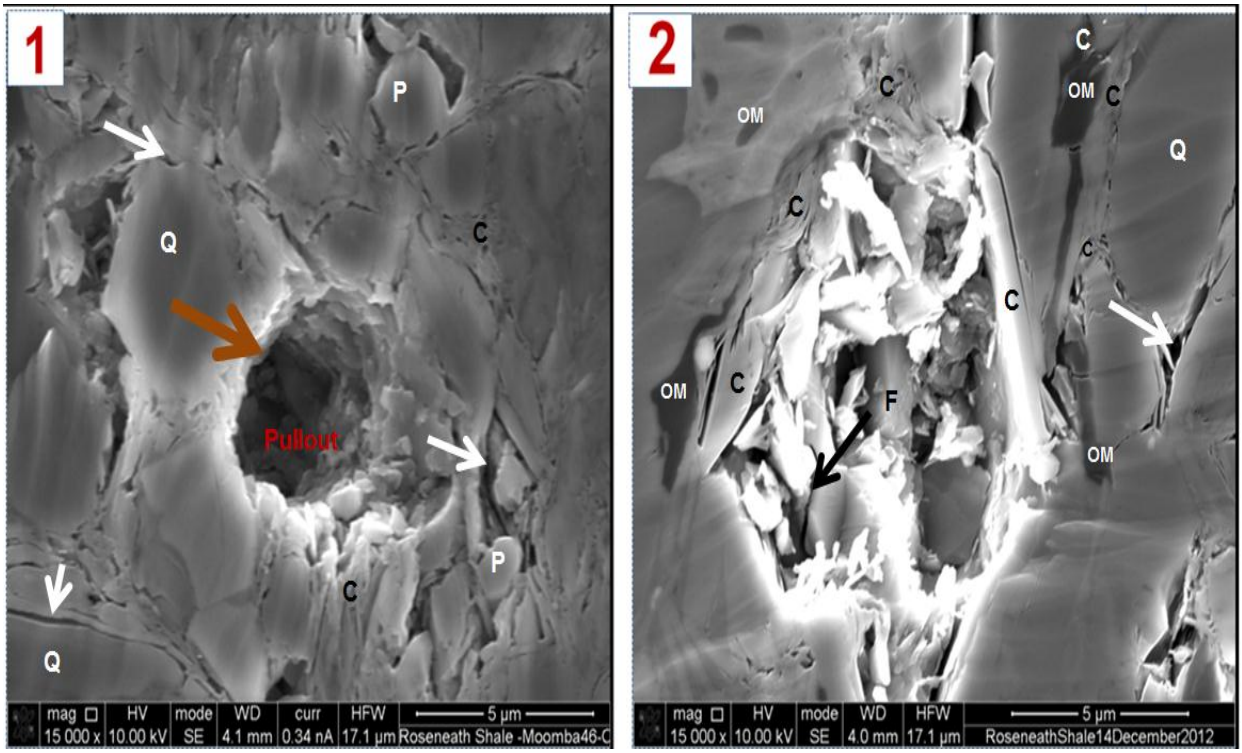

Figure B9: Example of grains pull out in 1, right in the middle of the image during ion milling sample preparation procedure, a large isolate porous zone surrounded by ductile clays platelets in panel 2. F (black arrow) =fracture, OM=organic matter, C=clays, Q=quartz, P=pyrite white arrows showing intergranular pores surrounding the hard grains.

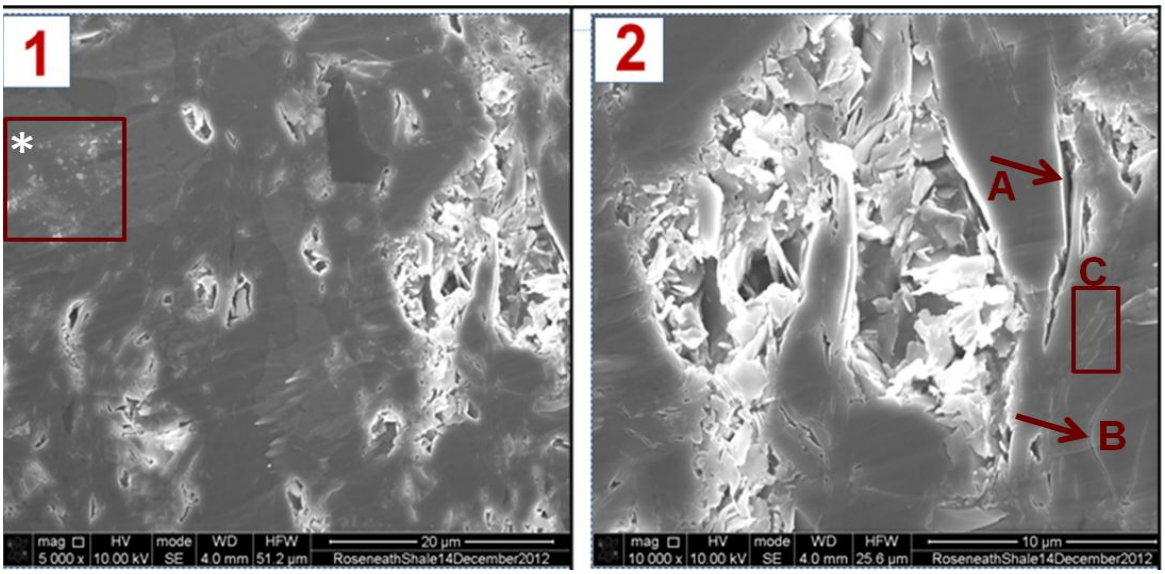

Figure B10: FIB/SEM image of Roseneath shale. This is not BSE image. Ion milled material from other parts of sample when deposited in the intergranular pores and clay cleavage pores can be differentiated from the surrounding matrix as marked by the white asterisk within maroon color rectangle in panel 1. Maroon color arrows, labelled as A and B in panel 2, represent open and partially closed cleavage cleavage plane pores in the clay platelets respectively while in maroon colored rectangle C are completely closed by the sectioned material. During this procedure there is loss of microporosity quantification when building 3D total porosity and pores interconnectivity.

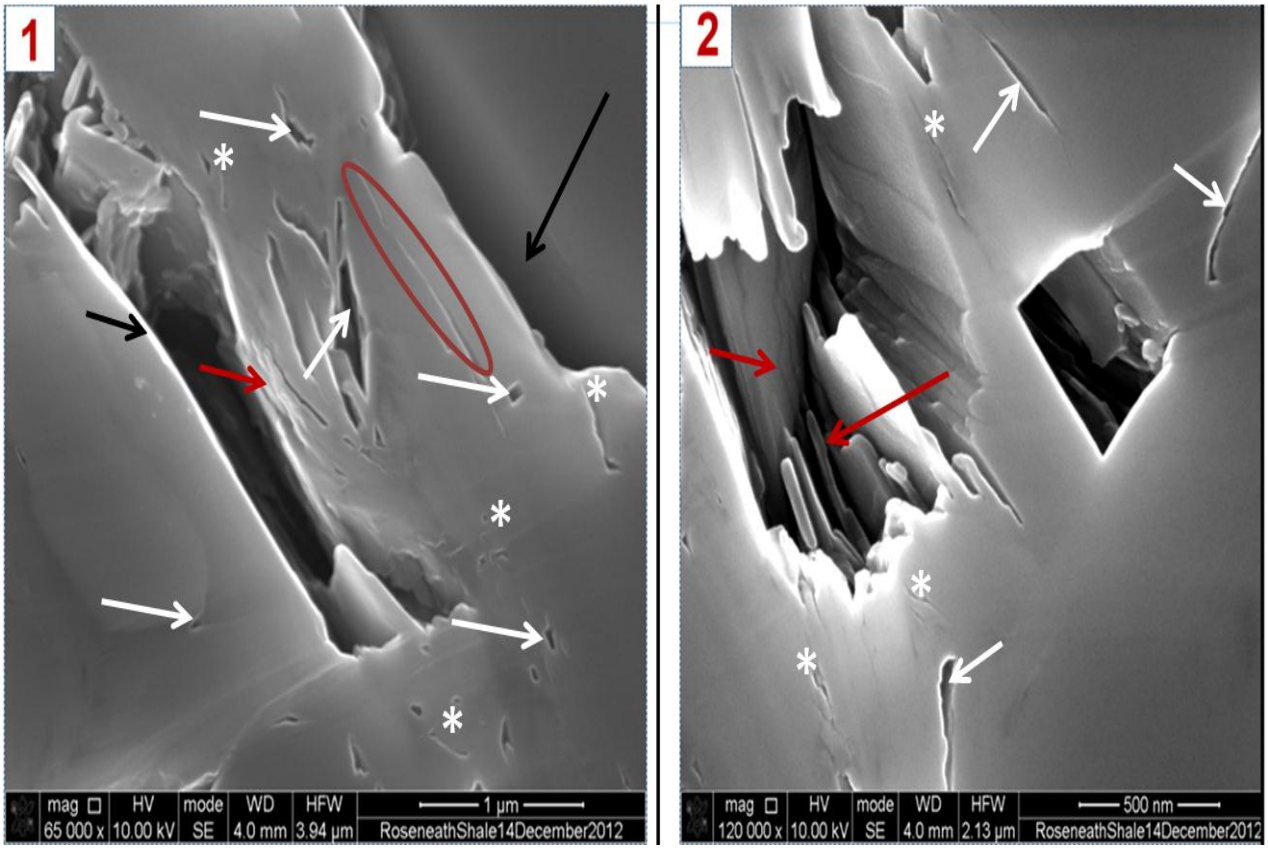

Figure B11: FIB/SEM imaged of Roseneath shale. Ion milled material has been deposited in the intergranular pores as marked by the white asterisks, as the cleavage plane pores in the clay platelets are partial closed by the sectioned material in ion milling procedure marked by maroon ellipse in panel 1. Maroon colour arrows show mica/clay platelets, black arrwos pointing toward large fractures while white arrows pointing the cleavage plane, elongated pores in 1 and 2 panels , rich in clay matrix. There is a very low ion milling curtain effect in both images image.

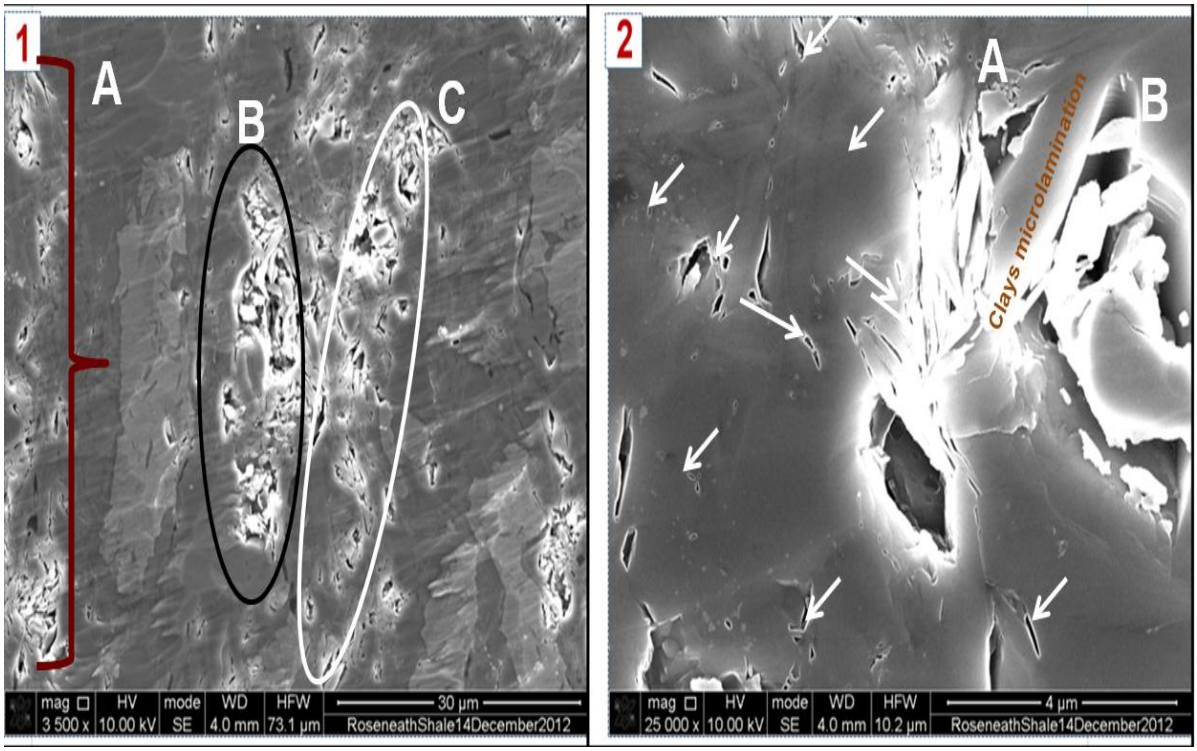

Figure B12: Three porous isolated network one at far left, and two in middle of figure marked by A, B and C in panel marked by 1 and dimensions of vugy porosity in higher resolution, to store compressed gas and help in the flow of the gas in panel 2. White arrows pointing to submicron isolated porosity. High fraction of free porosity is intergranular porosity. Fluids communication between Zone A and B is questionable, when using radiation and fluid penetration techniques.

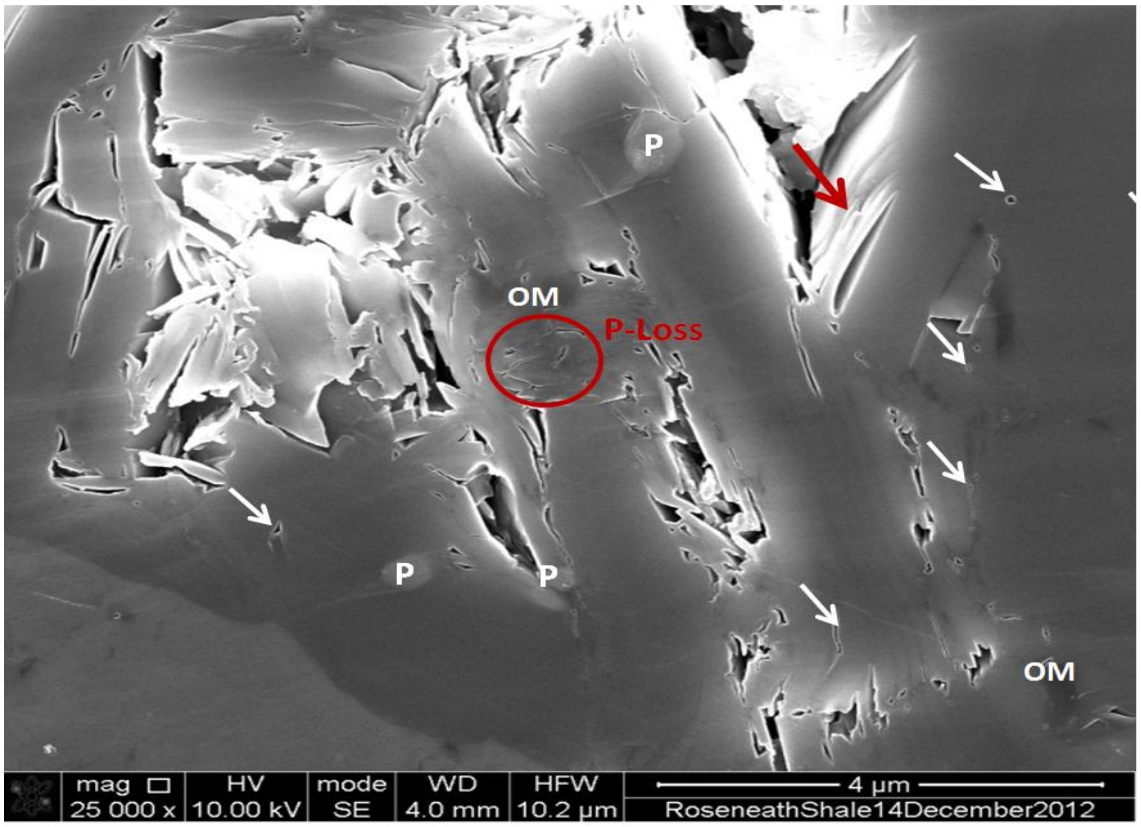

Figure B13: Network and pores is result of compaction after the deposition of the detrital grains, pores dimensions range from less than 1 micron to 2 microns. (sub-micro reservoirs for compressed gas, isolated cavities /vugs for free gas). P-Loss=Porosity loss during FIB operation, OM=organic matter, White arrows= Pointing partial closed pores during FIB operation. Red arrow = Loss porosity in clay platelet cleavage pores during FIB operation. P = pyrite crystals.

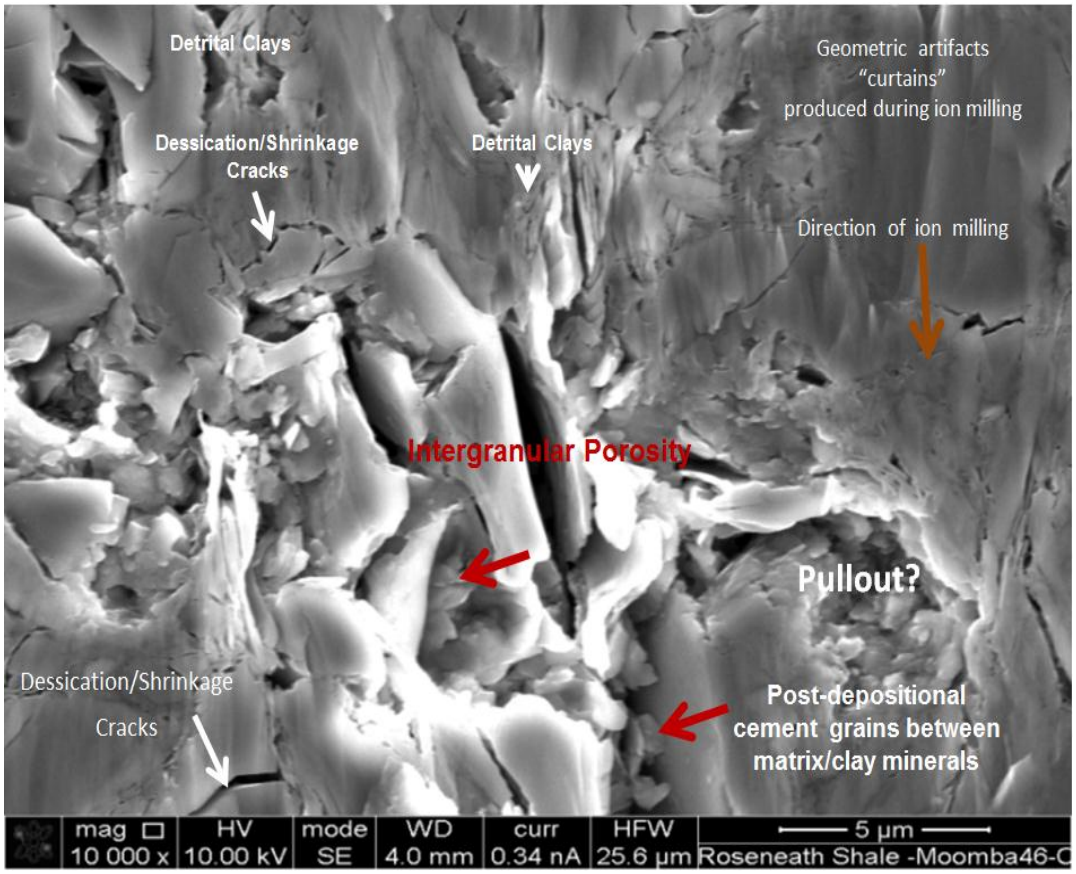

Figure B14: FIB/SEM image of Roseneath shale using Helios D433, application of secondary electrons for identification of intergranular porosity and matrix fracture system, pullouts, and cement identification, project well Moomba 46, Depth 8096.00-8097.5 ft.

Appendix-C

Mathematical Expressions & Nomenclatures for Shale Volume, Porosity, & Water Saturation Estimation

Clays/Shale:

$$I_{GR} = \left(\frac{GR_{\log} - GR_{\min}}{GR_{\max} - GR_{\min}} \right) \quad \text{....(C-1)}$$

$$V_{sh} = 0.083 \times [2^{(3.7 \times I_{IGR})} - 1.0] \quad \text{....(C-2)}$$

$$V_{sh} = 0.33 \times [2^{(2 \times I_{IGR})} - 1.0] \quad \text{....(C-3)}$$

$$V_{sh} = 1.7 - \sqrt{3.38 - (IGR + 0.7)^2} \quad \text{....(C-4)}$$

$$V_{sh} = \frac{0.5 \times IGR}{1.5 - IGR} \quad \text{....(C-5)}$$

$$V_{sh} = \frac{0.2 \times IGR}{1.2 - IGR} \quad \text{....(C-6)}$$

Porosity Calculations:

$$\Phi_{sonic} = \left(\frac{\Delta t_{\log} - \Delta t_{ma}}{\Delta t_f - \Delta t_{ma}}\right) \quad \text{....(C-7)}$$

$$\Phi_{Den} = \left(\frac{\rho_{ma} - \rho_b}{\rho_{ma} - \rho_f}\right) \quad \text{....(C-8)}$$

$$\Phi_{D-S} = \frac{0.36}{\left[\frac{\Phi_D + 0.37}{\Phi_S}\right] - 1} \quad \text{....(C-9)}$$

Sonic Porosity = $\Phi_{sonic} * 0.7$ (C-10)

$$\Phi_{sonic} = \frac{\Delta t_{\log} - \Delta t_{ma}}{B} \quad \text{....(C-11)}$$

$$\Phi = \frac{\Delta t_{\log} - \Delta t_{ma}}{BBc} \quad \text{....(C-12)}$$

Water Saturation

$$S_{W-In}=\left[\frac{1}{R_t\times\left(\frac{\Phi_e^m}{R_w}+\left[2\times\sqrt{\frac{\Phi_e^m\times V_{sh}^{(2-V_{sh})}}{R_w\times R_{sh}}}\right]+\frac{V_{sh}^{(2-V_{sh})}}{R_{sh}}\right)}\right]^{\frac{1}{n}} \quad \text{....(C13)}$$

$$S_{W-Si}=\left(\frac{0.45\times R_w}{\Phi_e^m}\right)\times\left(\left[\left(\frac{5.0\times\Phi_e^m}{R_w\times R_t}\right)+\left(\frac{V_{sh}}{R_{sh}}\right)^2\right]^{\frac{1}{n}}-\frac{V_{sh}}{R_{sh}}\right) \quad \text{....(C14)}$$

$$S_{W-To}=\frac{0.4\times R_w\times(1.0-V_{sh})}{\Phi_e^m}\times\left(\left(\frac{V_{sh}}{R_{sh}}\right)^2+\frac{\Phi_e^m}{0.2\times R_w\times(1.0-V_{sh})\times R_t}\right)^{\frac{1}{n}}-\frac{V_{sh}}{R_{sh}} \quad \text{....(C15)}$$

$$S_{W-Ar}=\left(\frac{0.62\times R_w}{\Phi^{2.15}\times R_t}\right)^{\frac{1}{n}} \quad \text{....(C16)}$$

$$G_{Total-Free-Gas}=\frac{32.0368}{B_g}\left[\left(\frac{\Phi(1-S_w)}{\rho_b}\right)\right] \quad \text{....(A17)}$$

Nomenclature:

$S_{W\text{-}Ar}$:	Water saturation from Archie's equation (Fraction)
$S_{W\text{-}In}$:	Water Saturation from Indonesian formula (Fraction)
$S_{W\text{-}Si}$:	Water saturation from Simandoux - formula (Fraction)
$S_{W\text{-}To}$:	Water saturation from total shale model (Fraction)
$Ø_S$:	Sonic porosity (Fraction)
$Ø_D$:	Density porosity (Fraction)
$Ø_{ef}$:	Effective porosity (Fraction)
$Ø_{S\text{-}H}$:	Hilchie's corrected sonic porosity (Fraction)
$Ø_{To}$:	Total porosity (Fraction)
$Ø_{S\text{-}D}$:	Sonic-density porosity (Fraction)
R_t:	Formation true resistivity (Ohm-m)
R_w:	Formation brine resistivity (Ohm-m)
V_{sh}:	Volume of shale (V/V)
R_{cl}:	Shale Resistivity (Ohm-m)
a:	Tortousity factor (Dimensionless)
m:	Cementation exponent (Dimensionless)
n:	Saturation exponent (Dimensionless)
Δt_{ma}:	Matrix transit time for shale (µs/ft.)
Δt_{log}:	Sonic log reading from shale interval (µs/ft.)
Δt_f:	Interval transit time fluid (µs/ft.)
ρ_b:	Bulk density (gm/cc)

ρ_{ma}:	Matrix density (gm/cc)
ρ_f:	Fluid density (gm/cc)
GR_{-min}:	Gamma ray in clean sand (API)
GR_{-max}:	Gamma ray in 100% shale (API)
GR_{-log}:	Gamma ray log reading in shale zone (API)
B_g:	Gas formation volume factor (ratio - CF/SCF)
$I_{GR:}$	Gamma ray Index (Fraction)
B =	214.6 (constant)
B_c =	2.33 (correction factor)
ρf =	1.237 gm/cc
ρma =	2.650 gm/cc
GR-min =	25(API)
GR-max =	172 (API)
Δtma=	68 (μs/ft.)
Δtf=	189 (μs/ft.)
B =	214.6 (A constant for shale)
Bc =	2.33 (Correction Factor)
$Z_{ef} = \sum f_i Z^n_i$	Effective atomic number of the sample
n =	Number of electrons in ith shell
f_i =	Electron concentration of the ith component of the sample.
E =	X-Ray Energy (Kev)
N_A =	Avogadro's Number
ρ =	Sample Bulk Density
μ =	Linear Attenuation Coefficient
ρg:	Grain density, in g/cm^3
M0:	Apparent mass in air (weight in air) (g) of the empty pyknometer.
M1:	Apparent mass in air (g) of the pyknometer plus solid.
M2:	Apparent mass in air (g) of the pyknometer plus solid plus water.
M3:	Apparent mass in air (g) of the pyknometer filled with water.
C :	Correction of air buoyancy in gm/ml
ρ_w:	Density of water in Kg/m^3 at the temperature of calibration
V_2 =	Volume of the sample chamber and lines to the air valve, cc
V_1 =	Volume of the reference chamber and lines, cc
P_1 =	Initial system pressure, atm
P_2 =	Pressure of the reference chamber and lines with air valve closed, atm
P_{eq} =	Equalization pressure of the system air valve open, atm
V_{ref} =	Volume of the reference core, cc
V_1 =	Volume of the reference chamber and lines, cc
P_1 =	Initial system pressure, atm
P_2 =	Pressure of reference chamber and lines with air valve closed, atm
P_{eq} =	Equalization pressure of the system air valve open, atm
P_{1r} =	Initial system pressure with reference core in the sample chamber, atm
P_{2r} =	Pressure of reference chamber and lines with air valve closed (with reference core in the sample chamber), atm
P_{eqr} =	Equalization pressure of the system (with reference core in the reference chamber) with air valve open, atm
PPL =	Petroleum Production License

APPENDIX – D

Murteree Shale Della#4 - Wireline Logs and Digital Data

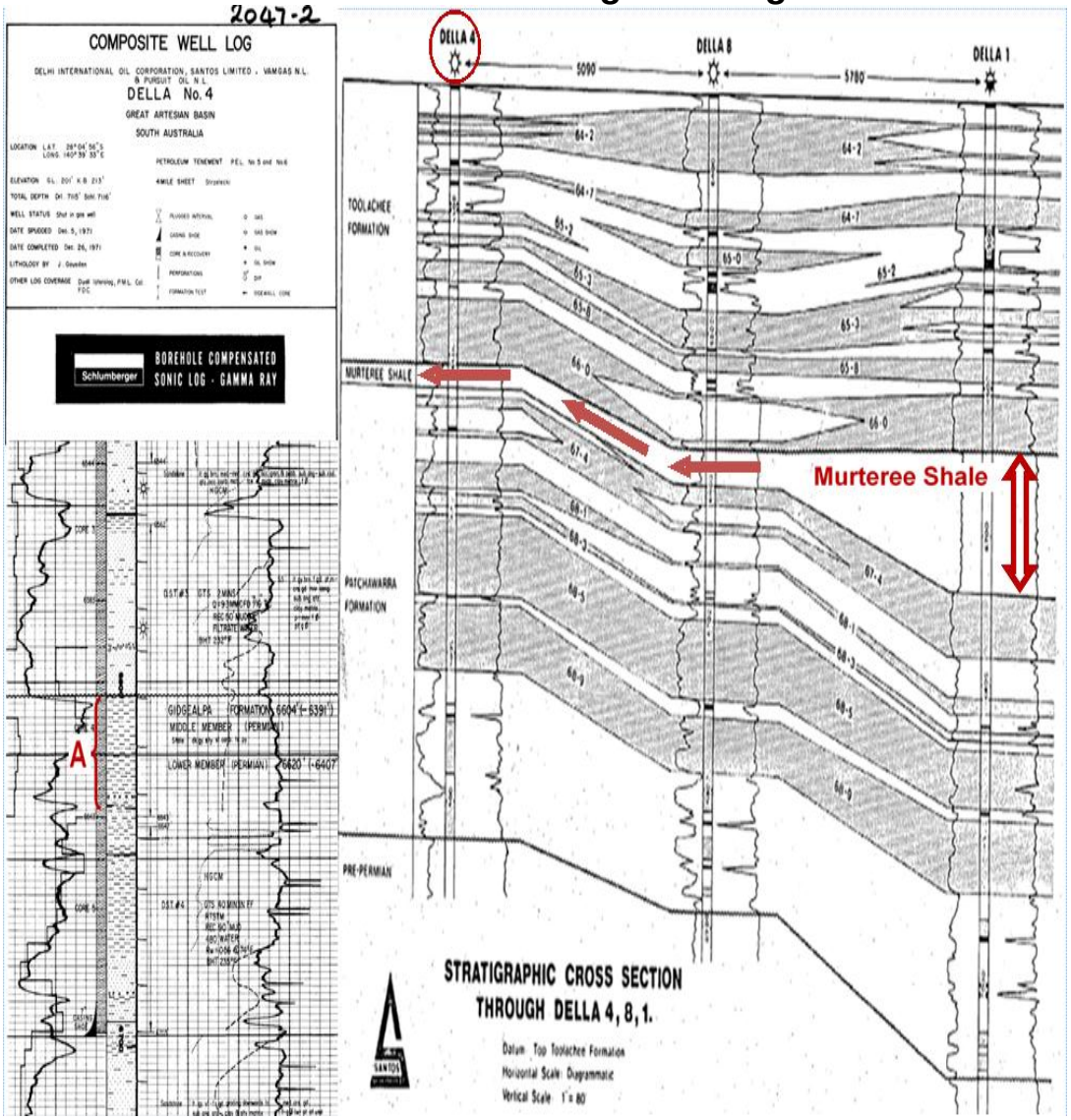

Figure D1: Murteree shale core samples and digital log core data depth location A; from Della#4 Composite Well Log (Source: Well Completion Reports of Della#4 left and Della#8 right PIRSA South Australia).

Table D1: Clay (Shale Volume - Illite (Muscovite); Chlorite & Koalinite) content% in Murteree shale from QEMSCAN and XRD, (M Ahmad and M. Haghighi, 2012) log based and Encounter#1 well completion report from laboratory results (Source: PIRSA SA Adelaide)

Della#4 Project Well (Murteree Shale) Scanned Core Samples QEMSCAN & XRD Results	Well Completion Report Della#4 Project Well Log based Mineralogy Results (Murteree Shale-Using Steiber Formula)	Enconter#1 Well Completion Report Murteree Shale (XRD - Quantitative Results) Source (PIRSA-SA Adelaide)
XRD Avg. 50.59% QEMSCAN Avg. 47.30%	Avg. 52.3 %	Avg. 53.4%

Table D2: Digital log data, of Murteree shale in Della#4; project well in Cooper Basin.

Depth (ft.)	Caliper (in)	Gamma Ray (API)	Δt Sonic Velocity (µs/ft.)	Rt True Resistivity Ohm.m	Rho-b (Bulk Density-gm/cc)
6626.00	9.58	104.70	69.80	59.39	2.51
6625.50	9.58	105.00	69.70	61.39	2.56
6625.00	9.56	105.00	70.03	65.27	2.60
6624.50	9.55	105.30	70.99	70.44	2.59
6624.00	9.55	104.10	71.75	74.93	2.55
6623.50	9.55	100.40	71.44	76.76	2.52
6623.00	9.55	98.35	70.34	75.47	2.53
6622.50	9.54	101.60	69.05	71.59	2.59
6622.00	9.53	108.20	68.55	68.18	2.64
6621.50	9.53	115.00	69.49	67.70	2.65
6621.00	9.53	121.20	70.89	67.68	2.63
6620.50	9.52	126.80	71.62	65.75	2.63
6620.00@	9.50	132.30	71.67	64.80	2.62
6619.50@	9.48	138.00	71.28	67.56	2.60
6619.00@	9.47	142.40	70.81	70.70	2.59
6618.50	9.45	144.20	70.58	70.73	2.61
6618.00	9.42	143.70	70.73	69.68	2.63
6617.50	9.40	142.20	71.26	70.30	2.64
6617.00	9.37	142.40	71.67	72.78	2.63
6616.50	9.35	146.00	71.47	76.12	2.64
6616.00	9.33	149.10	70.81	77.14	2.64
6615.50	9.29	148.10	70.02	73.52	2.63
6615.00	9.26	145.30	69.56	68.67	2.61
6614.50	9.27	143.90	69.84	66.32	2.59
6614.00	9.26	143.70	70.81	65.75	2.57
6613.50	9.21	144.50	72.16	65.64	2.57
6613.00	9.15	147.80	73.07	66.71	2.57
6612.50	9.12	154.30	72.94	69.41	2.57
6612.00	9.10	158.00	72.68	71.21	2.57
6611.50	9.06	154.40	73.20	70.25	2.57
6611.00	8.99	150.40	73.93	70.19	2.56
6610.50	8.90	152.50	74.14	73.56	2.55
6610.00	8.84	156.40	73.85	72.78	2.55

Legend:	
6620.00ft @	Derived log based values from exact location of Murteree Shale Core sample in Della#4 Project well
6619.50 ft.@	
6619.00ft @	

Table D3: Shale Volumes (Total Clay Fraction) Derived						
Depth (ft.)	Shale Volume=Gamma Ray Index(GRI-Fraction)	Tertiary Rocks Unconsolidated Formula (Fraction)	Tertiary Rocks Consolidated Formula (Fraction)	Older Rocks Consolidated High Shale Content Formula (Fraction)	Steiber Formula (Fraction)	Super Steiber Formula (Fraction)
6626.00	0.5420	0.2500	0.3700	0.6310	0.2830	0.1650
6625.50	0.5440	0.2520	0.3720	0.6320	0.2850	0.1660
6625.00	0.5440	0.2520	0.3720	0.6320	0.2850	0.1660
6624.50	0.5460	0.2540	0.3730	0.6330	0.2860	0.1670
6624.00	0.5380	0.2470	0.3660	0.6290	0.2800	0.1630
6623.50	0.5130	0.2260	0.3420	0.6170	0.2600	0.1490
6623.00	0.4990	0.2150	0.3290	0.6100	0.2490	0.1420
6622.50	0.5210	0.2330	0.3490	0.6210	0.2660	0.1530
6622.00	0.5660	0.2710	0.3930	0.6430	0.3030	0.1790
6621.50	0.6120	0.3160	0.4410	0.6660	0.3450	0.2080
6621.00	0.6540	0.3610	0.4870	0.6870	0.3870	0.2400
6620.50	0.6930	0.4080	0.5320	0.7070	0.4290	0.2730
6620.00@	0.7300	0.4570	0.5780	0.7250	0.4740	0.3110
6619.50@	0.7690	0.5130	0.6280	0.7440	0.5260	0.3560
6619.00@	0.7990	0.5610	0.6680	0.7590	0.5690	0.3980
6618.50	0.8110	0.5810	0.6860	0.7660	0.5890	0.4170
6618.00	0.8080	0.5760	0.6820	0.7640	0.5840	0.4120
6617.50	0.7970	0.5580	0.6660	0.7590	0.5670	0.3960
6617.00	0.7990	0.5610	0.6690	0.7600	0.5700	0.3990
6616.50	0.8230	0.6020	0.7030	0.7720	0.6080	0.4370
6616.00	0.8440	0.6400	0.7330	0.7820	0.6430	0.4740
6615.50	0.8370	0.6270	0.7230	0.7790	0.6310	0.4610
6615.00	0.8180	0.5930	0.6960	0.7690	0.6000	0.4280
6614.50	0.8090	0.5780	0.6830	0.7650	0.5850	0.4140
6614.00	0.8080	0.5760	0.6820	0.7640	0.5840	0.4120
6613.50	0.8130	0.5850	0.6890	0.7670	0.5920	0.4200
6613.00	0.8350	0.6230	0.7200	0.7780	0.6280	0.4580
6612.50	0.8800	0.7100	0.7880	0.8000	0.7100	0.5500
6612.00	0.9050	0.7620	0.8270	0.8130	0.7610	0.6140
6611.50	0.8800	0.7100	0.7880	0.8000	0.7100	0.5500
6611.00	0.8530	0.6570	0.7470	0.7870	0.6590	0.4920
6610.50	0.8670	0.6840	0.7680	0.7940	0.6850	0.5210
6610.00	0.8940	0.7390	0.8100	0.8070	0.7380	0.5840

Legend:	
6620.00ft @	Shale volume values from exact location of Murteree Shale Core sample in Della#4 Project well
6619.50 ft. @	
6619.00ft @	

Table D4: Porosities evaluated using various formulas with correction factors.						
Depth (ft.)	Sonic Porosity Wyllie Formula (Fraction)	Hilchie's Correction Factor (Sonic Porosity*0.7) (Fraction)	Sonic Porosity using B Correction Factor (Fraction)	Sonic Porosity using BBc Correction Factor (Fraction)	Density Porosity (Fraction)	Sonic-Density Cross Plot Porosity (Fraction)
6626.00	0.0178	0.0125	0.0084	0.0036	0.0970	0.0150
6625.50	0.0168	0.0118	0.0079	0.0034	0.0658	0.0142
6625.00	0.0201	0.0141	0.0095	0.0041	0.0389	0.0171
6624.50	0.0296	0.0207	0.0139	0.0060	0.0453	0.0257
6624.00	0.0371	0.0260	0.0175	0.0075	0.0715	0.0327
6623.50	0.0341	0.0239	0.0160	0.0069	0.0927	0.0297
6623.00	0.0232	0.0162	0.0109	0.0047	0.0870	0.0198
6622.50	0.0104	0.0073	0.0049	0.0021	0.0453	0.0086
6622.00	0.0054	0.0038	0.0026	0.0011	0.0050	0.0045
6621.50	0.0148	0.0104	0.0069	0.0030	0.0000	0.0124
6621.00	0.0286	0.0200	0.0135	0.0058	0.0120	0.0248
6620.50	0.0358	0.0251	0.0169	0.0072	0.0163	0.0316
6620.00	0.0363	0.0254	0.0171	0.0073	0.0212	0.0321
6619.50	0.0325	0.0228	0.0153	0.0066	0.0361	0.0284
6619.00	0.0278	0.0195	0.0131	0.0056	0.0446	0.0240
6618.50	0.0255	0.0179	0.0120	0.0052	0.0318	0.0220
6618.00	0.0270	0.0189	0.0127	0.0055	0.0142	0.0234
6617.50	0.0323	0.0226	0.0152	0.0065	0.0099	0.0283
6617.00	0.0363	0.0254	0.0171	0.0073	0.0113	0.0321
6616.50	0.0344	0.0241	0.0162	0.0069	0.0099	0.0302
6616.00	0.0278	0.0195	0.0131	0.0056	0.0092	0.0241
6615.50	0.0200	0.0140	0.0094	0.0040	0.0170	0.0170
6615.00	0.0154	0.0108	0.0073	0.0031	0.0304	0.0130
6614.50	0.0182	0.0127	0.0086	0.0037	0.0460	0.0154
6614.00	0.0278	0.0195	0.0131	0.0056	0.0566	0.0240
6613.50	0.0412	0.0288	0.0194	0.0083	0.0566	0.0367
6613.00	0.0502	0.0351	0.0236	0.0101	0.0538	0.0457
6612.50	0.0489	0.0342	0.0230	0.0099	0.0545	0.0444
6612.00	0.0463	0.0324	0.0218	0.0094	0.0573	0.0417
6611.50	0.0515	0.0361	0.0242	0.0104	0.0587	0.0469
6611.00	0.0587	0.0411	0.0276	0.0119	0.0616	0.0545
6610.50	0.0608	0.0426	0.0286	0.0123	0.0686	0.0566
6610.00	0.0579	0.0405	0.0273	0.0117	0.0743	0.0535

Legend:	
6620.00ft @	Porosity values from exact location of Murteree Shale Core sample in Della#4 Project well
6619.50ft @	
6619.00ft @	

Table D5: Four water saturation models results using shale volume from GRI – Gamma Ray shale formula and various derived porosities

Type of Porosity		Archie's Model Sw (Fraction)	Indonesian Model Sw (Fraction)	Simandoux Model Sw (Fraction)	Total Shale Model Sw (Schlumberger) (Fraction)
Sonic Porosity	0.0363	2.515	0.583	0.565	1.713
	0.0325	2.751	0.568	0.522	1.843
	0.0278	3.144	0.559	0.486	2.162
Hilchie's Porosity Formula	0.0254	3.594	0.626	0.579	3.094
	0.0228	3.921	0.605	0.532	3.369
	0.0195	4.482	0.591	0.492	4.036
Sonic Porosity B Factor	0.0171	5.338	0.664	0.587	6.301
	0.0153	5.843	0.637	0.537	6.990
	0.0131	6.671	0.617	0.495	8.485
Sonic Porosity BBc Factor	0.0073	12.505	0.715	0.593	32.451
	0.0066	13.546	0.679	0.540	35.681
	0.0056	15.606	0.652	0.497	44.655
Density Porosity	0.0212	4.306	0.645	0.584	4.256
	0.0361	2.477	0.555	0.518	1.557
	0.0446	1.960	0.505	0.470	1.019
Sonic - Density Porosity Cross Plot Porosity	0.0321	2.844	0.599	0.571	2.087
	0.0284	3.148	0.583	0.526	2.304
	0.0240	3.641	0.573	0.489	2.785

Table D6: Four water saturation models results using shale volume from tertiary rocks unconsolidated and high shale content formula and various derived porosities

Type of Porosity		Archie's Model Sw (Fraction)	Indonesian Model Sw (Fraction)	Simandoux Model Sw (Fraction)	Total Shale Model Sw (Schlumberger) (Fraction)
Sonic Porosity	0.0363	2.515	0.783	0.844	2.304
	0.0325	2.751	0.733	0.752	2.649
	0.0278	3.144	0.700	0.677	3.302
Hilchie's Porosity Formula	0.0254	3.594	0.863	0.892	4.063
	0.0228	3.921	0.796	0.780	4.799
	0.0195	4.482	0.750	0.692	6.172
Sonic Porosity B Factor	0.0171	5.338	0.937	0.922	8.114
	0.0153	5.843	0.853	0.797	9.896
	0.0131	6.671	0.794	0.701	12.992
Sonic Porosity BBc Factor	0.0073	12.505	1.042	0.944	41.050
	0.0066	13.546	0.931	0.809	50.249
	0.0056	15.606	0.852	0.708	68.457
Density Porosity	0.0212	4.306	0.899	0.908	5.533
	0.0361	2.477	0.712	0.740	2.245
	0.0446	1.960	0.617	0.635	1.556
Sonic -Density Porosity Cross Plot	0.0321	2.844	0.812	0.863	2.782
	0.0284	3.148	0.758	0.764	3.300
	0.0240	3.641	0.722	0.684	4.256

Table D7: Four water saturation models results using shale volume from older-rocks consolidated high shale content formula and various derived porosities

Type of Porosity		Archie's Model Sw (Fraction)	Indonesian Model Sw (Fraction)	Simandoux Model Sw (Fraction)	Total Shale Model Sw (Schlumberger) (Fraction)
Sonic Porosity	0.0363	2.515	0.672	0.694	2.143
	0.0325	2.751	0.642	0.629	2.405
	0.0278	3.144	0.624	0.576	2.935
Hilchie's Porosity Formula	0.0254	3.594	0.731	0.721	3.854
	0.0228	3.921	0.690	0.645	4.408
	0.0195	4.482	0.663	0.585	5.517
Sonic Porosity B Factor	0.0171	5.338	0.783	0.737	7.823
	0.0153	5.843	0.732	0.655	9.168
	0.0131	6.671	0.697	0.591	11.656
Sonic Porosity BBc Factor	0.0073	12.505	0.855	0.748	40.185
	0.0066	13.546	0.788	0.661	46.897
	0.0056	15.606	0.741	0.595	61.602
Density Porosity	0.0212	4.306	0.756	0.730	5.292
	0.0361	2.477	0.626	0.622	2.030
	0.0446	1.960	0.557	0.549	1.369
Sonic Density Porosity Cross Plot	0.0321	2.844	0.694	0.705	2.606
	0.0284	3.148	0.661	0.636	3.010
	0.0240	3.641	0.641	0.581	3.793

Table D8: Four water saturation models results using shale volume from clavier formula consolidated rocks formula and various porosities derived

Type of Porosity		Archie's Model Sw (Fraction)	Indonesian Model Sw (Fraction)	Simandoux Model Sw (Fraction)	Total Shale Model Sw (Schlumberger) (Fraction)
Sonic Porosity	0.0363	2.515	0.585	0.568	1.732
	0.0325	2.751	0.578	0.538	1.964
	0.0278	3.144	0.576	0.510	2.437
Hilchie's Porosity Formula	0.0254	3.594	0.629	0.583	3.129
	0.0228	3.921	0.617	0.549	3.599
	0.0195	4.482	0.610	0.517	4.568
Sonic Porosity B Factor	0.0171	5.338	0.667	0.591	6.372
	0.0153	5.843	0.651	0.555	7.481
	0.0131	6.671	0.638	0.521	9.634
Sonic BBc Factor	0.0073	12.505	0.719	0.597	32.824
	0.0066	13.546	0.695	0.559	38.242
	0.0056	15.606	0.675	0.524	50.829
Density Porosity	0.0212	4.306	0.648	0.588	4.303
	0.0361	2.477	0.565	0.534	1.659
	0.0446	1.960	0.519	0.492	1.141
Sonic -Density Porosity Cross Plot	0.0321	2.844	0.601	0.575	2.110
	0.0284	3.148	0.594	0.543	2.459
	0.0240	3.641	0.591	0.514	3.145

Table D9: Four water saturation models results using shale volume from Steiber-older consolidated rocks formula and various derived porosities

Type of Porosity		Archie's Model Sw (Fraction)	Indonesian Model Sw (Fraction)	Simandoux Model Sw (Fraction)	Total Shale Model Sw(Schlumberger) (Fraction)
Sonic Porosity	0.0363	2.515	0.764	0.820	2.291
	0.0325	2.751	0.721	0.736	2.630
	0.0278	3.144	0.694	0.668	3.282
Hilchie's Porosity Formula	0.0254	3.594	0.841	0.863	4.053
	0.0228	3.921	0.782	0.762	4.775
	0.0195	4.482	0.743	0.683	6.140
Sonic Porosity B Factor	0.0171	5.338	0.911	0.891	8.121
	0.0153	5.843	0.837	0.778	9.860
	0.0131	6.671	0.785	0.692	12.931
Sonic Porosity BBc Factor	0.0073	12.505	1.009	0.911	41.210
	0.0066	13.546	0.911	0.789	50.130
	0.0056	15.606	0.842	0.698	68.162
Density Porosity	0.0212	4.306	0.875	0.878	5.529
	0.0361	2.477	0.700	0.725	2.228
	0.0446	1.960	0.612	0.628	1.545
Sonic -Density Porosity Cross Plot	0.0321	2.844	0.792	0.837	2.769
	0.0284	3.148	0.745	0.747	3.279
	0.0240	3.641	0.715	0.675	4.232

Table D10: Four water saturation models results using shale volume from Super Steiber-older consolidated rocks & very high Vsh - more non-linear rocks formula and various derived porosities

Type of Porosity		Archie's Model Sw (Fraction)	Indonesian Model Sw (Fraction)	Simandoux Model Sw (Fraction)	Total Shale Model Sw (Schlumberger) (Fraction)
Sonic Porosity	0.0363	2.515	1.002	1.121	2.324
	0.0325	2.751	0.937	1.013	2.709
	0.0278	3.144	0.891	0.916	3.439
Hilchie's Porosity Formula	0.0254	3.594	1.138	1.233	3.906
	0.0228	3.921	1.043	1.082	4.723
	0.0195	4.482	0.974	0.955	6.254
Sonic Porosity B Factor	0.0171	5.338	1.269	1.312	7.457
	0.0153	5.843	1.144	1.126	9.430
	0.0131	6.671	1.048	0.978	12.905
Sonic Porosity BBc Factor	0.0073	12.505	1.470	1.379	35.948
	0.0066	13.546	1.287	1.161	46.487
	0.0056	15.606	1.152	0.995	66.878
Density Porosity	0.0212	4.306	1.201	1.275	5.202
	0.0361	2.477	0.903	0.986	2.325
	0.0446	1.960	0.761	0.825	1.696
Sonic -Density Porosity Cross Plot	0.0321	2.844	1.050	1.164	2.760
	0.0284	3.148	0.979	1.043	3.323
	0.0240	3.641	0.927	0.935	4.378

Table D11: Sensitivity analysis results using higher resistivity (R_t - Assumed) and log base density porosity ($Ø_D$) in Murteree Shale impact on Archie's formula derived water saturation.

True Resistivity Rt (Ohmm)	Density Porosity Ø (Fraction)	Shale Volume-Steiber Formula (Fraction)	Shale Resistivity Rcl (Ohmm)	Brine Resistivity Rw (Ohmm)	a	m	n	Archie's Model Sw(Fraction)	Indonesian Model Sw(Fraction)	Simandoux Model Sw(Fraction)	Total Shale Model Sw (Schlumberger) (Fraction)
64.800	0.0212	0.474	25	0.54	1.00	2.00	2.00	4.306	0.875	0.878	5.529
67.560	0.0361	0.526	25	0.54	1.00	2.00	2.00	2.477	0.700	0.725	2.228
70.700	0.0446	0.569	25	0.54	1.00	2.00	2.00	1.960	0.612	0.628	1.545
10.000	0.0212	0.474	25	0.54	1.00	2.00	2.00	10.961	2.227	4.807	8.556
20.000	0.0361	0.526	25	0.54	1.00	2.00	2.00	4.552	1.287	2.107	3.233
40.000	0.0446	0.569	25	0.54	1.00	2.00	2.00	2.605	0.814	1.041	1.841
50.000	0.0850	0.474	25	0.54	1.00	2.00	2.00	1.223	0.618	0.748	0.828
60.000	0.0900	0.526	25	0.54	1.00	2.00	2.00	1.054	0.523	0.603	0.680
70.000	0.0950	0.569	25	0.54	1.00	2.00	2.00	0.925	0.455	0.501	0.569
80.000	0.0950	0.474	25	0.54	1.00	2.00	2.00	0.865	0.461	0.498	0.591
90.000	0.1000	0.526	25	0.54	1.00	2.00	2.00	0.775	0.404	0.421	0.502
100.000	0.1050	0.569	25	0.54	1.00	2.00	2.00	0.700	0.362	0.363	0.431
150.000	0.1050	0.474	25	0.54	1.00	2.00	2.00	0.571	0.319	0.293	0.400
200.000	0.1100	0.526	25	0.54	1.00	2.00	2.00	0.472	0.258	0.213	0.320
250.000	0.1150	0.569	25	0.54	1.00	2.00	2.00	0.404	0.218	0.165	0.264
300.000	0.1150	0.474	25	0.54	1.00	2.00	2.00	0.369	0.214	0.161	0.271
350.000	0.1200	0.526	25	0.54	1.00	2.00	2.00	0.327	0.186	0.129	0.230
400.000	0.1250	0.569	25	0.54	1.00	2.00	2.00	0.294	0.165	0.107	0.197
500.000	0.0850	0.474	25	0.54	1.00	2.00	2.00	0.387	0.195	0.109	0.371
600.000	0.0900	0.526	25	0.54	1.00	2.00	2.00	0.333	0.165	0.084	0.315
700.000	0.0950	0.569	25	0.54	1.00	2.00	2.00	0.292	0.144	0.067	0.268
800.000	0.0950	0.474	25	0.54	1.00	2.00	2.00	0.273	0.146	0.069	0.278
900.000	0.1000	0.526	25	0.54	1.00	2.00	2.00	0.245	0.128	0.056	0.242
1000.000	0.1050	0.569	25	0.54	1.00	2.00	2.00	0.221	0.114	0.047	0.209
1200.000	0.0212	0.474	25	0.54	1.00	2.00	2.00	1.001	0.203	0.049	4.818
1300.000	0.0361	0.526	25	0.54	1.00	2.00	2.00	0.565	0.160	0.041	1.668
1400.000	0.0446	0.569	25	0.54	1.00	2.00	2.00	0.440	0.138	0.035	1.073

Table D12: Sensitivity analysis results using higher resistivity (R_t - Assumed) values and log derived density porosity ($Ø_{D)}$ and FIB/SEM visualized porosity in Murteree Shale impact on derived water saturation

True Resistivity Rt (Ohmm)	Density Porosity Ø (Fraction)	Shale Volume-Steiber Formula (Fraction)	Shale Resistivity Rcl (Ohmm)	Brine Resistivity Rw (Ohmm)	a	m	n	Archie's Model Sw(Fraction)	Indonesian Model Sw(Fraction)	Simandoux Model Sw(Fraction)	Total Shale Model Sw (Schlumberger) (Fraction)
64.800	0.0212	0.474	25	0.54	1.00	2.00	2.00	4.306	0.875	0.878	5.529
67.560	0.0361	0.526	25	0.54	1.00	2.00	2.00	2.477	0.700	0.725	2.228
70.700	0.0446	0.569	25	0.54	1.00	2.00	2.00	1.960	0.612	0.628	1.545
10.000	0.0212	0.474	25	0.54	1.00	2.00	2.00	10.961	2.227	4.807	8.556
20.000	0.0361	0.526	25	0.54	1.00	2.00	2.00	4.552	1.287	2.107	3.233
40.000	0.0446	0.569	25	0.54	1.00	2.00	2.00	2.605	0.814	1.041	1.841
50.000	0.0850	0.474	25	0.54	1.00	2.00	2.00	1.223	0.618	0.748	0.828
60.000	0.0900	0.526	25	0.54	1.00	2.00	2.00	1.054	0.523	0.603	0.680
70.000	0.0950	0.569	25	0.54	1.00	2.00	2.00	0.925	0.455	0.501	0.569
80.000	0.0950	0.474	25	0.54	1.00	2.00	2.00	0.865	0.461	0.498	0.591
90.000	0.1000	0.526	25	0.54	1.00	2.00	2.00	0.775	0.404	0.421	0.502
100.000	0.1050	0.569	25	0.54	1.00	2.00	2.00	0.700	0.362	0.363	0.431
150.000	0.1050	0.474	25	0.54	1.00	2.00	2.00	0.571	0.319	0.293	0.400
200.000	0.1100	0.526	25	0.54	1.00	2.00	2.00	0.472	0.258	0.213	0.320
250.000	0.1150	0.569	25	0.54	1.00	2.00	2.00	0.404	0.218	0.165	0.264
300.000	0.1150	0.474	25	0.54	1.00	2.00	2.00	0.369	0.214	0.161	0.271
350.000	0.1200	0.526	25	0.54	1.00	2.00	2.00	0.327	0.186	0.129	0.230
400.000	0.1250	0.569	25	0.54	1.00	2.00	2.00	0.294	0.165	0.107	0.197

Table D13: Sensitivity analysis results using density porosity ($Ø_{D)}$ values and visualized FIB/SEM porosity in Murteree shale impact on Archie's models and other water saturation models

True Resistivity Rt (Ohmm)	Density Porosity Ø (Fraction)	Shale Volume-Steiber Formula (Fraction)	Shale Resistivity Rcl (Ohmm)	Brine Resistivity Rw (Ohmm)	a	m	n	Archie's Model Sw(Fraction)	Indonesian Model Sw(Fraction)	Simandoux Model Sw(Fraction)	Total Shale Model Sw (Schlumberger) (Fraction)
64.800	0.0212	0.474	25	0.54	1.00	2.00	2.00	4.306	0.875	0.878	5.529
67.560	0.0361	0.526	25	0.54	1.00	2.00	2.00	2.477	0.700	0.725	2.228
70.700	0.0446	0.569	25	0.54	1.00	2.00	2.00	1.960	0.612	0.628	1.545
64.800	0.0850	0.474	25	0.54	1.00	2.00	2.00	1.074	0.543	0.617	0.739
67.560	0.0900	0.526	25	0.54	1.00	2.00	2.00	0.993	0.492	0.551	0.646
70.700	0.0950	0.569	25	0.54	1.00	2.00	2.00	0.920	0.452	0.497	0.566
64.800	0.0950	0.474	25	0.54	1.00	2.00	2.00	0.961	0.512	0.583	0.649
67.560	0.1000	0.526	25	0.54	1.00	2.00	2.00	0.894	0.467	0.523	0.570
70.700	0.1050	0.569	25	0.54	1.00	2.00	2.00	0.832	0.430	0.475	0.502
64.800	0.1050	0.474	25	0.54	1.00	2.00	2.00	0.869	0.485	0.552	0.578
67.560	0.1100	0.526	25	0.54	1.00	2.00	2.00	0.813	0.444	0.498	0.510
70.700	0.1150	0.569	25	0.54	1.00	2.00	2.00	0.760	0.410	0.453	0.451
64.800	0.1150	0.474	25	0.54	1.00	2.00	2.00	0.794	0.461	0.523	0.521
67.560	0.1200	0.526	25	0.54	1.00	2.00	2.00	0.745	0.423	0.474	0.462
70.700	0.1250	0.569	25	0.54	1.00	2.00	2.00	0.699	0.392	0.434	0.410

Table D14: Observations Correlation – Archie, Indonesian, Simandoux and Total Shale Model Equations for Water saturation in Murteree Shale Project Well Della#4.

Calculations & Observations – Water Saturation Archie's Equation Application	True Resistivity Rt (Ohmm)	Density Porosity Ø (Fraction)	Shale Volume-Steiber Formula (Fraction)	Shale Resistivity Rcl (Ohmm)	Brine Resistivity Rw (Ohmm)	a	m	n	Archie's Model Sw (Fraction)	Indonesian Model Sw (Fraction)	Simandoux Model Sw (Fraction)	Total Shale Model (Schlum) (Fraction)
A) General Archie's Formula - Using log derived density porosity Ø (Avg. =0.0340) & a=1.00, m=2.00 and n=2.00	64.80	0.0212	0.474	25.00	0.54	1.00	2.00	2.00	4.306	0.875	0.878	5.529
	67.56	0.0361	0.526	25.00	0.54	1.00	2.00	2.00	2.477	0.700	0.725	2.228
	70.70	0.0446	0.569	25.00	0.54	1.00	2.00	2.00	1.960	0.612	0.628	1.545
B) Practical Average Archie's Equation - Using derived density porosity Ø (Avg. =0.0340) & a=0.62, m=2.15 and n=2.00 (Malcolm 1996)	64.80	0.0212	0.474	25.00	0.54	0.62	2.15	2.00	4.527	0.922	0.894	9.303
	67.56	0.0361	0.526	25.00	0.54	0.62	2.15	2.00	2.502	0.747	0.748	3.330
	70.70	0.0446	0.569	25.00	0.54	0.62	2.15	2.00	1.948	0.655	0.651	2.212
C) Practical Average Archie's Equation -FIB/SEM observed porosity Ø (Avg. =9.00%) & a=0.62; m=2.15 and n=2.00 (Malcolm 1996)	64.80	0.0850	0.474	25.00	0.54	0.62	2.15	2.00	1.017	0.594	0.671	0.924
	67.56	0.0900	0.526	25.00	0.54	0.62	2.15	2.00	0.937	0.536	0.596	0.805
	70.70	0.0950	0.569	25.00	0.54	0.62	2.15	2.00	0.864	0.492	0.535	0.703
D) Practical Average Archie's Equation -FIB/SEM observed porosity **Ø (Avg. =9.00%)** & a= 0.62, m=2.00 & n=2.00 & Avg Sw (Archie's Model) = 0.784 (Fraction)	64.80	0.0850	0.474	25.00	0.54	0.62	2.00	2.00	**0.846**	0.543	0.617	0.739
	67.56	0.0900	0.526	25.00	0.54	0.62	2.00	2.00	**0.782**	0.492	0.551	0.646
	70.70	0.0950	0.569	25.00	0.54	0.62	2.00	2.00	**0.724**	0.452	0.497	0.566
E) Practical Average Archie's Equation - FIB/SEM observed porosity **Ø (Avg. = 9 %)** & a= 1.00; m= 2.00 and n= 2.00 & Avg. Sw (Archie's Model) = 0.995 (Fraction)	64.80	0.0850	0.474	25.00	0.54	1.00	2.00	2.00	1.074	0.543	0.617	0.739
	67.56	0.0900	0.526	25.00	0.54	1.00	2.00	2.00	0.993	0.492	0.551	0.646
	70.70	0.0950	0.569	25.00	0.54	1.00	2.00	2.00	0.920	0.452	0.497	0.566
F) Practical Average Archie's Equation -FIB/SEM observed porosity **Ø (Avg. = 10.00)** & a= 1.00, m=2.00 and n=2.00 & Avg Sw (Archie's Model) = 0.895 (Fraction)	64.80	0.0950	0.474	25.00	0.54	1.00	2.00	2.00	0.961	0.512	0.583	0.649
	67.56	0.1000	0.526	25.00	0.54	1.00	2.00	2.00	0.894	0.467	0.523	0.570
	70.70	0.1050	0.569	25.00	0.54	1.00	2.00	2.00	0.832	0.430	0.475	0.502
G) Practical Average Archie's Equation -FIB/SEM observed porosity **Ø (Avg. = 11.00 %)** & a= 1.00, m=2.00 and n=2.00 & Avg Sw (Archie's Model) = 0.814 (Fraction)	64.80	0.1050	0.474	25.00	0.54	1.00	2.00	2.00	0.869	0.485	0.552	0.578
	67.56	0.1100	0.526	25.00	0.54	1.00	2.00	2.00	0.813	0.444	0.498	0.510
	70.70	0.1150	0.569	25.00	0.54	1.00	2.00	2.00	0.760	0.410	0.453	0.451

APPENDIX – E

Roseneath Shale Moomba#46 - Wireline Logs and Digital Data

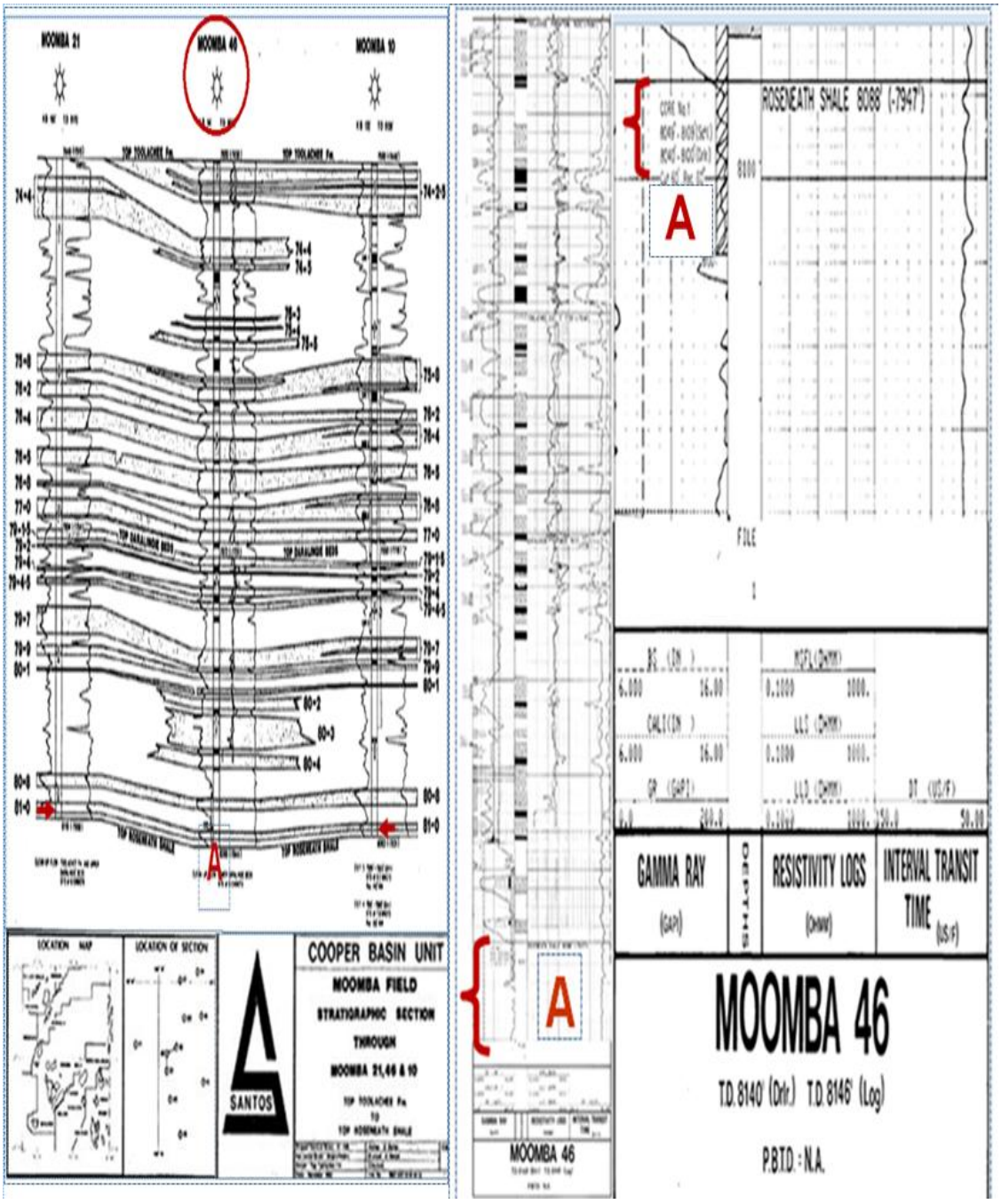

Figure E1 : Roseneath shale core samples and digital log core data depth location A; from Moomba#46 Composite Well Log (Source: Open File Envelope No. 4893; PPL 8 Well Completion Reports of Moomba#46 PIRSA South Australia).

Roseneath Shale Digital Data

Table E1 : Digital Data from Moomba#46

Depth ft.	Caliper in	Sonic Velocity DT µs/ft.	Gamma Ray GR API	Deep Laterolog LLD Ohm.m	Shallow Laterolog LLS Ohm.m	Spherically Focused Log SFL Ohm.m	Spontaneous Potential SP mvolts.
8088.00	-999.25	65.88	165.18	-999.25	-999.25	-999.25	-999.25
8088.50	-999.25	65.88	174.05	-999.25	-999.25	-999.25	-999.25
8089.00	-999.25	66.89	180.50	-999.25	-999.25	-999.25	-999.25
8089.50	-999.25	67.89	192.59	-999.25	-999.25	-999.25	-999.25
8090.00	-999.25	71.71	199.03	-999.25	-999.25	-999.25	-999.25
8090.50	-999.25	71.81	191.77	-999.25	-999.25	-999.25	-999.25
8091.00	-999.25	71.91	190.15	-999.25	-999.25	-999.25	-999.25
8091.50	-999.25	70.29	183.69	-999.25	-999.25	-999.25	-999.25
8092.00	-999.25	66.27	181.27	-999.25	-999.25	-999.25	-999.25
8092.50	-999.25	65.86	182.88	-999.25	-999.25	-999.25	-999.25
8093.00	-999.25	66.66	188.52	-999.25	-999.25	-999.25	-999.25
8093.50	-999.25	68.47	194.96	-999.25	-999.25	-999.25	-999.25
8094.00	-999.25	69.68	202.21	-999.25	-999.25	-999.25	-999.25
8094.50	-999.25	69.67	206.24	-999.25	-999.25	-999.25	-999.25
8095.00	-999.25	70.27	198.98	-999.25	-999.25	-999.25	-999.25
8095.50	-999.25	71.28	194.94	-999.25	-999.25	-999.25	-999.25
8096.00@	-999.25	71.28	179.61	-999.25	-999.25	-999.25	-999.25
8096.50@	-999.25	71.07	180.41	-999.25	-999.25	-999.25	-999.25
8097.00	-999.25	70.26	184.44	-999.25	-999.25	-999.25	-999.25
8097.50@	-999.25	69.05	195.73	-999.25	-999.25	-999.25	-999.25
8098.00	-999.25	68.45	199.75	-999.25	-999.25	-999.25	-999.25
8098.50	-999.25	68.54	199.75	-999.25	-999.25	-999.25	-999.25
8099.00	-999.25	68.64	193.29	-999.25	-999.25	-999.25	-999.25
8099.50	-999.25	69.04	192.48	-999.25	-999.25	-999.25	-999.25
8100.00	-999.25	69.44	199.73	-999.25	-999.25	-999.25	-999.25
8100.50	-999.25	69.64	198.92	-999.25	-999.25	-999.25	-999.25
8101.00	-999.25	69.54	190.85	-999.25	-999.25	-999.25	-999.25
8101.50	-999.25	69.44	186.81	-999.25	-999.25	-999.25	-999.25
8102.00	-999.25	70.04	189.23	-999.25	-999.25	-999.25	-999.25
8102.50	-999.25	69.63	191.64	-999.25	-999.25	-999.25	-999.25
8103.00	-999.25	68.82	186.79	-999.25	-999.25	-999.25	-999.25
8103.50	-999.25	68.42	187.60	-999.25	-999.25	-999.25	-999.25
8104.00	-999.25	68.01	196.46	-999.25	-999.25	-999.25	-999.25
8104.50	-999.25	67.81	195.65	-999.25	-999.25	-999.25	-999.25
8105.00	-999.25	65.19	194.84	-999.25	-999.25	-999.25	-999.25
8105.50	-999.25	62.97	197.25	-999.25	-999.25	-999.25	-999.25
8106.00	-999.25	62.57	194.02	-999.25	-999.25	-999.25	-999.25
8106.50	-999.25	62.77	198.05	-999.25	-999.25	-999.25	-999.25
8107.00	-999.25	68.20	196.43	-999.25	-999.25	-999.25	-999.25
8107.50	-999.25	71.42	193.20	-999.25	-999.25	-999.25	-999.25
8108.00	-999.25	72.02	189.16	-999.25	-999.25	-999.25	-999.25
8108.50	-999.25	72.21	182.71	-999.25	-999.25	-999.25	-999.25

Legend:	
8096.00ft @ 8096.50 ft.@ 8097.00ft @	Derived log based values Sonic Velocity & Gamma Ray from exact location of Roseneath Shale Core sample in Moomba#46 Project well

Roseneath Shale Digital Data

Table E2 : Digital Data from Moomba#46

Depth ft.	Caliper in	Sonic Velocity DT µs/ft.	Gamma Ray GR API	Deep Laterolog LLD Ohm.m	Shallow Laterolog LLS Ohm.m	Spherically Focused log SFL Ohm.m	Spontaneous Potential SP mvolts.
8109.00	-999.25	71.61	180.28	-999.25	-999.25	-999.25	-999.25
8109.50	-999.25	68.79	177.05	-999.25	-999.25	-999.25	-999.25
8110.00	-999.25	69.39	160.11	-999.25	-999.25	-999.25	-999.25
8110.50	-999.25	69.79	148.81	-999.25	-999.25	-999.25	-999.25
8111.00	-999.25	71.60	138.32	-999.25	-999.25	-999.25	-999.25
8111.50	-999.25	71.80	161.71	-999.25	-999.25	-999.25	-999.25
8112.00	-999.25	72.10	181.06	-999.25	-999.25	-999.25	-999.25
8112.50	-999.25	72.39	206.05	-999.25	-999.25	-999.25	-999.25
8113.00	-999.25	72.39	204.43	-999.25	-999.25	-999.25	-999.25
8113.50	-999.25	71.99	199.58	-999.25	-999.25	-999.25	-999.25
8114.00	-999.25	70.37	196.36	-999.25	-999.25	-999.25	-999.25
8114.50	-999.25	69.37	194.74	-999.25	-999.25	-999.25	-999.25
8115.00	-999.25	70.57	199.57	-999.25	-999.25	-999.25	-999.25
8115.50	-999.25	72.18	209.24	-999.25	-999.25	-999.25	-999.25
8116.00	-999.25	73.38	206.01	-999.25	-999.25	-999.25	-999.25
8116.50	-999.25	73.38	208.83	-999.25	-999.25	-999.25	-999.25
8117.00	-999.25	72.77	210.84	-999.25	-999.25	-999.25	-999.25
8117.50	-999.25	72.17	206.80	-999.25	-999.25	-999.25	-999.25
8118.00	-999.25	70.96	203.57	-999.25	-999.25	-999.25	-999.25
8118.50	-999.25	71.26	194.69	-999.25	-999.25	-999.25	-999.25
8119.00	-999.25	71.56	193.08	-999.25	-999.25	-999.25	-999.25
8119.50	-999.25	71.95	189.85	-999.25	-999.25	-999.25	-999.25
8120.00	-999.25	71.95	185.00	-999.25	-999.25	-999.25	-999.25
8120.50	-999.25	72.15	194.67	-999.25	-999.25	-999.25	-999.25
8121.00	-999.25	72.15	205.15	-999.25	-999.25	-999.25	-999.25
8121.50	-999.25	72.14	206.76	-999.25	-999.25	-999.25	-999.25
8122.00	-999.25	71.74	193.85	-999.25	-999.25	-999.25	-999.25
8122.50	-999.25	72.34	191.42	-999.25	-999.25	-999.25	-999.25
8123.00	-999.25	72.34	187.39	-999.25	-999.25	-999.25	-999.25
8123.50	-999.25	71.63	182.54	-999.25	-999.25	-999.25	-999.25
8124.00	-999.25	70.92	190.60	-999.25	-999.25	-999.25	-999.25
8124.50	-999.25	69.91	198.66	-999.25	-999.25	-999.25	-999.25
8125.00	-999.25	69.51	198.65	-999.25	-999.25	-999.25	-999.25
8125.50	-999.25	69.51	197.84	-999.25	-999.25	-999.25	-999.25
8126.00	-999.25	69.71	197.03	-999.25	-999.25	-999.25	-999.25
8126.50	-999.25	70.31	197.83	-999.25	-999.25	-999.25	-999.25
8127.00	-999.25	71.51	203.48	-999.25	-999.25	-999.25	-999.25
8127.50	-999.25	72.11	203.47	-999.25	-999.25	-999.25	-999.25
8128.00	-999.25	73.12	197.01	-999.25	-999.25	-999.25	-999.25
8128.50	-999.25	72.51	192.97	-999.25	-999.25	-999.25	-999.25
8129.00	-999.25	72.31	198.61	-999.25	-999.25	-999.25	-999.25

Roseneath Shale Digital Data

Table E2 : Digital Data from Moomba#46 (continued)

Depth ft.	Caliper in	Sonic Velocity DT µs/ft.	Gamma Ray GR API	Deep Laterolog LLD Ohm.m	Shallow Laterolog SLL Ohm.m	Spherically Focused log SFL Ohm.m	Spontaneous Potential SP mvolts.
8129.50	-999.25	72.60	196.19	-999.25	-999.25	-999.25	-999.25
8130.00	-999.25	72.50	193.76	-999.25	-999.25	-999.25	-999.25
8130.50	-999.25	72.70	197.79	-999.25	-999.25	-999.25	-999.25
8131.00	-999.25	72.50	196.98	-999.25	-999.25	-999.25	-999.25
8131.50	-999.25	72.29	192.14	-999.25	-999.25	-999.25	-999.25
8132.00	-999.25	71.89	196.16	-999.25	-999.25	-999.25	-999.25
8132.50	-999.25	71.58	208.25	-999.25	-999.25	-999.25	-999.25
8133.00	-999.25	71.28	207.44	-999.25	-999.25	-999.25	-999.25
8133.50	-999.25	71.48	198.57	-999.25	-999.25	-999.25	-999.25
8134.00	-999.25	71.47	195.33	-999.25	-999.25	-999.25	-999.25
8134.50	-999.25	71.47	191.30	-999.25	-999.25	-999.25	-999.25
8135.00	-999.25	71.67	191.29	-999.25	-999.25	-999.25	-999.25
8135.50	-999.25	71.87	188.86	-999.25	-999.25	-999.25	-999.25
8136.00	-999.25	71.86	184.83	-999.25	-999.25	-999.25	-999.25
8136.50	-999.25	71.76	183.21	-999.25	-999.25	-999.25	-999.25
8137.00	-999.25	71.66	186.03	-999.25	-999.25	-999.25	-999.25
8137.50	-999.25	71.59	186.42	-999.25	-999.25	-999.25	-999.25
8138.00	-999.25	71.52	184.80	-999.25	-999.25	-999.25	-999.25
8138.50	-999.25	71.45	181.57	-999.25	-999.25	-999.25	-999.25
8139.00	-999.25	71.45	177.54	-999.25	-999.25	-999.25	-999.25
8139.50	-999.25	71.44	179.15	-999.25	-999.25	-999.25	-999.25
8140.00	-999.25	71.44	185.19	-999.25	-999.25	-999.25	-999.25

APPENDIX – F

Murteree Shale Micro-XCT technique results from project well Della4

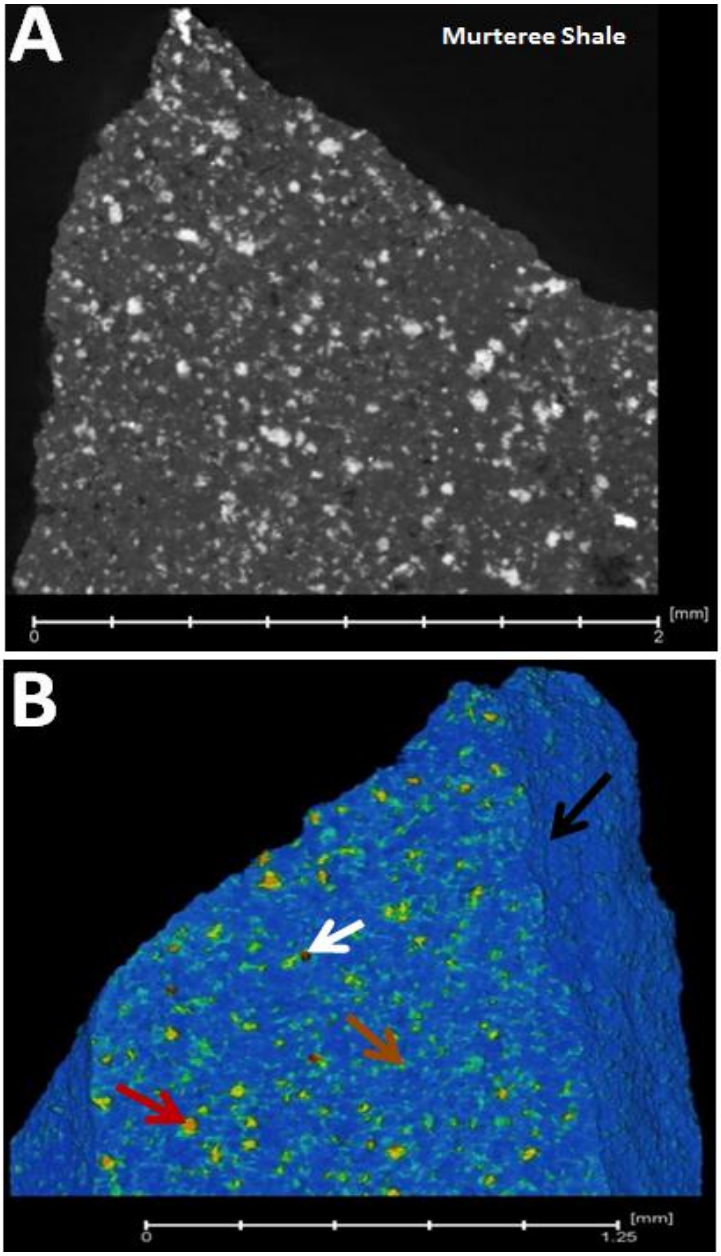

Figure F1: Grey scale image panel A, of virtual slice through Y-Z plane and panel B, volume render with cut–away in Y-Z plane of Murteree shale sample scanned using XCT facility at Ian Wark Research Institute University of South Australia. In panel B, to show the internal structure and features based on their density and atomic number, artificial colour were applied to identify different phases as labelled by arrows. A polychromatic source of x-rays rather monochromatic was used to get resolution less than 5 µ which did not work well to identify more than total 5 different phases in the microfocused XCT-analysis.

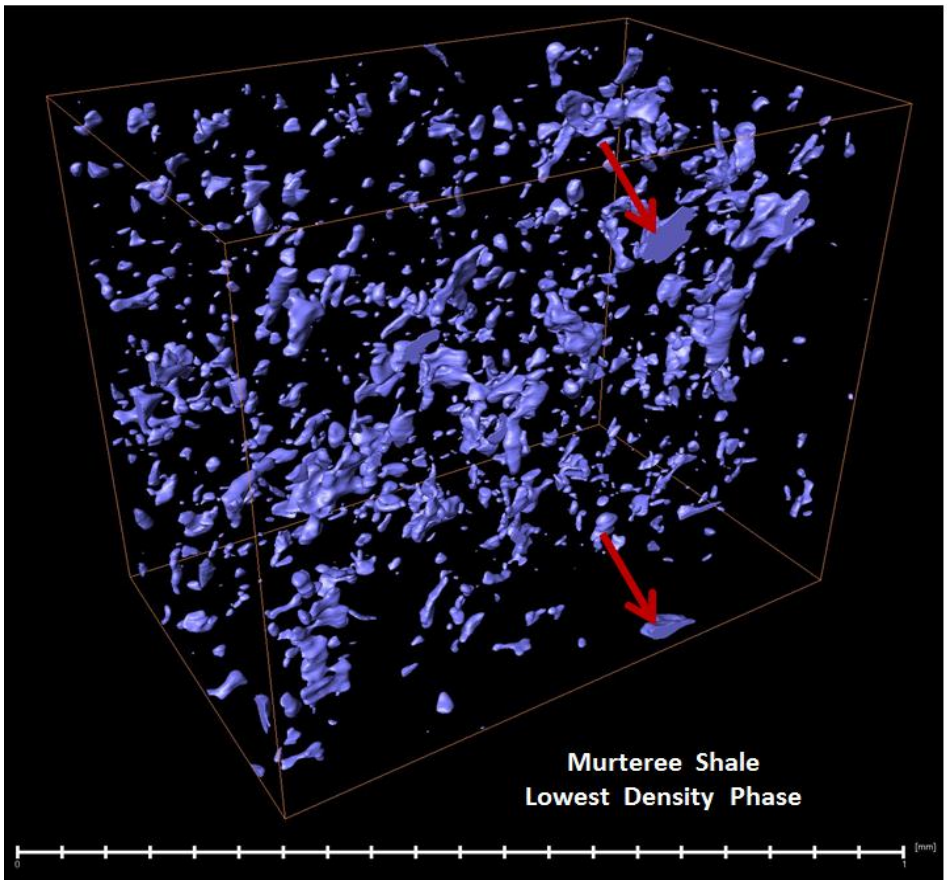

Figure F2: 3D model of Murteree Shale lowest density phase marked by red arrows, based on Micro XCT Data using Xradia Micro XCT-400 facility at Ian Wark Research Institute University of South Australia, Adelaide. The total lowest density phase contains pore volume, organic matter. The interconnectivity in this lowest density phases is much localized. Micro XCT or Nano-XCT was not capable to estimate total pore volume in carbonaceous shale gas reservoirs as observed in these results from Xradia Micro XCT-400 application.

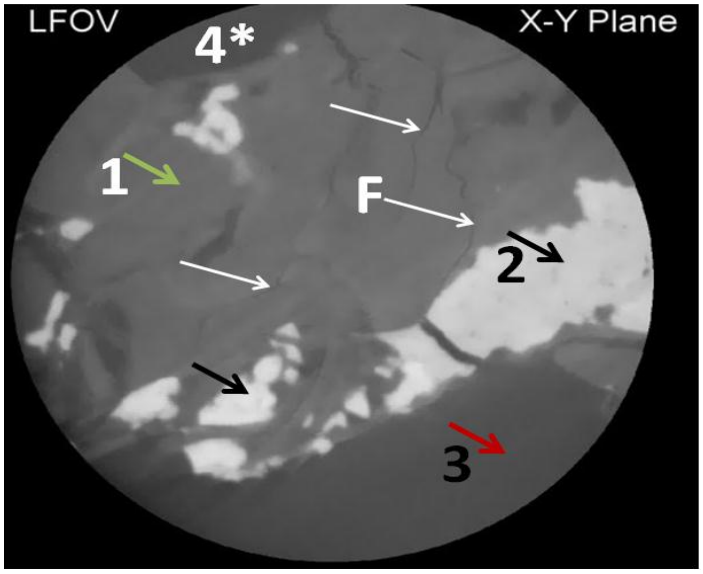

Figure F3: Murteree Shale sample scanned using microfocused computed tomography, Della4 project well, depth 6019.00-6020.00 ft. At resolution 5µm, maximum four mineral phases labelled as 1, 2, 3 and 4 are recognisable while at this resolution pores identification is not possible in this technique we applied to our samples. Microfracture system can be readily identified with some continuation in the samples labelled by white arrows and F. Heavy minerals like dull white, Siderite, very bright pyrite, rutile or sphalerite by white areas, green arrows quartz and silicates while area labelled with white asterisk could be organic matter.

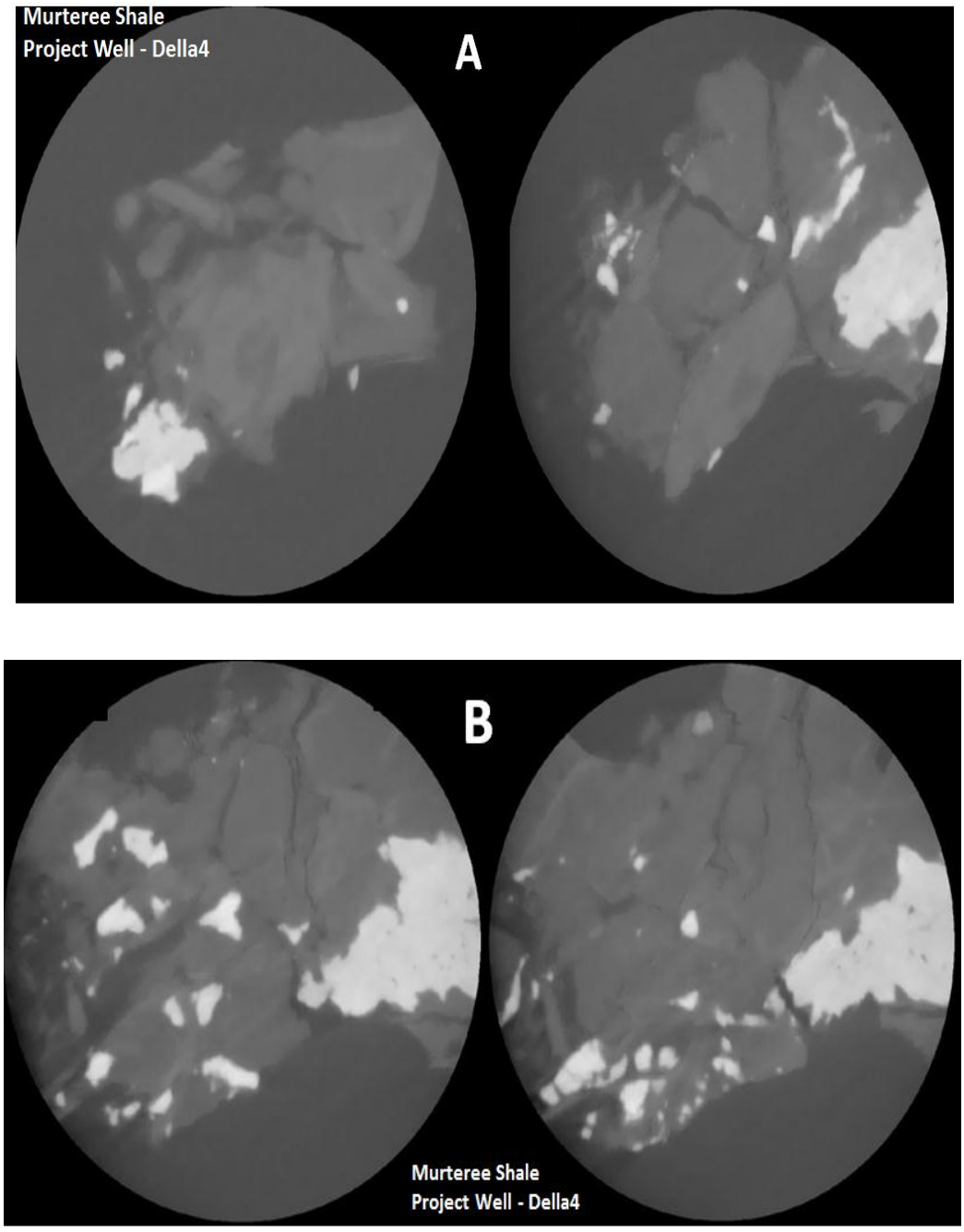

Figure F4: Two Murteree Shale samples, A and B, scanned using microfocused computed tomography xy slices, Della4 project well, depth 6019.00-6020.00 ft. At resolution 5µm as in figure F1, maximum four mineral phases recognisable and pores identification is not possible in this technique we applied. The arbitrary gray scale threshold for identification of a characteristic in the sample also has a role in CT-digital files and it varies from operator to operator. To identify the grains, pores, fracture system and its interconnectivity in organic mature shales we need submicron level resolution power which is not available in applied CT-scanning techniques.

APPENDIX – G

Murteree Shale QEMSCAN mineralogical and textural map from project well Della4

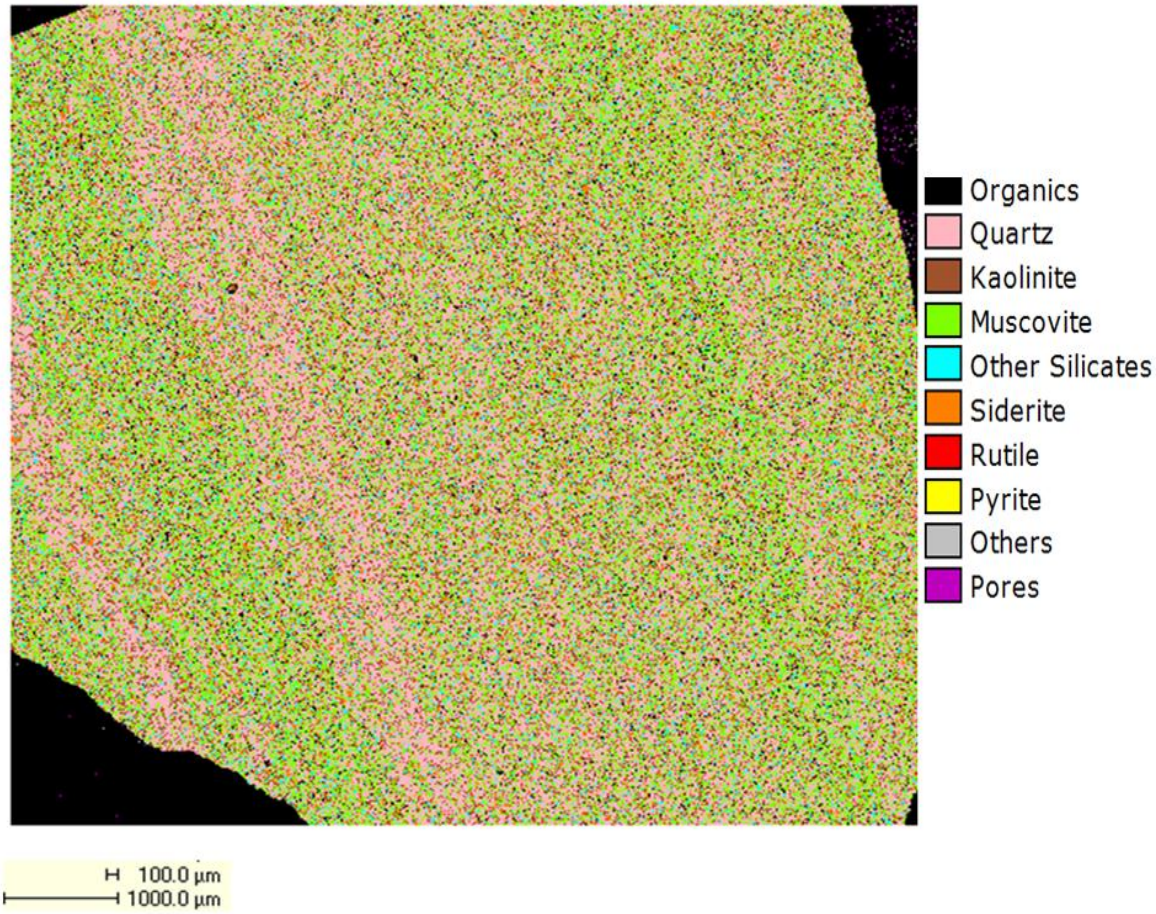

Figure G1: Murteree Shale – QEMSCAN false coloured mineralogical and textural map from project well Della4 depth 6019.00-6020.00 ft., Cooper Basin South Australia.

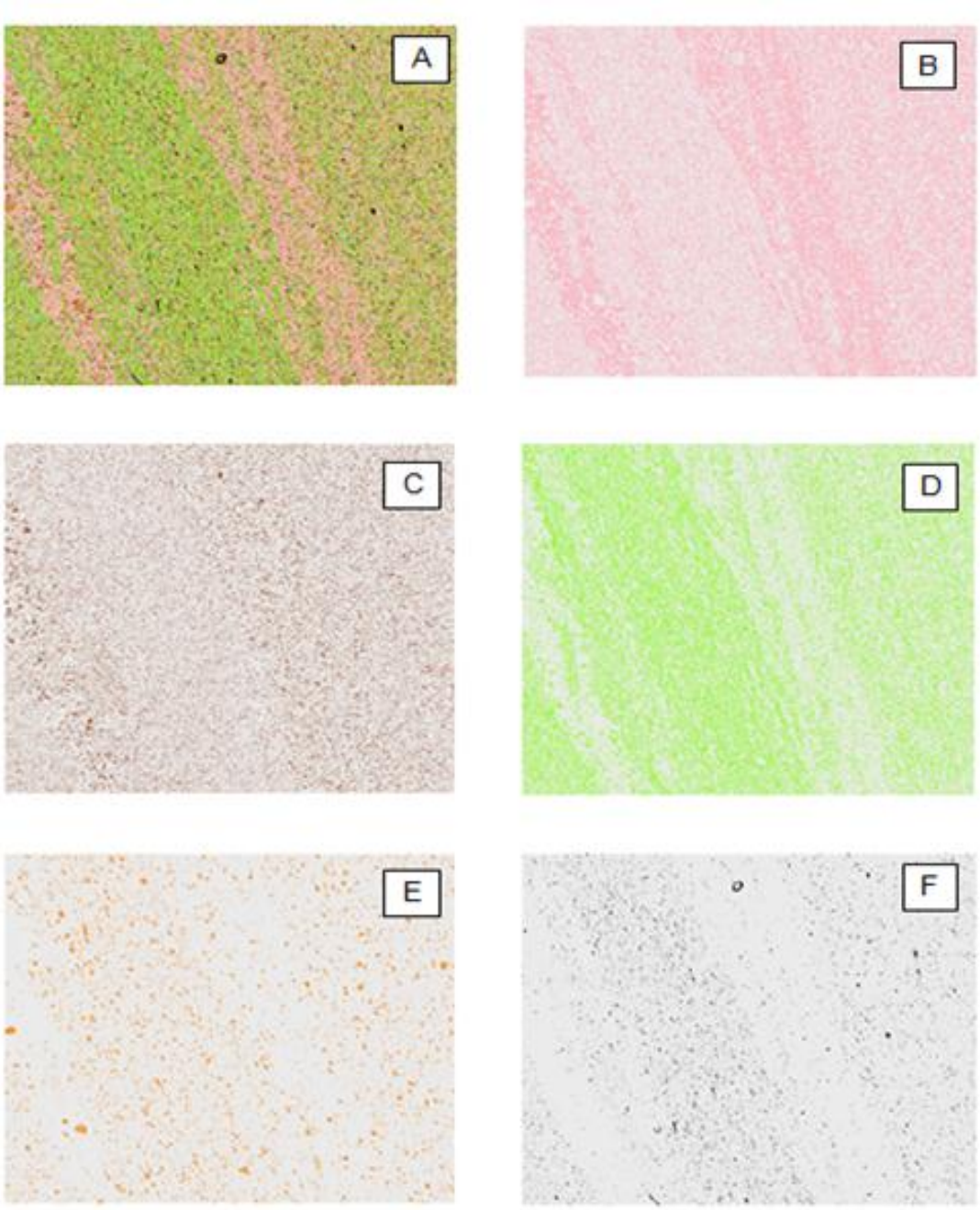

Figure G2: QEMSCAN images illustrating mineralogical and textural characteristics of all of the phases (A) found in the Murteree shale sample. Distribution of some phases was highlighted as follows: quartz (B), kaolinite (C), muscovite (D), siderite (E), organic matter (F).

REFERENCES

- Abad, Isabel (2007). "Physical Meaning and Applications of the illite Kübler Index: Measuring Reaction Progress in Low-grade Metamorphism." Diagenesis and Low-Temperature Metamorphism, Theory, Methods and Regional Aspects, Scenarios. Sociedad Espanola: Sociedad Espanola Mineralogia 53-64.
- Aguilera, R. (1978). “Log analysis of Gas-bearing Fracture Shales in the Saint Lawrence lowlands of Quebec.” In SPE Annual Fall Technical Conference and Exhibition.
- Aguilera, R. (2013). “Flow Units: From Conventional to Tight Gas to Shale Gas to Tight Oil to Shale Oil Reservoirs.” In SPE Western Regional & AAPG Pacific Section Meeting, 2013 Joint Technical Conference.
- Ahmad, M. and M. Haghighi (2012). “Mineralogy and Petrophysical Evaluation of Roseneath and Murteree Shale Formations, Cooper Basin, Australia Using QEMSCAN and CT-Scanning”. SPE Asia Pacific Oil and Gas Conference and Exhibition. Perth, Australia, Society of Petroleum Engineers.
- Ahmad, M., A. Alamar, R. Koo, H. Nguyen, M. Haghighi, (2012). “Evaluation of Free Porosity in Shale Gas Reservoirs (Roseneath and Murteree Formations Case Study)”, APPEA Journal 2012, Pages 603-610.
- Ambrose, R., Hartman, R., Diaz Campos, M., Akkutlu, I. Y., and Sondergeld, C. (2010). “New Pore-scale Considerations for Shale Gas in Place Calculations.” In SPE Unconventional Gas Conference.
- Amiri, M., Yunan, M. H., Zahedi, G., Jaafar, M. Z. and Oyinloye, E. (2012). "Introducing New Method to Improve Log Derived Saturation Estimation in Tight Shaly Sandstones-A Case Study from Mesaverde Tight Gas Reservoir." Journal of Petroleum Science and Engineering 92(93): 132-142.
- Archie (194). “The Electrical Resistivity Log as an Aid in Determining Some Reservoir Characteristics.” Trans. AIME 146, 54–62.
- Armitage, P. J., Worden, R. H., Faulkner, D. R., Aplin, A. C., Butcher, A. R., and Iliffe, J. (2010). “Diagenetic and Sedimentary Controls on Porosity in Lower Carboniferous Fine-Grained Lithologies, Krechba Field, Algeria: A Petrological Study of a Caprock to a Carbon Capture site.” Marine and Petroleum Geology, 27(7), 1395-1410.
- Asquith, G. B., D. Krygowski, and C.R. Gibson (2004). “Basic Well Log Analysis, American Association of Petroleum Geologists.”
- Baker, S. and P. J. Bare. (2011). “Australia Oil & Gas, Shale Gas, Grab a Surfboard, Research Report, Hong Kong, Morgan Stanley Asia/Pacific.”
- Barker, C. (1972). "Aquathermal Pressurizing: Role of Temperature in Development of Abnormal Pressure Zones,” Paper AAPG Bulletin, (October 1972), 65, (10), p. 2068-2071.

- Beer (1852). “Determination of the Absorption of Red Light in Colored Liquids.” Annalen der Physik und Chemie, vol. 86, pp. 78–88
- Bell, M. S. (2007). “Experimental Shock Decomposition of Siderite and the Origin of Magnetite in Martian Meteorite ALH 84001.” Meteoritics and Planetary Science, 42(6), 935-949.
- Bennett, R. H., Ransom, B., Kastner, M., Baerwald, R. J., Hulbert, M. H., Sawyer, W. B., and Lambert, M. W. (1999). “Early Diagenesis: Impact of Organic Matter on Mass Physical Properties and Processes, California continental margin. Marine Geology.” 159(1), 7-34.
- Bennett, R. H., O’Brien, N.R., and Hullbert, M.H. (1991) “Determinants of Clay Fabric Signature - Process and Mechanism.” In Bennet, R.H..Bryant, W.R < Hullbert, M.H., eds., Microstructure of Fine-Grained Sediments: New York, Springer-Verlag, p.-5-32.
- Bergenheier Lauren (2010). Australian Shale Gas: Permian of the Cooper, Bowen and Sydney Basins. Energy and Gas Institute.” The University of Utah USA.
- Boles R. James and Franks Stephen G. (1979) “Clay Diagenesis in Wilcox Sandstones of Southwest Texas-Implication of Smectite Diagenesis of Sandstones Cementation.” Journal of Sedimentology , Vol. 49, No.1 p 0055-0070
- Bolinger D. and Fink R. (1980). “A New Technique Ion Milling.” Solid Sate Technology November 1980.
- Boyce, M. L., and Carr, T. (2009). “Lithostratigraphy and Petrophysics of the Devonian Marcellus Interval in West Virginia and South-western Pennsylvania.”
- Bradshaw, Marita T., Irina Borissova, Dianne S Edwards, George M Gibson, Takehiko Hashimoto, Gabriel J Nelson, Nadege Rollet, Jennifer M Totterdell. (2007) “Out of Gondwana: Shaping a Nation-Geology of Australia.” Geoscience Australia.
- Breyer, J. A. (2012). “Shale Reservoirs, in J. A. Breyer, ed., Shale Reservoirs—Giant Resources for the 21st Century: AAPG Memoir 97”.
- Browning, I. B. (1935). “Relation of Structure to Shale Gas Accumulation: Devonian Shales.” A Symposium by the Appalachian Geological Society: Charleston. West Virginia, Appalachian Geological Society, 16-20.
- Bustin, R.M. And Bustin, A. M. M. (2008). “Impact of Shale Properties on Pore Structure and Storage Characteristics.” SPE Shale and Gas Production Conference, 16–18 November, Fort Worth, Texas, SPE 119892.
- Bustin M., Wust R., and Cui A. (2013). “Unconventional Tight Oil/Gas Plays: A Geological and Geomechanical Approach.” 2013 Trican Short Course and Core Workshop Lecture Notes. South Australia Adelaide, Nov. 7-8, 2013.
- Campbell Jr, R. L., and Truman, R. B. (1986). “Formation evaluation in the Devonian Shale.” Paper SPE, 15212, 18-21.
- Cane, R. F., 1976. Origin and formation of oil shale, in: Chilligarian, G. V. and Yen, T. F. (Eds.), Oil Shale. Elsevier, Amsterdam. 27-60.

- Castanier, L. M., and Reid, T. B. (1989). “An Introduction to Computerized X-Ray Tomography for Petroleum Research”. DOE.
- Centre, G. M. W. (2004). "Flow and Transport: Characterization and Modelling from Pore to Reservoir Scales."
- Chapman, D.R. (1975) “Shale Classification Tests and Systems: A comparative study.” Interim report phase 1. Joint highway research project, Purdue University School of Civil Engineering and Indiana Department of Highways Publication jhrp-75/11. Indiana: Purdue University and the Indiana State Highway Commission.
- Cheng, A. L. and Huang, W. L. (2004). “Selective Adsorption of Hydrocarbon Gases on Clays and Organic Matter.” Organic geochemistry, 35(4), 413-423.
- Clarkson, C. R., Jensen, J. L. and Blasingame, T. A. (2011). “Reservoir Engineering for Unconventional Gas Reservoirs: What Do We Have to Consider? In Paper SPE 145080 presented at SPE North American Unconventional Gas Conference and Exhibition held in The Woodlands, Texas (pp. 14-16).
- Clavier, C., Coates, G., and Dumanoir, J. (1984). “Theoretical and Experimental Bases for the Dual-Water Model for Interpretation of Shaly Sands.” Old SPE Journal, 24(2), 153-168.
- Coenen, J., Tchouparova, E., and Jing, X. (2004). “Measurement Parameters and Resolution Aspects of Micro X-Ray Tomography for Advanced Core Analysis.”
- Colin C.Ward and Paul G. Lennox (2007). “Petroleum Geology Geol9151.” Lecture Notres School of Biology Earth and Environmental Science. The University of New South Wales. Sydney NSW Australia.
- Curry, T.S. Dowedy, J.E., and Murry, R.C. (1990). “Christen’s Physics of Diagnostic Radiology, 4th Edition . Lea & Febiger, London, 522p.
- Curtis, M. E. C.H. Sondergeld, R.J. Ambrose and C.S. Rai (2012). “Microstructural Investigation of Gas Shales in Two and Three Dimensions Using Nanometre – Scale Resolution.” AAPG – Bulletin 96(4):665-677.
- Curtis, J. B. (2002). “Fractured Shale-Gas Systems”. AAPG bulletin, 86(11), 1921-1938.
- Curtis, M. E., Cardott, B. J., Sondergeld, C. H., and Rai, C. S. (2012). “Development of Organic Porosity in the Woodford Shale with Increasing Thermal Maturity.” International Journal of Coal Geology.
- Curtis, M., Ambrose, R., Sondergeld, C. and Rai, C. (2011). “Transmission and Scanning Electron Microscopy Investigation of Pore Connectivity of Gas Shales on the Nanoscale. In North American Unconventional Gas Conference and Exhibition.
- Curtis, M., Ambrose, R., Sondergeld, C., and Sondergeld, C. (2010). “Structural Characterization of Gas Shales on the Micro-and Nano-scales.” In Canadian Unconventional Resources and International Petroleum Conference.
- David L., Rolf Nüesch, and Janos L. (1995). “Consolidation of Water Saturated Shales at Great Depth under Drained Conditions.” 8th International Congress on Rock Mechanics, Tokyo, Japan, 25-29 September 1995.

- David H. and M. Garrick. (2011). “QEMSCAN Well Site: On-shore Field test in Papua New Guinea. Multiscale Imaging of Shale Samples in the Scanning Electron Microscope.” Application Note FEI fei-natural-resources.com.
- Davies, D., Bryabt, W.K., Vessell, R.K., and Burkett, P. J. (1991). “Porosities and Permeabilies, and Microfabrics of Devonian Shales.” In Bennett, R. H., Bryant, W.K., and Hullbert, M. H., eds., Microstructure of Fine Grain Sediments, From Mudstone to Shale, Springer-Verlag, New York, p.109-119.
- Decker, A. D., Hill, D. G., and Wicks, D. E. (1993). “Log-based Gas Content and Resource Estimates for the Antrim shale, Michigan Basin. In Low Permeability Reservoirs Symposium.”
- Department for Manufacturing, Innovation, Trade, Resources and Energy, Report by Energy Resources Division, Government of South Australia (2012). “Road Map for Unconventional Gas Projects in South Australia”
- Deshpande, V. P. (2008). “General Screening Criteria for Shale Gas Reservoirs and Production Data Analysis of Barnett Shale (Doctoral dissertation, Texas A&M University).”
- Diaz, Elizabeth. (2009). “Integration of DRP – Digital Rock Physics and Well Logging.” Ingrain Digital Rock Physics Lab
- Duane, W., and Hunt, F. L. (1913). American Physical Society. Physical Review.
- Duliu, G. O. (1999). “Computer Axial Tomography in Geosciences, An Overview.”
- Durand, B., (1980). “Kerogen, Insoluble Organic Matter from Sedimentary Rocks”. Paris, Editions Technip, 519 p.
- Dyrkacz, G. R. and Horwitz, E. P. (1982). “Separation of Coal Macerals.” Fuel 61(1), 3-12, 1982.
- Elgmati M., H. Zhang, B. Bai and F. Ralf, (2011) “Submicron Pore Chacterization of Shale Gas Plays.” SPE North American Unconventional Gas Conference and Exhibition held in The Woodlands, Texas, USA, 14-16 June 2011.
- Engler, W.Thomas. (2012). “Lecture notes for PET 370, Chapter 7 Gamma Ray Log.” Published by University of Oklahoma, USA.
- Eslinger, E., and R. V. Everett. (2012). “Extended abstract—Petrophysics in Gas Shales, in J. A. Breyer, ed., Shale Reservoirs—Giant Resources for the 21st Century: AAPG Memoir 97, p. 63– 68.
- Espitalie, J., Madec, M., Tissot, B., Mennig, J., and Leplat, P. (1977). “Source Rock Characterization Method for Petroleum Exploration.” In Offshore Technology Conference Houston, Texas
- Estupiñán Letamendi, J., Marfil Pérez, R., Delgado Huertas, A., and Permanyer I Bastardas, A. (2007). “The Impact of Carbonate Cements on the Reservoir Quality in the Napo Fm. Sandstones (Cretaceous Orient Basin, Ecuador). Geological Act, 5(1), 89.
- Fertl, W. H., and Hammack, G. W. (1971). A comparative look at water saturation computations in shaly pay sands. In Twelfth SPWLA Logging Symposium Transactions.

- Fertl, W. H. and Reik H.H. (1980). “Gamma Ray Spectral Evaluation Techniques Identify Fractured Shale Reservoirs and Source-Rock Characteristics.” Journal of Petroleum Technology, 32(11), 2053-2062.
- Fertl, W. H., and Chilingarian, G. V. (1990). “Hydrocarbon Resource Evaluation in the Woodford Shale Using Well Logs.” Journal of Petroleum Science and Engineering, 4 (1990) 347-357.
- Fertl, W. H., and Hammack, G. W. (1990). “Type and Distribution Modes of Clay Minerals from Well Logging Data.” Journal of Petroleum Science and Engineering, 3(1990) 321-332.
- Fisher, Q. J., Raiswell, R., & Marshall, J. D. (1998). Siderite concretions from nonmarine shales (Westphalian A) of the Pennines, England: Controls on their growth and composition. *Journal of Sedimentary Research*, *68*(5).
- Fishman, N. S., Hackley, P. C., Lowers, H. A., Hill, R. J., Egenhoff, S. O., Eberl, D. D. and Blum, A. E. (2012). “The Nature of Porosity in Organic-Rich Mudstones of the Upper Jurassic Kimmeridge Clay Formation, North Sea, offshore United Kingdom.” International Journal of Coal Geology.
- Fitts, T. G., and L. L. Summa. (2002). "The Relationship of the Smectite-illite Conversion to Pore Water Salinity Trends, Deep Water Offshore Niger Delta." In AGU Fall Meeting Abstracts, vol. 1, p. 0801. 2002.
- Foscolos, A. E. (1990). "Catagenesis of Argillaceous Sedimentary Rocks." Diagenesis: Ottawa, Geoscience Canada, Reprinted Series 4 (1990): 177-187.
- Foster, J.M. (1975) “A New Gas Supply.” The Devonian Shales, SPE 5451, Eastern Regional Meeting of SPE of AIME, Charleston, WVA, NOV. 6-7
- French, D., Ward, C.R. And Butcher, A. (2008). “QEMSCAN for Characterisation of Coal and Coal Utilisation by-Products.” Cooperative Research Centre for Coal in Sustainable Development Report 93. Pullenvale, Queensland: QCAT Technology Centre. Accessed 26 November 2011.
  <http://www.ccsd.biz/publications/files/rr/rr93qemscanforcharcoal_web.pdf>
- Gault, B. and Stotts, G. (2007). “Improve Shale Gas Production Forecast: Assessing the Potential of Shale Gas Resources Requires an Understanding of the Shale Properties.” Fekete Associates inc. Technical Paper. Houston: Hart Energy Publishing.
- Gelb, J., Gu, A., Fong, T. Hunter, L., Lau, SH, and Yun W. (2011). “A Closer Look at Shale, Representative Elementary Volume Analysis with Laboratory 3D X-Ray Computed Microtomography And Nanotomography”.
- Ghous, A., Knackstedt, M., Arns. C. H., Sheppard, A., Kumar, M., Sok, R., and Pinczewski, W. (2008). “3D Imaging of Reservoir Core at Multiple Scales; Correlations to Petrophysical Properties and Pore Scale Fluid Distributions.” In International Petroleum Technology Conference.

- Glorioso, J.C. and A.J. Rattia (2012). “Unconventional Reservoirs: Basic Petrophysical Concepts for Shale Gas.” SPE/EAGE European Unconventional Resources Conference and Exhibition. Vienna, Austria, Society of Petroleum Engineers.
- Gravestock, D. I., Alexander, E. M., Morton, J. G. G. and Sun, X. (1998). “Reservoirs & Seals.”
- Gravestock, D. I., Hibburt, J.E. and Drexel, J.F. (Eds), (1988). “The Petroleum Geology of South Australia.” D. O. P. I. A. Resources, Adelaide, Department of Primary Industries and Resources volume, 4..
- Gravestock, D. I., Hibburt, J.E. and Drexel, J.F. (Eds), (1988). “The Petroleum Geology of South Australia.” D. O. P. I. A. Resources, Adelaide, Department of Primary Industries and Resources volume, 4, 1988.
- Gravestock, D.I., Hibburt, J.E. And Drexel, J.F. (1998). “The Petroleum Geology of South Australia”. Volume 4: Cooper Basin, 1st edition. Report book 98/9. Adelaide: Primary Industries and Resources South Australia.
- Green C. (2012) “Shale Gas Background Note.” Department of Energy & Climate Change Government of UK. https://www.gov.uk/government/uploads/system/uploads/attachment_data/file/48332/5057-background-note-on-shale-gas-and-hydraulic-fractur.pdf (site visited on 28/07/2013).
- Guidry, F. K, Luffel, D. L., and Olszewski, A.J. (1996). "Devonian Shale Formation Evaluation Model Based on Logs, New Core Analysis Methods, and Production Tests." SPE REPRINT SERIES: 101-120.
- Haghighi, M., Bagheri, A. M., and Namani, M. (2008). “Investigation of Cementation Factor in Iranian Carbonate Reservoirs.” In Formation Evaluation Symposium of Japan (14th: 2008: Chiba, Japan).
- Halliburton (USA) (2008). “Shale Gas Report.” An Unconventional Resource - Unconventional Challenges www.halliburton.com, 2008.
- Handwerger, D.A., Keller, J., Vaughn, K., and Keller, J. (2011). “Improved Petrophysical Core Measurements on Tight Shale Reservoirs Using Retort and Crushed Samples.” In SPE Annual Technical Conference and Exhibition.
- Hartman, R. C., Lasswell, P., and Bhatta, N. (2008). “Recent Advances in the Analytical Methods Used for Shale Gas Reservoir Gas-in-Place Assessment.” In San Antonio, Texas: AAPG Annual Convention.
- Hartman, R.C., Bhatta, N. and Lasswell, P. (2008). “Recent Advances in the Analytical Methods Used for Shale Gas Reservoir Gas-in-Place Assessment. AAPG 2008 Annual Convention and Exhibition, 20–23 April, San Antonio, Texas.
- Herman, L., Butcher, A., and Botha, P.W.S.K. (2010) “FIB/SEM and Automated Mineralogy for Core and Cuttings Analysis.” SPE Russian Oil and Gas Conference and Exhibition. Moscow, Russia, Society of etroleum Engineers.
- Hilchie W.H. (1978). “Applied Open Hole Log Interpretation.” D.W. Hilchie , Golden, Co.

- Hill, A.J. and Gravestock, D.I., (1995).”Cooper Basin. In, Drexel, J.F. and Preiss, W.V. (eds.), The Geology of South Australia. Vol. 2, The Phanerozoic. South Australian Geological Survey Bulletin, 54, 78–87
- Hill D.G., and C.R. Nelson. (2002). “Gas Productive Fractured Shales-An Overview and Update: Gas TIPS.” V. 6, No. 2, P. 4-13.
- Hill, H.J., O.J. Shirley and G.E. Klein. (1979). Bound Water in Shaly Sand: Its Relation to Qv and Other Formation Properties, in M.H. Waxman and E.C. Thomas, eds., The Log Analyst, V. 20, no. 3, p. 3-19
- Horseman, S. T., J. J. W. Higgo, J. Alexander, and J. F. Harrington. (1996). "Water, Gas and Solute Movement Through Argillaceous Media." Nuclear Energy Agency Rep. CC-96/1. OECD, Paris.
- Houben, M. E., Desbois, G., and Urai, J. L. (2013). “Pore morphology and Distribution in the Shaly Facies of Opalinus Clay (Mont Terri, Switzerland): Insights from Representative 2D BIB–SEM Investigations on mm to nm Scale.” Applied Clay Science, 71, 82-97.
- Howard, J. J. (1991). Porosimetry Measurement of Shale Fabric and its Relationship to illite/smectite Diagenesis. Clays and Clay Minerals, 39(4), 355-361.
- Hunnur, A. T. (2006). “Smectite to illite Transformation: Relevence to Pore Pressure in the Subsurface (Doctoral Dissertation, University of Oklahoma).”
- Hunt J.M. (1996). “Petroleum Geochemistry and Geology.” W.H. Freeman and Company , New York, P.743
- Hutton, A. C., Bharati, S., and Roble, T. (1994). “Chemical and Petrographic Classification of Kerogen/Macerals.” Energy & fuels, 8(6), 1478-1488.
- Hutton, A. C. (1987). “Petrographic Classification of Oil Shales.” International Journal of Coal Geology, 8(3), 203-231.
- Ipek, G. (2002). “Log-Derived Cation Exchange Capacity of Shaly Sands: Application to Hydrocarbon Detection and Drilling Optimization.” Faculty of the Louisiana State University and Agricultural and Mechanical College in Partial Fulfilment of the Requirements for the Degree of Doctor of Philosophy in The Department of Petroleum Engineering by Gamze Ipek MS, Louisiana State University.
- Jacobi, D., Gladkikh, M., LeCompte, B., Hursan, G., Mendez, F., Longo, J. and Shoemaker, P. (2008). “Integrated Petrophysical Evaluation of Shale Gas Reservoirs.” In CIPC/SPE Gas Technology Symposium 2008 Joint Conference.
- Jacobi, D., Breig, J., LeCompte, B. and Kopal, M. (2009). “Effective Geochemical and Geomechanical Characterization of Shale Gas Reservoirs from the Wellbore Environment: Caney and the Woodford Shale.” SPE Annual Technical Conference and Exhibition.
- Gelb, J., Gu, A., Fong, T., Hunter, L., Lau, S. H., and Yun, W. (2011). “A Closer Look at Shale: Representative Elementary Volume Analysis with Laboratory 3D X-Ray Computed Microtomography and Nanotomography.” SCA2011-58.

- Javadpour, F. (2009). “Nanopores and Apparent Permeability of Gas Flow in Mudrocks (Shales and Siltstone).” Journal of Canadian Petroleum Technology, 48(8), 16-21.
- Josh, M., Esteban, L., Delle Piane, C., Sarout, J., Dewhurst, D.N., Clennell, M.B., (2012). “Laboratory Characterisation of Shale Properties.” Journal of Petroleum Science and Engineering.” DOI: 10.1016/j.petrol.
- Kale, S., Rai, C., and Sondergeld, C. (2010). “Petrophysical Characterization of Barnett shale.” In SPE Unconventional Gas Conference.
- Kamel, M. H. and W. M. Mabrouk. (2003). "Estimation of Shale Volume Using a Combination of the Three Porosity Logs." Journal of Petroleum Science and Engineering 40(3): 145-157.
- Kamel, M., Bayoumi, A. I. and Ibrahim H. (2001). "Formation Factor Parameters From Acoustic Logs: A Novel Approach"
- Kanitpanyacharoen, W., Parkinson, D. Y., De Carlo, F., Marone, F., Stampanoni, M., Mokso, R., & Wenk, H. R. (2012). “A Comparative Study of X-ray Tomographic microscopy on Shales at Different Synchrotron Facilities: ALS, APS and SLS. Journal of Synchrotron Radiation, 20(1), 0-0.”
- Kanitpanyacharoen, W., Wenk, H. R., Kets, F., Lehr, C., and Wirth, R. (2011). “Texture and Anisotropy Analysis of Qusaiba shales.” Geophysical Prospecting, 59(3), 536-556.
- Katahara, K. (2008). "What is Shale to a Petrophysicist?" The Leading Edge 27(6): 738-741.
- Katsube, T. J., Williamson, M., and Best, M. E. (1992). “Shale Pore Structure Evolution and its Effect on Permeability.” In Thirty-third Annual Symposium of the Society of Professional Well Log Analysts (SPWLA), Symposium (Vol. 3, pp. 1-22).
- Kawata, Y. and Fujita, K. (2001). “Some Predictions of Possible Unconventional Hydrocarbons Availability Until 2100”. Paper SPE, 68755.
- Ketcham, R. A., and Carlson, W. D. (2001). “Acquisition, Optimization and Interpretation of X-Ray Computed Tomographic Imagery: Applications to the Geosciences.” Computers & Geosciences, 27(4), 381-400.
- Kevin McCarthy, Kathrine Rojas, Martin Niemann, Daniel Palmowski, Kenneth Peters and Artur Stankiewicz. (2011). “Basic Petroleum Geochemistry for Source Rock Evaluation. “ Oilfield Review Summer 23, no. 2 Schlumberger.
- Killops, Stephen D., and Vanessa J. Killops. (2009). “Introduction to Organic Geochemistry.” Wiley. Com.
- Khaksar, A. (1994). “Techniques for Improving the Petrophysical Evaluation of the Patchawarra Formation in the Toolachee Field, Cooper Basin, South Australia.” University of Adelaide. National Centre for Petroleum Geology and Geophysics. M.Sc. Thesis.
- Khaksar, A. and Griffiths C.M., (1996). “Influence of Effective Stress on the Acoustic Velocity and Log Derived Porosity.” In: SPE Asia Pacific Oil and Gas Conference,

Adelaide, 1996. Proceedings. Society of Petroleum Engineers, pp.173-181. (SPE Paper 36981)

- Khaksar A and C. Griffiths. (1999). "Influence of Effective Stress on the Acoustic Velocity and Log-Derived Porosity." SPE Reservoir Evaluation & Engineering 2(1): 69-75.
- Knackstedt, M. A., Jaime, P., Butcher, A., Botha, P., Middleton, J., and Sok Rob. (2010). "Integrating Reservoir Characterization, 3D Dynamic, Petrophysical and Geological Description of Reservoir Facies." SPE Asia Pacific Oil and Gas Conference and Exhibition, Brisbane, Queensland, Australia, Society of Petroleum Engineers, 2010.
- Komar, C.A. (1976) "ERDA Research in Fracturing Technology." SPE Paper 6363, Eastern Region, Columbus, Ohio.
- Kundert, D. and Mullen, M., (2009) "Proper Evaluation of Shale Gas Reservoirs Leads to More Effective Hydraulic - Fracture Stimulation." SPE 123586, Presented at 2009 SPE Rocky Mountain Petroleum Technology Conference, Denver, Colorado, 14-16 April.
- Kuuskraa, V., Scott S, Tyler V. L. and Keith M. (2011). "World Shale Gas Resources: An Initial Assessment of 14 Regions Outside the United States, Energy Information Administration."
- Lafferty, R. C. (1935). "Occurrence of Gas in the Devonian shale." In Devonian Shales: A Symposium by Appalachian Geological Society: Charleston, West Virginia, Appalachian Geological Society (Vol. 1, pp. 14-15).
- Lancaster, D. E., McKetta, S. F., Hill, R. E., Guidry, F. K., and Jochen, J. E. (1992). "Reservoir Evaluation, Completion Techniques, and Recent Results from Barnett Shale development in the Fort Worth Basin". In SPE Annual Technical Conference and Exhibition.
- Lewis R. ,G. Baker and A. Suyanto (2010). "Gas Reserves Development in Eastern Australia – Projections Prepared for the GSOO." Report to AEMO by McLennan Megasanik Associates. www.mmassociates.com.au
- Lemmens, H.J. (2011). "Multiscale Imaging of Shale Samples in the Scanning Electron Microscope." Application Note FEI fei-natural-resources.com
- Lemmens, H., and Butcher, A. (2011). "A Workflow Concept To Characterize Core Samples From The Microscale to The Nanoscale." In SPE Annual Technical Conference and Exhibition.
- Lemmens, H. J., Butcher, A. R., and Botha, P. W. S. K. (2011). "FIB/SEM and SEM/EDX: A New Dawn for the SEM in the Core Lab?" Petrophysics-SPWLA-Journal of Formation Evaluation and Reservoir Description, 52(6), 452.
- Lemmens, H., Butcher, A., richards, D., Laughrey, C., & Dixon, M. (2011). "Imaging Techniques for 2D and 3D Characterization of Unconventional Reservoirs Core and Cuttings Samples-and How To Integrate Them." In North American Unconventional Gas Conference and Exhibition.

- Lewis, R., Ingraham, D., Pearcy, M., Williamson, J., Sawyer, W., and Frantz, J. (2004). “New Evaluation Techniques for Gas Shale Reservoirs.” In Reservoir Symposium, Schlumberger USA
- Lindsay, J. F. (2000). “Source Rock Potential and Algal-Matter Abundance, Cooper Basin.” South Australia. PIRSA Report Book, 32.
- Liu, G., Diaz, E., Grader, A., Armbruster, M., and Nur, A. (2009) “Digital Rock Physics for Oil Sands and Gas Shales.” Canadian Well Logging Society Journal, 2009.
- Liu, Y., Gupta, R., Sharma, A., Wall, T., Butcher, A., Miller, G., Gottlieb, P., and French, D. (2005). “Mineral Matter–Organic Matter Association Characterisation by QEMSCAN and Applications in Coal Utilisation.” Fuel 84(10) 1259-1267, 2005.
- Long, H., Swennen, R., Foubert, A., Dierick, M., and Jacobs, Patrick.(2009). “3D Quantification of Mineral Components and Porosity Distribution in Westphalian C Sandstone by Microfocus X-Ray Computed Tomography.” Journal of Sedimentology Volume 220, 116-125, 2009.
- Loucks, R. G., Reed, R. M. and Ruppel, S.C. (2012). "Spectrum of Pore Types and Networks in Mudrocks and a Descriptive Classification for Matrix-Related Mudrock Pores." AAPG Bulletin 96(6): 1071-1098.
- Loucks, R. G., Reed, R. M., Ruppel, S. C., and Jarvie, D. M. (2009). “Morphology, Genesis, and Distribution of Nanometre-scale Pores in Siliceous Mudstones of the Mississippian Barnett Shale.” Journal of Sedimentary Research, 79(12), 848-861.
- Loucks, R. G., Reed, R. M., Ruppel, S. C., and Hammes, U. (2010). “Preliminary classification of Matrix Pores in Mudrocks.” Gulf Coast Association of Geological Societies Transactions, 60, 435-441.
- Lu, X. C., Pepin, G. P., Moss, R. M., & Watson, A. T. (1992). “Determination of Gas Storage in Devonian Shales With X-ray-Computed Tomography.” In SPE Annual Technical Conference and Exhibition.
- Luffel, D. L., & Guidry, F. K. (1989). “Reservoir Rock Properties of Devonian Shale from Core and Log Analysis.” In Society of Core Analysts Conference.
- Luffel, D. L. and F. K. Guidry (1992). "New Core Analysis Methods for Measuring Reservoir Rock Properties of Devonian Shale." Journal of Petroleum Technology 44(11): 1184-1190.
- Luffel, D.l., Guidry, F. K. And Curtis, J.B. (1992). “Evaluation of Devonian Shale with New Core and Log Analysis Methods.” In: journal of Petroleum Technology, 44 (11), 1192–97. SPE 21297.
- Lui, Y., Gupta, R., and Wall, T.F., (2007) “A Comparison of CCSEM and QEMSCAN Analysis of Pulverized Coal, QCAT Technology Transfer Centre, 2007.”
- Mackie, S.I. (1987). “Cooper/Eromanga Basins Hydrocarbon Potential.” In: Oil and Gas Journal, 85 (45), 90–2.
- Magoon, L.B., and Dow, W.G. (1994). “The Petroleum System, in: Magoon, L. B., Dow, W. G. (Eds.), The Petroleum System - from source to trap. AAPG Memoir 60, 3-24.

- Miller, M., and Shanley, K. (2010). “Petrophysics in Tight Gas Reservoirs—Key Challenges Still Remain.” The Leading Edge, 29(12), 1464-1469.
- Milliken, Kitty L, Mark Rudnicki, David N., Awwiller, and Tongwei Zhang. (2013). “Organic Matter -Hosted Pore System Marcellus Formation (Devonian), Pennsylvania.” AAPG Bulletin, V.97, No.2 PP.177-200.
- Milner, M., and Shanley, K. (2010). “Petrophysics in Tight Gas Reservoirs—Key Challenges Still Remain.” The Leading Edge, 29(12), 1464-1469.
- Milner, M., McLin, R., and Petriello, J. (2010). “Imaging Texture and Porosity in Mudstones and Shales: Comparison of Secondary and Ion-Milled Backscatter SEM Methods.” In Canadian Unconventional Resources and International Petroleum Conference.
- Mitterer, R. M., and Cunningham Jr, R. (1985). “The Interaction of Natural Organic Matter with Grain Surfaces: Implications for Calcium Carbonate Precipitation”.
- Montgomery, S. L., Jarvie, D. M., Bowker, K. A., and Pollastro, R. M. (2005). “Mississippian Barnett Shale, Fort Worth basin, north-central Texas: Gas-Shale Play with Multi–Trillion Cubic Foot Potential.” AAPG bulletin, 89(2), 155-175.
- Moseby, G., (2010). “Cooper Basin Shale Gas. (2010). “IIR-2010-Shale Gas Briefing, Brisbane, 30 March 2010.” Adelaide: Beach Energy Limited.
- Knackstedt, M. A., Jaime, P., Butcher, A., Botha, P., Middleton, J., and Sok, R. (2010). “Integrating Reservoir Characterization: 3D Dynamic Petrophysical and Geological Description of Reservoir Facies.” In *SPE Asia Pacific Oil and Gas Conference and Exhibition*. Society of Petroleum Engineers.
- Nelson, Philip H. (2009). "Pore-Throat Sizes in Sandstones, Tight Sandstones, and Shales." AAPG Bulletin 93.3 (2009): 329-340.
- North, F. K. (1985). “Petroleum Geology”. Boston: Allen & Unwin.
- Oslon, K.R. and Grigg M.W. (2008). “Mercury Injection Capillary Pressure (MICP) A Useful Tool for Improved Understanding of Porosity and Matrix Permeability Distribution in Shale Reservoirs. Search and Discovery Article 40322.” Tulsa: Search and Discovery.
- Passey, Q. S., Creaney S., Kulla J.B. and Moretti F.J. (1990). "A Practical Model for Organic Richness from Porosity and Resistivity Logs." AAPG Bulletin 74(12): 1777-1794.
- Passey, Q.R., K. M., Bohacs, W.L. Esch, R. Klimentidis and S. Sinha. (2010). “From Oil-Prone Source Rock to Gas-Producing Shale Reservoir-Geologic and Petrophysical Characterization of Unconventional Shale Gas Reservoirs.” International Oil and Gas Conference and Exhibition in China.
- Pearce M.A., E. T. Nicholas, M. H. Robert and James S.C. (2013). “Reaction Mechanism for the Replacement of Calcite by Dolomite and Siderite: Implications for Geochemistry, Microstructure and Porosity Evolution during Hydrothermal Mineralization.” Contrib Mineral Petrol (2013) 166:995-1009.
- Peebles, M.W. H., (1980). “Evolution of the Gas Industry: New York, New York University Press, 235.

- Peng Wu and Roberto Aguilera, (2012). “Investigation of Gas Shales at Nanoscale Using Scan Electron Microscopy, Transmission Electron Microscopy and Atomic Force Microscopy.
- Peters, E. J. (2004). “Petrophysics: Department of Petroleum and Geosystems Engineering. The Text Note of the University of Texas at Austin.”
- Peters, K. E., and Cassa, M. R. (1994). “Applied Source Rock Geochemistry.” Memoirs-American Association of Petroleum Geologists, 93-93.
- Petricola, M., Hitoshi, T., and Shageaki A. (2002). “Saturation Evaluation in Micritic Reservoirs: Rising to the Challenge”. Abu Dhabi International Petroleum Exhibition and Conference.
- Pirson, S. J. (1963). "Handbook of Well Log Analysis for Oil and Gas Formation Evaluation."
- Planck, M. (1901). “On the law of distribution of energy in the normal spectrum.” Annalen der Physik, 4(553), 1.
- Popielski, A. C., Z. Heidari, and Torresverdine C. (2012). “Rock Classification from Conventional Well Logs in Hydrocarbon-Bearing Shale.” SPE Annual Technical Conference and Exhibition. San Antonio, Texas, USA, Society of Petroleum Engineers.
- Popielski, Andrew Christopher. (2012). "Rock Classification from Conventional Well Logs in Hydrocarbon-Bearing Shale."
- Poupon, A., and Leveaux, J. (1971). “Evaluation of Water Saturation in Shaly Formations.” The Log Analyst, 12(4), 3-8.
- Primary Industries and Resources South Australia. (1972). PEL 5 & 6 Nappacoongee-Murteree Block, Cooper and Eromanga Basins, Della#4 Well Completion Report. Open File Envelope No. 2047, Submitted by Delhi Petroleum Pty Ltd. Adelaide: Primary Industries and Resources South Australia.
- Primary Industries and Resources South Australia. (1982). PPL 8 Moomba Block, Cooper & Eromanga Basins, Moomba 46 Well Completion Report. Open File Envelope No. 4893, Submitted by Santos Ltd. Adelaide: Primary Industries and Resources South Australia.
- Primary Industries And Resources South Australia. (2011). PEL 218 South Australia, Cooper & Eromanga Basins, Encounter-1 Well Completion Report, Submitted by Beach Energy Limited Adelaide, July 2011.
- Primary Industries And Resources South Australia. (1972). PEL 5 & 6 Nappacoongee-Murteree Block, Cooper and Eromanga Basins, Della 4 Well Completion Report, Open File Envelope No. 2047, Submitted by Delhi Petroleum Pty Ltd. Adelaide, 1972.
- Primary Industries And Resources South Australia. (1982). PPL 8 Moomba Block, Cooper & Eromanga Basins, Moomba 46 Well Completion Report, Open File Envelope No. 4893, Submitted by SANTOS Ltd. Adelaide, 1982.
- Quirein, J., Witkowsky, J., Truax, J., Galford, J., Spain, D., and Odumosu, T. (2010). “Integrating Core Data and Wireline Geochemical Data for Formation Evaluation and

Characterization of Shale-Gas Reservoirs." In SPE Annual Technical Conference and Exhibition.

- Quihein, J., Galfohd, J., & Witkowsky, J. (2013). "Formation Evaluation and Characterization of Shale-Gas Reservoirs by Means of Core and Wireline Data Integration." *The Leading Edge*, *32*(12), 1486-1492.
- Ramirez, T., Klein, J., Bonnie, R., and Howard, J. (2011). "Comparative Study of Formation Evaluation Methods for Unconventional Shale Gas Reservoirs: Application to the Haynesville Shale (Texas)." In North American Unconventional Gas Conference and Exhibition.
- Reyntjens, S. and Puers, R. (2001). "A Review of Focused Ion Beam Applications in Microsystem Technology." J. Micromech. Microeng. , 287–300.
- Rezaee, M., Motiei And kazemzadeh E. (2007). "A New Method to Acquire m Exponent and Tortuosity Factor for Microscopically Heterogeneous Carbonates." Journal of Petroleum Science and Engineering 56(4): 241-251.
- Rezaee, M.R., Ali S., and Ben C. (2012). "Tight Gas Sands Permeability Estimation from Mercury Injection Capillary Pressure and Nuclear Magnetic Resonance Data." Journal of Petroleum Science and Engineering 88 (2012): 92-99.
- Richard Lewis, Grahame Baker and Albert Suyanto (2010). "Gas Reserves Development in Eastern Australia – Projections Prepared for the GSOO". Report to AEMO Ref: J1899.
- Rider, M. H. (1996). "The Geological Interpretation of Well Logs." Second Edition Whittles Publishing Roseleigh House, Lather wheel Caithness KW5 6DW
- Rieke, Herman H., and George V. Chilingar. (1974) "Compaction of Argillaceous Sediments." Vol. 16. Elsevier Science Limited.
- Riepe, L., Suhaimi, M., Kumar, M., and Knackstedt, M. (2011). "Application of High Resolution Micro-CT-Imaging and Pore Network Modelling (PNM) for the Petrophysical Characterization of Tight Gas Reservoirs-A Case History from a Deep Clastic Tight Gas Reservoir in Oman." In SPE Middle East Unconventional Gas Conference and Exhibition.
- Rietveld, H. (1969). "A Profile Refinement Method for Nuclear and Magnetic Structures." Journal of Applied Crystallography, 2(2), 65-71.
- Rogner, H. H. (1997). "An Assessment of World Hydrocarbon Resources. Annual Review of Energy and the Environment." 22(1), 217-262.
- Rokosh, D., Pawlowicz, J., Anderson, S., Berhane, M., and Beaton, A. (2009) "Shale Fabric, Mineralogy and Effective Porosity of the Upper Colorado Group." CSPG CSEG CWLS CONVENTION Calgary Alberta Canada
- Ross, D.J.K., And Bustin, R.M. (2007). "Impact of Mass Balance Calculations on Adsorption Capacities in Microporous Shale Gas Reservoirs." In: Fuel, 86 (17–18), 2696–706.
- Rossi C., Rafaela M., Karl R., and Albert P. (2001). "Facies Diagenesis and Multiphase Siderite Cementation and Dissolution in the Reservoir Sandstones of the Khataba

Formation, Egypt's Desert." Journal of Sedimentary Research Vol. 71, No. 3, May 2001 P. 459-472.

- Salem, H. S. and G. V. Chilingarian (1999). "The Cementation Factor of Archie's Equation for Shaly Sandstone Reservoirs." Journal of Petroleum Science and Engineering 23(2): 83-93.
- Sam Boggs Jr. (2006). "Principles of Sedimentology and Stratigraphy". Pearson Prentice Hall Upper Saddle River, New Jersey 07 458.
- Schieber Jürgen (1998). "Deposition of Mudstones and Shales: Overview, Problems and Challenges." In: J Schieber. W. Zimmerle, and P. Sethi (Editors), Shales and Mudstones (Vol. 1); Basin Studies, Sedimentology Palaeontology, Scheizerbartsche Verlaggsbuchhandlung, Stuttgart, p. 131-146.
- Schieber, Jürgen. (2010). "Common Themes in the Formation and Preservation of Intrinsic Porosity in Shales and Mudstones-Illustrated with Examples Across the Phanerozoic." SPE Unconventional Gas Conference.
- Schlumberger (1972). Log Interpretation, Volume 1-Principles: Schlumberger Ltd., New York, 113 pp.
- Schlumberger (1969). "Log Interpretation Charts." Schlumberger Well Services, Houston.
- Schön, S. (2011). "Nuclear/Radioactive Properties." Handbook of Petroleum Exploration and Production 8: 107-148.
- Schrider, L., Komar, C. A., and WK, O. (1977). "Natural gas from eastern US shales." In SPE Annual Fall Technical Conference and Exhibition.
- Serra, Oberto (1984). "Fundamentals of Well-log Interpretation: The Acquisition of Logging Data." Elsevier Science Limited.
- Shaw, J.C., Reynolds, M.M., and Burke, I.K. (2006). "Shale Gas Production Potential and Technical Challenges in Western Canada." Petroleum Society of Canada, Canadian International Petroleum Conference, Calgary, Alberta, 13–15 June, 2006-193.
- Simandoux, P. (1963). "Dielectric Measurements on Porous Media, Application to the Measurements of Water Saturation: Study of Behaviour of Argillaceous Formations." Revue de l'Institut Francais du Petrol, 18 (supplementary issue), 93-215.
- Silin, Dmitriy. (2010). "Petrophysical Studies of Unconventional Gas Reservoirs Using High-Resolution Rock imaging." Lawrence Berkeley. National Laboratory Earth Sciences Division. RPSEA Unconventional Gas Project Review Meeting Denver, CO April 06, 2010. ESD Berkley Lab Project: 07122-22.
- Sivakugan N. (2011). "Clay Mineralogy," James Cook University, Townsville Australia
- Sliwinski, Jon Harrington, J., Power M, Hughes, P., and Yeung, B. (2010) "A High-Definition Mineralogical Examination of Potential Gas Shales." Adapted from an oral presentation at AAPG Annual Convention and Exhibition, New Orleans, Louisiana, USA, Search and Discovery Article #50290.
- Soeder, D.J. (1988) "Porosity and Permeability of Easterm Devonian Gas Shale." SPE & SPE Formation Evaluation March., p.116-124.

- Sondergeld, C.H., Ambrose, R.J., Rai, C.S., And Moncrieff, J. (2010a) “Micro-Structural Studies of Gas Shales.” SPE Unconventional Gas Conference, Pittsburgh, Pennsylvania, 23–25 February, SPE 131771.
- Sondergeld, C.H., Newsham, K.E., Comisky, J.T., Rice, M.C., And Rai, C.S. (2010b). “Petrophysical Considerations in Evaluating and Producing Shale Gas Resources.” SPE Unconventional Gas Conference, Pittsburgh, Pennsylvania, 23–25 February, SPE 131768.
- Sondergeld, C.H. (2010) “New Perspective on Shale.” Presentation Material from Meetings 2010. http://www.ogs.ou.edu/level3-meetingsPRES2010.php
- Sundberg, K. (1980). "Effect of Impregnating Waters on Electrical Conductivity of Soils And Rocks." The Log Analyst 21(3).
- Steiber, R.G. (1973). “Optimization of Shale Volumes in the Open Hole Logs.” J. Pet. Techol. 31, 147-162.
- Strahler, A. N. (1981). Physical geology. Harper & Row.
- Steward, B.D., and Paniszczyn, F. (1977). “The Barnett Shale Play; Phoenix of the Fort Worth Basin, A history.” Published by The Fort Worth Geologic Society and The North Texas Geologic Society.
- Stuart, W.J. (1976). “The Genesis of Permian and Lower Triassic Reservoir Sandstones During Phases of Southern Cooper Basin Development.” APEA Journal, 16, 37–47
- Suárez-Ruiz, I., Flores, D., Mendonça Filho, J. G., & Hackley, P. C. (2012). Review and update of the applications of organic petrology: Part 1, geological applications. *International Journal of Coal Geology*, *99*, 54-112.
- Swanson, V. E., 1961. Geology and geochemistry of uranium in marine black shales-a review. U.S. Geol. Surv. Prof. Pap. 356-C, 67-112.
- Swierczek, Z. (2011). “Mineral Phase Investigation of a Murteree Shale Sample Using QEMSCAN Analysis.” Technical Report, Ian Wark Institute, ARC, Special Research Centre, University of South Australia (Unpublished), 2012.
- Talukdar, C. Suhas (2010). “Application of Geochemistry for Shale Gas Assessment” Presentation, Weatherford Core Laboratories Houston TX. USA
- Thornton, R.C.N. (1979). “Regional Stratigraphic Analysis of the Gidgealpa Group, Southern Cooper Basin, Australia.” South Australia. Geological Survey, Bulletin, 49
- Thyberg, B., Jahren, J., Winje, T., Bjorlykke, K., and Faleide, J. I. (2009). “From Mud to Shale: Rock Stiffening by Micro-Quartz Cementation.” First Break, 27, 53.
- Trudgill, B. D., and Arbuckle W. C. (2009). “Reservoir Characterization of Clastic Cycle Sequences in the Paradox Formation of the Hermosa Group.” Paradox Basin, Utah, Utah Geological Survey Open-File Report 543, p. 106, 2009.
- Truman, R. B., Howard, W. E., and Luffel, D. L. (1989). “Shale Porosity Its Impact on Well Log Modelling and Interpretation.” In SPWLA 30th Annual Logging Symposium.

- Taud, H., Martinez-Angeles, R., Parrot, J. F., and Hernandez-Escobedo, L. (2005). “Porosity estimation method by X-ray computed tomography.” Journal of Petroleum Science and Engineering, 47(3), 209-217.
- United States (USA) Energy Information Administration, and Kuuskraa, V. (2011). “World Shale Gas Resources: An initial Assessment of 14 Regions Outside the United States. US Department of Energy. http://www.adv-res.com/pdf/A_EIA_ARI_2013
- Van Krevelen, D.W. (1961). “Coal.” New York, Elsevier, 514p.
- Vavra, C.L., Kaldi, J.G., And Sneider, R. M. (1992). “Geological Applications of Capillary Pressure: A Review.” In: AAPG Bulletin, 76 (6), 840–50.
- Vinegar, H. J., De Waal, J. A., and Wellington, S.L. (1991). “CT Studies of Brittle Failure in Castlegate Sandstone.” Pergamon, 1991.
- Volkert, C. A., and Minor, A. M. (2007). “Focused Ion Beam Microscopy and Micromachining.” Mrs Bull, 32(5), 389-395.
- Walls, J. D., Diaz, E., and Cavanaugh, T. (2012). “Shale Reservoir Properties from Digital Rock Physics.” In SPE/EAGE European Unconventional Resources Conference & Exhibition-From Potential to Production.
- Washburn, E.W. (1921). “Note on a Method of Determining the Distribution of Pore Sizes in Porous Material. “ Proceedings of the National Academy of Science, 7: 115-116.
- Wirth, R. (2009). “Focused Ion Beam (FIB) Combined with SEM and TEM: Advanced Analytical Tools for Studies of Chemical Composition, Microstructure and Crystal Structure in Geomaterials on a Nanometre Scale.” Chemical Geology, 261(3), 217-229.
- Wang, F. P., and Reed, R.M. (2009) “Pore Networks and Fluid Flow in Gas Shales.” SPE-124253, Paper Presented at the Annual Technical Conference and Exhibition, SPE, New Orleans, LA, October 4-7, 2009.
- Ward, C. R., and French D. (2004) “Analysis and Significance of Mineral Matter in Coal seams.” International Journal of Coal Geology 50(1), 135-168.
- Watson, A. T., and Mudra, J. (1994). “Characterization of Devonian Shales With X-Ray-Computed Tomography.” SPE Formation Evaluation, 9(3), 209-212.
- Wellington, S., and Vinegar, H. J. (1987). “X-ray Computerized Tomography”. Journal of Petroleum Technology 39(8): 885-898, 1987.
- Wolf, Karl H., and G. V. Chilingarian. (1975) "Diagenesis of Sandstones and Compaction." Developments in Sedimentology 18 (1975): Elsevier 69-444.
- Worthington, P.F. (2011) “The Petrophysics of Problematic Reservoirs.” Journal of Petroleum Technology 63(12) 88-97.
- Wu, Peng, and Roberto Aguilera. (2012) "Investigation of Gas Shales at Nanoscale - Using Scanning Electron Microscopy, Transmission Electron Microscopy and Atomic Force Microscopy." SPE Annual Technical Conference and Exhibition. 2012.
- Wyllie M.R.J. (1963) “The Fundamentals of Well Log Interpretation.” Third Edition, Academic Press New York and London.

- Yu, G., and Aguilera, R. (2011) “Use of Pickett Plots for Evaluation of Shale Gas Formations.”
- Zuber, M. D., J.H. Frantz Jr., and J.M. Gatens. (1994). “Reservoir Characterization and Production Forecasting for Antrim Shale Wells: An Integrated Reservoir Analysis Methodology.” In SPE Annual Technical Conference and Exhibition.
- Zhao, H., Givens, N. B., and Curtis, B. (2007). “Thermal maturity of the Barnett Shale Determined from Well-log Analysis.” AAPG bulletin, 91(4), 535-549.